Coupled-cluster theory for infinite matter

Gustav Baardsen

A dissertation submitted for the degree of
Philosophiae Doctor (PhD)

Centre of Mathematics for Applications
and
Department of Physics
University of Oslo

June 2014

Series of dissertations submitted to the
Faculty of Mathematics and Natural Sciences, University of Oslo
No. 1530

ISSN 1501-7710

Cover: Inger Sandved Anfinsen.
Printed in Norway: AIT Oslo AS.

Produced in co-operation with Akademika Publishing.
The thesis is produced by Akademika Publishing merely in connection with the thesis defence. Kindly direct all inquiries regarding the thesis to the copyright holder or the unit which grants the doctorate.

Acknowledgments

The work presented in this thesis is a result of collaboration with many people. During the years of my PhD studies, I have learned a lot from a countless number of discussions with my advisors, colleagues, and collaborators. Several people have given their valuable help and, not the least, encouraged me to finish the thesis. The encouragement has been particularly important at challenging times. In addition, financial and practical support has made it possible to accomplish the project. I am deeply indebted for all this help and support.

First, I am thankful to Centre of Mathematics for Applications (CMA) and its director Ragnar Winther for financial support and for the possibility to do a PhD project. In particular, I want to thank Helge Galdal and Aslaug Kleppe Lyngra for help with practicalities during my time at CMA. Likewise, I am grateful to Department of Physics at the University of Oslo for providing working facilities and practical assistance.

It has been very instructive to work with my first supervisor, Morten Hjorth-Jensen, and I highly appreciate the way he has generously shared his knowledge and insight in nuclear and computational physics, as well as in science in general. Many thanks to you, Morten, for the large number of useful discussions, for all your patience when things have taken time, and for being a friendly advisor and fellow human. Morten has contributed to all subprojects of this thesis with essential ideas, advice, and discussions. I am thankful to him for suggesting the topic of this thesis, for the main ideas of the coupled-cluster approach in Paper II, for useful advice considering derivations and implementations in the studies of both nuclear matter and the electron gas, and for many helpful comments on the manuscripts, to name a few things. Also, thanks to Morten for sharing his code, which I have used as a basis when I have developed my own computer programs for nuclear matter.

As part of my PhD research, I worked nine months at Oak Ridge National Laboratory (ORNL). Thanks to ORNL for hospitality during my stay in the USA. When working at ORNL, Gaute Hagen was an informal instructor for me in my PhD project. I learned a lot about computational nuclear physics through frequent discussions with

Gaute. Gaute also contributed to the first parts of Paper II, which were developed when I was at ORNL. The collaboration with Gaute was important in the initial stage of this PhD work, and I want to express my gratitude for all his help. The main ideas of the spherical model for nuclear matter, presented in Section 5.2.5, are by Gaute Hagen, Morten Hjorth-Jensen, and Thomas Papenbrock. Thanks for letting me include these ideas in this thesis.

At several different occasions when I have got stuck into complicated problems with derivations, Simen Kvaal has helped me with analyzing the problems. I have had useful discussions with Simen considering problems related to the CC approach presented in Paper II, the BHF method, and to Ewald's interaction for the electron gas. The ideas of the proof given in Eqs. (5.21) and (5.22) are by Simen, and he has given many useful comments on the manuscript of this thesis. The discussions I have had with Simen have been significant for the completion of this work, and I am indebted for his willingness to help.

I am thankful to my second supervisor, Trygve Helgaker, for discussions, and for showing interest in my work. Andreas Ekström and Boris Carlsson deserve thanks for many interesting and useful discussions considering nuclear physics and programming while sharing office at Department of Physics in Oslo. Gustav Jansen has given helpful advice, in particular related to the implementation presented in Sec. 5.2.2, for which I am thankful. Likewise, I want to thank Xavier Raynaud for help with the derivation of the relations presented in Appendix B.1, and Scott Bogner for discussions and for sharing numbers that I used to validate my Hartree-Fock and particle-particle ladder codes for nuclear matter. Thanks to Rodolfo Id Betan, Øyvind Jensen, Markus Kortelainen, and Sølve Selstø for useful discussions. Also, many thanks to Sarah Reimann and Karl Leikanger for the collaboration on the electron-gas project, for discussions, and for letting me include your results in this thesis.

During my PhD project, I have met many people, for which I am grateful. Thanks to all colleagues with whom I have had interesting discussions about physics, mathematics, science, or something else related or unrelated to this project. Thanks for all conversations, short or lengthy, and for all kind words.

Finally, but not the least, my family and friends have given me balance that has been essential to deal with the challenging project a PhD thesis is. I am thankful to my parents for all their encouragement and support along the years. Thanks also to my cousin and friend Magnus Enlund for many discussions about scientific research and our PhD projects. As mentioned above, many people have been helpful while working on this thesis. However, the most important support I have got from my beloved wife,

Paula. Paula has been positive and encouraged me at all stages of the PhD work. I am highly grateful for your love, for our discussions, and for giving me balance in my life. Similarly, I want to thank our pretty daughter Ada Emilia for giving us joy and duties beyond the PhD project.

Oslo, May 2014 Gustav Baardsen

List of papers

Paper I: Andreas Ekström, Gustav Baardsen, Christian Forssén, Gaute Hagen, Morten Hjorth-Jensen, Gustav R. Jansen, Ruprecht Machleidt, Witold Nazarevicz, Thomas Papenbrock, Jason Sarich, and Stefan M. Wild, Physical Review Letters **110**, 192502 (2013).

Paper II: Gustav Baardsen, Andreas Ekström, Gaute Hagen, and Morten Hjorth-Jensen, Physical Review C **88**, 054312 (2013).

Paper III: Gaute Hagen, Thomas Papenbrock, Andreas Ekström, Kyle A. Wendt, Gustav Baardsen, Stefano Gandolfi, Morten Hjorth-Jensen, and Charles J. Horowitz, Physical Review C **89**, 014319 (2014).

Contents

1 Introduction **1**

2 Background **5**

2.1 Infinite nuclear matter 5

2.1.1 Connection to astrophysics 6

2.1.2 The infinite nuclear matter problem 10

2.2 The homogeneous electron gas 17

3 Microscopic models of fermionic matter **23**

3.1 A quantum many-particle system 23

3.1.1 The Hamiltonian equation 23

3.1.2 Second quantization 25

3.1.3 Momentum single-particle basis 27

3.1.4 Other single-particle bases 30

3.1.5 Interaction matrix elements 32

3.2 The nuclear interaction 33

3.2.1 Background 34

3.2.2 Chiral perturbation theory 36

3.2.3 Optimized interaction model 37

3.2.4 The Minnesota potential 38

4 The Brueckner-Hartree-Fock approximation for nuclear matter **39**

4.1 Many-body perturbation theory 39

4.2 Brueckner-Hartree-Fock approximation 45

4.3 Transformation to partial-wave expansion 46

4.3.1 The first orders of perturbation theory 47

4.3.2 The BHF approximation 52

4.4 Implementations and results 56

4.4.1 The first orders of perturbation theory 56

4.4.2 The BHF approximation 56

5 Coupled-cluster approximations for infinite matter 63
5.1 Coupled-cluster theory 64
5.2 Applications for nuclear matter 71
5.2.1 A reparametrized interaction model 72
5.2.2 Ladder approximation at the thermodynamic limit 73
5.2.3 Finite-box approximations of nuclear matter 80
5.2.4 Problems with particle-hole diagrams 82
5.2.5 Spherical approximation of nuclear matter 85
5.3 Applications for the electron gas 94
5.3.1 Finite-box approximations of the electron gas 95

6 Conclusions 113

A Technical details 135
A.1 Antisymmetrization 135

B Mathematical tools 137
B.1 Coupled delta distributions 137

C Erratum to Paper II 139

Chapter 1

Introduction

To explain how heavy atomic nuclei have been formed from their constituents, and to solve many other problems related to astrophysics or to the basic properties of matter, we need a profound understanding of how a large number of protons and neutrons interact with each other [1]. In this thesis, we study infinite nuclear matter [2], which contains an infinite number of interacting nucleons. Infinite nuclear matter is useful for testing of nuclear interaction models, and its equation of state and symmetry energy provide valuable information about astrophysical systems and processes [3–6]. The nuclear matter equation of state has been studied using first-principle methods through many decades [7, 8], but still different approaches give deviating predictions (see Refs. [9, pp. 139–143] and [10]). Open questions are related to, among other, the nuclear forces [11–16], many-body correlations [17–23], and relativistic effects [9]. Here we concentrate on many-body approaches and their application to infinite nuclear matter.

It is a long-term goal in the nuclear theory community to couple descriptions with different levels of predictability, such as lattice QCD, quantum mechanical *ab initio* methods, and mean-field theory, to each other [1, 24]. Infinite nuclear matter plays an important role when first-principles methods are connected with mean-field theory, as the nuclear matter equation of state may be used to extract energy-density functionals or Skyrme forces for nuclear systems [10, 25–28]. In this thesis, we apply an *ab initio* many-particle method, called coupled-cluster (CC) theory [29–33], to infinite nuclear matter. Coupled-cluster theory has proven to be a reliable and efficient tool to study finite nuclei (see, for example, Refs. [34–42], or, for reviews, Refs. [43, 44]). Instead of using the Bochum truncation [43], as was done in the earliest CC studies of nuclear matter [17, 43], we formulate the CC equations similarly as has been done in recent CC studies of nuclei [44], with truncations after n-particle-n-hole excitations [33]. Our aim is to reintroduce CC theory to the toolbox of modern *ab initio* many-body methods

that are used to study infinite nuclear matter [18–22, 45–48], and thereby provide more insight about many-body correlations in this system.

In condensed matter physics, the electron gas [49] plays a similar role as infinite nuclear matter in nuclear physics. Coupled-cluster theory has been applied to the three-dimensional electron gas in several studies, both in the thermodynamic limit [50–53] and lately using finite-cube approximations [54–58]. As an application of CC theory, we study the two-dimensional electron gas using similar techniques as in Refs. [54–58]. In these calculations, we include CC correlations beyond the level of approximations that Freeman used in his studies [59, 60].

Contributions

My most important contributions to this thesis are presented in Paper II. We approximated the CC equations for nuclear matter by retaining only particle-particle and hole-hole ladder diagrams in the CC doubles (CCD) [61, p. 258] amplitude equation. Particle-particle and hole-hole ladder approximations are common in, for example, self-consistent Green's function theory (see Refs. [62] and [63, pp. 413–416]). I derived and implemented the CC ladder equations in a partial-wave basis using exact Pauli exclusion operators. Our formulation uses ideas first applied by Suzuki *et al.* [64] to the Brueckner-Hartree-Fock (BHF) method [7, 8, 65–69].

As a first application of the CC ladder approximation, I studied pure neutron matter using different nucleon-nucleon interaction models derived from effective field theory (Ref. [70] and Paper I). The results, which are given in Paper I, show that the optimized $\mathrm{NNLO_{opt}}$ parametrization of Ekström performs well for neutron matter as compared to the $\mathrm{N^3LO}$ interaction of Entem and Machleidt [70]. To verify the CC ladder method, I have implemented the well-studied BHF approximation using angular-averaged Pauli operators [67] and continuous single-particle states [68, 69]. As a third application of the CC ladder approximation, we used our results to verify another CC method for nuclear matter, presented in Paper III. In the latter method, the CC equations are formulated using cubic boxes containing a finite number of nucleons, similarly as has been done in Monte Carlo methods [71] for nuclear matter and in CC studies of the electron gas [54–58]. When using twist-averaged boundary conditions [72] to approximate the thermodynamic limit, we obtained very similar results with the two quite different CC ladder approximations. To compare with the accurate auxiliary-field diffusion Monte Carlo (AFDMC) method [73], I implemented and used the simple Minnesota potential [74]. Both the CCD approximation of Paper III and the CC ladder

approximation of Paper II gave neutron matter equations of state in close agreement with the AFDMC method (see Paper III).

In Chapter 5, we discuss a possible implementation of CC theory for nuclear matter that uses a spherical Bessel basis, following ideas by Gaute Hagen, Morten Hjorth-Jensen, and Thomas Papenbrock.

Finally, I have implemented the CCD approximation for the electron gas using finite-size boxes, as was done in [54–58] and, for nuclear matter, in Paper III. To verify the implementation of the CCD approximation, I wrote a general CC code in the singles-doubles (CCSD) approximation [61, p. 258] that I applied to parabolic quantum dots, similarly as in Ref. [75]. Following Refs. [54–58], we modeled the effective electron-electron interaction using Ewald's method [76–79] when studying the electron gas. In this thesis, we apply the CCD method to the two-dimensional electron gas, and we compare correlation energies with in-medium-SRG (IM-SRG) [80] results [81, 82] and full configuration-interaction quantum Monte Carlo (FCIQMC) [83, 84] results [85, 86]. Our study shows that correlations beyond the CCD truncation are necessary to model finite-size approximations of the two-dimensional electron gas with high accuracy.

Outline

In Chapter 2, we define infinite nuclear matter and the electron gas. We explain why the nuclear matter equation of state is important in astrophysics and nuclear theory, and we mention microscopic methods that have been used to study infinite nuclear and neutron star matter. Furthermore, we briefly review studies of the electron gas. Chapter 3 is devoted to the infinite-matter many-body problem, including the Hamiltonian operator, single-particle bases, and many-particle wave functions. In Chapter 4, we discuss many-body perturbation theory [61, pp. 18–53] and the BHF approximation. We also sketch how we have implemented the BHF method and low-order approximations of many-body perturbation theory. The results of this thesis are mainly discussed in Chapter 5. We start with a short introduction to CC theory. Thereafter, we present Papers I–III, including the main ideas, details on implementation and verification, and some results. We also discuss a different way to implement CC theory for nuclear matter, in which the infinite system is approximated using a spherical box. Finally, we show how we have formulated, implemented, and verified the CCD approximation for the two-dimensional electron gas. We compare CCD energies for the two-dimensional electron gas with results obtained with the SRG [81, 82] and FCIQMC [85, 86] methods, as well as with previous studies. In Chapter 6, we give a summary of the thesis, and discuss possible ways to extend our CC studies of infinite matter.

Chapter 2

Background

The subject of this thesis is related to fields as different as nuclear astrophysics and nanotechnology. On a general level, we are interested in questions considering, for example, the origin of the chemical elements, the stability of nuclear matter [1], and physical properties of technological devices on a nanoscale [87]. To learn more about these subjects, we can study complex systems such as neutron stars, supernovae, atomic nuclei, and nanoscale transistors. The way to approach complicated systems in physics is by using simplified models. Hopefully, the models can tell us something essential about the behavior of real physical objects. In this thesis, we study theoretical approaches for one such class of models: infinite matter. Papers I–III consider the nuclear interaction and nuclear structure theory, and the main emphasis of the thesis is, therefore, on applications to nuclear physics. As we define it, nuclear matter is a many-fermion system. Another well-known extended fermion system is the homogeneous electron gas [49]. Due to the formal similarity, these two systems can often be studied using the same theoretical methods. We therefore use the homogeneous electron gas as a benchmark system, for comparisons with other established methods, and to illuminate different aspects of the theoretical methods. In the following sections, we define infinite nuclear matter and the homogeneous electron gas, explain why the systems are important, and briefly review some of the related research.

2.1 Infinite nuclear matter

As far as we know, there are four different fundamental types of interactions in nature. These are the strong, weak, electromagnetic, and gravitational interactions. At high energies, the weak and electromagnetic interactions are shown to converge towards the same interaction; the electroweak interaction (see Refs. [88, pp. 261–325] and [89, pp. 177–213]). All these fundamental interactions are present in nucleonic matter,

which we define as matter with nucleons as building blocks. As predicted initially by Gell-Mann and Zweig and verified later experimentally (see Refs. [90] and [89, p. 4]), nucleons have internal structure. Hadrons, including nucleons, consist of quarks and gluons, where the latter mediate the strong interaction between the quarks. According to the successful standard model of elementary particles, strong interactions are described by a theory called Quantum Chromodynamics (QCD) (see Refs. [89, pp. 149–151] and [91]). Nucleons are important both as building blocks of atomic nuclei and as basic consitutents in stellar matter.

Similarly as described in, for example, a review article by Day [2], we define infinite nuclear matter as an infinitely large system of homogeneously distributed nucleons. In particular, we study two different nuclear matter systems: symmetric nuclear matter, which contains the same amout of protons and neutrons, and neutron matter, which has only neutrons as building blocks. Symmetric nuclear matter is by definition a system with zero electrical charge [2]. In finite nuclei, the gravitational force is vanishingly small [92, pp. 2–3] compared to the other fundamental interactions, whereas in macroscopic nuclear objects, such as supernovae [93] and neutron stars [3, 5], the gravitational force plays an important role. However, the gravitational interaction only affects the density of the system. When studying infinite nuclear matter, we neglect the weak interaction, which causes β decays [89, p. 5], and concentrate only on residual effects of the strong interaction.

2.1.1 Connection to astrophysics

To understand more about the origin of the chemical elements, the evolution of stars, and the inner mechanisms of the building blocks of matter, we need more knowledge about the structure of nucleons and how they interact. In this thesis, we focus on the nuclear matter equation of state. This equation of state describes strongly interacting matter containing only protons and neutrons [2]. As is reviewed in, for example, Ref. [91], strongly interacting matter is predicted to appear in many different phases depending on the temperature and the baryochemical potential [1]. For example, at sufficiently high temperature and baryochemical potential, quarks and gluons become much less confined and form a so-called quark-gluon plasma [91].[2] In our work, we assume that the temperature and baryochemical potential (or density) are sufficiently low such that the quarks and gluons are confined as hadrons. According to Ref. [3],

[1] The baryochemical potential tells how much energy is needed to add one baryon, such as, for example, a nucleon, to the medium [3].

[2] At the European Organization for Nuclear Research (CERN) [94] and at Brookhaven National Laboratory [95], formation of quark-gluon plasma is studied using heavy-ion collisions.

phases containing deconfined quarks occur at densities around two to three times the saturation density of nuclear matter, which is approximately $2.8 \cdot 10^{14}$ g cm^{-3}. In this thesis, we study infinite nuclear matter at densities up to at most 10^{15} g cm^{-3}. One should keep in mind that at the highest densities we study, hadrons may be mixed with deconfined quark-gluon plasma. At densities above the saturation point, other hadrons, such as pions, kaons, and hyperons may also coexist with nucleons [3, 4].

Presently, we do not have satisfying explanations for how all the different chemical elements heavier than iron have been formed. One of the currently best explanations for the formation of heavy neutron-rich elements is a mechanism called the rapid-neutron-capture process (r-process) (see Refs. [96] and [97, p. 265]). There is no agreement of where in the universe the necessary conditions for r-processes are fulfilled, but core-collapse supernovae and merging neutron stars are among the suggested locations [96]. According to Arnould [96], accurate r-process simulations require very precise data for a large number of stable and unstable nuclei. It is costly and difficult to measure all the required nuclei experimentally; therefore, predictive theoretical methods will be necessary to understanding the r-process [96]. Ideally, a predictive microscopic model for many-nucleon systems should reproduce the experimental saturation point of nuclear matter. In that way, nuclear matter calculations are a good test-bed for microscopic theories. As part of a larger effort, such calculations are needed to model r-processes accurately [96]. The nuclear matter equation of state, as well as the closely related symmetry energy, are also important components, for example, when predicting theoretically how much energy is released in a supernova type II explosion [98]. Likewise, the same equation of state is an essential input to neutron star models [3, 5]. Let us, therefore, briefly consider the formation and composition of neutron stars.

We define a Type II supernova following Boyd [97]: Consider a heavy star with a mass larger than ten times the solar mass. When the star has burnt up its fuel, the core contains elements lighter than or equal to iron. When the fusion processes do not release more energy, the core of this big star may start to collapse due to the strong gravitational field. The stellar matter of the core gets compressed until the density is a few times the saturation value. This results in a giant explosion where matter is thrown out. Eventually the core is left. In the so-called Type II supernova, the dense core may become a neutron star [97, pp. 238–239].

There are many reasons why neutron stars are scientifically interesting objects. Firstly, neutron stars are part of several different hypotheses for where the r-process could occur [96, 99]. Secondly, we can learn more about how strongly interacting matter behaves at high densities by comparing different theoretical neutron star models with

astrophysical observations [4]. According to current observational data and theory [5], neutron stars have masses between one and three times the solar mass inside a radius that is roughly 12 kilometers. Some recent observations indicate that neutron stars may be even smaller, with a radius of only 9 kilometers [6]. General relativity, causality, and rotational arguments give upper and lower limits for the mass, as well as maximum radii corresponding to different masses [4]. Different theoretical approaches predict different relationships between the neutron star radius and mass [3, 4, 100].

In our description of the composition of neutron stars, we follow Refs. [3, 4]. Neutron stars contain strongly interacting matter in a number of different phases. The phases are believed to exist in layers, forming an onion-shell-like structure. The main body of the star contains inner and outer cores, constituting around 99 % of the total mass, as well as inner and outer crusts. Outside the crust, there is an envelope, and finally a gaseous phase surrounds the solid sphere. The neutron star composition is illustrated in, for example, Figure 3 of Ref. [4]. In Table 2.1, we list the compositions and the estimated densities of the core and crust. It is still uncertain exactly what kind of phases exist in the inner core, but possibly there is a mix of nucleons, hyperons, Bose condensates of kaons and pions, and maybe deconfined quark matter. The outer core contains mostly superfluid neutrons, but also a fraction of superconducting protons. Electrons and muons neutralize this layer. In the crust, neutron-rich and heavy nuclei appear in lattice structures. The crust also contains electrons and superfluid neutrons [3, 4].

Neutron star models have many different sources of uncertainties. As described in, for example, Refs. [3, 101], the nuclear matter equation of state is a central ingredient in neutron star models. Despite more than half a century of research, most theoretical approaches are unable to predict the correct saturation properties of symmetric nuclear matter [3, 20–23, 45, 101–106]. The symmetric nuclear matter equation of state is, therefore, still poorly understood. A source of uncertainty in neutron star models is nuclear forces including hyperons [3, 107]. In neutron stars, the neutron-proton ratios are typically highly asymmetric, and it is, therefore, necessary to have good models for asymmetric nuclear matter [3]. As we explain in the next paragraph, the symmetry energy is also important in neutron star models [6]. The symmetry energy is defined as the difference between the energy per nucleon of pure neutron matter and symmetric nuclear matter. Because of the uncertainties related to the nuclear matter equation of state, there are large differences in theoretical predictions of the symmetry energy [45, 108–112].

Layer	Density ($g \cdot cm^{-3}$)	Composition
Inner core	$\approx 10^{15}$	Nucleons and possibly hyperons, Bose condensate of kaons and pions, and deconfined quark matter
Outer core	$2 \cdot 10^{14} - 10^{15}$	Superfluid neutrons, superconducting protons, electrons and muons
Inner crust	$4 \cdot 10^{11} - 2 \cdot 10^{14}$	Neutron-rich nuclei, superfluid neutrons, and electrons
Outer crust	$10^{6} - 4 \cdot 10^{11}$	Heavy nuclei and electrons

Table 2.1: The composition of a neutron star, as described in Refs. [3, 4]. For comparison, the saturation density of nuclear matter is approximately $2.8 \cdot 10^{14}$ g cm^{-3}.

Let us give a few examples that illustrate the importance of the symmetry energy. First, it is well known that the composition of both neutron stars [4] and supernova cores [113] are sensitive to the symmetry energy. The composition, in turn, may determine what cooling mechanisms are possible for the neutron star [3]. According to current understanding, neutron stars cool by neutrino emission, among other [4]. The modified Urca process, which is slow, and the fast so-called direct Urca process are two important neutrino-emission cooling mechanisms that have been suggested [114]. The direct Urca process may occur only in neutron stars with a sufficiently high proton-neutron ratio. As the proton-neutron ratio depends on the symmetry energy at β equilibrium, reliable predictions of the symmetry energy are necessary to understand how neutron stars cool [3]. The reader is referred to, for example, Refs. [3, 4] for more details about the connection between the direct Urca process and nuclear matter models. Also other neutron star observables, such as the radius-mass relation, are strongly dependent on the neutron-proton ratio, and thereby the symmetry energy [115]. Better theoretical predictions for the symmetry energy will therefore give more reliable astrophysical models. For a recent review considering the symmetry energy, the reader is referred to Ref. [6].

The nuclear matter equation of state and the symmetry energy have been studied experimentally using heavy-ion collisions, giving constraints at densities above and below the saturation point [6, 116, 117]. Experimental information about the symmetry

energy has also been obtained by measuring the neutron skin thickness, as well as properties related to giant monopole and dipole resonances [6].

2.1.2 The infinite nuclear matter problem

Infinite nuclear matter is, as we define it, a relativistic quantum system with an infinite number of interacting nucleons. Given the homogeneous structure, naively one may assume infinite nuclear matter to be a very simple system to study. In fact, many theoretical many-body methods can be formulated easier for a homogeneous system than for, for example, finite nuclei. In particular, the single-particle basis, which for infinite nuclear matter is the plane-wave basis, is much simpler than for finite nuclei. Nevertheless, infinite nuclear matter has been studied using microscopic approaches for more than half a century [7, 8], yet still there are large deviations ([9, pp. 139–143] and [10]) between predictions of different theoretical methods for this system.

Commonly, infinite nuclear matter is modeled using either *ab initio* many-body methods [9, 118] or mean-field approaches [27, 119]. The *ab initio* methods use a Hamiltonian operator containing two- and many-body interactions. Normally, the only adjustable parameters in an *ab initio* calculation are in the Hamiltonian. Optimal parameter values for the two-body interaction are obtained by fitting phase shifts to experimental nucleon-nucleon scattering data [14]. The three-body interaction may have additional parameters which are adjusted to, for example, observables of triton or helium [16], or to the saturation density and/or energy of symmetric nuclear matter [21, 101, 120, 121]. In principle, *ab initio* methods provide a systematic way of improving the result towards the exact solution, given a Hamiltonian operator. However, the results are truly based on first principles only if that is also the case for the Hamiltonian operator.

Self-consistent mean-field approaches [119], such as the Skyrme-Hartree-Fock method, the Gogny model, and relativistic mean-field theory, are methods closely related to density functional theory [122], which is very popular in quantum chemistry and condensed matter physics. However, the former methods are tailored to nuclear physics applications. In these methods [119], an effective density-dependent interaction is used in self-consistent calculations. The effective interaction contains several free parameters, which are typically fitted to reproduce, optimally, observables of many different nuclei, and possibly also saturation properties of symmetric nuclear matter [10]. In self-consistent mean-field methods, the many-body problem is reduced to an effective one-body problem, which makes these methods computationally considerably simpler

than *ab initio* approaches. As a result, self-consistent mean-field approximations can be used to study nuclei from the lightest to superheavy elements [119].

Because self-consistent mean-field methods cannot be systematically improved, for example as a function of a convergence parameter, as is common in *ab initio* methods [118], the mean-field approaches are believed to have less predictive power than *ab initio* approximations. *Ab initio* calculations provide therefore important tests for mean-field parametrizations. In this context, *ab initio* predictions for the nuclear matter equation of state play an important role [10]. *Ab initio* methods, such as the nonrelativistic BHF and the relativistic Dirac-Brueckner-Hartree-Fock (DBHF) [123–128] approach, have been used [10, 25–27] to extract density functionals or Skyrme forces. Even if the resulting mean-field methods have a microscopic foundation, the quality of these approximations are currently not as good as more empirical Skyrme-Hartree-Fock models [10]. The quality of local density approximations for nuclear systems would probably improve if we had more realistic nuclear matter equations of state [22, 28].

As pointed out by van Dalen and Müther [103], one might first assume that relativistic effects are small in nucleonic systems, because the saturation energy per particle in nuclear matter is much smaller than the nucleon mass in energy units. On the contrary, calculations show [103] that relativistic effects give important contributions for infinite nuclear matter, in particular as compared to nonrelativistic approaches with only a two-body interaction. Dalen and Müther also found not negligible relativistic effects in finite nuclei [103]. According to Ref. [103], relativistic *ab initio* calculations for finite nuclei are complicated and have, therefore, not yet been done. Instead, nonrelativistic approaches for finite nuclei have been widely used [44, 62, 129, 130], giving results in good agreement with experiments, in particular when three-body forces are included [41, 129–133]. Relativistic and nonrelativistic mean-field methods are used for finite nuclei and nuclear matter side by side, and in the best calculations both approaches give approximately the same accuracy [10]. As we see, nonrelativistic and relativistic microscopic methods have a complementary role in describing low-energy nuclear systems. Because this thesis considers nonrelativistic *ab initio* methods, we concentrate on this group of methods in the rest of the present section.

When studying infinite nuclear matter, an important test for the microscopic method is to compare the theoretical saturation properties with experimental data. Inside a heavy nucleus, the density is approximately constant and similar for different nuclei [134, pp. 13–14]. The density in the center of nuclei can be obtained from electron scattering experiments, and different estimates around 0.16–0.17 fm^{-3} are used in the literature (see Refs. [135] and [136, p. 2]). This is believed to be the saturation density

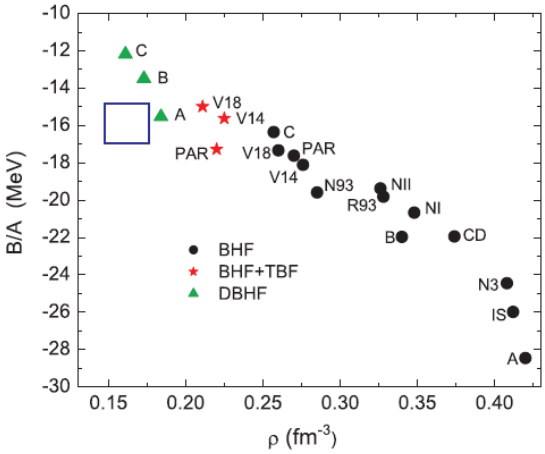

Figure 2.1: Even if different two-body interactions are optimized to reproduce the same nucleon-nucleon phase shifts, they give very different predictions for the saturation point of symmetric nuclear matter. The figure shows results [45] obtained with the nonrelativistic Brueckner-Hartree-Fock method (BHF) and only two-body interactions, with the Brueckner-Hartree-Fock method including three-body forces (BHF+TBF), and relativistic results obtained with the Dirac-Brueckner-Hartree-Fock (DBHF) method. The saturation points are given as the energy per particle B/A at a density ρ. Different points with the same color represent calculations with different two-body interactions. The unfilled square represents the uncertainty region of the experimental saturation point. The figure is courtesy of Ref. [45]. Reprinted figure with permission from Z. H. Li, U. Lombardo, H.-J. Schulze, W. Zuo, L. W. Chen, and H. R. Ma, Phys. Rev. C **74**, 047304 (2006). Copyright (2006) by the American Physical Society. `http://link.aps.org/abstract/PRC/v74/p047304`

of nuclear matter, also in the infinite-matter limit. According to the semiempirical mass formula, the energy of a nucleus is [134, p. 17]

$$E = -c_{\mathrm{V}}A + c_{\mathrm{S}}A^{2/3} + c_C Z^2 A^{-1/3} + c_M (A-2Z)^2 A^{-1} + c_P \delta A^{-3/4}, \tag{2.1}$$

where A is the total number of nucleons, Z is the number of protons, δ is a constant that depends on the parity of Z and A, and c_V, c_S, c_C, c_M, and c_P are constants related to the volume, surface, Coulomb, symmetry, and pairing terms, respectively. In the special case of symmetric nuclear matter, only the volume term is nonzero. The parameters in the semiempirical mass formula can be determined by simultaneously optimizing with respect to many different nuclei [135]. Such an optimization gives an estimate for the volume term, and thus also for the experimental binding energy of symmetric nuclear matter. According to Chabanat *et al.* [135], the experimental binding energy of nuclear matter is $-(16 \pm 0.2)$ MeV per nucleon.

Figure 2.1 shows a typical set of saturation points for symmetric nuclear matter, as obtained with different *ab initio* many-body methods and different interaction models. The figure, which is from Ref. [45], presents saturation points obtained with the nonrelativistic BHF method [7, 8, 65–69] and the DBHF method [123–128]. The latter approach is a relativistic counterpart of the BHF approximation. The uncertainty region of the experimental saturation point is marked by a blue unfilled square. As can be seen from the figure, saturation points obtained with the nonrelativistic BHF method and different two-body interaction models (black circles) occur approximately on a line that does not cross the experimental uncertainty region. The phenomenon of saturation points obtained with the same many-body method and different interaction models aligning so that a higher saturation density means more binding is well-known for both nonrelativistic [137] and relativistic calculations [9, p. 141]. When including only a two-body interaction, nonrelativistic calculations typically give a so-called Coester band much farther from the experimental saturation region than relativistic calculations do [9, p. 141]. Figure 2.1 also shows another commonly observed feature: When including three-body forces in nonrelativistic calculations, the saturation point is usually closer to the experimental value than in calculations neglecting three-body interactions. It is a prevailing understanding (see Refs. [9, pp. 139–143] and [133]) that either three-body interactions are needed in nonrelativistic calculations or a relativistic many-body method is necessary to obtain saturation properties in agreement with experimental data.

In many-body perturbation theory, the energy can be expressed in terms of Goldsone diagrams [61, Chapter 5]. The hole-line approximation [2, 66] builds on the assumption that the total contribution from all Goldstone diagrams with n independent

hole lines is larger than the contribution from all diagrams containing $n+1$ hole lines. Given a truncation level n, all diagrams containing more than n hole lines are therefore neglected from the perturbative expansion. As Day explains [2], the truncation in the number of hole lines is justified only at sufficiently low densities. According to Song *et al.* [18], the approximation breaks down above $3\rho_0$, where ρ_0 is the experimental saturation density of nuclear matter. The above mentioned BHF method is equivalent to the lowest-order approximation of the hole-line expansion, including diagrams with maximally two independent hole lines [66]. The BHF approach is one of the standard methods for infinite nuclear matter, and has been used and developed in a large number of studies, starting in the 1950s with the publications of Brueckner and co-workers [7, 8, 138, 139] and continuing until the present [2, 18, 45, 64–69, 109, 140–150]. Mahaux *et al.* introduced continuous single-particle energies [68, 69] in the G matrix, giving a faster convergence [18, 142] in terms of hole lines than the traditional gap choice [67]. The BHF approximation has been extended to finite temperatures [141, 147], asymmetric nuclear matter [143, 151, 152], and hyperonic matter [145, 153], among others. In Chapter 4, we review the theory and give details about the implementation of the BHF method.

In addition to the many BHF calculations, there are only a few studies of nuclear matter using higher-order hole-line approximations [18, 154, 155]. By definition, Bethe-Brueckner-Goldstone (BBG) theory [2, 66, 156] does not determine the exact form of the energy denominator. A necessary condition for convergence in the number of hole lines is that the calculation does not depend on the choice of single-particle potentials in the energy denominator [66]. Song *et al.* have compared [18] a three-hole-line approximation using the traditional gap choice with a calculation using continuous single-particle energies. In the study of Song *et al.* [18], the two approaches gave approximately the same binding energy, differing by less than 1 MeV around the saturation density. The weak dependence on the choice of single-particle potentials may indicate that a three-hole-line approximation is sufficient to obtain converged results. In agreement with studies using other methods, the results of Song *et al.* show that it is necessary to take into account three-body forces in order to reproduce the experimental saturation point [18].

A method that is related to the hole-line approximation is coupled-cluster theory [29–33]. The first coupled-cluster calculations for nuclear matter were done using the so-called Bochum truncation scheme [17, 43]. Day and Zabolitzky did calculations [17] containing three-body equations, and also included an estimate of the four-body amplitudes. Whereas the inclusion of three-body terms gave a significant contribution

to the binding energy, their estimate including a subset of the four-body terms gave results very similar to the three-body approximation. Provided that the approximation of the four-body equations was reasonable, the results showed convergence for the Bochum coupled-cluster method. Day and Zabolitzky also compared their coupled-cluster calculations with the hole-line approximation. For Fermi momenta between 1.4 and 1.8 fm^{-1}, the four-hole line approximation gave binding energies differing at most almost 3 MeV from their most accurate coupled-cluster results [17]. In Paper II, we explain the differences between our coupled-cluster implementation and the Bochum scheme. In Chapter 5, we give an introduction to coupled-cluster theory.

Symmetric nuclear matter, pure neutron matter, and asymmetric neutron star matter have been studied using many other nonrelativistic *ab initio* methods, and we will mention some of these only briefly. There exist a large number of different methods derived from perturbation theory, some of which are obtained by partial summation of certain diagrammatic classes to infinite order [157, pp. 266–289]. When using a bare interaction, nuclear matter is commonly known to be a nonperturbative system [158]. The G matrix, which is used in BBG theory, was introduced to deal with this problem [2]. Renormalization group (RG) theory provides an alternative, modern approach to obtain softer interactions that give the same phase shifts as bare nuclear interaction models [80].

Nuclear matter calculations have been done [22, 80, 158–160] using two- and three-body interactions evolved to low momenta by using either the so-called $V_{\text{low}k}$ or the similarity renormalization group (SRG) method. When using a low-momentum interaction in symmetric nuclear matter, the third-order particle-particle and hole-hole diagrams give only a small additional contribution compared to second-order perturbation theory [22]. This perturbative behavior in calculations with low-momentum potentials is potentially a great advantage. On the other hand, in these calculations the RG interactions have a cutoff dependency that is not negligible and increasing for larger densities [22].

Lately, Tews *et al.* [47] have done perturbation-theory calculations for neutron matter with nuclear interactions derived from chiral perturbation theory including the full next-to-next-to-next-to-leading order (N^3LO) contribution, with three- and four-body forces. Compared to calculations with three-body interactions defined only to next-to-next-to-leading order (NNLO), the inclusion of all N^3LO diagrams was found to be important [47].

The nonrelativistic particle-hole ring approximation has been implemented for nuclear matter to fourth order [161]. Other methods derived from many-body pertur-

bation theory are, for example, the model-space BHF [162–164] and the model-space particle-particle ring [164–167] approximations. In the particle-particle ring diagram approximation, particle-particle and hole-hole diagrams are summed to infinite order [165], and this method is, therefore, similar to our coupled-cluster ladder approximation presented in Paper II.

In the self-consistent Green's function (SCGF) method [62, 118, 168], single-particle and two-particle propagators are used to evaluate expectation values of different operators. The standard SCGF approximation for extended nuclear matter includes particle-particle and hole-hole ladder diagrams to infinite order [169]. In contrast to, for example, the BHF and coupled-cluster methods, in the SCGF approach the Fermi sea is correlated, and the propagators are said to be 'dressed' [62]. According to Dickhoff and Müther [168], perturbations of the Fermi surface can become significant in systems with strong correlations. Due to the symmetry between particle and hole states, one can show that the number of particles is a conserved quantity in SCGF calculations. Calculations in SCGF theory also have the advantage that they can be conveniently compared to experiments through spectral functions, which are evaluated using propagators [168]. As reviewed by Dickhoff and Barbieri [62], there are many approaches to deal with pairing instabilities, which occur in the SCGF method. In Paper II, we explain why the pairing instability problem is not present in coupled-cluster equations. The developments of the SCGF method for nuclear matter until 2004 are reviewed in, for example, Ref. [62]. During the last decade, several new studies of infinite nuclear and neutron matter have been presented [21, 23, 112, 170–180].

Beside BBG, CC, and SCGF theory, different variational and Monte Carlo methods have been important in the study of infinite nuclear matter. Let us first consider two variational methods: the Fermi hypernetted chain (FHNC) [181] and the variational Monte Carlo (VMC) [71, p. 342–347] approximations. In both the VMC and FHNC methods, the variational energy is written using a Jastrow-type wave-function ansatz. The Jastrow-type ansatz of a nuclear system is often expanded as a sum of different operators (see Refs. [71, p. 342] and [181, pp. 138 and 140]). In the VMC approach, the variational energy is calculated using a Monte Carlo method [71, p. 346–347]. In contrast, the FHNC approach results in a set of integral equations [181, p. 165–169]. The so-called variational chain summation (VCS) technique, in which the Fermi-hypernetted-chain-single-operator (FHNC-SOC) equations are solved, has been used in several studies of nuclear and neutron star matter [19, 101, 182–184]. The VMC method has likewise been applied to model infinite nuclear systems [19]. Whereas FHNC approximations can be formulated with integral equations in the thermodynamic

limit, only finite systems can be studied using Monte Carlo methods [181, p. 121]. Infinite nuclear or neutron matter is, therefore, typically approximated by a box with a finite number of particles [19, 20, 185]. Gandolfi *et al.* [185] have used twist-averaged boundary conditions to approximate the thermodynamic limit.

The variational energy estimate of the VMC method is restricted by the chosen Jastrow-type ansatz [186, pp. 373–380]. The Green's function Monte Carlo (GFMC) method [71, p. 347–355] provides a recipe to improve the VMC energy to almost the exact value. In the GFMC method, the Schrödinger equation is multiplied by a trial wave function and formulated as a diffusion equation by using an imaginary time variable. The stationary GFMC solution is obtained in the limit of infinite imaginary time, using random walks that are guided by approximative Green's functions for finite time steps [187, pp. 77–100]. Due to the fermion sign problem [13], GFMC calculations cannot be systematically improved to the exact solution. Carlson *et al.* have used the GFMC method to study pure neutron matter in both the normal [19] and superfluid phases [188]. The GFMC method is computationally expensive and is, therefore, restricted to small systems. As suggested by Schmidt and Fantoni [73], the computational scaling of the GFMC approach can be significantly improved by using a Hubbard-Stratonovich transformation, which makes it possible to sample both position and spin randomly. This approach, which is called the auxiliary-field diffusion Monte Carlo (AFDMC) method, has been used by Gandolfi *et al.* in calculations of symmetric nuclear matter [20], neutron matter [185], and neutron star matter [121]. The AFDMC method has also been applied with a Jastrow-BCS wave-function ansatz to model neutron matter in the superfluid phase [189]. In Refs. [46, 190], another Monte Carlo projection method using lattice discretization has been applied to neutron matter at low densities.

Examples of other recent developments for infinite nuclear matter are, for example, the chiral perturbation theory approaches of Holt, Kaiser, and Weise [191], and the study of Inoue *et al.* [150], in which the authors use a nuclear interaction model derived from lattice QCD. In the latter calculations, the lattice QCD two-body force still has unphysically large quark masses [150].

2.2 The homogeneous electron gas

The focus of this thesis is on coupled-cluster theory for nuclear matter. Another important system with infinite extension is the electron gas [49]. The homogeneous electron gas is defined as a system of interacting electrons with a constant, neutralizing background charge [192, p. 21]. The electron gas, in one, two or three dimensions, is

interesting as a test-bed for electron-electron correlations. The three-dimensional electron gas is particularly important as a cornerstone of the local-density approximation in density-functional theory [122, pp. 176–183]. In the physical world, systems similar to the three-dimensional electron gas can be found in, for example, alkali metals and doped semiconductors. Two-dimensional electron fluids are observed on metal and liquid-helium surfaces, as well as at metal-oxide-semiconductor interfaces. These and other physical realizations of the electron gas are presented and discussed in the textbook of Giuliani [49, pp. 5–12]. We use the electron gas as a benchmark system to compare coupled-cluster theory with other many-body methods. In particular, we concentrate on the two-dimensional electron gas, for which there are very few coupled-cluster studies [59, 60].

As we explain in Section 3.2, the nucleon-nucleon interaction has a range of only a few fermi, but is strongly repulsive when the nucleons are close to each other [193, pp. 5–7]. Consequently, short-range correlations are important in nuclear matter, while the role of longe-range correlations is more debated [169]. At low density, the electrons become localized and form a lattice [194]. This so-called Wigner crystallization [195] is a direct consequence of the long-range repulsive interaction. At higher densities, the electron gas is better described as a liquid [53, 194, 196, 197]. When using, for example, Monte Carlo methods [198], the electron gas must be approximated by a finite system. The long-range Coulomb interaction in the electron gas causes additional finite-size effects [77, 79, 199] that are not present in infinite nuclear matter (for the latter, see, for example, Paper III). Because of these differences, coupled-cluster approximations face other challenges when applied to the electron gas than when used to study infinite nuclear matter.

The electron gas has been studied using a large number of different approaches, and we will here only mention some of the most important works that are relevant for this thesis. We start with the three-dimensional electron gas, which has got most attention in the literature. It is a well-known fact that the correlation energy of the three-dimensional electron gas diverges at second order in perturbation theory [200, pp. 44–46]. As is shown in the textbook of Bruus and Flensberg [200, pp. 246–250], the particle-hole ring diagrams dominate in the limit of high density. Even though all these diagrams diverge when calculated separately, the energy converges when summing all direct particle-hole ring diagrams to infinite order [200, p. 256]. Gell-Mann and Brueckner obtained for this so-called random-phase approximation (RPA) the first terms of the exact energy in the high-density limit [201].

In systems with not very high densities, short-range correlations are not negligible [202]. Singwi *et al.* [202] and Lowy and Brown [203] came up with early attempts to combine RPA with contributions for short-range correlations. The calculations of Singwi *et al.* were based on dielectric function theory [202], whereas Lowy and Brown interpolated between short- and long-range models using a diagrammatic technique [203].

In 1978, Ceperley used [196] the variational Monte Carlo (VMC) method [71, p. 342–347] to study the two- and three-dimensional electron gas. The obtained VMC ground-state energies were shown to be close to other results at that time [196]. The electron gas has also been studied [204] using the Fermi hypernetted chain (FHNC) method [181], which is another variational approach to the quantum many-body problem. In the VMC method, the energy estimate is restricted by the chosen Slater-Jastrow wave-function ansatz [71, p. 342]. As we discussed in Section 2.1.2, higher accuracy can be obtained with the diffusion Monte Carlo (DMC) method (this method is also named Green's function Monte Carlo). Ceperley and Alder [194] did DMC calculations for the three-dimensional electron gas in which the fermion sign problem [13] was handled using a released-node approximation. Similar accuracy has been obtained in more recent calculations using the backflow-correlation technique [205], which is used to relax the simpler fixed-node approximation. Backflow correlations have also been used in more recent DMC studies, such as Refs. [206–208]. Ortiz and Ballone did DMC calculations with a normal fixed-node approximation but studied systems with different degrees of spin polarization [209].

When modeling the electron gas using a finite box, as is commonly done in Monte Carlo methods, the energy has an error compared to the electron gas at the thermodynamic limit [79]. At the thermodynamic limit, plane-wave single-particle states fill the Fermi sphere with a continuous spectrum. However, as is illustrated in Figure 1 of Ref. [72], when the system is approximated using a finite box, the single-particle spectrum becomes discrete. This discretization gives an error that is common to systems with short-range and long-range interactions [72]. The perhaps most obvious way to correct for finite-size effects related to a discrete single-particle basis is by using an extrapolation formula. As is described in Ref. [79], results from Hartree-Fock and density-functional theory calculations can be used to construct extrapolation methods. Another approach that efficiently reduces the finite-size error is a technique that utilizes so-called twisted boundary conditions [72]. In calculations with twisted boundary conditions, the single-particle wave function is multiplied by a complex phase factor when moving from one simulation cell to a neighboring cell. When averaging over results

obtained with different twist angles, the energy estimates become much more accurate than when using periodic boundary conditions [72]. In Paper III, twist-averaged boundary conditions are used to deal with finite-size effects in nuclear matter.

Finite-size approximations of extended Coulombic systems, such as the electron gas, have additional errors that are caused by the long-range interaction [77, 79, 199]. Interactions with electrons in neighboring cells can be summed using, for example, Ewald's method [76–79] (see also Section 5.3). In Ewald's approach, each electron in the simulation cell interacts with an infinite number of image charges located at the same local position in all other cells [78]. As is shown in Refs. [77, 199], Ewald's interaction cannot describe the exchange-correlation energy correctly. Chiesa *et al.* used a static structure factor and a Jastrow factor derived from RPA to estimate the correction to Ewald's method [199]. The correction technique of Chiesa *et al.* [199] is directly applicable only to Monte Carlo methods. Fraser *et al.* suggested [77] two different effective interactions that avoid screening effects caused by Ewald's interaction. The most successful alternative was to use a normal Coulomb interaction combined with the minimum-image convention [77]. The reader is referred to Ref. [79] for more details about finite-size effects and different approaches to correct for the related errors.

The full configuration-interaction quantum Monte Carlo (FCIQMC) method [83] is a new approach to the quantum many-body problem, in which the full configuration-interaction (FCI) equations [157, p. 180] are solved approximately using a Monte Carlo technique. Similarly as in the DMC method, the Schrödinger equation is written as a diffusion equation with an imaginary time variable [84]. In the FCI method, the total wave-function ansatz is expressed as a linear combination of Slater determinants constructed from a given single-particle basis [157, p. 178]. In FCIQMC, the coefficients in the expansion of Slater determinants are obtained as the large-time limit of a random walk [84]. As we discussed above, Monte Carlo calculations of the electron gas have an error related to the finite number of particles in the simulation cell [72, 77, 79, 199]. Methods such as FCIQMC, CC, and partial summations derived from many-body perturbation theory have an additional error when studying systems with a discrete single-particle basis: The result depends on the given set of both occupied and unoccupied single-particle states [54]. This error can be corrected for by using, for example, the single-point extrapolation technique [54, 210] introduced by Shepherd *et al.* The FCIQMC method has recently been applied to finite electron-gas systems [54, 84, 210], giving results [84] in close agreement with DMC calculations utilizing backflow correlations [207]. In Section 5.3, we compare our CC calculations for the electron gas with FCIQMC results of Leikanger [85].

Singal and Das [50] were the first to study the electron gas using a CC approach. The approximation they used is similar to the BHF method [67], and does not properly include particle-hole ring diagrams. Later, Freeman did CC calculations [51] in which only ring diagrams and their exchange parts were retained in a CC doubles approximation. The results of both Singal and Das [50] and Freeman [51] compared well with dielectric-function approaches.

Presently, the most accurate CC calculations of the three-dimensional electron gas are those of Bishop and Lührmann [52, 53]. Bishop and Lührmann derived a CC SUB2 approximation (also called CCD) for the electron gas, extended with some ladder contributions from higher-order amplitudes [53]. As the authors describe in Ref. [52], the CCD approximation contains many more diagrammatic classes than partial-summation techniques derived from perturbation theory. The CCD approximation takes account of particle-particle and hole-hole ladders, particle-hole ring diagrams including exchange terms, and many other diagrams to infinite order in perturbation theory (see Refs. [52] and [157, pp. 346–353]). In their CC approximations [53], Bishop and Lührmann replaced summations over hole states by averages. In fact, the nine-dimensional CC amplitudes were simplified to one-dimensional objects, with the absolute value of the transfer momentum being the only variable. The authors showed that the state-average approximation is accurate in the RPA approximation. Bishop and Lührmann neglected some diagrammatic classes, such as the hole-hole ladders and mixed ladders, which they assumed to be small. Despite all these approximations, the final CC correlation energies are very accurate in a typical metallic density range. Relative differences of less than one percent compared to DMC calculations of Ceperley and Alder [211] may indicate that the extended CCD approximation describes most of the relevant correlations in the three-dimensional electron gas [53].

The CC study of Bishop and Lührmann [52, 53] was very successful, but still the calculations are based on a large number of approximations. It would be desirable to apply CC theory to the electron gas without the same simplifications. Recently, Shepherd *et al.* [54–57] have taken up again the CC effort for the three-dimensional electron gas. The CC calculations for the electron gas from the 1970s and 1980s were all done at the thermodynamic limit [50–53]. Shepherd *et al.* approximate the electron gas using finite cubic boxes [54–57]. When using finite-size systems, the CC equations are simpler, and it is possible to study few-particle systems that require less computational power. Instead, one has to deal with errors related to finite particle numbers and single-particle bases, similarly as in the FCIQMC method [54, 84, 210].

Let us finally turn our attention to the two-dimensional electron gas. The two-dimensional electron gas is defined in the same way as the three-dimensional counterpart, and similar approaches can therefore often be used to study both systems. As a first example, the classical derivation of the high-density RPA approximation by Gell-Mann and Brueckner [201] has been extended to the two-dimensional electron gas by Rajagopal and Kimball [212].

As far as we know, the only CC calculations that have been done for the two-dimensional electron gas are the ring [59] and particle-particle ladder [60] approximations of Freeman. Because of stronger correlations in the purely two-dimensional system, the ring approximation was not as reliable in two dimensions as it was in the three-dimensional case [59]. In Figure 1 of Ref. [197], the CC ring and ladder approximations are compared with the GFMC results of Tanatar and Ceperley. The CC ladder energies are similar to those of the DMC method, whereas the CC ring results clearly deviate at intermediate densities [197]. In Section 5.3, we present results for the two-dimensional finite-size electron gas with all correlations of the CCD approximation included.

As we mentioned above, Ceperley studied both two- and three-dimensional systems in the VMC calculations of Ref. [196]. Tanatar and Ceperley did calculations for the two-dimensional electron gas using DMC approximated by the fixed-node technique [197]. After extrapolation to the thermodynamic limit, the DMC correlation energies were close to, but variationally lower than, CC ladder results of Freeman [60], dielectric calculations of Jonson [213], and FHNC energies of Sim *et al.* [214] for scaled average electron-electron distances r_s between one and ten. The CC ring-diagram results of Freeman [59] were found to differ significantly from the DMC energy estimates of Tanatar and Ceperley [197]. The work of Tanatar and Ceperley has been followed by several improved DMC studies [215–219]. The most accurate DMC results for the two-dimensional electron gas were obtained in calculations using backflow-correlation techniques [215, 217–219].

In this chapter, we have defined infinite nuclear matter and the electron gas. We have given motivations for studying these systems, and we have also reviewed some of the research on infinite matter that is relevant for the studies presented in this thesis. In the next chapter, we take a step backward and formulate the infinite-matter problem using quantum many-body theory.

Chapter 3

Microscopic models of fermionic matter

In the previous chapter, we defined both infinite nuclear matter and the electron gas as systems in which the d-dimensional real space $\mathbb{R}^d$ is filled by homogeneously distributed quantum particles. For nuclear matter, we assumed that nucleons are appropriate degrees of freedom in the density range we are going to study. As is well known, nucleons and electrons have spin 1/2 and obey fermionic statistics. Infinite matter is, therefore, as we define it, a system containing an infinite number of interacting fermions. Following our arguments in Chapter 2, we choose to model infinite nuclear matter within nonrelativistic quantum mechanics.

In the present chapter, we formulate the nonrelativistic quantum many-body problem for infinite matter. Furthermore, we define notations that are used in this thesis, and we give a short review of the nuclear interaction.

3.1 A quantum many-particle system

We start by formulating the nonrelativistic many-body problem. Because nuclear matter is the major topic of this thesis, we mostly concentrate on that system. However, the formulation for the electron gas is similar, and details specific to the electron gas are given in Chapter 5. Along the way, we define our notation. For a general introduction to nonrelativistic many-fermion theory, see, for example, Refs. [61, 63, 157, 192].

3.1.1 The Hamiltonian equation

The physics of a general, nonrelativistic, and time-independent quantum mechanical system is described by the Hamiltonian eigenvalue equation

$$\hat{H}|\Psi\rangle = E|\Psi\rangle, \tag{3.1}$$

where $\hat{H}$ is the Hamiltonian operator, $|\Psi\rangle$ is the quantum state vector, and the eigenvalue E is the energy. In infinite nuclear matter, the Hamiltonian operator can be written as [134, p. 21]

$$\hat{H} = \hat{T} + \hat{V}, \tag{3.2}$$

where $\hat{T}$ is the kinetic energy operator and $\hat{V}$ is the interaction operator. As we mentioned in Chapter 2, nucleons are composed of quarks and gluons, and are not point particles (see Refs. [89, p. 4] and [90]). Interactions between three or more nucleons are, therefore, generally nonzero [133]. The total nuclear interaction operator is of the form

$$\hat{V} = \hat{V}_{NN} + \hat{V}_{NNN} + \hat{V}_{NNNN} + \dots \tag{3.3}$$

where $\hat{V}_{NN}$, $\hat{V}_{NNN}$, and $\hat{V}_{NNNN}$ are the two-, three-, and four-body interaction operators, respectively. In particular for finite nuclei, it is a reasonable first approximation to neglect three- and many-body interactions. However, as several recent studies show, inclusion of three-nucleon forces may change the energy by around 10–20 percent, giving final results considerably closer to experimental values [41, 129, 130, 132]. When using a soft two-body interaction for infinite nuclear matter, the contribution from the three-body interaction may be even larger, altering the total energy by up to 50 percent at the experimental saturation density [22, 23, 106]. As the good agreement with experiments for finite nuclei including two- and three-nucleon forces indicate, four- and many-nucleon forces are probably less important than three-body interactions [133]. In our calculations using the BHF and the partial-wave-expanded CC ladder approximation (see Paper II), we neglect three- and many-body interactions.

In coordinate space, the Hamiltonian operator for infinite nuclear matter has the form

$$\hat{H} = -\frac{\hbar^2}{2m}\sum_{i=1}^{A}\nabla_i^2 + \sum_{i<j}^{A}\hat{v}_{NN}(\mathbf{r}_i,\mathbf{r}_j) + \sum_{i<j<k}^{A}\hat{v}_{NNN}(\mathbf{r}_i,\mathbf{r}_j,\mathbf{r}_k) + \dots, \tag{3.4}$$

where A is the total number of nucleons, m is the nucleon mass, $\hbar$ is the reduced Planck constant, and $\mathbf{r}_i$ is the coordinate of nucleon i. The nuclear interaction operators $\hat{v}_{NN}$, $\hat{v}_{NNN}$, etc., are also functions of spin and isospin, which we have neglected for simplicity. The projection of the state vector $|\Psi\rangle$ to the position space depends on A position vectors, that is,

$$\langle \mathbf{r}_1 \dots \mathbf{r}_A|\Psi\rangle = \Psi(\mathbf{r}_1,\dots,\mathbf{r}_A), \tag{3.5}$$

where $\mathbf{r}_i$ is particle i's position vector. Again, we implicitly assume that the total wave function depends on spin and isospin.

In the many-body methods we are going to consider – the hole-line expansion [2, 66] and the coupled-cluster method [61, pp. 251-291] – the A-particle wave function $\Psi(\mathbf{r}_1, \ldots, \mathbf{r}_A)$ is expanded in a basis, that is,

$$\Psi(\mathbf{r}_1, \mathbf{r}_2, \ldots, \mathbf{r}_A) = \sum_m c_m \Phi_m(\mathbf{r}_1, \mathbf{r}_2, \ldots, \mathbf{r}_A), \tag{3.6}$$

where the basis functions Φ_m are Slater determinants

$$\Phi_m(\mathbf{r}_1, \mathbf{r}_2, \ldots, \mathbf{r}_A) = \frac{1}{\sqrt{A!}} \begin{vmatrix} \phi_{\alpha_1^{(m)}}(\mathbf{r}_1) & \phi_{\alpha_2^{(m)}}(\mathbf{r}_1) & \ldots & \phi_{\alpha_A^{(m)}}(\mathbf{r}_1) \\ \phi_{\alpha_1^{(m)}}(\mathbf{r}_2) & \phi_{\alpha_2^{(m)}}(\mathbf{r}_2) & \ldots & \phi_{\alpha_A^{(m)}}(\mathbf{r}_2) \\ \vdots & \vdots & \ddots & \vdots \\ \phi_{\alpha_1^{(m)}}(\mathbf{r}_A) & \phi_{\alpha_2^{(m)}}(\mathbf{r}_A) & \ldots & \phi_{\alpha_A^{(m)}}(\mathbf{r}_A) \end{vmatrix} \tag{3.7}$$

constructed from a chosen single-particle basis $\{\phi_\alpha(\mathbf{r})\}_\alpha$. Here the label α contains spin, isospin, and possibly also other quantum numbers. The structure of the Slater determinants ensures that the total wave function is antisymmetric, which is a requirement for a fermion system.

3.1.2 Second quantization

In the present subsection, we follow the textbook of Shavitt and Bartlett [61, p. 9 and pp. 54–72] when no other references are given.

When working with many-particle quantum systems, it is convenient to utilize the power of the second quantization formalism (see Refs. [192, pp. 3–31], [61, pp. 54–89]). In second quantization, the quantum states belong to the Fock space [220, p. 11], which means that they can be constructed from an arbitrary number of single-particle states. The states are given in occupation representation, in which $|n_1 n_2 \ldots\rangle$ is a state with n_1 particles in the single-particle state 1, n_2 particles in single-particle state 2 and so on. The single-particle states are elements of a chosen basis, and because the system is fermionic, the occupation numbers can only take the values 0 or 1. Below, we use the alternative notation

$$|\alpha_1 \alpha_2 \ldots\rangle \equiv |\ldots n_{\alpha_1} \ldots n_{\alpha_2} \ldots\rangle, \tag{3.8}$$

in which only indices of occupied states are given explicitly.

Let us define the fermion creation and annihilation operators $a_\alpha^\dagger$ and a_α, respectively, such that $a_\alpha^\dagger$ creates a fermion in the state $|\alpha\rangle$ and a_α annihilates a fermion in the same state. When operating on single-particle states, the operators have the properties

$$a_\alpha^\dagger|0\rangle = |\alpha\rangle, \qquad a_\alpha^\dagger|\alpha\rangle = 0 \tag{3.9}$$

and

$$a_\alpha|0\rangle = 0, \qquad a_\alpha|\alpha\rangle = |0\rangle. \tag{3.10}$$

Above, $|0\rangle$ is the physical vacuum state. The fermion creation and annihilation operators obey the anticommutator relations

$$\begin{aligned} &\{a_\alpha^\dagger, a_\beta^\dagger\} = 0, \qquad \{a_\alpha, a_\beta\} = 0, \\ &\{a_\alpha, a_\beta^\dagger\} = \delta_{\alpha,\beta}, \end{aligned} \tag{3.11}$$

where the curly brackets denote anticommutation operators and $\delta_{\alpha,\beta}$ is the Kronecker delta function. The anticommutator relations are necessary for getting antisymmetric many-particle states, as required for fermion systems.

In second quantization, a vector with the single-particle states $\alpha_1, \alpha_2, \ldots, \alpha_A$ occupied is written in terms of creation operators as

$$|\alpha_1\alpha_2\ldots\alpha_A\rangle = a_{\alpha_1}^\dagger \ldots a_{\alpha_A}^\dagger|0\rangle, \tag{3.12}$$

where $|0\rangle$ is the vacuum state. Because the occupation number for fermions is always zero or one, one can label a vector by only those single-particle states that are occupied. A general one-body operator is written as

$$\hat{U} = \sum_{p,q}\langle p|\hat{u}|q\rangle a_p^\dagger a_q \tag{3.13}$$

and a two-body operator as

$$\hat{W} = \frac{1}{4}\sum_{p,q,r,s}\langle pq|\hat{w}|rs\rangle_{AS} a_p^\dagger a_q^\dagger a_s a_r, \tag{3.14}$$

where the brackets are inner products and the summations are taken over all single-particle states. In Eq. (3.14) we have used the definition

$$\langle pq|\hat{w}|rs\rangle_{AS} \equiv \langle pq|\hat{w}|rs\rangle - \langle pq|\hat{w}|sr\rangle \tag{3.15}$$

to denote an antisymmetrized interaction matrix element.

Let the reference state $|\Phi_0\rangle$ be constructed of A single-particle states chosen from a given basis. As is common in quantum chemistry (see Refs. [221], [222, pp. 685–697], and [61, p. 72]), we denote states occupied in the reference state by $i, j, k, \ldots$, states not occupied in $|\Phi_0\rangle$ by $a, b, c, \ldots$, whereas indices $p, q, r, \ldots$ are used for arbitrary single-particle states in the given basis. Using creation operators, the reference state is

$$|\Phi_0\rangle = a_{i_1}^\dagger a_{i_2}^\dagger \ldots a_{i_A}^\dagger|0\rangle, \tag{3.16}$$

where $|0\rangle$ is the physical vacuum state. Let us further define states of the form

$$|\Phi_{ij\ldots}^{ab\ldots}\rangle = a_a^\dagger a_b^\dagger \ldots a_j a_i |\Phi_0\rangle \tag{3.17}$$

as particle-hole excitations of the reference state. In a space spanned by the given single-particle basis, the total state vector may be written as

$$|\Psi\rangle = |\Phi_0\rangle + \sum_{ia} c_i^a |\Phi_i^a\rangle + \sum_{ijab} c_{ij}^{ab} |\Phi_{ij}^{ab}\rangle + \ldots, \tag{3.18}$$

where we have assumed the intermediate norm $\langle\Psi|\Phi_0\rangle = 1$. This expansion can be truncated after a finite number of terms, and the coefficients are typically found using a numerical method [61, p. 9 and pp. 54–72].

3.1.3 Momentum single-particle basis

Later, we study infinite-matter systems in two and three dimensions. Similarly as explained by, for example, Fetter and Walecka [192, p. 21] and Giuliani and Vignale [49, p. 13], we use d-dimensional hypercubic potential wells to model infinite-matter systems. Figure 3.1 illustrates hypercubes in one, two, and three dimensions. Let us define the single-particle basis following Refs. [192, p. 21] and [49, pp. 27–29]. The external potential is assumed to be zero inside the hypercube, and infinitely large outside the box. In coordinate representation, the Schrödinger equation of a single nucleon inside a hypercube is

$$-\frac{\hbar^2}{2m}\nabla^2\phi(\mathbf{x}) = \varepsilon\phi(\mathbf{x}), \tag{3.19}$$

provided that spin and isospin are neglected. Here $\phi(\mathbf{x})$ is the orbital part of the single-particle wave function, ε is the single-particle energy, $\mathbf{x}$ is a d-dimensional position vector $\mathbf{x} \equiv (x_1, \ldots, x_d)$, m is the nucleon mass, and $\hbar$ is the reduced Planck constant. The single-particle Schrödinger equation has solutions of the form

$$\phi_{\mathbf{k}}(\mathbf{x}) = \frac{1}{L^{d/2}} e^{i\mathbf{k}\cdot\mathbf{x}}, \tag{3.20}$$

where $|\mathbf{k}| = \sqrt{2m\varepsilon/\hbar^2}$. Continuing the approach as outlined by Fetter and Walecka [192, p. 21], we use periodic boundary conditions

$$\begin{aligned} \phi_{\mathbf{k}}(x_1 + L, \ldots, x_d) &= \phi_{\mathbf{k}}(x_1, \ldots, x_d), \\ &\vdots \\ \phi_{\mathbf{k}}(x_1, \ldots, x_d + L) &= \phi_{\mathbf{k}}(x_1, \ldots, x_d + L), \end{aligned} \tag{3.21}$$

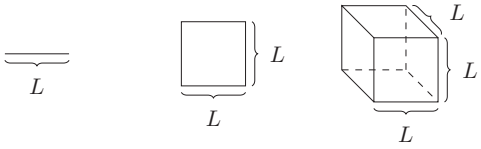

Figure 3.1: Infinite-matter systems may be modeled using hypercubes in one, two and three dimensions [49, p. 13].

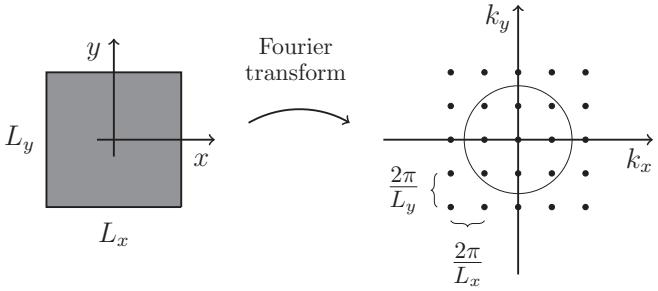

Figure 3.2: Fourier transform in two dimensions. The finite, continuous, and rectangular region in coordinate space is mapped to a set of infinitely many discrete points in momentum space (Fourier space). The finite size of the coordinate space domain gives a finite distance between points in momentum space [192, p. 21]. The number of Fourier grid points inside the Fermi sea, denoted by a circle, is by definition the same as the number of particles in the physical box.

which give the conditions

$$k_i = \frac{2\pi}{L} n_i, \qquad n_i = 0, \pm 1, \pm 2, \ldots \tag{3.22}$$

for the component i of the wave vector $\mathbf{k}$. A general single-particle state represents a set of quantum numbers $(n_1, \ldots, n_d)$ (Refs. [192, p. 21] and [49, pp. 27–29]).

Single-particle states in fermionic matter have a spin projection m_s, and for nuclear matter also an isospin projection m_t. In nuclear matter, we write a single-particle state vector as

$$|\mathbf{k}_n m_s m_t\rangle = |n_1 \ldots n_d m_s m_t\rangle, \tag{3.23}$$

where the quantum numbers n_i are as defined in Eq. (3.22). We choose to label neutrons by $m_t = +\frac{1}{2}$ and protons by $m_t = -\frac{1}{2}$. In the electron gas, there is no isospin dependency, but otherwise the single-particle states are equal to those in nuclear matter.

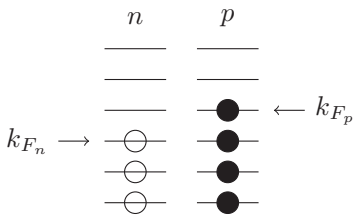

Figure 3.3: The Fermi momentum for neutrons, k_{F_n}, is defined as the momentum of the highest-lying occupied neutron state. Similarly, the Fermi momentum for protons, k_{F_p} is defined as the momentum of the highest-lying occupied proton state. In other words, the proton and neutron Fermi levels, k_{F_n} and k_{F_p}, determine together the ratio of the two nucleon types in the considered system [223].

Following Fetter and Walecka [192, p. 21], we construct infinite-matter systems by filling hypercubes with interacting nucleons, as shown for two dimensions at the left in Figure 3.2. Infinite matter is obtained in the limit when the box length L and the number of particles A approach infinity, whereas the particle density $\rho \equiv A/L^2$ is kept constant [192, p. 21]. Expressions in the momentum basis may be considered as Fourier transforms of corresponding coordinate-space equations. Figure 3.2 shows how a finite number of particles in the continuous coordinate space is transformed to an infinite number of discrete points in the Fourier space. As is apparent from Eq. (3.22), the spacing between points in Fourier space is inversely related to the hypercube side. In Fourier space, the physical particles may be represented by all momentum points inside the Fermi sphere.

Let us neglect spin and isospin degrees of freedom and write the reference state as

$$|\Phi_0\rangle = a^\dagger_{\mathbf{k}_1} a^\dagger_{\mathbf{k}_2} \dots a^\dagger_{\mathbf{k}_A} |0\rangle, \tag{3.24}$$

where each particle $i \in \{1, 2, \dots, A\}$ has a unique momentum vector $\mathbf{k}_i$. Assume that the reference state is occupied by the A single-particle states with the lowest single-particle energies

$$\varepsilon_{\mathbf{k}} = \frac{\hbar^2 k^2}{2m}, \tag{3.25}$$

where $k \equiv |\mathbf{k}|$ is the length of the momentum vector. Then the Fermi momentum k_F is defined as the momentum $|\mathbf{k}|$ of the highest-lying occupied state. As illustrated in Figure 3.3, in nuclear matter the Fermi momentum is defined separately for protons and neutrons. In a calculation, the proton-neutron ratio can be controlled by adjusting the neutron and proton Fermi momenta k_{F_n} and k_{F_p} [223]. Symmetric nuclear matter

is obtained by choosing the same Fermi level for both protons and neutrons, whereas in pure neutron matter the proton Fermi momentum k_{F_p} is set to zero.

Assuming that the d-dimensional hypercube with side length L is filled by A fermions, the particle density becomes

$$\rho \equiv \frac{A}{L^d} = \frac{1}{L^d} \sum_{m_s m_t} \sum_{|\mathbf{k}| \leq k_F(m_t)} , \tag{3.26}$$

where the Fermi momentum k_F may be dependent on the isospin projection. The summation is taken over all occupied single-particle states, restricted by Eq. (3.22) and a Fermi momentum.

3.1.4 Other single-particle bases

In the expressions for infinite matter arising in many-body perturbation theory and coupled-cluster theory, there are summations over single-particle momenta $\mathbf{k}_p$ (see Chapters 4 and 5). In the limit when the box side of the hypercube L approaches infinity, a sum over discrete Fourier states $\mathbf{k}_p$ can be approximated by an integral according to

$$\sum_{\mathbf{k}_p} \longrightarrow \left(\frac{L}{2\pi}\right)^d \int d\mathbf{k}_p, \tag{3.27}$$

where the integration is over the d-dimensional space spanned by the Fourier states. In the energy expressions, the summations are often taken over only particle or hole states. At the thermodynamic limit, a sum over two different hole states, i and j, is replaced by two integrals, as in Eq. (3.27). The restriction to only occupied states is ensured by a hole-hole Pauli exclusion operator

$$Q_{hh}(|\mathbf{k}_i|, |\mathbf{k}_j|, k_F) \equiv \theta(k_F - |\mathbf{k}_i|)\theta(k_F - |\mathbf{k}_j|), \tag{3.28}$$

where $\theta(x)$ is the Heaviside step function. Similarly, a sum over two particle states, a and b, is transformed to two d-dimensional integrals with a particle-particle Pauli exclusion operator

$$Q_{pp}(|\mathbf{k}_a|, |\mathbf{k}_b|, k_F) \equiv \theta(|\mathbf{k}_a| - k_F)\theta(|\mathbf{k}_b| - k_F), \tag{3.29}$$

which ensures that the integration is taken over only unoccupied states. As before, k_F denotes the Fermi momentum.

The coordinates of two particles, $\mathbf{x}_p$ and $\mathbf{x}_q$, may be expressed in terms of a relative vector, $\mathbf{x}$, and a center-of-mass (CM) vector, $\mathbf{X}$, such that

$$\mathbf{x} = \mathbf{x}_p - \mathbf{x}_q, \qquad \mathbf{X} = (\mathbf{x}_p + \mathbf{x}_q)/2. \tag{3.30}$$

Assuming that the reduced Planck constant $\hbar = 1$, the momentum $\mathbf{p} \equiv \hbar\mathbf{k}$ is equal to the wave vector $\mathbf{k}$. Provided that the two particles have equal mass m, the reduced mass is $m_r = \frac{1}{2}m$ and the total mass $M = 2m$. Using the definitions in Eq. (3.30), the relative and CM momentum vectors, $\mathbf{k}$ and $\mathbf{K}$, become

$$\mathbf{k} = (\mathbf{k}_p - \mathbf{k}_q)/2, \qquad \mathbf{K} = \mathbf{k}_p + \mathbf{k}_q, \tag{3.31}$$

where $\mathbf{k}_p$ and $\mathbf{k}_q$ are the momenta of particles p and q in laboratory coordinates.

In relative and center-of-mass (RCM) coordinates, the hole-hole Pauli exclusion operator becomes

$$Q_{hh}(\mathbf{k}, \mathbf{K}, k_F) = \theta(k_F - |\mathbf{k} + \mathbf{K}/2|)\theta(k_F - |-\mathbf{k} + \mathbf{K}/2|) \tag{3.32}$$

and the particle-particle Pauli exclusion operator

$$Q_{pp}(\mathbf{k}, \mathbf{K}, k_F) = \theta(|\mathbf{k} + \mathbf{K}/2| - k_F)\theta(|-\mathbf{k} + \mathbf{K}/2| - k_F). \tag{3.33}$$

Observe that in RCM coordinates, the Pauli operators are dependent on the radial coordinates of both the relative and the CM momentum vectors, as well as on the angle between these two vectors.

Methods derived from MBPT [64, 67, 224] and SCGF [225, pp. 70–72] approaches are often implemented in a partial-wave basis with relative momenta. The basis commonly used is of the form

$$|k\mathcal{J}m_{\mathcal{J}}(lS)m_{t_1}m_{t_2}\rangle, \tag{3.34}$$

where $k \equiv |\mathbf{k}|$ is the length of a relative momentum vector $\mathbf{k}$, l is the relative orbital angular momentum related to $\mathbf{k}$, S is the total two-particle spin, $\mathcal{J}$ is equal to the total relative angular momentum $l+S$, $m_{\mathcal{J}}$ is the z projection of $\mathcal{J}$, and m_{t_1} and m_{t_2} label the nucleon types of particles 1 and 2, respectively. If charge independence breaking and charge symmetry breaking are neglected, m_{t_1} and m_{t_2} can be replaced by a coupled isospin T with the projection M_T. Charge symmetry and charge independence are defined in, for example, Refs. [16] and [226, pp. 119–121].

When transforming from an RCM basis $|\mathbf{k}\mathbf{K}m_{s_1}m_{t_1}m_{s_2}m_{t_2}\rangle$ to the basis of Eq. (3.34), we need the completeness relations

$$\sum_{lm_l} |lm_l\rangle\langle lm_l| = \hat{\mathbb{1}}, \tag{3.35}$$

$$\sum_{SM_S} |SM_S\rangle\langle SM_S| = \hat{\mathbb{1}}, \tag{3.36}$$

where m_l and M_S are z projections of l and S, respectively, and $\hat{\mathbb{1}}$ is the unity operator. Furthermore, we need the equalities

$$\langle \hat{\mathbf{k}} | l m_l \rangle \equiv Y_{lm_l}(\hat{\mathbf{k}}), \tag{3.37}$$

$$\int d\hat{\mathbf{k}} Y^*_{lm_l}(\hat{\mathbf{k}}) Y_{l'm_{l'}}(\hat{\mathbf{k}}) = \delta_{ll'}\delta_{m_l m_{l'}}, \tag{3.38}$$

$$Y_{lm_l}(\pi - \theta_{\mathbf{k}}, \phi_{\mathbf{k}} + \pi) = (-1)^l Y_{lm_l}(\theta_{\mathbf{k}}, \phi_{\mathbf{k}}), \tag{3.39}$$

where $\hat{\mathbf{k}} = (\theta_{\mathbf{k}}, \phi_{\mathbf{k}})$ is the angular vector of the relative momentum $\mathbf{k}$, $Y_{lm_l}(\hat{\mathbf{k}})$ is the spherical harmonics function, and δ_{pq} is the Kronecker delta function. The angular momenta are coupled and decoupled according to

$$|\mathcal{J} m_{\mathcal{J}} l S\rangle = \sum_{m_l M_S} \langle l m_l S M_S | \mathcal{J} m_{\mathcal{J}} l S \rangle | l m_l S M_S \rangle, \tag{3.40}$$

$$|l m_l S M_S\rangle = \sum_{\mathcal{J} m_{\mathcal{J}}} \langle \mathcal{J} m_{\mathcal{J}} l S | l m_l S M_S \rangle | \mathcal{J} m_{\mathcal{J}} l S \rangle, \tag{3.41}$$

where the brackets denote Clebsch-Gordan coefficients. We also need the property

$$\langle j_p m_p j_q m_q | J M_J \rangle = (-1)^{j_p + j_q - J} \langle j_q m_q j_p m_p | J M_J \rangle \tag{3.42}$$

of Clebsch-Gordan coefficients. The relations (3.38) – (3.42) and other useful angular momentum relations are given in, for example, the text of Varshalovich *et al.* [227, pp. 131,141,236, and 245].

Sometimes we denote coupling of angular momenta using square brackets. Following Lawson [228, p. 15], we define

$$\left[Y_{l_p m_{l_p}}(\hat{\mathbf{k}}_p) Y_{l_q m_{l_q}}(\hat{\mathbf{k}}_q) \right]_{\lambda m_\lambda} \equiv \sum_{m_{l_p} m_{l_q}} \langle l_p m_{l_p} l_q m_{l_q} | \lambda m_\lambda \rangle Y_{l_p m_{l_p}}(\hat{\mathbf{k}}_p) Y_{l_q m_{l_q}}(\hat{\mathbf{k}}_q), \tag{3.43}$$

where two spherical-harmonics functions associated with with the orbital angular momenta $(l_p m_{l_p})$ and $(l_q m_{l_q})$ have been coupled to a state with the total orbital angular momentum (λm_λ). In an abstract vector space, Eq. (3.43) becomes

$$|\lambda m_\lambda l_p l_q\rangle = \sum_{m_{l_p} m_{l_q}} \langle l_p m_{l_p} l_q m_{l_q} | \lambda m_\lambda l_p l_q \rangle | l_p m_{l_p} l_q m_{l_q} \rangle, \tag{3.44}$$

similarly as in Eq. (3.40).

3.1.5 Interaction matrix elements

Next, we derive a transformation between relative and center-of-mass (RCM) and laboratory coordinates for the two-body interaction, generalizing the approach of Fetter and Walecka [192, p. 23] to d dimensions. Interaction matrix elements are defined as

$$\langle pq | \hat{v} | rs \rangle = \int d\mathbf{x}_1 \int d\mathbf{x}_2 \phi^*_p(\mathbf{x}_1) \phi^*_q(\mathbf{x}_2) v(\mathbf{x}_1, \mathbf{x}_2) \phi_r(\mathbf{x}_1) \phi_s(\mathbf{x}_2), \tag{3.45}$$

where $v(\mathbf{x}_1, \mathbf{x}_2)$ is the two-body interaction expressed in coordinate space, $\phi_m(\mathbf{x})$ is the coordinate-space projection of the single-particle state $|m\rangle$, and a star denotes the complex conjugate. If we take the single-particle states to be eigenfunctions of a finite hypercube with side length L, that is, plane waves as in Eq. (3.20), the matrix elements become

$$\begin{aligned}\langle \mathbf{k}_p\mathbf{k}_q|\hat{v}|\mathbf{k}_r\mathbf{k}_s\rangle &= \int d\mathbf{x}_1 \int d\mathbf{x}_2 \phi^*_{\mathbf{k}_p}(\mathbf{x}_1)\phi^*_{\mathbf{k}_q}(\mathbf{x}_2)v(\mathbf{x}_1,\mathbf{x}_2)\phi_{\mathbf{k}_r}(\mathbf{x}_1)\phi_{\mathbf{k}_s}(\mathbf{x}_2) \\ &= \frac{1}{L^{2d}} \int d\mathbf{x}_1 \int d\mathbf{x}_2 e^{-i\mathbf{k}_p\cdot\mathbf{x}_1} e^{-i\mathbf{k}_q\cdot\mathbf{x}_2} v(\mathbf{x}_1,\mathbf{x}_2) e^{i\mathbf{k}_r\cdot\mathbf{x}_1} e^{i\mathbf{k}_s\cdot\mathbf{x}_2}. \end{aligned} \tag{3.46}$$

If we use the definitions (3.31), and do the change of integration variables

$$\mathbf{r} = \mathbf{x}_1 - \mathbf{x}_2, \qquad \mathbf{R} = (\mathbf{x}_1 + \mathbf{x}_2)/2, \tag{3.47}$$

where $\mathbf{r}$ and $\mathbf{R}$ are relative and center-of-mass coordinates, respectively, we get the matrix element into the form

$$\langle \mathbf{k}_p\mathbf{k}_q|\hat{v}|\mathbf{k}_r\mathbf{k}_s\rangle = \underbrace{\left[\frac{1}{L^d}\int d\mathbf{r} e^{-i(\mathbf{k}-\mathbf{k}')\cdot\mathbf{r}} v(\mathbf{r})\right]}_{\equiv\langle \mathbf{k}|\hat{v}|\mathbf{k}'\rangle} \delta_{\mathbf{K},\mathbf{K}'}. \tag{3.48}$$

Here we have assumed that the interaction is invariant under translations, which means that the interaction depends only on the distance $\mathbf{r} = \mathbf{x}_1 - \mathbf{x}_2$, and not on the specific positions of the two particles. We have also used the definition

$$\delta_{\mathbf{K},\mathbf{K}'} = \frac{1}{L^d}\int_\Omega d\mathbf{R} e^{i(\mathbf{K}-\mathbf{K}')\cdot\mathbf{R}} \tag{3.49}$$

of the d-dimensional Kronecker delta function, where the integration is over the d-dimensional hypercube [192, p. 23].

3.2 The nuclear interaction

More than hundred years after the atomic nucleus was discovered by Rutherford [229], an exact theoretical description of the nuclear force is still lacking. Baryons, such as nucleons and hyperons, are composed of strongly interacting quarks and gluons, and a model for the interaction between baryons should therefore be derived directly from QCD. Nonperturbative QCD problems, such as systems consisting of nucleons, can be solved using lattice QCD, and, for example, Ishii *et al.* have derived simple nuclear potentials [230, 231] using such stochastic calculations. Lattice QCD calculations involving baryons are computationally expensive, and due to limitations in computing

time, the calculations are done with unphysically large quark masses [150, 230]. Since realistic nuclear interaction models cannot be derived directly from QCD, we need other effective approaches to obtain more accurate potentials.

Due to the internal structure of nucleons, nuclear Hamiltonians contain two-nucleon, three-nucleon, and many-nucleon interactions (for a modern review, see, for example, Ref. [133]). However, as we discussed in the text following Eq. (3.3), in finite nuclei approximations neglecting three- and other many-body interactions give reasonable first estimates of, for example, the binding energy [41, 129, 130, 132]. In infinite nuclear matter, the three-nucleon force may have a larger impact on the total energy, but generally the two-body part gives the largest contribution to the potential energy [21–23, 45, 106]. Let us, therefore, start with the nucleon-nucleon force.

3.2.1 Background

Interactions between nucleons can be studied in, for example, elastic scattering experiments [232]. As explained by Brown and Jackson [193, pp. 1–18], the nuclear interaction is known to have a range of only a few fermi. In the region between 1 fm and 2 fm it is attractive, and at distances comparable to the nucleon size, the force becomes strongly repulsive [92, pp. 109–111] (see Figure 3.4). On a very general level, the nucleon-nucleon interaction obeys certain symmetries, such as conservation of the center of mass and total momentum, rotational and time-reversal symmetry, and conservation of parity. The nucleon-nucleon force has a rich operator structure, the most important terms being a central, a spin-orbit, and a tensor-force part. The reader is referred to Refs. [92, pp. 65–116] and [233, pp. 147–156] for a more thorough introduction to basic properties of the nuclear force. Let us instead turn our attention to the development of nuclear interaction models.

Machleidt gives a historical review [234] from the first decades of nuclear interaction models, starting with the discovery of the atomic nucleus in 1911 and continuing until the year 1989. Here we very briefly sketch this development following Ref. [234]. At an early stage, in 1935, Yukawa proposed [236] a theoretical model in which mesons are mediator particles for the nuclear force. It soon became an established fact that the long-range part of the nuclear interaction is accurately described by one-pion exchange. As Machleidt outlines, it was much less straightforward to obtain successful models for the intermediate- and short-range parts. Various more or less phenomenological approaches were investigated, including approaches with two- and multi-pion exchange as well as one-boson exchange models. In the latter models, two- and multi-pion exchange terms are replaced by heavy single-boson mediator particles, such as the ω,

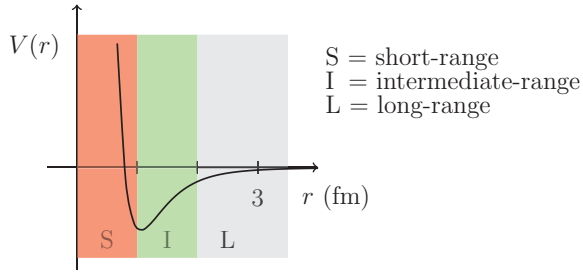

Figure 3.4: The nucleon-nucleon interaction consists of a strongly repulsive short-range part ($r \leq 1$ fm), an attractive intermediate-range part (1 fm $< r <$ 2 fm), and a rapidly vanishing long-range part ($r \geq 2$ fm) [92, pp. 109–111]. Theoretically, each of these regions corresponds to different types of contributions. For example, the long-range part is known to be dominated by one-pion exchange [234]. A similar figure is shown in, for example, Refs. [193, p. 7], [235, p. 11], and [92, p. 111].

ρ, and σ mesons. While the ω and ρ particles were detected early, still in 2013 a sufficiently light σ meson had not been found [237] in experiments. Besides the efforts in quantum field theory, dispersion theory was also used to derive nuclear interactions [234].

In the early 1990s, a group at University of Nijmegen collected a large amount of data from nucleon-nucleon (NN) scattering experiments [232]. The Nijmegen data basis, and in some cases also more recent data, were used to parametrize several very accurate NN potentials. These potentials, named Nijm I, Nijm II, Reid93 [238], Argonne v_{18} [239], and CD-Bonn [240], are fitted to the experimental data with a χ^2 per datum close to one. Machleidt and Slaus compare [14] these interaction models with each other. In all of these modern potentials, the long-range part is described by one-pion exchange, whereas the intermediate- and short-range parts are treated differently. The CD-Bonn potential has a nonlocal one-pion-exchange contribution, whereas the other interactions use local approximations for this part [14]. In Ref. [240] it is shown that the nonlocality gives triton and α-particle binding energies closer to experiments. The short- and intermediate-range parts of the CD-Bonn, Nijm I, and Nijm II potentials are based on the one-boson-exchange model, whereas in the Reid93 and Argonne v_{18} potentials this part is treated phenomenologically. These modern NN potentials are all charge dependent, but the approximations are different [14].

Recently, different variations of the Urbana three-nucleon force [11–13] have been used in nuclear matter studies [21, 185]. In the Urbana three-body interaction, an attractive two-pion exchange part is combined with a repulsive phenomenological term

[11, 21]. According to Epelbaum *et al.* [15], the Urbana three-nucleon force has the disadvantage that it is not consistent with any two-body forces. In 1989, Grangé *et al.* constructed a three-body interaction [241] that was consistent with the Paris two-body potential [242], which is constructed using dispersion theory [243]. During the last decade, nuclear interactions derived from chiral perturbation theory [15, 16, 244] have become increasingly popular. Chiral perturbation theory gives, in a natural way, two- and many-nucleon forces as terms of the same perturbative expansion [16]. In our studies, we have used nuclear interaction models derived from chiral perturbation theory mostly, and we, therefore, devote the next subsection to chiral interactions.

3.2.2 Chiral perturbation theory

Machleidt and Entem [16] and Epelbaum [245] have written pedagogical introductions to chiral perturbation theory for nuclear forces. In the current subsection, we follow these texts when not referring explicitly to other works. Chiral effective field theory has also been reviewed in, for example, Refs. [15, 244].

When dealing with energy scales typical in atomic nuclei, it is computationally more reasonable to work with nucleons and pions than with quarks and gluons. In chiral perturbation theory, as described in Refs. [16, 245], nucleons and pions are considered as particles in an effective field theory. If the quark masses were zero, right- and left-handed quark fields would be independent in QCD. In nuclear systems, the quark masses are relatively small but nonzero. This results in coupling of right- and left-handed fields, and consequently the chiral symmetry is broken. The broken chiral symmetry gives pions with nonzero masses as Goldstone bosons in the effective field theory where nucleons interact, and, therefore, the Lagrangian can be expanded perturbatively in terms of the pion mass.

To limit the number of terms, the diagrams are ordered using a perturbative smallness parameter Q/Λ_χ, where Q is the pion mass or a comparable momentum and Λ_χ is a fixed number, which is chosen to be approximately 1 GeV. Chiral perturbation theory results in so-called contact terms for the short-range part of the interaction, as well as one-pion, two-pion, and multi-pion exchange terms. According to Machleidt and Entem [16], the contact terms are used for renormalization purposes as well as to model heavy mesons, which are not included explicitly in the theory. When using an order parameter as defined in Refs. [16, 245], the lowest-order (LO) contribution contains contact terms and one-pion exchange, whereas two-pion exchange occurs at next-to-lowest order (NLO). Chiral perturbation theory has the advantage that three-, four-, and up to A-body interactions are introduced at increasingly higher orders of

perturbation theory. Therefore, at next-to-next-to-lowest order (NNLO), for example, only two- and three-body forces are present. If the chiral expansion converges order by order, the total contribution from next-to-next-to-next-to-lowest order (N^3LO), which contains four-body interactions for the first time, should be smaller than that from NNLO [16, 133].

To avoid singularities in the Lippmann-Schwinger equation, chiral interactions are regularized. One can define the regulator in different ways. Typically, the reguator is dependent on a cutoff parameter that has to be chosen appropriately. Ideally, the nuclear interaction should be independent on the particular form and chosen cutoff of the regulator. However, as we report in Paper III, for example, the results of a many-body calculation may depend strongly on regulator properties.

In some of our nuclear matter calculations, we have used the chiral nucleon-nucleon interaction of Entem and Machleidt [246], which contains all two-body contributions to N^3LO. Epelbaum, Glöckle, and Meißner have later developed another chiral two-nucleon interaction [247], which, among other, uses different regularization schemes than the interaction of Entem and Machleidt. In Paper I, we present an NNLO chiral interaction that is parametrized with respect to phase shifts using a new, efficient optimization tool. We have used this two-body interaction, called $NNLO_{opt}$, in Papers I–III, and we, therefore, say a few words about the optimization procedure in the next subsection.

3.2.3 Optimized interaction model

Nuclear interactions derived from chiral perturbation theory are dependent on a number of so-called low-energy constants. These parameters can be fitted to reproduce phase shifts that have been determined using experimental data [16]. When using the optimization algorithm called Practical Optimization Using No Derivatives (for Squares) (POUNDERS) [248, 249], Ekström *et al.* obtained better agreement with experimentally extracted phase shifts compared to previous parametrizations (see Paper I). As is explained in Paper I, the parameters of the $NNLO_{opt}$ two-body interaction were obtained by comparing phase shifts calculated with the new interaction with the experimentally extracted phase shifts of the Nijmegen group [232]. The POUNDERS optimization algorithm is described in Refs. [248, 249]. This algorithm is designed to do least-squares optimizations without calculating derivatives [249]. According to Kortelainen *et al.* [248], the POUNDERS algorithm is a quasi-Newton method in which the derivatives in the second-order Taylor expansion are replaced by parametrized functions. The approximative second-order Taylor polynomial is parametrized so that it

gives exact values at certain known data points [248]. The POUNDERS algorithm is a so-called trust-region method [250]. Roughly, this means that at each step, the optimization parameter space is restricted to trust regions defined around the previous values of the optimization parameters [248, 249]. According to Ref. [250, pp. 173–174], trust regions are used among other to get a faster optimization method.

3.2.4 The Minnesota potential

In Paper III, we compare different coupled-cluster approximations with the auxiliary-field diffusion Monte Carlo method using the simple phenomenological Minnesota potential [74]. This potential has the form

$$\begin{aligned} v(r) = &\left(v_R + \left(1 + P_{12}^{\sigma}\right) v_T/2 + \left(1 - P_{12}^{\sigma}\right) v_S/2\right) \\ &\times \left(\alpha + (2 - \alpha)\, P_{12}^{r}\right)/2 + (1 + m_{t,1})\,(1 + m_{t,2})\,\frac{e^2}{4r}, \end{aligned} \tag{3.50}$$

where $r = |\mathbf{r}_1 - \mathbf{r}_2|$ is the distance between particles 1 and 2, $m_{t,1}$ and $m_{t,2}$ are isospin projections (± 1) of the two particles, and P_{12}^{σ} and P_{12}^{r} are exchange operators for spin and position, respectively. In Eq. (3.50), we have used the definitions

$$v_R = v_{0R} e^{-k_R r^2}, \qquad v_T = -v_{0T} e^{-k_T r^2}, \qquad v_S = -v_{0S} e^{-k_S r^2}, \tag{3.51}$$

where the constants v_{0R}, v_{0T}, v_{0S}, k_R, k_T, and k_S are as given in Ref. [74]. In our calculations, we have chosen the parameter α to be one. Then the potential for pure neutron matter can be written as

$$v(r) = \begin{cases} v_{0R} e^{-k_R r^2} - v_{0S} e^{-k_S r^2}, & \text{if } S = 0, \\ v_{0R} e^{-k_R r^2} - v_{0T} e^{-k_T r^2}, & \text{if } S = 1, \end{cases} \tag{3.52}$$

where S is the total two-particle spin. In this special case, the Minnesota potential is a function of only the total spin and the interparticle distance.

We have now formulated the infinite nuclear matter problem in terms of nonrelativistic many-fermion quantum mechanics. Some useful definitions have been given, and we have discussed the nuclear interactions we use in Papers I–III. The emphasis of this thesis is on many-body methods for the infinite-matter problem. In particular, we apply CC theory to infinite nuclear matter and the electron gas. We use the more familiar BHF method to verify our nuclear matter calculations, and to put the theory in perspective. There are also other similar many-body methods that could equally well have been used for benchmarking, such as, for example, the self-consistent Green's function theory [62] and the model-space ring approximation [165]. In the next chapter, we present many-body perturbation theory and the BHF approximation.

Chapter 4

The Brueckner-Hartree-Fock approximation for nuclear matter

Being the lowest-order approximation of both Brueckner-Goldstone theory and the hole-line approximation [2, 66], the Brueckner-Hartree-Fock (BHF) approximation [2, 7, 8, 65, 66, 138, 139] is one of the standard many-body methods for infinite nuclear matter studies. In Paper II, we have derived a CC ladder approximation in a partial-wave basis using exact Pauli exclusion operators. As we show in the paper, the CC ladder approximation is closely related to the BHF method. Because of the similarity between the two methods, we have chosen to use the BHF approximation as a benchmark. In the work with Paper II, we have used a modification of the BHF method to verify important parts of our CC ladder implementations. In Paper II, we have also compared CC and BHF results.

One can derive the BHF method as a partial summation to infinite order of ladder diagrams given by many-body perturbation theory (see Refs. [66] and [157, p. 273–276]). When deriving the BHF approximation in this way, the starting point is Rayleigh–Schrödinger perturbation theory (RSPT) [61, p. 18–45]. In this chapter, we discuss the basic principles of RSPT and the BHF approximation. Furthermore, we show how we have implemented the BHF method and the lowest orders of perturbation theory for nuclear matter systems. Apart from minor details related to the practical implementations, most of the material presented in this chapter is based on well-known theory.

4.1 Many-body perturbation theory

Rayleigh–Schrödinger perturbation theory [61, p. 18–46] is one of the standard many-body methods for nonrelativistic quantum systems. RSPT has the advantage that it is

size-extensive [61, pp. 46–46 and 165–176], which means, using the wording of Shavitt and Bartlett [61, p. 11], that "the energy of a system computed with this model scales correctly with the size of the system". Shavitt and Bartlett [61, pp. 11–17] explain the concept of size-extensivity, and show that RSPT is size-extensive for a special system with equal, noninteracting atoms.

Unfortunately, the strong short-range interaction between nucleons makes nuclear systems nonperturbative, and generally it is necessary to renormalize the interaction before doing perturbative many-body calculations [251]. Brueckner-Goldstone theory and the hole-line approximation [2, 66] are approaches related to RSPT in which the interaction has been replaced by a so-called G matrix. The G matrix is obtained by summing to infinite order in perturbation theory certain correlation contributions that are important for short-range correlations [251]. In the following, we derive the BHF method, which is the lowest-order approximation of the hole-line expansion [66], as a partial summation of diagrams in perturbation theory. In particular, we start with the RSPT formulation of many-body perturbation theory.

We follow Shavitt and Bartlett [61, pp. 18–153] when introducing many-body perturbation theory (MBPT). For the interested reader, the textbook of Harris, Monkhorst, and Freeman [157] also gives a thorough introduction to MBPT. If there is no external potential, the physics of a time-independent nuclear system is determined by a Hamiltonian operator

$$\hat{H} = \hat{T} + \hat{V}, \tag{4.1}$$

where $\hat{T}$ is the kinetic energy operator and $\hat{V}$ is the interaction operator. The Hamiltonian operator $\hat{H}$ can be regrouped into a noninteracting part $\hat{H}_0$ and a perturbation operator $\hat{H}_I$, that is,

$$\hat{H} = \hat{H}_0 + \hat{H}_I, \tag{4.2}$$

where

$$\hat{H}_0 = \hat{T} + \hat{U}, \tag{4.3}$$

$$\hat{H}_I = \hat{V} - \hat{U}. \tag{4.4}$$

Here $\hat{U}$ is an arbitrary single-particle potential operator that preferably is chosen to be such that the contribution of the perturbation $\hat{H}_I$ is as small as possible.

Let the state $|\Psi\rangle$ be the eigenvector of the total Hamiltonian $\hat{H}$ corresponding to the lowest eigenvalue, that is,

$$\hat{H}|\Psi\rangle = E|\Psi\rangle, \tag{4.5}$$

and let $|\Phi_0\rangle$ be the eigenvector of the noninteracting part $\hat{H}_0$ corresponding to the lowest eigenvalue, that is,

$$\hat{H}_0|\Phi_0\rangle = E_0|\Phi_0\rangle. \tag{4.6}$$

Here E and E_0 are the ground state total and noninteracting energy, respectively. In the following, we assume that the ground state is nondegenerate. We define further the operators $\hat{P}$ and $\hat{Q}$ such that

$$\hat{P}|\Psi\rangle = |\Phi_0\rangle \tag{4.7}$$

and $\hat{P} + \hat{Q} = \hat{I}$, where $\hat{I}$ is the unity operator.

As Shavitt and Bartlett show [61, pp. 29–33], the total energy can be written as

$$E = E_0 + \Delta E, \tag{4.8}$$

where the energy perturbation

$$\Delta E = \sum_{n=1}^{\infty} \Delta E^{(n)} \tag{4.9}$$

is expanded in powers of the perturbation $\hat{H}_I$. The energy contribution to the n:th power of $\hat{H}_I$ is [61, p. 31 and 33]

$$\Delta E^{(n)} = \langle \Phi_0 | \hat{H}_I \left(\hat{R} \left(E - \mu - \hat{H}_I \right) \right)^{n-1} |\Phi_0\rangle, \tag{4.10}$$

where $\hat{R}$ is the resolvent operator, defined as

$$\hat{R} \equiv \left(\hat{Q} \left(\hat{H}_0 - \mu \right) \hat{Q} \right)^{-1}, \tag{4.11}$$

and μ is an arbitrary constant. The Rayleigh-Schrödinger perturbation theory (RSPT) is defined such that $\mu = E_0$. In this thesis, we consider only perturbative methods derived from RSPT.

Expressed in second quantization, the single-particle operators can be written as

$$\hat{T} = \sum_{p,q} \langle p|\hat{t}|q\rangle a_p^\dagger a_q, \tag{4.12}$$

$$\hat{U} = \sum_{p,q} \langle p|\hat{u}|q\rangle a_p^\dagger a_q, \tag{4.13}$$

and the two-particle operator becomes

$$\hat{V} = \sum_{p,q,r,s} \langle pq|v|rs\rangle_{AS} a_p^\dagger a_q^\dagger a_s a_r. \tag{4.14}$$

Let us define the Fock operator as

$$\hat{F} = \sum_{p,q} \langle p|\hat{f}|q\rangle a_p^\dagger a_q, \tag{4.15}$$

where

$$\langle p|\hat{f}|q\rangle = \langle p|\hat{t}|q\rangle + \langle p|\hat{u}|q\rangle. \tag{4.16}$$

In the laboratory coordinate momentum basis, the matrix elements of the kinetic energy operator are diagonal.

Observe that the explicit expressions of $\Delta E^{(n)}$ in Eq. (4.10) depend on which operator $\hat{U}$ is used. Let us first choose the single-particle potential

$$\langle p|\hat{u}|q\rangle = \sum_i \langle pi|\hat{v}|qi\rangle_{AS}, \tag{4.17}$$

where i denotes a state that is occupied in the Fermi vacuum. Provided the Fock operator contains the single-particle potential (4.17), the Hartree-Fock equations are [157, pp. 42–43]

$$\begin{aligned} \langle p|\hat{f}|q\rangle &= \varepsilon_q \langle p|q\rangle, \\ \langle p|q\rangle &= \delta_{pq}, \end{aligned} \tag{4.18}$$

where the single-particle states are restricted to be orthonormal. A Hartree-Fock single-particle basis is a basis that fulfills Eq. (4.18) [157, p. 43]. If the interaction $\hat{v}$ conserves the total momentum, the Fock matrix becomes diagonal in the plane-wave basis. Consequently, the Hartree-Fock equations (4.18) are fulfilled in this basis, and, as stated in Ref. [192, p. 352], the momentum basis is a Hartree-Fock single-particle basis for infinite nuclear matter.

From now on, we use a notation with explicit momentum states. For brevity, we do not write out the spin and isospin degrees of freedom explicitly. The state vectors and sums

$$|\mathbf{k}\rangle \quad \text{and} \quad \sum_{\mathbf{k}} \tag{4.19}$$

should therefore be read as

$$|\mathbf{k}\rangle|m_s m_t\rangle \quad \text{and} \quad \sum_{m_s m_t} \sum_{\mathbf{k}}, \tag{4.20}$$

where m_s and m_t are the z projections of the single-particle spin and isospin, respectively. Let us define the reference energy as

$$E_{REF} \equiv \langle \Phi_0|\hat{H}|\Phi_0\rangle = E_0 + \Delta E^{(1)}. \tag{4.21}$$

As shown by Fetter and Walecka [192, p. 354], the explicit expression for the reference energy is

$$E_{REF} = \sum_{\mathbf{k}_i} \langle \mathbf{k}_i | \hat{t} | \mathbf{k}_i \rangle + \frac{1}{2} \sum_{\mathbf{k}_i, \mathbf{k}_j} \langle \mathbf{k}_i \mathbf{k}_j | \hat{v} | \mathbf{k}_i \mathbf{k}_j \rangle_{AS}. \tag{4.22}$$

By definition, the Hartree-Fock energy is the reference energy of a system calculated in a Hartree-Fock basis [157, p. 36, 40, and 41]. As can be seen from Eq. (4.18), the Fock matrix defined by Eqs. (4.16) and (4.17) is diagonal in a Hartree-Fock basis. Consequently, one-particle-one-hole diagrams vanish when using the plane-wave basis in infinite matter. With the chosen operator $\hat{U}$, the second-order contribution is [61, p. 131–132]

$$\Delta E^{(2)} = \frac{1}{4} \sum_{\mathbf{k}_i, \mathbf{k}_j} \sum_{\mathbf{k}_a, \mathbf{k}_b} \frac{\langle \mathbf{k}_i \mathbf{k}_j | \hat{v} | \mathbf{k}_a \mathbf{k}_b \rangle_{AS} \langle \mathbf{k}_a \mathbf{k}_b | \hat{v} | \mathbf{k}_i \mathbf{k}_j \rangle_{AS}}{\varepsilon_{\mathbf{k}_i} + \varepsilon_{\mathbf{k}_j} - \varepsilon_{\mathbf{k}_a} - \varepsilon_{\mathbf{k}_b}}, \tag{4.23}$$

where we have used the definition

$$\varepsilon_{\mathbf{k}} \equiv \langle \mathbf{k} | \hat{f} | \mathbf{k} \rangle. \tag{4.24}$$

In the special case with the Hartree-Fock operator $\hat{U}$, the contribution to third order is [61, pp. 132–133]

$$\Delta E^{(3)} = \Delta E^{(3)}_{pp} + \Delta E^{(3)}_{hh} + \Delta E^{(3)}_{ph} + \Delta E^{(3)}_{h} + \Delta E^{(3)}_{p}. \tag{4.25}$$

Here the third-order energy contains the so-called particle-particle term

$$\begin{aligned} \Delta E^{(3)}_{pp} = \frac{1}{8} \sum_{\mathbf{k}_a, \mathbf{k}_b} \sum_{\mathbf{k}_c, \mathbf{k}_d} \sum_{\mathbf{k}_i, \mathbf{k}_j} & \frac{\langle \mathbf{k}_i \mathbf{k}_j | \hat{v} | \mathbf{k}_a \mathbf{k}_b \rangle_{AS} \langle \mathbf{k}_a \mathbf{k}_b | \hat{v} | \mathbf{k}_c \mathbf{k}_d \rangle_{AS}}{\left(\varepsilon_{\mathbf{k}_i} - \varepsilon_{\mathbf{k}_j} - \varepsilon_{\mathbf{k}_a} - \varepsilon_{\mathbf{k}_b} \right)} \\ \times & \frac{\langle \mathbf{k}_c \mathbf{k}_d | \hat{v} | \mathbf{k}_i \mathbf{k}_j \rangle_{AS}}{\left(\varepsilon_{\mathbf{k}_i} - \varepsilon_{\mathbf{k}_j} + \varepsilon_{\mathbf{k}_c} - \varepsilon_{\mathbf{k}_d} \right)}, \end{aligned} \tag{4.26}$$

the hole-hole term

$$\begin{aligned} \Delta E^{(3)}_{hh} = \frac{1}{8} \sum_{\mathbf{k}_a, \mathbf{k}_b} \sum_{\mathbf{k}_i, \mathbf{k}_j} \sum_{\mathbf{k}_k, \mathbf{k}_l} & \frac{\langle \mathbf{k}_i \mathbf{k}_j | \hat{v} | \mathbf{k}_a \mathbf{k}_b \rangle_{AS} \langle \mathbf{k}_a \mathbf{k}_b | \hat{v} | \mathbf{k}_k \mathbf{k}_l \rangle_{AS}}{\left(\varepsilon_{\mathbf{k}_i} + \varepsilon_{\mathbf{k}_j} - \varepsilon_{\mathbf{k}_a} - \varepsilon_{\mathbf{k}_b} \right)} \\ \times & \frac{\langle \mathbf{k}_k \mathbf{k}_l | \hat{v} | \mathbf{k}_i \mathbf{k}_j \rangle_{AS}}{\left(\varepsilon_{\mathbf{k}_k} + \varepsilon_{\mathbf{k}_l} - \varepsilon_{\mathbf{k}_a} - \varepsilon_{\mathbf{k}_b} \right)}, \end{aligned} \tag{4.27}$$

and the particle-hole term

$$\begin{aligned} \Delta E^{(3)}_{ph} = - \sum_{\mathbf{k}_a, \mathbf{k}_b} \sum_{\mathbf{k}_c, \mathbf{k}_i} \sum_{\mathbf{k}_j, \mathbf{k}_k} & \frac{\langle \mathbf{k}_i \mathbf{k}_j | \hat{v} | \mathbf{k}_a \mathbf{k}_b \rangle_{AS} \langle \mathbf{k}_k \mathbf{k}_b | \hat{v} | \mathbf{k}_i \mathbf{k}_c \rangle_{AS}}{\left(\varepsilon_{\mathbf{k}_i} + \varepsilon_{\mathbf{k}_j} - \varepsilon_{\mathbf{k}_a} - \varepsilon_{\mathbf{k}_b} \right)} \\ \times & \frac{\langle \mathbf{k}_a \mathbf{k}_c | \hat{v} | \mathbf{k}_i \mathbf{k}_j \rangle_{AS}}{\left(\varepsilon_{\mathbf{k}_k} + \varepsilon_{\mathbf{k}_j} - \varepsilon_{\mathbf{k}_a} - \varepsilon_{\mathbf{k}_c} \right)}, \end{aligned} \tag{4.28}$$

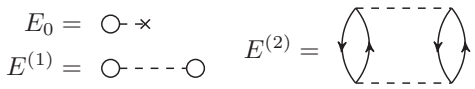

Figure 4.1: Diagrammatic representation of the energy to second order in perturbation theory, as obtained when assuming a Hartree-Fock single-particle potential $\hat{U}$ [61, pp. 131–132].

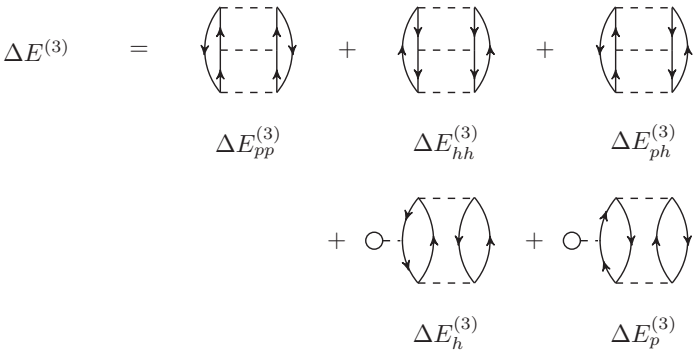

Figure 4.2: MBPT diagrams for the third-order energy correction, when the operator $\hat{U}$ is as in Eq. (4.17). For other choices than the Hartree-Fock operator $\hat{U}$, there are additional third-order diagrams containing the Fock operator [61, p. 133].

as well as $\Delta E^{(3)}_h$ and $\Delta E^{(3)}_p$, which we give only diagrammatically in Figure 4.2. The reference and second-order energy terms of Eqs. (4.22) and (4.23) are given diagrammatically in Figure 4.1. We use the diagrammatic rules defined in Ref. [61, pp. 90–131]. A vertical line with an arrow pointing up (down) represents the summation over a particle (hole) state, whereas a ring without an arrow represents a summation over a hole state. We have denoted the kinetic energy operator by a horizontal dashed line with a cross in one of the ends and the antisymmetrized two-body operator by a horizontal dashed line that is connected to four vertical lines. Between every pair of interaction lines, there is an energy denominator. For an introduction to the diagrammatic rules, the reader is referred to Refs. [157, pp. 119–176], [61, pp. 90–131], and [221]. The third-order diagrams for this special case are given in Figure 4.2. Shavitt and Bartlett [61, pp. 138–152] show all MBPT diagrams up to fourth order for the general case.

As stated in the linked-diagram theorem, the RSPT energy may be constructed "as the sum of all distinct closed connected perturbation-theory diagrams that contain one or more fragments of H'" [157, p. 255] (here H' is equal to our $\hat{H}_I$). A Goldstone

diagram is defined to be closed if there are no open lines, and it is connected if all parts of the diagram are tied by lines. As explained in Ref. [61, pp. 156–159], a method is size-extensive when obeying the linked-diagram theorem. Size-extensivity is crucial when studying large systems. For example, Harris *et al.* show [157, p. 217] that the configuration interaction doubles approximation, which is not size-extensive, gives zero correlation energy per particle for the electron gas.

4.2 Brueckner-Hartree-Fock approximation

As described in the textbook of Harris, Monkhorst, and Freeman [157, pp. 273–274], the perturbation series contains diagrams similar to the particle-particle diagram $\Delta E_{pp}^{(3)}$, given in Figure 4.2, with one, two, three, and up to infinitely many interaction matrix elements. That class of terms is commonly called particle-particle ladder diagrams. In a similar way, the RSPT contains hole-hole ladder diagrams to infinite order. The hole-hole ladder diagrams are obtained from the particle-particle ladders by exchanging all particle and hole lines with each other. Following Ref. [157, pp. 273–274], the complete set of particle-particle ladder diagrams can be constructed using the so-called G matrix [138], which is defined by the implicit equation

$$\begin{aligned}\langle \mathbf{k}_p\mathbf{k}_q|\hat{g}|\mathbf{k}_r\mathbf{k}_s\rangle &= \langle \mathbf{k}_p\mathbf{k}_q|\hat{v}|\mathbf{k}_r\mathbf{k}_s\rangle \\ &\quad + \sum_{\mathbf{k}_c\mathbf{k}_d} \frac{\langle \mathbf{k}_p\mathbf{k}_q|\hat{v}|\mathbf{k}_c\mathbf{k}_d\rangle\langle \mathbf{k}_c\mathbf{k}_d|\hat{g}|\mathbf{k}_r\mathbf{k}_s\rangle}{\varepsilon_{\mathbf{k}_p}+\varepsilon_{\mathbf{k}_q}-\varepsilon_{\mathbf{k}_c}-\varepsilon_{\mathbf{k}_d}},\end{aligned} \tag{4.29}$$

where the single-particle energies are defined as in Eq. (4.24) and the summation is over only particle states. Observe that the G matrix occurs on both sides of the equation, and the single-particle energies depend on the auxiliary potential $\hat{U}$. In terms of antisymmetric matrix elements, the same equation can be written as

$$\begin{aligned}\langle \mathbf{k}_p\mathbf{k}_q|\hat{g}|\mathbf{k}_r\mathbf{k}_s\rangle_{AS} &= \langle \mathbf{k}_p\mathbf{k}_q|\hat{v}|\mathbf{k}_r\mathbf{k}_s\rangle_{AS} \\ &\quad + \frac{1}{2}\sum_{\mathbf{k}_c\mathbf{k}_d} \frac{\langle \mathbf{k}_p\mathbf{k}_q|\hat{v}|\mathbf{k}_c\mathbf{k}_d\rangle_{AS}\langle \mathbf{k}_c\mathbf{k}_d|\hat{g}|\mathbf{k}_r\mathbf{k}_s\rangle_{AS}}{\varepsilon_{\mathbf{k}_p}+\varepsilon_{\mathbf{k}_q}-\varepsilon_{\mathbf{k}_c}-\varepsilon_{\mathbf{k}_d}},\end{aligned} \tag{4.30}$$

where the sum is now multiplied by a factor of one half.

The strong short-range forces of the nuclear interaction induce correlations that cannot be accounted for in a mean-field theory such as the Hartree-Fock approximation [158]. If the bare interaction is replaced by a G matrix, important parts of the correlations are included already at the lowest order of perturbation theory [18]. The Brueckner-Goldstone (BG) expansion [2] is obtained by replacing all interaction matrix

elements in the RSPT with G matrices. In BG theory, the diagonal matrix elements of the auxiliary potential $\hat{U}$ are commonly chosen to be [2]

$$\langle \mathbf{k}_p|\hat{u}|\mathbf{k}_p\rangle = \sum_{\mathbf{k}_i}\langle \mathbf{k}_p\mathbf{k}_i|\hat{g}|\mathbf{k}_p\mathbf{k}_i\rangle_{AS} \tag{4.31}$$

for single-particle states that are occupied in the uncorrelated Fermi vacuum. In the first-order approximation of Brueckner-Goldstone theory, which corresponds to the reference energy in RSPT, the energy becomes [66]

$$E_{BHF} = \sum_{\mathbf{k}_i}\langle \mathbf{k}_i|\hat{t}|\mathbf{k}_i\rangle + \frac{1}{2}\sum_{\mathbf{k}_i,\mathbf{k}_j}\langle \mathbf{k}_i\mathbf{k}_j|\hat{g}|\mathbf{k}_i\mathbf{k}_j\rangle_{AS}. \tag{4.32}$$

This approximation is commonly called the Brueckner-Hartree-Fock (BHF) method [251], because the interaction in the Hartree-Fock energy has been replaced by a self-consistently solved Brueckner G matrix. Observe that the matrix elements of the auxiliary potential is not yet defined for single-particle states above the Fermi level. There have been different approaches to handling the single-particle potential for particle states, such as the conventional gap option [251], in which the single-particle potential is set to zero above the Fermi level, and the continuous option [68, 69], in which the potential in Eq. (4.31) is used for both particle and hole single-particle states. In our calculations, we use the latter approach. Day has written a pedagogical introduction [2] to Brueckner-Goldstone theory and its application to infinite nuclear matter.

According to Rajaraman and Bethe [156], the Brueckner-Goldstone expansion does not converge when using the G matrix as a convergence parameter. Instead, they argue that the number of independent hole lines is a more appropriate cutoff parameter in the perturbation series [156]. The first-order energy in the Brueckner-Goldstone theory, the BHF approximation, is equal to the Brueckner-Bethe approximation including up to two hole lines [66]. The hole-line approximation builds on the assumption that every nucleon has only a small number of close neighbors, and the method is, therefore, accurate only at sufficiently low densities [2, 118].

4.3 Transformation to partial-wave expansion

The nuclear interaction is often given explicitly in the partial-wave basis

$$|k\mathcal{J}m_{\mathcal{J}}(lS)m_{t_1}m_{t_2}\rangle,$$

which was defined in Eq. (3.34). Next, we rewrite some of the previously defined expressions derived from RSPT and the BHF approximation in the partial-wave basis

(3.34). In this basis, the equations can be considerably simplified by approximating the Pauli exclusion operators (3.32) and (3.33) by averages over the angle between the relative and CM momentum vectors [8]. Similar expressions as we present in the partial-wave basis have been given many places in the literature (see Refs. [64, 67, 224, 252] and [225, pp. 63–101 and C1–C4], but we write out the equations to get all details and to make the text more self-contained.

4.3.1 The first orders of perturbation theory

Nuclear matter contains by definition an infinite number of particles, and one is, therefore, normally interested in, for example, the energy per particle instead of the total energy.

Assuming an uncorrelated Fermi sphere, the kinetic energy per nucleon can be calculated analytically, and is for both PNM and SNM simply [192, p. 355]

$$\begin{aligned}\frac{E_{kin}}{A} &= \frac{\Omega}{A}\frac{1}{(2\pi)^3}\sum_{m_s,m_t}\int_{|\mathbf{k}|\leq k_F} d\mathbf{k}\frac{\hbar^2 k^2}{2m} \\ &= \frac{3\hbar^2 k_F^2}{10m},\end{aligned} \tag{4.33}$$

where $\Omega \equiv L^3$ is the volume, A is the number of nucleons, k_F is the Fermi momentum, m is the nucleon mass, and $\hbar$ is the reduced Planck constant. To obtain the final expression in Eq. (4.33), the number of particles A is calculated as

$$A = \frac{\Omega}{(2\pi)^3}\sum_{m_s,m_t}\int_{|\mathbf{k}|\leq k_F} d\mathbf{k}, \tag{4.34}$$

that is, by counting all nucleons under the Fermi surface.

Nucleon masses occur in the kinetic energy, both as part of the single-particle operator in the reference energy and in the energy denominators of the MBPT, BHF, and CC correlation-energy expressions. Using different masses for protons and neutrons, the kinetic energy (4.33) becomes

$$\frac{E_{kin}}{A} = \frac{3\hbar^2 k_F^2}{20}\left(\frac{1}{m_P}+\frac{1}{m_N}\right), \tag{4.35}$$

where m_P and m_N are the proton and neutron masses, respectively. Given the transformation between laboratory and RCM coordinates

$$\mathbf{k} = (\mathbf{k}_p - \mathbf{k}_q)/2, \qquad \mathbf{K} = \mathbf{k}_p + \mathbf{k}_q,$$

the kinetic energies in the energy denominators may be written as

$$\frac{k_p^2}{2m_p} + \frac{k_q^2}{2m_q} = \frac{1}{2}\left(\frac{1}{m_p} + \frac{1}{m_q}\right)\left(k^2 + \frac{1}{4}K^2\right) + \frac{1}{2}\left(\frac{1}{m_p} - \frac{1}{m_q}\right)\mathbf{k}\cdot\mathbf{K}, \tag{4.36}$$

where m_p and m_q are nucleon masses that depend on the isospins of the single-particle states p and q. As we explain in Paper II, the CC implementations simplify considerably if we can write the energy denominators without explicit angles between the relative and CM momentum vectors. In our PNM calculations, we use the neutron mass m_N, whereas in the SNM calculations we replace proton and neutron masses by the average $\overline{m} \equiv (m_N + m_P)/2$. Using the average mass $\overline{m}$, the last term of Eq. (4.36), which contains the angular coordinate, vanishes. In our studies, we use the masses $m_N = 939.565379$ MeV and $m_P = 938.272046$ MeV [253]. Then the relative error of the average nucleon-mass approximation is 0.0000474% for the kinetic-energy expression (4.35) and 0.0688735% for the kinetic energy in the energy denominator. Whereas the former error is very small, the latter may be not negligible. However, we hope that the error associated with approximative masses in the energy denominators is smaller than other uncertainties in our implementations, which we argue to be less than 3% of the total energy (see Papers II and III and Section 5.2).

The expressions for the potential energy are obtained by first writing the equations in terms of relative momenta, and then transforming to a partial-wave basis [64, 67]. When transforming the potential energy expressions to the desired form, we first rewrite the sums as integrals using the transformation (3.27). Next, the equations are written in an RCM basis, as defined in Eq. (3.31), and the identity operators (3.35) and (3.36) are used to to introduce angular momenta. A coupled angular momentum basis is obtained by using the relation (3.41). In this chapter, we approximate all Pauli exclusion operators (3.32) and (3.33) by averages over the angle between the relative and CM momentum vectors, $\theta_{\mathbf{kK}}$. That is, the exact Pauli operators are replaced by the angular-averaged hole-hole operator

$$\overline{Q}_{hh}(k, K, k_F) = \frac{1}{2}\int_{-1}^{1} d\cos\theta_{\mathbf{kK}} \times \theta(k_F - |\mathbf{k} + \mathbf{K}/2|)\theta(k_F - |-\mathbf{k} + \mathbf{K}/2|), \tag{4.37}$$

and the angular-averaged particle-particle operator

$$\overline{Q}_{pp}(k', K, k_F) = \frac{1}{2}\int_{-1}^{1} d\cos\theta_{\mathbf{k'K}} \times \theta(|\mathbf{k}' + \mathbf{K}/2| - k_F)\theta(|-\mathbf{k}' + \mathbf{K}/2| - k_F). \tag{4.38}$$

Explicit expressions for the angular-averaged Pauli exclusion operators are given in, for example, Ref. [252]. Finally, the dependency on the angular coordinates of the relative momentum vectors are integrated out using Eq. (3.38).

With a transformation as described above, the first-order correction to the energy per nucleon becomes

$$\begin{aligned}\frac{\Delta E^{(1)}}{A} = C \sum_{\mathcal{J}Sl} \sum_{M_T} (2\mathcal{J}+1) \\ \times \int_0^{k_F} dk k^2 \left(1 - \frac{3}{2}\frac{k}{k_F} + \frac{1}{2}\left(\frac{k}{k_F}\right)^3\right) \\ \times \langle k\mathcal{J}lSM_T|\hat{v}|k\mathcal{J}lSM_T\rangle,\end{aligned} \tag{4.39}$$

where the constant C is 1 for symmetric nuclear matter and 2 for pure neutron matter. The summation over M_T takes the values -1, 0, 1 for symmetric nuclear matter and only 0 for pure neutron matter. Here and in the following, all interaction matrix elements are assumed to be multiplied by the operator (A.5), which ensures proper antisymmetry and conservation of parity. A similar expression as Eq. (4.39) is given for symmetric nuclear matter by MacKenzie [224] using isospin symmetry. The differing factor $4/\pi$ comes from a different definition of the Fourier-Bessel transform in the interaction matrix elements.

Similarly, the second-order perturbation correction (4.23) can be written as

$$\begin{aligned}\frac{\Delta E^{(2)}}{A} = C \frac{3}{16 k_F^3} \sum_{\mathcal{J}S} \sum_{ll'} \sum_{M_T} (2\mathcal{J}+1) \int_0^{2k_F} dK K^2 \\ \times \int_0^{\sqrt{k_F^2 - K^2/4}} dk k^2 \int_{\sqrt{k_F^2 - K^2/4}}^{\infty} dk' k'^2 \\ \times |\langle k\mathcal{J}lSM_T|\hat{v}|k'\mathcal{J}l'SM_T\rangle|^2 \\ \times \frac{\overline{Q}_{hh}(k,K,k_F)\overline{Q}_{pp}(k',K,k_F)}{\Delta\varepsilon_{ave}(k,k',K,M_T)},\end{aligned} \tag{4.40}$$

where we have used angular-averaged Pauli exclusion operators and the constant C is as defined for the Hartree-Fock term. In Eq. (4.40), the energy denominator has been approximated by the expression

$$\begin{aligned}\Delta\varepsilon_{ave}(k,k',K) = \varepsilon(\overline{|\mathbf{k} + \mathbf{K}/2|}) + \varepsilon(\overline{|-\mathbf{k} + \mathbf{K}/2|}) \\ - \varepsilon(\overline{|\mathbf{k}' + \mathbf{K}/2|}) - \varepsilon(\overline{|-\mathbf{k}' + \mathbf{K}/2|}),\end{aligned} \tag{4.41}$$

where angular-averaged arguments are marked with an overline. We explain below how the arguments in the energy denominator are averaged. In Eq. (4.40), the isospin

dependence in the energy denominator has been neglected for brevity. A similar expression as Eq. (4.40) is given in Ref. [224], in which they assume isospin symmetry.

The exact energy denominator contains the single-particle energy terms

$$\varepsilon(k_i) + \varepsilon(k_j) = \varepsilon(|\mathbf{k} + \mathbf{K}/2|) + \varepsilon(|-\mathbf{k} + \mathbf{K}/2|), \tag{4.42}$$

where, on the right-hand side of the equation, the laboratory frame momenta k_i and k_j have been written using RCM momenta. When approximating the arguments of the single-particle energies, we use a technique first suggested by Brueckner and Gammel [8] and explained further in the doctoral thesis of Ramos (see [225, pp. 66–69] and [252]). In this method, the single-particle energy is first approximated by a polynomial expansion. Because nuclear matter is an isotropic medium, the single-particle energy must be a symmetric function of the laboratory-frame momentum, and, therefore, only even powers in the polynomial have a nonzero contribution. The single-particle energy is approximated by a polynomial

$$\varepsilon(k) = \alpha + \beta k^2 + \gamma k^4 + \ldots, \tag{4.43}$$

where α, β, and γ are constants, and consequently

$$\begin{aligned}
\varepsilon(k_i) + \varepsilon(k_j) &= 2\alpha + \beta(k_i^2 + k_j^2) + \gamma(k_i^4 + k_j^4) + \ldots \\
&= \ldots \\
&= 2\alpha + 2\beta(k^2 + K^2/4) \\
&\quad + 2\gamma\left((k^2 + K^2/4)^2 + (\mathbf{k}\cdot\mathbf{K})^2\right) + \ldots .
\end{aligned} \tag{4.44}$$

As Ramos points out, the first dependence on the angle between $\mathbf{k}$ and $\mathbf{K}$ comes at second order [225, p. 66].

Following Ramos [225, p. 66], we are using the angular-average approximation

$$(\mathbf{k}\cdot\mathbf{K})^2 \approx K^2 k^2 \overline{\cos^2\theta_{\mathbf{kK}}}, \tag{4.45}$$

where

$$\begin{aligned}
\overline{\cos^2\theta_{\mathbf{kK}}} &= \frac{1}{2}\int_{-1}^{1} d\cos\theta_{\mathbf{kK}} \cos^2\theta_{\mathbf{kK}} \\
&\quad \times \theta(k_F - |\mathbf{k} + \mathbf{K}/2|)\theta(k_F - |-\mathbf{k} + \mathbf{K}/2|)
\end{aligned} \tag{4.46}$$

for hole states and

$$\begin{aligned}
\overline{\cos^2\theta_{\mathbf{kK}}} &= \frac{1}{2}\int_{-1}^{1} d\cos\theta_{\mathbf{kK}} \cos^2\theta_{\mathbf{kK}} \\
&\quad \times \theta(|\mathbf{k} + \mathbf{K}/2| - k_F)\theta(|-\mathbf{k} + \mathbf{K}/2| - k_F)
\end{aligned} \tag{4.47}$$

for particle states. The angular-averaged value can be shown to be

$$\overline{\cos^2\theta_{\mathbf{kK}}} = \frac{1}{3}\overline{Q}^3(k,K,k_F), \tag{4.48}$$

where $\overline{Q}$ is replaced by the angular-averaged Pauli exclusion operator $\overline{Q}_{hh}$ for two-hole states, and by $\overline{Q}_{pp}$ for two-particle states. Now we get the angular-averaged input momenta [225, pp. 66–69]

$$\begin{aligned} k_i^2 &= \overline{|\mathbf{k}+\mathbf{K}/2|^2} \\ &= k^2 + K^2/4 + \frac{1}{\sqrt{3}}kK\overline{Q}_{hh}^{3/2}(k,K,k_F) \end{aligned} \tag{4.49}$$

and

$$\begin{aligned} k_j^2 &= \overline{|-\mathbf{k}+\mathbf{K}/2|^2} \\ &= k^2 + K^2/4 - \frac{1}{\sqrt{3}}kK\overline{Q}_{hh}^{3/2}(k,K,k_F). \end{aligned} \tag{4.50}$$

Angular-averaged input momenta for particle states k_a and k_b are defined in a similar way. Explicit expressions for the single-particle energies are obtained from Eqs. (4.62) and (4.63) by replacing the G matrix with a bare interaction.

The particle-particle term in third-order perturbation theory, Eq. (4.26), can be written as

$$\begin{aligned} \frac{\Delta E_{pp}^{(3)}}{A} = C\frac{3}{32k_F^3}\sum_{\mathcal{J}S}\sum_{ll'l''}\sum_{M_T}(2\mathcal{J}+1)\int_0^{2k_F}dKK^2 \\ \times\int_0^{\sqrt{k_F^2-K^2/4}}dkk^2\int_{\sqrt{k_F^2-K^2/4}}^{\infty}dpp^2\int_{\sqrt{k_F^2-K^2/4}}^{\infty}dp'p'^2 \\ \times\frac{\langle k\mathcal{J}(lS)M_T|\hat{v}|p\mathcal{J}(l'S)M_T\rangle\langle p\mathcal{J}(l'S)M_T|\hat{v}|p'\mathcal{J}(l''S)M_T\rangle}{\Delta\varepsilon_{ave}(k,p,K)\Delta\varepsilon_{ave}(k,p',K)} \\ \times\langle p'\mathcal{J}(l''S)M_T|\hat{v}|k\mathcal{J}(lS)M_T\rangle \\ \times\overline{Q}_{hh}(k,K,k_F)\overline{Q}_{pp}(p,K,k_F)\overline{Q}_{pp}(p',K,k_F), \end{aligned} \tag{4.51}$$

where C is 1 for symmetric nuclear matter and 2 for pure neutron matter. In Eq. (4.51), the Pauli exclusion operators in the numerator have been approximated by angular-averaged operators. A similar expression for the particle-particle term is given by MacKenzie [224] for symmetric nuclear matter with isospin symmetry. In Ref. [224], there is an additional factor $(4/\pi)^3$ owing to a different definition of the interaction matrix elements.

4.3.2 The BHF approximation

The Brueckner-Hartree-Fock approximation is a standard approach for calculating the binding energy of infinite nuclear matter [2, 66, 104, 118]. Implementations of the G-matrix equation have therefore been discussed many places in the literature (see, for example, Refs. [67, 68, 251], [225, pp. 63–101 and C1–C4], and [235, pp. 111–114]). In addition to being an essential part of the Brueckner-Goldstone theory [2], the G matrix is encountered also in, for example, ladder approximations of the self-consistent Green's function method [252]. We have solved the G-matrix equation using the matrix inversion technique of Haftel and Tabakin [67], but using continuous single-particle energy spectra [68, 69]. Using continuous single-particle spectra means that the operator $\hat{U}$ is chosen to be such that the definition (4.31) is used for both hole and particle single-particle states.

Our implementation of the BHF approximation follows to a large degree Haftel and Tabakin [67], using angular-averaged Pauli exclusion operators. As given in Ref. [67], the G-matrix equation (4.30) can be written in a partial-wave expansion basis as

$$\begin{aligned}
&\langle k\mathcal{J}(lS)M_T|\hat{g}(K)|k'\mathcal{J}(l'S)M_T\rangle \\
&= \langle k\mathcal{J}(lS)M_T|\hat{v}|k'\mathcal{J}(l'S)M_T\rangle \\
&+ \frac{1}{2}\sum_{l''}\int_0^\infty dpp^2\overline{Q}_{pp}(p,K,k_F) \\
&\times \frac{\langle k\mathcal{J}(lS)M_T|\hat{v}|p\mathcal{J}(l''S)M_T\rangle\langle p\mathcal{J}(l''S)M_T|\hat{g}(K)|k'\mathcal{J}(l'S)M_T\rangle}{\Delta\varepsilon_{ave}(k',p,K,M_T)},
\end{aligned} \tag{4.52}$$

where we notice that the G matrix depends on the radial part of the CM momentum. The energy denominator is defined as in Eq. (4.41).

Next, let us consider the energy denominator. The single-particle energy of a state $|\mathbf{k}_p, m_s, m_t\rangle$ is

$$\begin{aligned}
\varepsilon(\mathbf{k}_p, m_s, m_t) = \frac{\hbar^2 k_p^2}{2m} + \sum_{m_{s'}}\sum_{m_{t'}}\int d\mathbf{k}_j\theta(k_F - |\mathbf{k}_j|) \\
\times \langle \mathbf{k}_p m_s m_t \mathbf{k}_j m_{s'} m_{t'}|\hat{g}|\mathbf{k}_p m_s m_t \mathbf{k}_j m_{s'} m_{t'}\rangle_{AS},
\end{aligned} \tag{4.53}$$

where m_s and m_t are the z projections of spin and isospin, respectively, and a factor $\Omega/(2\pi)^3$ is included in the two-body interaction. If the integration variable is changed to relative coordinates, that is,

$$\mathbf{k} = (\mathbf{k}_p - \mathbf{k}_j)/2, \qquad \mathbf{K} = \mathbf{k}_p + \mathbf{k}_j, \tag{4.54}$$

where $\mathbf{k}$ and $\mathbf{K}$ are relative and CM coordinates, respectively, the single-particle potential becomes

$$\begin{aligned} U(\mathbf{k}_p, m_s, m_t) = 8 \sum_{m_{s'}} \sum_{m_{t'}} \int_{\min\{0,(k_p-k_F)/2\}}^{(k_p+k_F)/2} dk k^2 \int_0^{2\pi} d\phi_{\mathbf{k}} \int_{-1}^{1} d(\cos\theta_{\mathbf{k}}) \\ \times \langle \mathbf{k} m_s m_t m_{s'} m_{t'} | \hat{g}(\mathbf{K}) | \mathbf{k} m_s m_t m_{s'} m_{t'} \rangle_{AS} \\ \times \theta(k_F - |-2\mathbf{k} + \mathbf{k}_p|). \end{aligned} \tag{4.55}$$

See also Ref. [225, pp. C1–C4] for a similar calculation. Because infinite nuclear matter is an isotropic medium, the single-particle energy should not depend on the direction of $\mathbf{k}_p$. The input momentum vector is chosen to be directed along the positive z axis.

In our calculations we have replaced the CM momentum by $\overline{K^2}$, defined as the average of $|\mathbf{K}|^2$ when integrating with respect to the vector $\mathbf{k}$. If $\mathbf{k}_p$ is directed along the z axis, the average of the squared CM momentum becomes

$$\overline{K^2} \equiv \frac{1}{2} \int_{-1}^{1} d\cos\theta_{\mathbf{k}} \, |2(\mathbf{k}_p - \mathbf{k})|^2 \, \theta(k_F - |-2\mathbf{k} + \mathbf{k}_p|). \tag{4.56}$$

By evaluating this expression, we got the explicit formula

$$\overline{K^2} = \begin{cases} 4(k_p^2 + k^2), & \text{if } 0 \le 2k \le k_F - k_p \\ & \text{and } k_p \le k_F, \\ 4(k_p^2 + k^2) + \frac{1}{8kk_p} \left[-16k_p k^3 \right. & \\ -4(7k_p^2 + k_F^2)k^2 - 16k_p^3 k & \\ \left. + k_F^4 + 2k_F^2 k_p^2 - 3k_p^4 \right], & \text{if } |k_F - k_p| \le 2k \le k_F + k_p. \end{cases} \tag{4.57}$$

Haftel and Tabakin [67] have given a similar averaged CM momentum that is defined only when $k_p \le k_F$. Our expression differs from Haftel and Tabakin's in the second interval, but the limits of the intervals are the same. In Figure 4.3, our formula for $\overline{K^2}$ is compared with that of Ref. [67]. Observe that our definition of the CM momentum vector $\mathbf{K}$ is different from the definition

$$\mathbf{P} = (\mathbf{k}_i - \mathbf{k}_j)/2, \tag{4.58}$$

used by Haftel and Tabakin. In Figure 4.3, both expressions were calculated using the definition (4.58). In contrast to the expression given by Haftel and Tabakin [67], our average CM momentum vanishes at $k = (k_p + k_F)/2$, as is required by the definition (4.56). It seems therefore that the formula for $\overline{K^2}$ given in Ref. [67] is wrong.

In addition to using the averaged CM momentum (4.56), we replace the Pauli exclusion operator in Eq. (4.55) by the angular-averaged operator

$$\overline{Q}(k, k_p, k_F) = \frac{1}{2} \int_{-1}^{1} d\cos\theta_{\mathbf{k}} \theta(k_F - |-2\mathbf{k} + \mathbf{k}_p|), \tag{4.59}$$

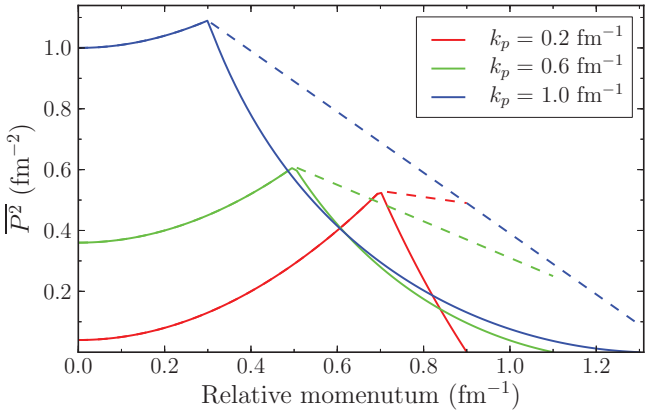

Figure 4.3: Average of the squared CM momentum, $\overline{P^2} = \overline{K^2}/4$, plotted as a function of the relative momentum for given lab momenta k_p. The Fermi momentum k_F was fixed to 1.6 fm^{-1}. The dashed lines represent results calculated with the formula for $\overline{P^2}$ given in Eq. (3.19) of Ref. [67]. In contrast to the formula given in Ref. [67], our formula for $\overline{K^2}$ gives the correct values at the end points of the relative momentum interval.

similarly as done in Ref. [67]. Applying angular momentum algebra, we got the expression

$$\begin{aligned} U(k_p, m_t) =& 16 \sum_{m_{t'}} \sum_{\mathcal{J}lS} (2\mathcal{J}+1) \left[\theta(k_F - |k_p|) \int_0^{|k_F - k_p|/2} dk k^2 \right. \\ &\left. + \int_{|k_F-k_p|/2}^{(k_F+k_p)/2} dk k^2 \left(\frac{-4k^2 + 4kk_p - k_p^2 + k_F^2}{8kk_p} \right) \right] \\ &\times \left[\langle k\mathcal{J}(lS) m_t m_{t'} | g(K_{av}) | k\mathcal{J}(lS) m_t m_{t'} \rangle \right. \\ &\left. - (-1)^{1+S+l} \langle k\mathcal{J}(lS) m_t m_{t'} | g(K_{av}) | k\mathcal{J}(lS) m_{t'} m_t \rangle \right], \end{aligned} \tag{4.60}$$

not very different from Eq. (C.14) in Ref. [225]. Above, the single-particle potential is given as a function of a single-particle isospin projection m_t. In the energy denominator, the single-particle potential always occurs in pairs

$$W(k_p, m_{t_p}, k_q, m_{t_q}) \equiv U(k_p, m_{t_p}) + U(k_q, m_{t_q}). \tag{4.61}$$

The function W is a function of the two-particle isospin projection $M_T = m_{t_p} + m_{t_q}$, that is,

$$W^{M_T}(k_p, k_q) \equiv U^{M_T,+}(k_p) + U^{M_T,-}(k_q), \tag{4.62}$$

where the explicit expressions of the single-particle potentials are

$$\begin{aligned} U^{M_T,\pm}(k_p) =& 16 \sum_{\mathcal{J}lS} (2\mathcal{J}+1) \left[\theta(k_F - |k_p|) \int_0^{|k_F - k_p|/2} dk k^2 \right. \\ &\left. + \int_{|k_F-k_p|/2}^{(k_F+k_p)/2} dk k^2 \left(\frac{-4k^2 + 4kk_p - k_p^2 + k_F^2}{8kk_p} \right) \right] \\ &\times \mathcal{B}^{M_T,\pm} \langle k\mathcal{J}(lS) | g(K_{av}) | k\mathcal{J}(lS) \rangle, \end{aligned} \tag{4.63}$$

and the antisymmetrization operator $\mathcal{B}^{M_T,\pm}$ is defined in Eqs. (A.6) and (A.7).

Finally, let us write the BHF energy (4.32) in the partial-wave basis. If the angular-average approximation (4.37) is used for the hole-hole Pauli exclusion operator, the BHF energy per nucleon is

$$\begin{aligned} \frac{\Delta E_{BHF}}{A} =& \frac{3\pi}{2k_F^3} \sum_{\mathcal{J}lS} \sum_{M_T} (2\mathcal{J}+1) \int_0^{k_F} dk k^2 \\ &\times \left\{ \int_0^{2(k_F-k)} dK K^2 - \int_{2(k_F-k)}^{2\sqrt{k_F^2-k^2}} dK K^2 \frac{k^2 - k_F^2 + K^2/4}{kK} \right\} \\ &\times \langle k\mathcal{J}lSM_T | g(K) | k\mathcal{J}lSM_T \rangle, \end{aligned} \tag{4.64}$$

where the G-matrix elements are assumed to be multiplied by the antisymmetrization and parity-conservation operator $\mathcal{A}^{llSM_T}$, defined in Eq. (A.5). Haftel and Tabakin have given expressions [67] similar to Eqs. (4.52) and (4.64) for a system in which the interaction depends only on the total two-particle isospin. Suzuki *et al.* have derived the BHF equations in a partial-wave basis using exact Pauli exclusion operators [64]. In Paper II, we derive CC ladder equations for nuclear matter using exact Pauli operators in a similar way as Suzuki *et al.* [64] did for the BHF approximation.

4.4 Implementations and results

4.4.1 The first orders of perturbation theory

The energy expressions for the lowest orders of perturbation theory, given in Eqs. (4.39), (4.40), and (4.51), were straightforwardly implemented using numerical integration with Gauss-Legendre quadrature [254, pp. 140–146]. The expressions for the angular-averaged Pauli exclusion operators are discontinuous with respect to the first derivative [225, p. 67]. In all our implementations, we split the integration intervals at the discontinuity points of the Pauli operators to avoid convergency problems in the numerical integrations.

4.4.2 The BHF approximation

We solve the G-matrix equation using a matrix inversion technique introduced by Haftel and Tabakin [67]. As outlined in Ref. [67], the G-matrix equation (4.52) may be written as

$$\mathbf{V} = \mathbf{U}\mathbf{G}, \tag{4.65}$$

where, for coupled channels, $\mathbf{G}$ is a $2(N+1) \times 2(N+1)$ matrix

$$\mathbf{G} = \begin{bmatrix} \mathbf{G}_{l_{\min},l_{\min}} & \mathbf{G}_{l_{\min},l_{\max}} \\ \mathbf{G}_{l_{\max},l_{\min}} & \mathbf{G}_{l_{\max},l_{\max}} \end{bmatrix}, \tag{4.66}$$

and $l_{\min} = \mathcal{J} - 1$ and $l_{\max} = \mathcal{J} + 1$. The matrices $\mathbf{V}$ and $\mathbf{U}$ are set up similarly for coupled channels. For uncoupled channels, the matrices $\mathbf{V}$, $\mathbf{U}$, and $\mathbf{G}$ contain only one submatrix. In Eq. (4.66), the submatrices have matrix elements

$$[\mathbf{G}_{l,l'}]_{i,j} \equiv \langle k_i \mathcal{J}(lS) M_T | \hat{g}(K) | k_j \mathcal{J}(l'S) M_T \rangle, \tag{4.67}$$

for $i, j \in \{1, \ldots, N+1\}$. Similarly, the matrix $\mathbf{V}$ is defined by the interaction matrix elements

$$[\mathbf{V}_{l,l'}]_{i,j} \equiv \langle k_i \mathcal{J}(lS) M_T | \hat{v} | k_j \mathcal{J}(l'S) M_T \rangle \tag{4.68}$$

and $\mathbf{U}$ by the elements

$$[\mathbf{U}_{l,l'}]_{i,j} \equiv \delta_{ij} + u_j \, [\mathbf{V}_{l,l'}]_{i,j} \, , \tag{4.69}$$

where

$$u_j = \begin{cases} -\frac{\omega_{k_j} k_j^2 Q_{pp}(k_j, K, k_F)}{\Delta\varepsilon_{av}(k_j, k_0, K)}, & \text{if } j \leq N, \\ \sum_{p=1}^{N} \frac{\omega_{k_p} k_0^2 Q_{pp}(k_0, K, k_F)}{\Delta\varepsilon_{av}(k_p, k_0, K)}, & \text{if } j = N+1, \end{cases} \tag{4.70}$$

and $u_{j+N+1} = u_j$ for $j = 1, 2, \ldots, N+1$. The coefficients ω_{k_j} are the quadrature weights corresponding to the grid points k_j, and k_0 is the relative momentum point we want to evaluate the G matrix at. Following Haftel and Tabakin [67], we calculate only the principal value of the integral in the G-matrix equation (4.52). As shown in Ref. [67], the singularity in the integrand is removed by adding a term that integrates to zero. A more proper way of dealing with the singularity is to solve a complex G-matrix equation, as is explained in, for example, the doctoral thesis of Engvik [235, pp. 112–114]. In the submatrices (4.67), (4.68), and (4.69), the momentum mesh points are $[k_1, k_2, \ldots, k_N, k_0]$, where the elements $k_1, k_2, \ldots, k_N$ are integration points used to integrate from zero to infinity and k_0 is the chosen evaluation point [67].

When solving the G-matrix equation, the grid points must be set up carefully to avoid convergency problems in the numerical integrations [235, p. 113]. The angular-averaged Pauli exclusion operator $\overline{Q}_{pp}(k, K, k_F)$ has a discontinuous first derivative at certain momenta k that depend on the CM momentum K and the Fermi momentum k_F [225, p. 67]. Therefore, we split the integration interval in relative momentum k at the discontinuity points of the Pauli operator. Even if the singularity point of the G-matrix equation is removed by calculating only the principal value, the region where the energy denominator is small still may cause convergence problems in the numerical integration. According to Engvik [235, p. 113], better numerical accuracy can be obtained by choosing integration points symmetrically around the singularity point where the denominator vanishes. Using this technique, the setup of the integration points $[k_1, \ldots, k_N]$ becomes therefore dependent on both K, which is the CM momentum, and k_0, which is the singularity point of the integrand. We set up the relative momentum grid points using the algorithm given in Figure 4.4. In her doctoral thesis [225, pp. B1-B6], Ramos has set up the momentum grid points in a similar way. However, we have written an algorithm to find a grid with certain conditions.

ALGORITHM – SETUP OF MOMENTUM GRID POINTS

Assume a CM momentum K and a pole k_0 are given.

1. Get the discontinuity points of the Pauli exclusion operator. Label these points by $L_1(K)$ and $L_2(K)$.

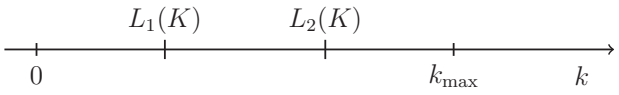

2. Locate in which subinterval the given pole k_0 is.

3. Determine whether k_0 is closer to the lower or upper limit in the subinterval it is in. Label the limit which is closest to k_0 by L_C.

4. Get the mirror point of L_C with respect to k_0 and label it by the symbol $L_3(k_0)$.

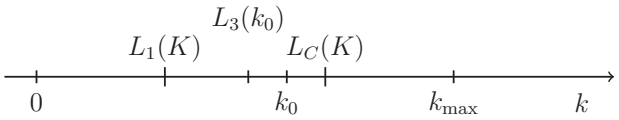

5. Set up Gauss-Legendre quadratures in all the intervals obtained by splitting the total interval at L_1, L_2, and L_3.

Figure 4.4: We use this algorithm to set up the momentum grid points for the G matrix. The principles of this setup are similar as in Refs. [225, pp. B1–B6] and [235, p. 113], but here we automatically find a suitable grid.

Results

In Figure 4.5, we compare equations of state for symmetric nuclear matter, calculated with different many-body methods. All the results in this figure were obtained with the $\mathrm{NNLO_{opt}}$ nucleon-nucleon interaction of Paper I, and the total angular momentum was truncated after $\mathcal{J} = 8$ in the correlation energy and after $\mathcal{J} = 24$ in the Hartree-Fock or Born approximations. In all the methods presented in the figure, we used angular-averaged Pauli exclusion operators. As seen from Figure 4.5, the MBPT(3) approximation containing only particle-particle ladders gives almost the same energies as the CC particle-particle ladder (PP-LAD) approximation of Paper II, in which ladder diagrams are summed to infinite order. The BHF approximation gives more binding than the other approaches, probably due to renormalized single-particle potentials. Similarly as in all our calculations with the relatively soft chiral interactions from Ref. [70] and Paper I, the saturation point is far from the experimental uncertainty region, which is marked in the figure by a square.

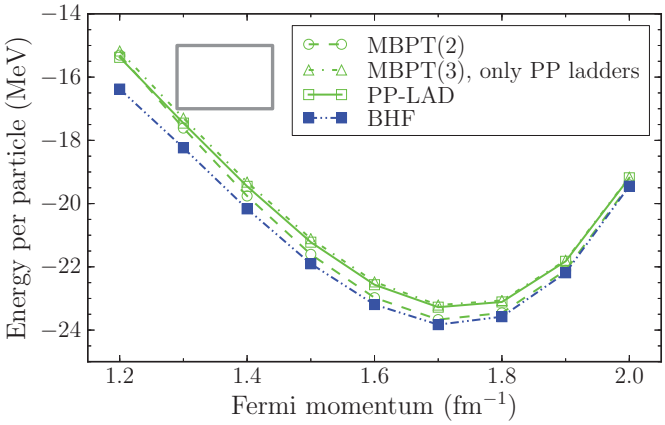

Figure 4.5: Equations of state for symmetric nuclear matter, as obtained with MBPT(2), MBPT(3) containing only particle-particle ladders, the CC particle-particle ladder approximation presented in Paper II, and with the BHF approach. All the calculations were done with angular-averaged Pauli exclusion operators using the $\mathrm{NNLO_{opt}}$ chiral nucleon-nucleon interaction from Paper I. Observe the small difference between energies given by particle-particle ladder approximations to third (MBPT(3)) and infinite (PP-LAD) order. The experimental saturation point is marked by a square.

As seen from Figure 4.6, the HF and MBPT(2) approximations are clearly insuf-

ficient to describe the correlations in symmetric nuclear matter, when using the hard Argonne v_{18} (AV18) [239] nucleon-nucleon interaction. This problem is well-known, and is discussed in, for example, Ref. [158]. When using the AV18 potential in an MBPT(2) calculation, we obtain a more repulsive equation of state than that of Bogner *et al.* [158]. However, whereas Bogner *et al.* approximated the single-particle energies using effective masses [158], we include the single-particle potential explicitly, as described in Sec. 4.3. In the effective mass approximation, the single-particle kinetic energy plus potential are fitted to a parabolic equation

$$\varepsilon^*(k) = \frac{\hbar^2 k^2}{2m^* m} + W,$$

where k is the laboratory-frame momentum, m is the nucleon mass, W is a constant potential, and m^* is the so-called effective mass (see Refs. [67, 158]). When doing, for example, a least-squares fitting [255, pp. 77–84], it is necessary to use a finite number of momentum points, with a largest data point k_n of finite size. We performed calculations in the effective-mass approximation in which the maximum momentum in the least-squares fitting was chosen to be a value between 1 fm^{-1} and 30 fm^{-1}, and found that the obtained effective mass m^* is strongly dependent on the interval in which the fitting is done. Different effective masses, in turn, result in largely deviating equations of states. Depending on the chosen interval for the least-squares fitting, it is possible to get results similar to those of Bogner *et al.* [158] or similar to ours, where our results were obtained using explicit single-particle potentials.

The results in Figure 4.6 were obtained with a cutoff in total angular momentum $\mathcal{J} \leq 6$ when using the AV18 nucleon-nucleon interaction. In calculations with the NNLO$_{\text{opt}}$ interaction, we included partial waves up to $\mathcal{J} = 24$ in the Hartree-Fock approximation and up to $\mathcal{J} = 8$ in the correlation energy.

Whereas perturbative approximations fail when using the strong AV18 interaction, we obtain a converging result with saturation when using the PPHH-LAD approximation of Paper II (see Figure 4.6). In this CC approach, particle-particle and hole-hole ladder diagrams are summed to infinite order. For comparison, HF, MBPT(2), and PPHH-LAD results are also shown in Figure 4.6 as obtained with the NNLO$_{\text{opt}}$ interaction. The difference between MBPT(2) and the CC ladder approximation is considerably smaller with the soft NNLO$_{\text{opt}}$ interaction than with the strong AV18 potential.

In this chapter, we have reviewed the basic ideas of many-body perturbation theory, with emphasis on RSPT. Starting from RSPT, we have derived the BHF approxima-

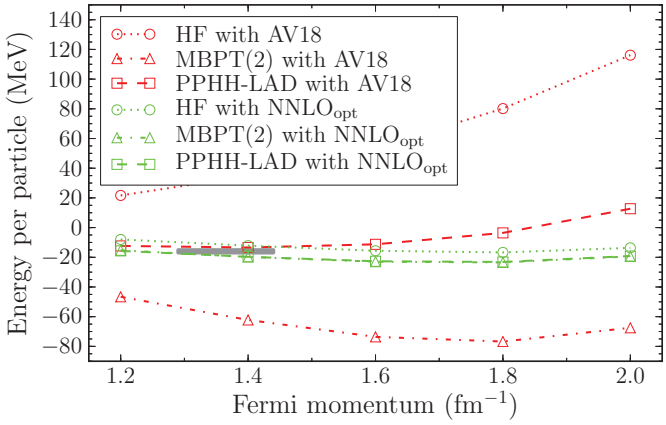

Figure 4.6: It is a well-known fact that symmetric nuclear matter is strongly nonperturbative when using the Argonne v_{18} (AV18) potential [239] (see Ref. [158]). When summing ladder diagrams to infinite order, as in the CC PPHH-LAD approximation, presented in Paper II, the saturation energy is less than 2 MeV from the experimental uncertainty region (gray box). In contrast to the calculations with the AV18 interaction, MBPT(2) gives almost the same energies as the PPHH-LAD approximation when using the NNLO$_{\text{opt}}$ interaction model of Paper I. The HF results obtained with the NNLO$_{\text{opt}}$ nuclear force are from Paper II. All the calculations were done with angular-averaged Pauli operators.

tion, which is commonly used in nuclear structure theory. We have given explicit energy expressions for nuclear matter in the lowest orders of perturbation theory and in the BHF approximation. In addition, we have given details considering our implementations of these approaches, and we have discussed some results. Next, we turn our attention to the main topic of this thesis, which is CC applications for infinite matter.

Chapter 5

Coupled-cluster approximations for infinite matter

As we discussed in Chapter 2, a wide range of quantum-mechanical *ab initio* methods have been used to study both infinite nuclear matter and the electron gas. Infinite nuclear matter has been studied using variational wave-function approaches, such as FHNC [181], VMC, GFMC [71], and AFDMC [20, 73, 185], nonvariational wave-function methods, such as the hole-line approximation and BHF [2, 18, 66, 154, 155], and propagator techniques, such as the SCGF method [62, 118, 168], to name a few. In electron-gas applications, GFMC [194] and dielectric-function [202] methods have been important, in particular for the local-density approximation of density-functional theory [122]. In this landscape, CC theory [29–33, 61] is a nonvariational wave-function method, which has been applied to both nuclear matter [17, 43] and the electron gas [50–60].

With Papers II and III, as well as this thesis, we want to reintroduce coupled-cluster theory to the study of infinite nuclear matter. The electron gas is a well-studied system, but still, to the best of our knowledge, CC theory has not been applied to the two-dimensional electron gas beyond the ladder [60] and ring [59] diagram approximations of Freeman. To start filling this gap, we study finite-size systems of the two-dimensional electron gas using a CC truncation beyond the ladder and ring approximations.

In Section 5.1, we outline the basic principles of CC theory and give explicit equations in a plane-wave basis. Section 5.2 is devoted to the nuclear matter CC studies of this thesis. We discuss the results of Papers I–III, the implementation of the partial-wave-expanded ladder approximation presented in Paper II, and the verification of the code. An approach based on spherical Bessel functions is also discussed. In Section 5.3, we explain how finite electron-gas systems have been modeled using Ewald's interaction. Finally, we present new results for the two-dimensional electron gas, discuss

implementation issues, and verify our results by comparing with other methods.

5.1 Coupled-cluster theory

Coupled-cluster theory is one of the standard tools in quantum chemistry [33, 222]. The method has its roots in the field of nuclear physics [29, 30, 43], but was for a long time mainly used and developed within the quantum-chemistry community [33, 256]. Since the late 1990s, CC theory has become an increasingly popular method for nuclear structure studies [44]. Recently, CC theory has been used to calculate the binding energy of light and medium-mass nuclei [34, 35, 37, 39, 42, 257], it has been applied to nuclei around the neutron drip line [41, 258], spectroscopic factors have been calculated [259], and simple time-dependent nuclear models have been studied using CC theory [260], among other things. The last decade's development of CC theory for nuclear applications has been reviewed by Hagen *et al.* [44].

At the core of CC theory is an exponential wave-function ansatz, which Coester suggested [29] to obtain a theory that fulfills the linked-diagram theorem [61, p. 152–153]. Theories that fulfill the linked-diagram theorem are size-extensive, which is a prerequisite to model large systems [157, p. 217]. Coupled-cluster theory scales polynomially with the number of occupied and unoccupied orbitals, and it is an efficient and accurate tool for calculations with small and medium-sized molecules and nuclei [33, 44]. Both CC theory and RSPT are size-extensive [61, p. 255] and nonvariational ([221, pp. 25–26] and [157, p. 219]) methods. In the CC singles and doubles (CCSD) approximation, which we define below, the CC equations contain certain RSPT diagrams, such as particle-particle and hole-hole ladders, mixed ladders, and particle-hole ring diagrams, summed to infinite order [52]. As shown in Refs. [157, pp. 315–317] and [221], the exponential form also arises naturally if different terms of the wave function ansatz contain all possible n-cluster correlations for $1 \leq n \leq A$, where A is the total number of particles. With this property, it is both convenient and, for many systems, physically motivated to truncate at a given maximum cluster size, including thereby, for example, only one- and two-particle clusters [157, pp. 313–315]. However, for sufficiently strongly correlated systems, such as liquid ^{3}He, wave functions truncated at a small maximum cluster size fail to describe the most important physics [43].

We follow here Refs. [61, pp. 251–291], [157, pp. 313–353], and [221] when introducing the general concepts of CC theory. Coupled-cluster theory starts from the assumption that the total wave function can be written in the exponential form

$$|\Psi_{CC}\rangle = e^{\hat{T}}|\Phi_0\rangle, \tag{5.1}$$

where $|\Phi_0\rangle$ is the Fermi vacuum state, the total cluster operator $\hat{T}$ is defined as the sum of cluster operators

$$\hat{T} = \sum_{m=1}^{A} \hat{T}_m, \tag{5.2}$$

and a single m-particle-m-hole cluster operator is defined as

$$\hat{T}_m = \left(\frac{1}{m!}\right)^2 \sum_{\substack{i_1,\ldots,i_m \\ a_1,\ldots,a_m}} t_{i_1,\ldots,i_m}^{a_1,\ldots,a_m} a_{a_1}^\dagger \ldots a_{a_m}^\dagger a_{i_m} \ldots a_{i_1}. \tag{5.3}$$

Here the labels $i_1, \ldots, i_m$ and $a_1, \ldots, a_m$ denote states occupied and unoccupied in $|\Phi_0\rangle$, respectively, $a_p^\dagger$ and a_p are creation and annihilation operators, respectively, and the CC amplitudes $t_{i_1,\ldots,i_m}^{a_1,\ldots,a_m}$ are unknowns that can be obtained by solving a set of nonlinear equations.

As explained in Refs. [157, pp. 322] and [221], the CC equations are obtained by projecting the Schrödinger equation

$$\hat{H} e^{\hat{T}} |\Phi_0\rangle = E e^{\hat{T}} |\Phi_0\rangle \tag{5.4}$$

onto the bra vectors

$$\langle \Phi_0 | e^{-\hat{T}}, \qquad \langle \Phi_{i_1,\ldots,i_m}^{a_1,\ldots,a_m} | e^{-\hat{T}}, \tag{5.5}$$

where $m = 1, 2, \ldots, A$ in the latter vector. In other words, the Hamiltonian operator $\hat{H}$ is replaced by a similarity-transformed operator $\overline{H}$, defined as

$$\overline{H} = e^{-\hat{T}} \hat{H} e^{\hat{T}}, \tag{5.6}$$

and the Hamiltonian equation of $\overline{H}$ is projected against the bra vectors $\langle \Phi_0|$ and $\langle \Phi_{i_1,\ldots,i_m}^{a_1,\ldots,a_m}|$, which form a complete basis in the given space of single-particle orbitals. The CC equations consist of the energy equation

$$\langle \Phi_0 | \overline{H} | \Phi_0 \rangle = E \tag{5.7}$$

and the amplitude equations

$$\langle \Phi_{i_1,\ldots,i_m}^{a_1,\ldots,a_m} | \overline{H} | \Phi_0 \rangle = 0, \qquad m = 1, 2, \ldots A. \tag{5.8}$$

In practical calculations, the CC amplitudes $t_{i_1,\ldots,i_m}^{a_1,\ldots,a_m}$ are first obtained by solving Eq. (5.8). Thereafter the CC amplitudes are used to calculate the energy from Eq. (5.7).

The coupled-cluster equations is, as presented above, an exact reformulation of the Schrödinger energy eigenvalue problem. Except for very simple model systems, few-

or many-body problems cannot be solved exactly. In quantum chemistry, the most common approach for approximating the coupled-cluster equations is to truncate the cluster operator (5.2) after $m = n$, where n is smaller than the number of particles [33, 221]. This truncation corresponds to including all possible combinations of clusters with a maximal size n. Approximations including $\hat{T}_1$, $\hat{T}_2$, $\hat{T}_3$, etc., are in the CC literature commonly denoted by singles (S), doubles (D), triples (T), etc., respectively [221]. For example, the CCSD approximation includes only $\hat{T}_1$ and $\hat{T}_2$, whereas in the CCD approximation only $\hat{T}_2$ is nonzero. The same approximations are sometimes called SUBn truncations [52], where, for example, the SUB2 approximation is equal to CCSD. An alternative family of approximations is the so-called Bochum truncation scheme [43], which is tailored for systems with hard-core interaction models. In this work, we consider only the SUBn truncation scheme of CC theory.

In the following, we give the explicit CC equations in the CCD approximation, as have been derived by, for example, Crawford and Schaefer [221]. The same equations are given in Papers II and III, but we repeat the basic expressions to make it easier to follow the discussions. In addition, these equations are also used in our studies of the homogeneous electron gas, which we present in Section 5.3. As is explained, for example, in Refs. [2, 52], conservation of momentum and symmetry makes the $\hat{T}_1$ amplitudes vanish for infinite homogeneous matter. For homogeneous matter, the CCD approximation is, therefore, equal to CCSD. We give the general equations in a momentum basis. For brevity, we neglect the spin and isospin degrees of freedom in the equations below.

The total CCD energy is split into two terms, that is,

$$E_{CCD} = E_{REF} + \Delta E_{CCD}, \tag{5.9}$$

where E_{REF} is the reference energy, defined as the Fermi vacuum expectation value

$$E_{REF} = \langle \Phi_0 | \hat{H} | \Phi_0 \rangle, \tag{5.10}$$

and ΔE_{CCD} is the remaining correction in the given approximation. Assuming that the Hamiltonian is of the form

$$\begin{aligned} \hat{H} = &\sum_{\mathbf{k}_p \mathbf{k}_q} \langle \mathbf{k}_p | h_0 | \mathbf{k}_q \rangle a^\dagger_{\mathbf{k}_p} a_{\mathbf{k}_q} \\ &+ \frac{1}{4} \sum_{\mathbf{k}_p \mathbf{k}_q} \sum_{\mathbf{k}_r \mathbf{k}_s} \langle \mathbf{k}_p \mathbf{k}_q | v | \mathbf{k}_r \mathbf{k}_s \rangle_{AS} a^\dagger_{\mathbf{k}_p} a^\dagger_{\mathbf{k}_q} a_{\mathbf{k}_s} a_{\mathbf{k}_r} + \frac{1}{2} A v_0, \end{aligned} \tag{5.11}$$

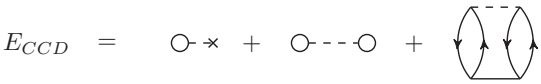

Figure 5.1: A diagrammatic expression for the CCD energy, as given in Figure 2 of Paper II. Reprinted by permission from G. Baardsen, A. Ekström, G. Hagen, and M. Hjorth-Jensen, Phys. Rev. C **88**, 054312 (2013). Copyright (2013) by the American Physical Society. `http://link.aps.org/abstract/PRC/v88/p054312`

where A is the number of particles and v_0 is a constant that is nonzero only in the finite-size electron gas, the reference energy is [221]

$$E_{REF} = \sum_{\mathbf{k}_i} \langle \mathbf{k}_i | \hat{h}_0 | \mathbf{k}_i \rangle + \frac{1}{2} \sum_{\mathbf{k}_i, \mathbf{k}_j} \langle \mathbf{k}_i \mathbf{k}_j | \hat{v} | \mathbf{k}_i \mathbf{k}_j \rangle_{AS} + \frac{1}{2} A v_0 \tag{5.12}$$

and the CCD correction [221]

$$\Delta E_{CCD} = \frac{1}{4} \sum_{\mathbf{k}_i, \mathbf{k}_j} \sum_{\mathbf{k}_a, \mathbf{k}_b} \langle \mathbf{k}_i \mathbf{k}_j | \hat{v} | \mathbf{k}_a \mathbf{k}_b \rangle_{AS} \langle \mathbf{k}_a \mathbf{k}_b | \hat{t} | \mathbf{k}_i \mathbf{k}_j \rangle, \tag{5.13}$$

where in the latter equation the CC amplitude is written using a bracket notation. In the following, we always use the bracket notation for the CC amplitudes. Figure 5.1 shows the CCD energy diagrammatically. In a Hartree-Fock single-particle basis, as is the plane-wave basis in infinite nuclear matter, the reference energy E_{REF} equals the Hartree-Fock energy and the rest is by definition the correlation energy.

Let us define the Fock operator as

$$\hat{F} = \sum_{p,q} \langle p | \hat{f} | q \rangle a_p^\dagger a_q, \tag{5.14}$$

where

$$\langle p | \hat{f} | q \rangle = \langle p | \hat{h}_0 | q \rangle + \sum_i \langle pi | \hat{v} | qi \rangle_{AS}. \tag{5.15}$$

The explicit expression of the CC $\hat{T}_2$ amplitude equation is given in, for example, Ref. [221]. Restricting ourself to the CCD approximation and writing the equations in a momentum basis, we get the $\hat{T}_2$ amplitude equation (see also Paper III)

$$\begin{aligned}
&\Big\{ \langle \mathbf{k}_i | \hat{f} | \mathbf{k}_i \rangle + \langle \mathbf{k}_j | \hat{f} | \mathbf{k}_j \rangle - \langle \mathbf{k}_a | \hat{f} | \mathbf{k}_a \rangle - \langle \mathbf{k}_b | \hat{f} | \mathbf{k}_b \rangle \Big\} \langle \mathbf{k}_a \mathbf{k}_c | \hat{t} | \mathbf{k}_i \mathbf{k}_j \rangle \\
&= \langle \mathbf{k}_a \mathbf{k}_b | \hat{v} | \mathbf{k}_i \mathbf{k}_j \rangle_{AS} \\
&+ \frac{1}{2} \sum_{\mathbf{k}_c, \mathbf{k}_d} \langle \mathbf{k}_a \mathbf{k}_b | \hat{v} | \mathbf{k}_c \mathbf{k}_d \rangle_{AS} \langle \mathbf{k}_c \mathbf{k}_d | \hat{t} | \mathbf{k}_i \mathbf{k}_j \rangle
\end{aligned}$$

$$
\begin{aligned}
&+\frac{1}{2}\sum_{\mathbf{k}_k,\mathbf{k}_l}\langle \mathbf{k}_a\mathbf{k}_b|\hat{t}|\mathbf{k}_k\mathbf{k}_l\rangle \\
&\times\left\{\langle \mathbf{k}_k\mathbf{k}_l|\hat{v}|\mathbf{k}_i\mathbf{k}_j\rangle_{AS}+\frac{1}{2}\sum_{\mathbf{k}_c,\mathbf{k}_d}\langle \mathbf{k}_k\mathbf{k}_l|\hat{v}|\mathbf{k}_c\mathbf{k}_d\rangle_{AS}\langle \mathbf{k}_c\mathbf{k}_d|\hat{t}|\mathbf{k}_i\mathbf{k}_j\rangle\right\} \\
&+\hat{P}(\mathbf{k}_i\mathbf{k}_j)\hat{P}(\mathbf{k}_a\mathbf{k}_b)\sum_{\mathbf{k}_k,\mathbf{k}_c}\langle \mathbf{k}_a\mathbf{k}_c|\hat{t}|\mathbf{k}_i\mathbf{k}_k\rangle \\
&\times\left\{\langle \mathbf{k}_k\mathbf{k}_b|\hat{v}|\mathbf{k}_c\mathbf{k}_j\rangle_{AS}+\frac{1}{2}\sum_{\mathbf{k}_l,\mathbf{k}_d}\langle \mathbf{k}_k\mathbf{k}_l|\hat{v}|\mathbf{k}_c\mathbf{k}_d\rangle_{AS}\langle \mathbf{k}_d\mathbf{k}_b|\hat{t}|\mathbf{k}_l\mathbf{k}_j\rangle\right\} \\
&-\frac{1}{2}\hat{P}(\mathbf{k}_i\mathbf{k}_j)\sum_{\mathbf{k}_k}\langle \mathbf{k}_a\mathbf{k}_b|\hat{t}|\mathbf{k}_i\mathbf{k}_k\rangle\left\{\sum_{\mathbf{k}_l}\sum_{\mathbf{k}_c,\mathbf{k}_d}\langle \mathbf{k}_k\mathbf{k}_l|\hat{v}|\mathbf{k}_c\mathbf{k}_d\rangle_{AS}\langle \mathbf{k}_c\mathbf{k}_d|\hat{t}|\mathbf{k}_j\mathbf{k}_l\rangle\right\} \\
&-\frac{1}{2}\hat{P}(\mathbf{k}_a\mathbf{k}_b)\sum_{\mathbf{k}_c}\langle \mathbf{k}_a\mathbf{k}_c|\hat{t}|\mathbf{k}_i\mathbf{k}_j\rangle\left\{\sum_{\mathbf{k}_k,\mathbf{k}_l}\sum_{\mathbf{k}_d}\langle \mathbf{k}_k\mathbf{k}_l|\hat{v}|\mathbf{k}_c\mathbf{k}_d\rangle_{AS}\langle \mathbf{k}_b\mathbf{k}_d|\hat{t}|\mathbf{k}_k\mathbf{k}_l\rangle\right\}, \qquad (5.16)
\end{aligned}
$$

where the permutation operator $\hat{P}$ is defined such that

$$
\hat{P}(x,y)\eta(x,y)=\eta(x,y)-\eta(y,x), \qquad (5.17)
$$

given an arbitrary function $\eta(x,y)$. In Eq. (5.16) we have assumed that the Fock operator is diagonal, as it is in homogeneous matter when the interaction conserves total momentum. The CC amplitude equations are commonly factorized to reduce the computational cost (see Ref. [221] and Paper III). Let us denote the expressions in brackets on right-hand side of Eq. (5.16) by

$$
\langle \mathbf{k}_k\mathbf{k}_l|I_1|\mathbf{k}_i\mathbf{k}_j\rangle,\langle \mathbf{k}_k\mathbf{k}_b|I_2|\mathbf{k}_c\mathbf{k}_j\rangle,\langle \mathbf{k}_k|I_3|\mathbf{k}_j\rangle,\langle \mathbf{k}_b|I_4|\mathbf{k}_c\rangle,
$$

so that the $\hat{T}_2$ amplitude equation (5.16) becomes (see Paper III)

$$
\begin{aligned}
&\left\{\langle \mathbf{k}_i|\hat{f}|\mathbf{k}_i\rangle+\langle \mathbf{k}_j|\hat{f}|\mathbf{k}_j\rangle-\langle \mathbf{k}_a|\hat{f}|\mathbf{k}_a\rangle-\langle \mathbf{k}_b|\hat{f}|\mathbf{k}_b\rangle\right\}\langle \mathbf{k}_a\mathbf{k}_c|\hat{t}|\mathbf{k}_i\mathbf{k}_j\rangle \\
&=\langle \mathbf{k}_a\mathbf{k}_b|\hat{v}|\mathbf{k}_i\mathbf{k}_j\rangle_{AS} \\
&+\frac{1}{2}\sum_{\mathbf{k}_c,\mathbf{k}_d}\langle \mathbf{k}_a\mathbf{k}_b|\hat{v}|\mathbf{k}_c\mathbf{k}_d\rangle_{AS}\langle \mathbf{k}_c\mathbf{k}_d|\hat{t}|\mathbf{k}_i\mathbf{k}_j\rangle \\
&+\frac{1}{2}\sum_{\mathbf{k}_k,\mathbf{k}_l}\langle \mathbf{k}_a\mathbf{k}_b|\hat{t}|\mathbf{k}_k\mathbf{k}_l\rangle\langle \mathbf{k}_k\mathbf{k}_l|I_1|\mathbf{k}_i\mathbf{k}_j\rangle \\
&+\hat{P}(\mathbf{k}_i\mathbf{k}_j)\hat{P}(\mathbf{k}_a\mathbf{k}_b)\sum_{\mathbf{k}_k,\mathbf{k}_c}\langle \mathbf{k}_a\mathbf{k}_c|\hat{t}|\mathbf{k}_i\mathbf{k}_k\rangle\langle \mathbf{k}_k\mathbf{k}_b|I_2|\mathbf{k}_c\mathbf{k}_j\rangle \\
&-\frac{1}{2}\hat{P}(\mathbf{k}_i\mathbf{k}_j)\sum_{\mathbf{k}_k}\langle \mathbf{k}_a\mathbf{k}_b|\hat{t}|\mathbf{k}_i\mathbf{k}_k\rangle\langle \mathbf{k}_k|I_3|\mathbf{k}_j\rangle
\end{aligned}
$$

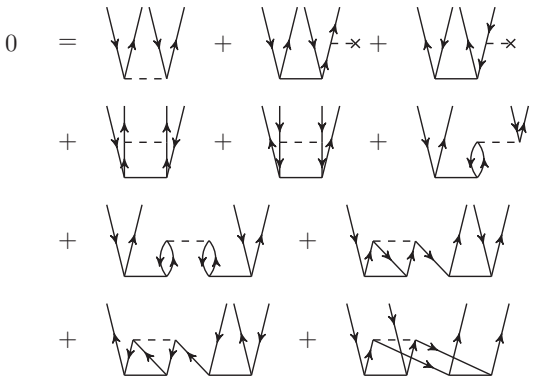

Figure 5.2: The CCD $\hat{T}_2$ amplitude equation, as illustrated in Figure 1 of Paper II. Reprinted by permission from G. Baardsen, A. Ekström, G. Hagen, and M. Hjorth-Jensen, Phys. Rev. C **88**, 054312 (2013). Copyright (2013) by the American Physical Society. `http://link.aps.org/abstract/PRC/v88/p054312`

$$-\frac{1}{2}\hat{P}(\mathbf{k}_a\mathbf{k}_b)\sum_{\mathbf{k}_c}\langle\mathbf{k}_a\mathbf{k}_c|\hat{t}|\mathbf{k}_i\mathbf{k}_j\rangle\langle\mathbf{k}_b|I_4|\mathbf{k}_c\rangle. \tag{5.18}$$

As was suggested first by Scuseria *et al.* [261], the computational cost is significantly reduced by computing the intermediates separately before substituting them into the amplitude equation. For example, the computational cost of evaluating the second term of I_1 may be reduced from the order $\sim n_h^4 n_p^4$ to $\sim n_h^4 n_p^2$, where n_h and n_p are the number of occupied and unoccupied orbitals, respectively [221]. Typically, n_p is much larger than n_h, and the scaling in terms of n_p is, therefore, the dominant contribution to the computational cost. The CCD $\hat{T}_2$ amplitude equation is given diagrammatically in Figure 5.2.

As explained in Paper II, we solve the system of CC amplitude equations using a fixed-point iteration scheme [221]. Let $\mathbf{T}_n$ be the CC $\hat{T}_2$ amplitude matrix, as obtained in iteration n when solving the amplitude equations. In systems with strong correlations, such as symmetric nuclear matter calculated with the AV18 potential [239] and the two-dimensional electron gas at not very high densities, the iteration scheme described in Paper II does not converge. When studying such systems, convergency can in many cases be obtained by updating the $\hat{T}_2$ amplitude matrix as [262]

$$\mathbf{T}_n \leftarrow \alpha\mathbf{T}_n + (1-\alpha)\mathbf{T}_{n-1}, \tag{5.19}$$

where $\alpha \in (0,1)$, $\mathbf{T}_{n-1}$ is the amplitude matrix of the previous iteration, and the arrow denotes the assignment operator. The solution obtained using Eq. (5.19) is also a

solution to the normal fixed-point equation

$$\mathbf{T} = R(\mathbf{T}), \tag{5.20}$$

where R is the function of $\mathbf{T}$ on right-hand side. Let us show it briefly, following arguments by Simen Kvaal. Assuming that the iteration has converged at step $n-1$, it holds that

$$\mathbf{T}_{n+1} = R(\alpha\mathbf{T}_n + (1-\alpha)\mathbf{T}_{n-1}) \tag{5.21}$$

and $\mathbf{T}_{n+1} = \mathbf{T}_n = \mathbf{T}_{n-1}$ to the chosen accuracy. This gives

$$\begin{aligned}\mathbf{T}_{n+1} &= R(\alpha\mathbf{T}_n + (1-\alpha)\mathbf{T}_n) \\ &= R(\mathbf{T}_n),\end{aligned} \tag{5.22}$$

which means that the solution obtained using Eq. (5.19) is also a solution to the normal fixed-point equation (5.20).

Let us for a moment consider only the terms that are linear in the $\hat{T}_2$ amplitudes on right-hand side of Eq. (5.16). The terms on the second, third and fifth to the sixth row on the right-hand side have summations over two particle states, two hole states and one hole and one particle state, respectively. The term with summation over two particle states, that is, the term

$$\frac{1}{2}\sum_{\mathbf{k}_c,\mathbf{k}_d}\langle\mathbf{k}_a\mathbf{k}_b|\hat{v}|\mathbf{k}_c\mathbf{k}_d\rangle_{AS}\langle\mathbf{k}_c\mathbf{k}_d|\hat{t}|\mathbf{k}_i\mathbf{k}_j\rangle$$

is commonly called the particle-particle ladder contribution. Similarly, the linear term with summation over two hole states, that is,

$$\frac{1}{2}\sum_{\mathbf{k}_k,\mathbf{k}_l}\langle\mathbf{k}_a\mathbf{k}_b|\hat{t}|\mathbf{k}_k\mathbf{k}_l\rangle\langle\mathbf{k}_k\mathbf{k}_l|\hat{v}|\mathbf{k}_i\mathbf{k}_j\rangle_{AS}$$

is called the hole-hole ladder contribution. The term

$$\hat{P}(\mathbf{k}_i\mathbf{k}_j)\hat{P}(\mathbf{k}_a\mathbf{k}_b)\sum_{\mathbf{k}_k,\mathbf{k}_c}\langle\mathbf{k}_a\mathbf{k}_c|\hat{t}|\mathbf{k}_i\mathbf{k}_k\rangle\langle\mathbf{k}_k\mathbf{k}_b|\hat{v}|\mathbf{k}_c\mathbf{k}_j\rangle_{AS},$$

with summation over one particle and one hole state, gives particle-hole ring contributions. The linear particle-particle ladder, hole-hole ladder, and particle-hole ring terms, respectively, are given diagrammatically on the second line of Figure 5.2. As is described in Papers II and III, the particle-particle and hole-hole ladder approximation (PPHH-LAD) is obtained from the CCD equations by setting the second term of I_1, as well as I_2, I_3, and I_4, to zero. The particle-particle ladder approximation (PP-LAD)

is otherwise like PPHH-LAD, but in PP-LAD the entire intermediate I_1 is neglected. Diagrammatically, the PPHH-LAD approximation is given by the five first diagrams, and the PP-LAD approximation by the four first diagrams, in Figure 5.2. We have given explicit linear CC ladder equations in Papers II and III.

As explained in Ref. [52], the PP-LAD approximation generates short-range correlation contributions in a similar way as in the Brueckner G-matrix equation. In the PPHH-LAD approximation, particle-particle and hole-hole ladder diagrams are summed to infinite order, similarly as, for example, in the ladder approximation of the self-consistent Green's function (SCGF) method [62]. The CC ladder approximations differ from the BHF and SCGF methods in that the single-particle potentials are not solved self-consistently, but instead include only the Hartree-Fock contribution. As shown in Refs. [51, 52], the linear particle-hole term together with the interaction term generate the direct and exchange parts of ring diagrams with forward time-order. Bishop and Lührmann [52] explain thoroughly how the full CCD approximation contains ladder diagrams, the random phase approximation (RPA), and a large number of other diagrams to infinite order. Observe that in CC theory, the different contributions also couple to each other, thereby generating additional diagrams [52, 53].

In the following sections, we discuss applications of the CC method for nuclear matter and the electron gas.

5.2 Applications for nuclear matter

As we described in Chapter 2, it has been a long-standing problem in nuclear physics to properly model the nuclear matter equation of state using realistic nuclear interaction models (for historical reviews, see, for example, Refs. [2, 3, 9, 43, 62, 65, 66, 118, 140, 168, 182]). In this context, an important quantity is the energy per nucleon as a function of the particle density. In our studies, we assume that the temperature is much smaller than the Fermi temperature so that a zero-temperature approximation is appropriate. We have also chosen to model the systems using nonrelativistic quantum mechanics. In most many-body quantum approaches, including the CC method, the energy at zero temperature is obtained from the basic formulation of the theory. Therefore, we get essential input to the nuclear matter equation of state by solving the CC equations as explained in Section 5.1.

More than thirty years ago, Day and Zabolitzky studied the nuclear matter equation of state [17] using the Bochum truncation [43] of CC theory. Day and Zabolitzky did calculations including reduced two- and three-particle subsystem amplitudes, as well as an estimate of the four-particle amplitude [17]. One aim of this thesis has been to

take up again the work on coupled-cluster theory for nuclear matter, now using the n-particle-n-hole, or SUBn, truncation scheme explained in Section 5.1 together with modern nuclear interaction models. The latter truncation scheme has been successfully applied to finite nuclei [35, 37, 39, 41, 257–259, 263], and it is, therefore, of interest to extend the method to the limit of infinitely many nucleons.

In Section 5.2.1, we give a short presentation of Paper I. Section 5.2.2 is devoted to Paper II, where we have derived CC ladder equations in a partial-wave basis using exact Pauli exclusion operators [64]. We discuss how we have implemented the CC ladder equations for nuclear matter at the thermodynamic limit. Thereafter, we show how the method and code have been verified, and we mention some of the results from Paper II. In Paper III, infinite nuclear matter is modeled using finite-sized boxes, and the thermodynamic limit is approximated by using twist-averaged boundary conditions [72]. Paper III is presented in Section 5.2.3. As we explain in Section 5.2.4, it seems difficult to extend the partial-wave-expanded CC ladder approximation of Paper II to a complete CCD approximation. In Section 5.2.5, we discuss how the CC equations for nuclear matter can be implemented using a spherical Bessel basis.

5.2.1 A reparametrized interaction model

Our collaborators have obtained a new parametrization of a nuclear interaction model derived from chiral perturbation theory [15]. This optimized interaction is presented in Paper I. The parameters of the nucleon-nucleon interaction, which is truncated after next-to-next-to-lowest order, are optimized to reproduce experimentally extracted phase-shifts given by the Nijmegen group [232]. The optimization is done using the efficient POUNDERS optimization algorithm [248, 249], as described in Paper I and in Chapter 3. To test the optimized nucleon-nucleon force, $\mathrm{NNLO_{opt}}$, we do calculations on different physical systems, in which the three-nucleon force is known to be important. When studying excitation energies of ^{10}B and various Ca isotopes, as well as binding energies of neutron-rich oxygen isotopes, our collaborators get better agreement with experiments than when using the N^{3}LO chiral interaction of Entem and Machleidt [70]. We also study pure neutron matter using the CC particle-particle and hole-hole ladder approximation of Paper II. In Paper I, the calculations are wrongly said to be done using the particle-particle ladder approximation. Similarly as in the studies of nuclei, we get closer agreement with calculations that include a three-nucleon force when using the $\mathrm{NNLO_{opt}}$ as compared to calculations with the N^{3}LO interaction of Ref. [70] (see Paper I).

5.2.2 Ladder approximation at the thermodynamic limit

As a first step towards new and improved CC calculations for nuclear matter, we have approximated the CCD amplitude equations (5.16) by including only particle-particle ladder diagrams, which are necessary to properly treat the short-range correlations between nucleons [7, 62], and hole-hole ladder diagrams, which constitute the symmetric counterpart for hole states. Our work has been described in detail in Paper II, and here we only give a brief introduction.

In Chapter 4, we explained how the BHF equations for infinite nuclear matter are commonly simplified using an angular-average approximation of the Pauli exclusion operators (3.32) and (3.33). The angular-average approximation, defined by Eqs. (4.37) and (4.38), is obtained by replacing the exact Pauli operators with averages integrated over the angle between the relative and CM momentum vectors. This approximation makes the BHF equations considerably simpler, as the G matrix becomes diagonal in the total angular momentum $\mathcal{J}$ and its projection $m_{\mathcal{J}}$ [64]. As shown in Refs. [64, 144], the error in the BHF binding energy of symmetric nuclear matter introduced by using angular-averaged Pauli exclusion operators is of the order 0.2–0.5 MeV.

Suzuki *et al.* [64] have suggested an approach to expand the exact Pauli operators of the BHF equations in partial waves. In Paper II, we derive explicit expressions for the CC ladder equations using this technique. When using exact Pauli operators, the CC ladder equations become complex, and storing the amplitude matrix becomes intractable. To make the computations manageable, we simplify the amplitude matrix by employing an angular-average approximation [8] of the momentum arguments in the single-particle energies, as shown in Eqs. (4.41), (4.49) and (4.50). When using these approximated single-particle energies, the amplitude matrix gets a symmetry that makes it possible to evaluate the matrix elements for only one direction of the CM momentum vector, and then use a rotation matrix to obtain matrix elements for other CM momentum directions (see Paper II and Ref. [64]). Using the rotation matrix, we are, therefore, able to decrease the size of the amplitude matrix further. The angular-average approximation in the single-particle energies also opens the possibility to use simplified formulae for the exact Pauli operators, as introduced by Suzuki *et al.* [64].

Implementation

Next, we discuss our implementation of the partial-wave-expanded CC ladder equations with exact Pauli operators, given as Eqs. (18) and (23) in Paper II. The ladder equations with angular-averaged Pauli operators may be implemented in a similar way.

As stated above, the nuclear interaction is diagonal in the total two-particle spin S, in the isospin projection M_T, and in the total relative angular momentum $\mathcal{J}$. Because of this symmetry, we store the interaction matrices in blocks of the conserved quantum numbers, as is commonly done in quantum chemistry [221]. Utilization of block diagonality decreases the memory consumption significantly, and it can also greatly reduce the number of floating-point operations. However, as shown in Paper II, the Pauli exclusion operators and the $\hat{T}_2$ amplitude matrix are not diagonal in $\mathcal{J}$ and its projection $m_{\mathcal{J}}$. Furthermore, these matrices depend on the radial CM momentum K, and the Pauli operators are also functions of the angle θ_K related to the CM momentum.

The CC energy equation (18) of Paper II may be written as

$$\begin{aligned}\Delta E_{CCD}/A = \text{Constant} \times &\sum_{SM_T} \sum_{\mathcal{J}m_{\mathcal{J}}} \sum_{\mathcal{J}''m_{\mathcal{J}''}} \sum_{\mathcal{J}'''m_{\mathcal{J}'''}} \sum_{m_{\mathcal{J}'}} \\ \times &\sum_{K_i} K_i^2 \omega_{K_i} \sum_{\theta_j} \sin\theta_j \omega_{\theta_j} d^{\mathcal{J}''}_{m_{\mathcal{J}''}m_{\mathcal{J}'}}(\theta_j) d^{\mathcal{J}'''}_{m_{\mathcal{J}'''}m_{\mathcal{J}'}}(\theta_j) \\ \times &\operatorname{Tr}\left[\mathbf{V}^{SM_T\mathcal{J}} \mathbf{Q}_{pp}^{SM_TK_i\mathcal{J}m_{\mathcal{J}}\mathcal{J}''m_{\mathcal{J}''}\theta_j} \mathbf{T}^{SM_TK_i\mathcal{J}''m_{\mathcal{J}'}\mathcal{J}'''} \mathbf{Q}_{hh}^{SM_TK_i\mathcal{J}'''m_{\mathcal{J}'''}\mathcal{J}m_{\mathcal{J}}\theta_j}\right], \end{aligned} \tag{5.23}$$

where the two-body interaction, the Pauli operators and the $\hat{T}_2$ amplitudes are expressed as matrices. Here K_i and θ_j are radial and angular coordinates of the CM momentum, ω_{K_i} and ω_{θ_j} are the corresponding quadrature weights, and the function d is part of the Wigner D function, defined in Ref. [227, pp. 72–74 and 76]. Using the relation [264, p. 19]

$$\operatorname{Tr}[\mathbf{AB}] = \operatorname{Tr}[\mathbf{BA}] \tag{5.24}$$

for the trace of a matrix-matrix product, we can replace the trace in Eq. (5.23) by

$$\operatorname{Tr}\left[\mathbf{M}^{SM_TK_i\mathcal{J}m_{\mathcal{J}}\mathcal{J}''m_{\mathcal{J}''}\mathcal{J}'''m_{\mathcal{J}'''}\theta_j} \mathbf{T}^{SM_TK_i\mathcal{J}''m_{\mathcal{J}'}\mathcal{J}'''}\right], \tag{5.25}$$

where

$$\begin{aligned}\mathbf{M}^{SM_TK_i\mathcal{J}m_{\mathcal{J}}\mathcal{J}''m_{\mathcal{J}''}\mathcal{J}'''m_{\mathcal{J}'''}\theta_j} = &\mathbf{Q}_{hh}^{SM_TK_i\mathcal{J}'''m_{\mathcal{J}'''}\mathcal{J}m_{\mathcal{J}}} \\ &\times \mathbf{V}^{SM_T\mathcal{J}} \mathbf{Q}_{pp}^{SM_TK_i\mathcal{J}m_{\mathcal{J}}\mathcal{J}''m_{\mathcal{J}''}\theta_j}. \end{aligned} \tag{5.26}$$

The matrix $\mathbf{M}$ does not change during the CC self-consistency loop and is, therefore, set up only once at the beginning of the calculations. We evaluate the trace as

$$\operatorname{Tr}[\mathbf{MT}] = \sum_{\alpha} \left(\sum_{\beta} M_{\alpha\beta} T_{\beta\alpha} \right), \tag{5.27}$$

and a matrix-matrix multiplication is therefore not necessary. Assuming that $\mathbf{M}$ has dimension $n \times m$ and $\mathbf{T}$ dimension $m \times n$, the simplification in Eq. (5.27) reduces the order of floating-point operations from the order of m^2n^2 [265, p. 18] to mn.

We further simplify the CC energy equation and write it as

$$\Delta E_{CCD}/A = \text{Constant} \times \sum_{K_i} \sum_{SM_T} \sum_{\mathcal{J}'' m_{\mathcal{J}'}} \sum_{\mathcal{J}'''} \times \sum_{\alpha} \left(\sum_{\beta} \tilde{T}_{\alpha\beta}^{SM_T K_i \mathcal{J}'' m_{\mathcal{J}'} \mathcal{J}'''} O_{\beta\alpha}^{SM_T K_i \mathcal{J}'' m_{\mathcal{J}'} \mathcal{J}'''} \right), \tag{5.28}$$

where the matrix elements $\tilde{T}_{\alpha\beta}$ are defined as

$$\tilde{T}_{\alpha\beta}^{SM_T K_i \mathcal{J}'' m_{\mathcal{J}'} \mathcal{J}'''} = T_{\alpha\beta}^{SM_T K_i \mathcal{J}'' m_{\mathcal{J}'} \mathcal{J}'''} / \Delta\tilde{\varepsilon}(k_\alpha, k_\beta, K_i), \tag{5.29}$$

that is, a $\hat{T}_2$ amplitude divided by an energy denominator. The matrix $\mathbf{O}$ is defined such that

$$\mathbf{O}^{SM_T K_i \mathcal{J}'' m_{\mathcal{J}'} \mathcal{J}'''} = \sum_{\mathcal{J} m_{\mathcal{J}}} \sum_{m_{\mathcal{J}''} m_{\mathcal{J}'''}} \sum_{\theta_j} \mathbf{N}^{(SM_T K_i \mathcal{J}'' m_{\mathcal{J}'} \mathcal{J}''')(\mathcal{J} m_{\mathcal{J}} m_{\mathcal{J}''} m_{\mathcal{J}'''} \theta_j)}, \tag{5.30}$$

where

$$\begin{aligned} &\mathbf{N}^{(SM_T K_i \mathcal{J}'' m_{\mathcal{J}'} \mathcal{J}''')(\mathcal{J} m_{\mathcal{J}} m_{\mathcal{J}''} m_{\mathcal{J}'''} \theta_j)} \\ &= K_i^2 \omega_{K_i} \sin\theta_j \omega_{\theta_j} d^{\mathcal{J}''}_{m_{\mathcal{J}''} m_{\mathcal{J}'}}(\theta_j) d^{\mathcal{J}'''}_{m_{\mathcal{J}'''} m_{\mathcal{J}'}}(\theta_j) \\ &\times \mathbf{M}^{SM_T K_i \mathcal{J} m_{\mathcal{J}} \mathcal{J}'' m_{\mathcal{J}''} \mathcal{J}''' m_{\mathcal{J}'''} \theta_j}. \end{aligned} \tag{5.31}$$

Similarly as for the energy equation, we write the amplitude equation as

$$\begin{aligned} \mathbf{T}^{SM_T K_i \mathcal{J}' m_{\mathcal{J}} \mathcal{J}} &= \mathbf{V}^{SM_T \mathcal{J}} \delta_{\mathcal{J}\mathcal{J}'} \\ &+ \frac{1}{2} \sum_{\mathcal{J}''} \tilde{\mathbf{T}}^{SM_T K_i \mathcal{J}' m_{\mathcal{J}} \mathcal{J}''} \mathbf{W}^{SM_T K_i \mathcal{J}'' m_{\mathcal{J}} \mathcal{J}} \\ &+ \frac{1}{2} \sum_{\mathcal{J}''} \mathbf{U}^{SM_T K_i \mathcal{J}' m_{\mathcal{J}} \mathcal{J}''} \tilde{\mathbf{T}}^{SM_T K_i \mathcal{J}'' m_{\mathcal{J}} \mathcal{J}}, \end{aligned} \tag{5.32}$$

where we have used the definitions

$$\mathbf{W}^{SM_T K_i \mathcal{J}'' m_{\mathcal{J}} \mathcal{J}} = \mathbf{Q}_{hh}^{SM_T K_i \mathcal{J}'' m_{\mathcal{J}} \mathcal{J} m_{\mathcal{J}}} \mathbf{V}^{SM_T \mathcal{J}} \tag{5.33}$$

and

$$\mathbf{U}^{SM_T K_i \mathcal{J}' m_{\mathcal{J}} \mathcal{J}''} = \mathbf{V}^{SM_T \mathcal{J}'} \mathbf{Q}_{pp}^{SM_T K_i \mathcal{J}' m_{\mathcal{J}} \mathcal{J}'' m_{\mathcal{J}}}. \tag{5.34}$$

The different matrices are stored in lists of matrices, where the list index is determined by the superscript quantum numbers. For example, the matrices $\mathbf{O}^{SM_TK_i\mathcal{J}''m_{\mathcal{J}'}\mathcal{J}'''}$ are stored as elements in a list in which the quantum numbers S, M_T, K_i, $\mathcal{J}''$, $m_{\mathcal{J}'}$, and $\mathcal{J}'''$ determine the location. To obtain sufficient accuracy, the grid in relative momentum must be set up such that the total interval is split at the points where the derivatives of the Pauli operators are discontinuous. In our numerical integrations, we use Gauss-Legendre quadrature [254, pp. 140–146].

In our calculations, we set up the matrices $\mathbf{O}$, $\mathbf{W}$, and $\mathbf{U}$ only once, and then we use Eqs. (5.28) and (5.32) to evaluate the energy in each iteration of the CC self-consistency loop. In large calculations, most of the computing time is used to set up the matrix $\mathbf{O}$. By setting up this matrix only once, the computing time of a typical symmetric nuclear matter calculation, therefore, decreases by approximately a factor of ten. To utilize the computing power of large computing clusters, we have parallelized the code using both the Message Passing Interface (MPI) Standard [266, 267] and OpenMP [268]. MPI is a standard for parallelization that is designed to work on computers with distributed memory [266, pp. 1–20]. Therefore, we use MPI to share work load between different computing nodes on a supercomputer. We split the CC ladder equations into parts corresponding to different CM momentum values K_i and distribute these parts to different MPI processes. As mentioned above, most of the computing time is used to set up the matrix $\mathbf{O}$. The code can therefore be further optimized by parallelizing the setup of $\mathbf{O}$ on each computing node. In our program, we use OpenMP to parallelize the setup of the matrices $\mathbf{O}^{SM_TK_i\mathcal{J}''m_{\mathcal{J}'}\mathcal{J}'''}$ locally on the different computing nodes.

Verification and results

We have verified our Hartree-Fock code for nuclear matter by comparing with results in Ref. [158] and with numbers provided by Scott Bogner. Our implementations of the BHF method were tested against results in Refs. [45, 67, 104]. When comparing different BHF energies, we found sometimes not negligible deviations, probably due to differences in the implementations, such as angular-average approximations [67], handling of singularities in the G matrix (see Refs. [67] and [235, pp. 112–114]), and in some older calculations possibly too low momentum cutoffs in the single-particle potentials [269]. As mentioned in Paper II, our BHF saturation energy for symmetric nuclear matter, obtained with the N^{3}LO interaction [70], differs approximately 0.5 MeV from the energy given by Li *et al.* [45]. As explained in Appendix C, the BHF results in Figs. 7 and 8 of Paper II were accidentally calculated using wrong partial waves.

This error was done only when making the figures, and the numbers given in Paper II are not affected.

As can be seen from the CC ladder equations, the first iteration of both the PP-LAD and PPHH-LAD approximations give the MBPT(2) energy. Similarly, the second iteration of the PP-LAD approximation is identical to the MBPT(2) approximation plus the particle-particle ladder diagram (4.26) of third-order perturbation theory. The second iteration of the hole-hole ladder (HH-LAD) approximation, which is obtained from PPHH-LAD by removing the particle-particle ladders, gives the same result as MBPT(2) plus the hole-hole ladder term (4.27) present in third-order perturbation theory. As part of the verification of our CC ladder approximations, we compared the first iterations of the CC calculations with results from many-body perturbation theory.

If the G-matrix elements in the single-particle potential (4.31) of the BHF equations are replaced by bare interaction-matrix elements, the PP-LAD approximation is obtained (see Paper II). We used such a modified BHF approximation to verify our implementation of the PP-LAD approach with angular-averaged Pauli exclusion operators. When comparing the modified BHF method with the PP-LAD approximation, we obtained the same results to an accuracy of 0.01 MeV.

We have also compared our MBPT(2) and PP-LAD implementations utilizing angular-averaged Pauli operators with results provided by Scott Bogner. When using the N^{3}LO chiral nucleon-nucleon interaction of Ref. [70], we got differences of approximately 0.001–0.05 MeV for Fermi momenta between 1.2 and 1.8 fm^{-1}. In these calculations, Scott Bogner used the method explained in Ref. [22], modified here to include only the Hartree-Fock single-particle potential.

Our implementations of the exact Pauli operators were tested using different formulae given by Suzuki *et al.* [64]. The CC ladder equations with angular-averaged Pauli operators are given in Eqs. (26) and (27) of Paper II, and the same equations for exact Pauli operators in Eqs. (18) and (23) of the same publication. As seen from the expressions, the equations with exact Pauli operators are much more complex than the counterpart with angular-averaged Pauli operators. To compare our implementations of these equations, we replaced the exact Pauli operators in Eqs. (18) and (23) of Paper II by the operator

$$\begin{aligned}\overline{Q}(l\mathcal{J}m_{\mathcal{J}}, l'\mathcal{J}', m_{\mathcal{J}'}; SM_TkK\theta_K\phi_Kk_F) = \mathcal{A}^{lSM_T}\mathcal{A}^{l'SM_T} \\ \times \overline{Q}(k, K, k_F)\delta_{ll'}\delta_{\mathcal{J}\mathcal{J}'}\delta_{m_{\mathcal{J}}m_{\mathcal{J}'}},\end{aligned} \tag{5.35}$$

given in Eq. (2.16) of Ref. [64]. Here $\overline{Q}(k, K, k_F)$ is a normal angular-averaged Pauli operator, given by Eqs. (4.37) and (4.38), and $\mathcal{A}^{lSM_T}$ is the antisymmetrization operator

defined in Eq. (A.5). With this replacement, the CC ladder equations designed for exact and angular-averaged Pauli operators give the same result.

Our implementation of the CC ladder approximations with exact Pauli operators was further verified in Paper III. Given that convergence is obtained in the number of momentum grid points, the only approximations of the CC ladder equations in Paper II are the angular-average approximation in the single-particle potential and a finite cutoff in angular momentum. As seen from Figure 6 of Paper II, the error owing to the cutoff in angular momentum is smaller than approximately 0.3 MeV. We have not been able directly to quantify the error related to the angular-average approximation in the single-particle potentials. However, in Paper III we show that a CC ladder approximation with a finite number of particles in a box and twist-averaged boundary conditions gives energies within 0.1–0.2 MeV from the ladder approximation described above. The good agreement between these two quite different approaches indicates that the error owing to the angular-averaged single-particle potentials is small. Different CC ladder approximations are compared with the BHF method in Paper II. As we describe in Section 5.2.3, in Paper III we also compare our CC ladder approximation with the AFDMC approach.

In Paper II, we study CC ladder approximations with exact and angular-averaged Pauli exclusion operators. Using exact Pauli operators, we get energies that are at most about 0.2 MeV from the energies obtained using angular-averaged Pauli operators. Similarly as observed in the BHF method [64, 144], exact treatment of the Pauli exclusion operators gives more binding for symmetric nuclear matter. In pure neutron matter, we find that the angular-average approximation of Pauli operators has a much smaller effect on the binding energy (see Paper II). In Figure 5.3, we compare equations of state for symmetric nuclear matter, as obtained in MBPT(2) using angular-averaged and exact Pauli operators. As a nuclear two-body interaction, we use the optimized chiral interaction $\mathrm{NNLO}_{\mathrm{opt}}$ given in Paper I, and both calculations are done with a cutoff in total angular momentum $\mathcal{J} \leq 8$ for the correlation energy and $\mathcal{J} \leq 24$ for the Hartree-Fock potential. The energy denominators are approximated by an angular-average approximation, as described in Paper II. The difference between the equations of state obtained with exact and angular-averaged Pauli operators is of the same size as the differences we observed for the PP-LAD and PPHH-LAD approximations in Paper II.

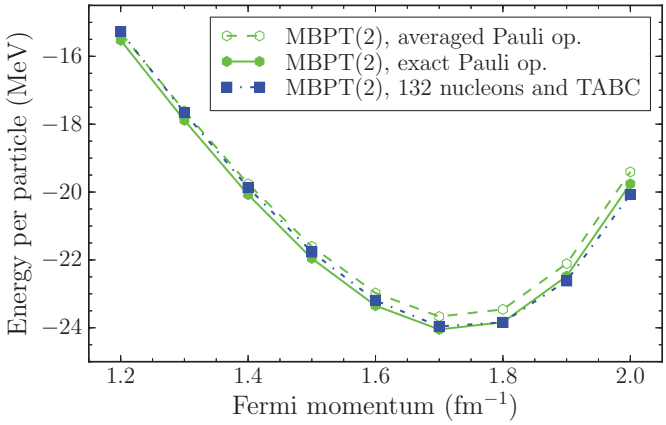

Figure 5.3: Energy per particle for symmetric nuclear matter given as a function of the Fermi momentum k_F. Similarly as in the PPHH-LAD and BHF approximations, the energy in second-order perturbation theory (MBPT(2)) has more binding with exact than with angular-averaged Pauli exclusion operators. The approximations with exact and angular-averaged Pauli operators differ by 0.22–0.38 MeV. For comparison, the figure also shows energies in MBPT(2) as obtained with 132 nucleons and twist-averaged boundary conditions (TABC) using three twist points in each Cartesian direction. The latter results are from Paper III. The energies obtained with partial-wave expansion, exact Pauli operators, and angular-averaged single-particle energies at the thermodynamic limit differ from the results obtained with a finite number of particles by at most 0.26 MeV, and at the saturation density by only 0.09 MeV. All calculations were done with the $\mathrm{NNLO}_{\mathrm{opt}}$ nucleon-nucleon interaction, which was presented in Paper I.

5.2.3 Finite-box approximations of nuclear matter

As we discuss in Section 5.2.4, it is not easy to extend the CC ladder approximation of Paper II to a full CCD approximation. The particle-hole diagrams, for example, become complicated when expressed in relative coordinates using a partial-wave expansion. In Paper III, the CC equations for infinite nuclear matter are written in laboratory-frame coordinates, with discretization in momentum space. The CC equations are generally defined in laboratory coordinates [221], and it is, therefore, straightforward to extend the approach described in Paper III to different truncation levels, such as CCD, CCDT, etc.

In Paper III, infinite nuclear matter is approximated by a finite cubic box containing a fixed number of nucleons. The single-particle basis is as defined in Eqs. (3.20)–(3.23), with discretization in Cartesian momentum coordinates. The total momentum is zero, and the symmetry is correct, for certain closed-shell configurations. When using a finite number of particles to approximate infinite nuclear matter, there will be an error related to the discretization in momentum space [72]. To get faster convergence towards the thermodynamic limit as the total nucleon number is increased, our collaborators take average over different twisted boundary conditions, similarly as was done in Ref. [72] for the electron gas (see Paper III).

The CC ladder approximation described in Paper II is formulated at the thermodynamic limit. The calculations have an error related to a cutoff in total angular momentum, which we estimate to be less than 0.3 MeV (see Figure 6 in Paper II). In addition, the single-particle energies are calculated using an angular-average approximation, which gives an error that we did not quantify in Paper II. In Paper III, we compare two different implementations of the CC ladder approximation for nuclear matter: the approach of Paper III, with twist-averaged boundary conditions, is compared with calculations defined at the thermodynamic limit, as described in Paper II. The two approaches give binding energies closer than the error associated with the angular-momentum cutoff of the latter method (see Paper III). This agreement between the two quite different implementations indicates that the twist-average technique is able to approximate the thermodynamic limit well. Furthermore, it seems that the error related to the angular-averaged single-particle energies is small. The same conclusion can be drawn from the MBPT(2) results in Figure 5.3.

To validate the CC approaches of Papers II and III, in Paper III we compare the CC approximations with the AFDMC [73] method, which is considered to be an accurate many-body approach. We do the calculations using the Minnesota potential [74]; see Section 3.2.4. As shown in Figure 5.4, both the CCD approximation of Paper

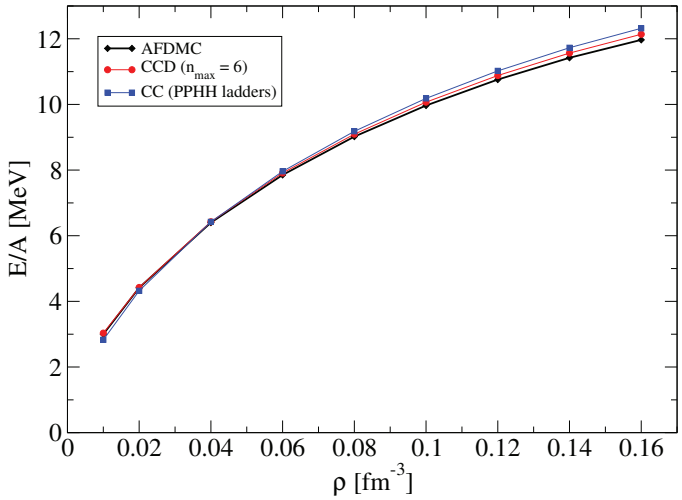

Figure 5.4: Neutron matter equations of state, as obtained with the AFDMC [73] method, the CCD approximation of Paper III, and the CC particle-particle and hole-hole ladder approximation of Paper II, using the Minnesota nucleon-nucleon interaction [74]. The figure is from Paper III. Reprinted by permission from G. Hagen, T. Papenbrock, A. Ekström, K. A. Wendt, G. Baardsen, S. Gandolfi, M. Hjorth-Jensen, and C. J. Horowitz, Phys. Rev. C **89**, 014319 (2014). Copyright (2014) by the American Physical Society. `http://link.aps.org/abstract/PRC/v89/p014319`

III, which uses twist-averaged boundary conditions, and the CC ladder approximation of Paper II, which is defined in the thermodynamic limit, give results close to those of the AFDMC method (see Paper III). These results indicate that the CC ladder approximation describes the most important correlations in pure neutron matter, at least in the special case when the nucleon-nucleon interaction is modeled using the simple Minnesota potential. Calculations using more realistic chiral interactions from Paper I also show that the CCD and CCD(T) approximations give no apparent important contributions to the neutron matter equation of state beyond the results obtained with CC ladder approximation (see Paper III). Based on the results of Paper III, we may conclude that the CC ladder approximation is an accurate tool to model neutron matter.

In contrast, the results of Paper III show that higher-order correlations are crucial in symmetric nuclear matter. Perturbative triples amplitudes are shown to be significant. It is necessary to include all three-body terms in the triples amplitudes, and a normal-ordered two-body approximation can only be used in the doubles amplitude (see Paper III). The CC ladder approximation is, therefore, not sufficient to accurately model symmetric nuclear matter. Unfortunately, the CC results of Paper III are strongly dependent on the chosen regulator in the chiral three-body force. As pointed out in Paper III, it may be necessary to improve the chiral interaction models to get a weaker regulator dependency. The interaction models we use do not account for Δ resonances, which may be important in nuclear structure calculations [16]. Finally, our collaborators show in Paper III that the constants c_D and c_E of the three-body force cannot be chosen to give both the experimental saturation properties of nuclear matter and the correct binding energy for triton.

5.2.4 Problems with particle-hole diagrams

In three-dimensional nuclear matter, the CC $\hat{T}_2$ amplitudes are functions of four three-dimensional momentum vectors. One vector can be removed owing to momentum conservation, but still the size of the $\hat{T}_2$ amplitude matrix may become very large. The realistic two-particle nuclear interactions we use are given in a coupled angular-momentum basis with relative momentum coordinates. We have therefore chosen to transform the CC equations to the coupled angular-momentum and relative momentum basis

$$|k\mathcal{J}m_{\mathcal{J}}(lS)m_{t_1}m_{t_2}\rangle,$$

which was defined in Chapter 3. As discussed in the previous subsection, the partial-wave-expanded CC ladder equations may be considerably simplified using angular-

averaged single-particle potentials. In this approximation, the size of the amplitude matrix decreases by two dimensions. Unfortunately, as we now show, the complete CCD equations become considerably more complicated in the partial-wave basis.

In the following, we repeat parts of the theory explained in Paper II, but we extend the discussion to include terms that are neglected in the article. For simplicity, let us for a moment consider only those terms in the CCD $\hat{T}_2$ amplitude equation (5.16) that are linear in the CC amplitudes. Using integrals in the limit when the box size approaches infinity, as in Eq. (3.27), the linear part of the amplitude equation becomes

$$\begin{aligned}
0 &= \langle \mathbf{k}_a \mathbf{k}_b | \hat{v} | \mathbf{k}_i \mathbf{k}_j \rangle_{AS} \\
&+ (\varepsilon(\mathbf{k}_a) + \varepsilon(\mathbf{k}_b) - \varepsilon(\mathbf{k}_i) - \varepsilon(\mathbf{k}_j)) \langle \mathbf{k}_a \mathbf{k}_b | \hat{t} | \mathbf{k}_i \mathbf{k}_j \rangle \\
&+ \frac{1}{2} \left(\frac{L}{2\pi} \right)^6 \int d\mathbf{k}_k \int d\mathbf{k}_l \langle \mathbf{k}_a \mathbf{k}_b | \hat{t} | \mathbf{k}_k \mathbf{k}_l \rangle \langle \mathbf{k}_k \mathbf{k}_l | \hat{v} | \mathbf{k}_i \mathbf{k}_j \rangle_{AS} \\
&\times \theta(k_F - |\mathbf{k}_k|) \theta(k_F - |\mathbf{k}_l|) \\
&+ \frac{1}{2} \left(\frac{L}{2\pi} \right)^6 \int d\mathbf{k}_c \int d\mathbf{k}_d \langle \mathbf{k}_a \mathbf{k}_b | \hat{v} | \mathbf{k}_c \mathbf{k}_d \rangle_{AS} \langle \mathbf{k}_c \mathbf{k}_d | \hat{t} | \mathbf{k}_i \mathbf{k}_j \rangle \\
&\times \theta(|\mathbf{k}_c| - k_F) \theta(|\mathbf{k}_d| - k_F) \\
&+ \hat{P}(\mathbf{k}_i, \mathbf{k}_j) \hat{P}(\mathbf{k}_a, \mathbf{k}_b) \left(\frac{L}{2\pi} \right)^6 \int d\mathbf{k}_k \int d\mathbf{k}_c \langle \mathbf{k}_a \mathbf{k}_c | \hat{t} | \mathbf{k}_i \mathbf{k}_k \rangle \\
&\times \langle \mathbf{k}_k \mathbf{k}_b | \hat{v} | \mathbf{k}_c \mathbf{k}_j \rangle_{AS} \theta(k_F - |\mathbf{k}_k|) \theta(|\mathbf{k}_c| - k_F),
\end{aligned} \tag{5.36}$$

where $\theta(x)$ is the Heaviside step function. In Eq. (5.36) we have used the definition $\varepsilon(\mathbf{k}) \equiv \langle \mathbf{k} | f | \mathbf{k} \rangle$. The term that we give on the third and fourth lines of Eq. (5.36) has summations over two hole states. The corresponding diagram is the one in the middle in the second row of Figure 5.2. This is the hole-hole ladder (HHLAD) diagram, which generates diagrams similar to the hole-hole ladders in many-body perturbation theory [157, pp. 346–347]. In the same way, there is a summation over two particle states in the term on the fifth and sixth lines of Eq. (5.36). The corresponding diagram is given in the second row at left of Figure 5.2. This term generates diagrams similar to the particle-particle ladders encountered in many-body perturbation theory [157, pp. 351–352], and we call the term the particle-particle ladder (PPLAD) diagram. In the last term of Eq. (5.36), there is a summation over one hole and one particle state. The corresponding diagram is the one at the right in the second row of Figure 5.2. We call this the particle-hole (PH) diagram.

Similarly as in Paper II, we write the linear part of the CCD amplitude equation in RCM coordinates, but including here also the PH term. The amplitude equation becomes

$$0 = \langle \mathbf{k}' | \hat{v} | \mathbf{k} \rangle_{AS} + (\varepsilon(|\mathbf{k}' + \mathbf{K}/2|) + \varepsilon(|-\mathbf{k}' + \mathbf{K}/2|)$$

$$
\begin{aligned}
&-\varepsilon(|\mathbf{k}+\mathbf{K}/2|)-\varepsilon(|-\mathbf{k}+\mathbf{K}/2|))\,\langle\mathbf{k}'|\hat{t}|\mathbf{k}\rangle \\
&+\frac{1}{2}\int d\mathbf{h}\langle\mathbf{k}'|t(\mathbf{K})|\mathbf{h}\rangle\langle\mathbf{h}|\hat{v}|\mathbf{k}\rangle_{AS} \\
&\times\theta(k_F-|\mathbf{h}+\mathbf{K}/2|)\theta(k_F-|-\mathbf{h}+\mathbf{K}/2|) \\
&+\frac{1}{2}\int d\mathbf{p}\langle\mathbf{k}'|\hat{v}|\mathbf{p}\rangle_{AS}\langle\mathbf{p}|\hat{t}|\mathbf{k}\rangle \\
&\times\theta(|\mathbf{p}+\mathbf{K}/2|-k_F)\theta(|-\mathbf{p}+\mathbf{K}/2|-k_F) \\
&+\int d\mathbf{B}\langle\mathbf{B}/4+3\mathbf{k}'/4-\mathbf{k}/4-\mathbf{K}/4|\hat{v}|\mathbf{B}/4-\mathbf{k}'/4+3\mathbf{k}/4-\mathbf{K}/4\rangle_{AS} \\
&\times\langle-\mathbf{B}/4+3\mathbf{k}'/4-\mathbf{k}/4+\mathbf{K}/4|\hat{t}|\mathbf{B}/4+3\mathbf{k}/4-\mathbf{k}'/4+\mathbf{K}/4\rangle \\
&\times\theta(k_F-|\mathbf{B}/2+(\mathbf{k}'-\mathbf{k})/2|)\theta(|\mathbf{B}/2-(\mathbf{k}'-\mathbf{k})/2|-k_F)+\ldots,
\end{aligned}
\tag{5.37}
$$

where the last term is the part of the particle-hole diagram that is not permuted. Here we have used the definitions

$$
\mathbf{h}=(\mathbf{k}_k-\mathbf{k}_l)/2, \qquad \mathbf{p}=(\mathbf{k}_c-\mathbf{k}_d)/2, \tag{5.38}
$$

and the relative momentum vectors $\mathbf{k}$, $\mathbf{k}'$ and CM momentum vector $\mathbf{K}$ are defined in Eq. (3.31).

In Paper II we wrote the amplitude equation into such a form that both the interaction and the CC amplitude were given in a coupled angular-momentum and relative-momentum basis

$$
|k\mathcal{J}m_{\mathcal{J}}(lS)M_T\rangle, \tag{5.39}
$$

where $k\equiv|\mathbf{k}|$ is the length of a relative momentum vector $\mathbf{k}$, l is the orbital angular momentum related to $\mathbf{k}$, S is the total two-particle spin, $\mathcal{J}$ is equal to the total angular momentum $l+S$, $m_{\mathcal{J}}$ is the z projection of $\mathcal{J}$, and M_T is the projection of the total two-particle isospin.

Let us now consider the simpler linear equation in which the PH diagrams are neglected, as was done in Paper II. When using an angular-average approximation for the inputs in the single-particle potentials $\varepsilon(|\mathbf{p}|)$ of the amplitude equation, all the vectors $|\mathbf{k}\rangle$, $|\mathbf{k}'\rangle$, and their conjugates can simply be replaced by vectors as in Eq. (5.39). The resulting CC amplitude equation is of the form (see Paper II)

$$
\begin{aligned}
&\Delta\tilde{\varepsilon}(k,k',K)\langle k'\mathcal{J}'m_{\mathcal{J}'}(l'S)M_T|\hat{t}(K)|k\mathcal{J}m_{\mathcal{J}}(lS)M_T\rangle \\
&=\langle k'\mathcal{J}'m_{\mathcal{J}'}(l'S)M_T|\hat{v}|k\mathcal{J}m_{\mathcal{J}}(lS)M_T\rangle\delta_{\mathcal{J}\mathcal{J}'}\delta_{m_{\mathcal{J}}m_{\mathcal{J}'}}
\end{aligned}
$$

$$
\begin{aligned}
&+\frac{1}{2}\sum_{\mathcal{J}''m_{\mathcal{J}''}}\sum_{l''l'''}\int_0^{k_F} h^2dh \\
&\times\langle k'\mathcal{J}'m_{\mathcal{J}'}(l'S)M_T|\hat{t}(K)|h\mathcal{J}''m_{\mathcal{J}''}(l''S)M_T\rangle \\
&\times\langle h\mathcal{J}m_{\mathcal{J}}(l'''S)M_T|\hat{v}|k\mathcal{J}m_{\mathcal{J}}(lS)M_T\rangle \\
&\times Q_{hh}(l''\mathcal{J}''m_{\mathcal{J}''},l'''\mathcal{J}m_{\mathcal{J}};SM_ThK\theta_K\phi_K) \\
&+\frac{1}{2}\sum_{\mathcal{J}''m_{\mathcal{J}''}}\sum_{l''l'''}\int_0^{\infty} p^2dp \\
&\times\langle k'\mathcal{J}'m_{\mathcal{J}'}(l'S)M_T|\hat{v}|p\mathcal{J}'m_{\mathcal{J}'}(l''S)M_T\rangle \\
&\times\langle p\mathcal{J}''m_{\mathcal{J}''}(l'''S)M_T|\hat{t}(K)|k\mathcal{J}m_{\mathcal{J}}(lS)M_T\rangle \\
&\times Q_{pp}(l''\mathcal{J}'m_{\mathcal{J}'},l'''\mathcal{J}''m_{\mathcal{J}''};SM_TpK\theta_K\phi_K),
\end{aligned}
\tag{5.40}
$$

where the exact Pauli operators Q_{hh} and Q_{pp} and the function $\tilde{\varepsilon}(k,k',K)$ are defined in Paper II. Unfortunately, the PH terms in Eq. (5.37) have complicated dependencies on the angular parts of $\mathbf{k}$ and $\mathbf{k}'$. When including the PH term, the angular parts of $\mathbf{k}$ and $\mathbf{k}'$ can therefore no longer be separated out in a simple way. Consequently, the size of the $\hat{T}_2$ matrix becomes intractably large in the thermodynamic limit, and the equations become considerably more complex. Because of this problem, we have omitted the PH diagrams from our CC amplitude equation in Paper II.

An advantage of using partial waves is that one can calculate the CC amplitude matrix for only one direction of the CM momentum vector $\mathbf{K}$, for example only vectors $\mathbf{K}=(0,0,K)$, and then one can obtain the matrix elements for other directions by using rotation matrices. In Paper II, the CC $\hat{T}_2$ amplitude matrix was rotated as

$$
\begin{aligned}
&\langle k'\mathcal{J}'m_{\mathcal{J}'}(l'S)|\hat{t}(\mathbf{K})|k\mathcal{J}m_{\mathcal{J}}(lS)\rangle \\
&=\sum_{m_{\mathcal{J}'''}m_{\mathcal{J}''}} D^{\mathcal{J}'}_{m_{\mathcal{J}'}m_{\mathcal{J}'''}}(\phi_K,\theta_K,0)D^{\mathcal{J}*}_{m_{\mathcal{J}}m_{\mathcal{J}''}}(\phi_K,\theta_K,0) \\
&\times\langle k'\mathcal{J}'m_{\mathcal{J}'''}(l'S)|\hat{t}(K)|k\mathcal{J}m_{\mathcal{J}''}(lS)\rangle,
\end{aligned}
\tag{5.41}
$$

where $D^{\mathcal{J}}_{m_{\mathcal{J}}m_{\mathcal{J}'}}(\phi,\theta,\sigma)$ is a rotation matrix defined by Varshalovich *et al.* [227, pp. 72–74]. It is possible to solve the amplitude equation using three-dimensional momentum vectors, but then we loose the rotational symmetry of the CC amplitude matrix. Consequently, the CC amplitude matrix needs two degrees more of freedom, which increases the demand for computer memory.

5.2.5 Spherical approximation of nuclear matter

As discussed in the previous subsection, the CCSD amplitude equations become very complicated in the partial-wave expansion using RCM coordinates. It would therefore

be advantageous to use an approach in which the CC equations can be written explicitly in laboratory-frame coordinates. In Paper III, a Cartesian momentum basis defined in the laboratory frame was successfully applied to nuclear matter systems. In the present section, we discuss another approach to implementing coupled-cluster theory for infinite matter, following ideas by Gaute Hagen, Morten Hjorth-Jensen, and Thomas Papenbrock (see also Ref. [270] for a discussion of the first part). In this approach, infinite nuclear matter is modeled as a spherical system. First, the interaction matrix elements are transformed from the relative partial-wave basis (3.34) to a single-particle basis in laboratory coordinates. Once the interaction matrix elements have been transformed to a laboratory-frame basis, it is straightforward to derive and implement explicit coupled-cluster equations.

A seemingly appealing approach is to transform the interaction matrix to the laboratory-frame single-particle basis

$$|k_p j_p m_{j_p} l_p s_p m_{t_p}\rangle, \tag{5.42}$$

where k_p is the laboratory momentum, l_p is the orbital angular momentum, s_p is the spin, j_p is the angular momentum, m_{j_p} is the z projection of j_p, and m_{t_p} is the isospin projection. Hagen *et al.* have shown [271] how more efficient coupled-cluster implementations can be obtained by coupling single-particle angular momenta j_p and j_q to a total angular momentum J. This kind of angular momentum coupling is possible because the nuclear interaction is rotationally invariant [233, p. 151] and, therefore, conserves the total angular momentum. We would therefore like to write the two-nucleon states in the basis

$$|k_p j_p l_p, k_q j_q l_q; J m_{t_p} m_{t_q}\rangle, \tag{5.43}$$

where the single-particle angular momenta j_p and j_q have been coupled to a total angular momentum.

Let us show how the interaction matrix elements can be transformed to the basis (5.43). Assume for a while that we have the continuous plane wave basis

$$\psi_{\mathbf{k}}(\mathbf{x}) = \frac{1}{(2\pi)^{3/2}} e^{i\mathbf{k}\cdot\mathbf{x}}, \tag{5.44}$$

instead of the discrete box-potential plane-wave basis of Eq. (3.20). A bra vector $\langle \mathbf{k}_p \mathbf{k}_q|$ can be expanded as [272]

$$\langle \mathbf{k}_p \mathbf{k}_q| = \langle \mathbf{k}_p \mathbf{k}_q| \left(\sum_{l_p m_{l_p}} \sum_{l_q m_{l_q}} |l_p m_{l_p} l_q m_{l_q}\rangle \langle l_p m_{l_p} l_q m_{l_q}| \right)$$

$$
\begin{aligned}
&= \langle \mathbf{k}_p \mathbf{k}_q | \sum_{l_p m_{l_p}} \sum_{l_q m_{l_q}} |l_p m_{l_p} l_q m_{l_q}\rangle \\
&\times \left(\sum_{\lambda\mu} \langle l_p m_{l_p} l_q m_{l_q} | \lambda\mu \rangle \langle \lambda\mu l_p l_q | \right) \\
&= \frac{1}{k_p k_q} \sum_{l_p l_q \lambda\mu} \langle k_p l_p k_q l_q, \lambda\mu | \left[Y_{l_p m_{l_p}}(\hat{\mathbf{k}}_p) Y_{l_q m_{l_q}}(\hat{\mathbf{k}}_q) \right]_{\lambda m_\lambda},
\end{aligned} \tag{5.45}
$$

where the functions $Y_{lm_l}(\hat{\mathbf{k}}) \equiv \langle \hat{\mathbf{k}} | l m_l \rangle$ are spherical harmonics, the bracket denotes a Clebsch-Gordan coefficient [227, pp. 235–236], l_p and l_q are orbital angular momenta of the two particles, λ is the total orbital angular momentum, and m_λ its projection in the z direction. In Eq. (5.45) the square brackets represent coupling of orbital angular momenta, as in Eq. (3.43). We define the radial states with the normalization condition

$$
\langle k l m_l | k' l' m_{l'} \rangle = \delta(k - k') \delta_{ll'} \delta_{m_l m_{l'}}, \tag{5.46}
$$

similarly as in Ref. [272]. When projecting to the real space, we get

$$
\varphi_{klm_l}(\mathbf{r}) \equiv \langle \mathbf{r} | k l m_l \rangle = \sqrt{\frac{2}{\pi}} k j_l(kr) Y_{lm_l}(\theta_r, \phi_r), \tag{5.47}
$$

where $j_l(x)$ is the spherical Bessel function. Equation (5.47) differs from the function given in [273, p. 417] due to different normalizations. Observe that continuous momentum variables give a Dirac delta distribution in the normalization expression (5.46).

Following Eq. (2.16) of Ref. [272], radial ket vectors can be transformed between the laboratory and RCM coordinate systems using the relation

$$
|k_p l_p k_q l_q, \lambda m_\lambda\rangle = \int dk \int dK \sum_{lL} |klKL, \lambda m_\lambda\rangle \langle klKL, \lambda | k_p l_p k_q l_q, \lambda\rangle, \tag{5.48}
$$

where k and K are radial coordinates of relative and CM momenta, respectively, l and L are corresponding orbital angular momenta, and the coefficient denoted by a bracket is called a vector bracket [272, 274]. According to Eqs. (3.3), (3.4), (3.11) and (3.14) of Ref. [272], the vector bracket can be written as

$$
\langle klKL, \lambda | k_p l_p k_q l_q, \lambda\rangle = (4\pi)^2 \delta(u) \theta(1 - v^2) A(v), \tag{5.49}
$$

where

$$
\begin{aligned}
A(v) = &\frac{1}{(2\lambda + 1)} \sum_{m_\lambda} \left[Y_{lm_l}(\hat{\mathbf{k}}) \times Y_{LM_L}(\hat{\mathbf{K}}) \right]^*_{\lambda m_\lambda} \\
&\times \left[Y_{l_p m_{l_p}}(\hat{\mathbf{k}}_p) \times Y_{l_q m_{l_q}}(\hat{\mathbf{k}}_q) \right]_{\lambda m_\lambda},
\end{aligned} \tag{5.50}
$$

as formulated by Balian and Brezin [272, 275], and

$$u = k^2 + \frac{1}{4}K^2 - \frac{1}{2}(k_p^2 + k_q^2), \tag{5.51}$$

$$v = \frac{1}{kK}\left(k_p^2 - k^2 - \frac{1}{4}K^2\right). \tag{5.52}$$

The delta distribution ensures that the kinetic energy is conserved in the transformation between coordinate systems. The variable v may also be written as

$$v = \cos(\theta_{\mathbf{kK}}),$$

where $\theta_{\mathbf{kK}}$ is the angle between the relative and CM momentum vectors $\mathbf{k}$ and $\mathbf{K}$. The step function $\theta(1-v^2)$, therefore, gives the geometric restriction $|\cos(\theta_{\mathbf{kK}})| \leq 1$ [274].

We want to write a vector $|(k_p l_p j_p)(k_p l_p j_p)(JM_J)\rangle$ as a linear combination of vectors $|klKL(\mathcal{J})SJM_J\rangle$. This transformation has been given in, for example, Refs. [274, 276]. In the following, we sketch a derivation of the transformation between the two bases. We do the derivation in several steps. First we recouple from the $j-j$ scheme to the $L-S$ scheme, as in Eq. (4.13) of Ref. [228]. Further, we do the recoupling $JM_J\lambda S \longrightarrow \lambda\mu SM_S$, and get

$$\begin{aligned}|(k_p l_p j_p)(k_q l_q j_q)(JM_J)\rangle = \sum_{\lambda m_\lambda}\sum_{SM_S} \hat{j}_p\hat{j}_q\hat{\lambda}\hat{S} \begin{Bmatrix} l_p & \frac{1}{2} & j_p \\ l_q & \frac{1}{2} & j_q \\ \lambda & S & J \end{Bmatrix} \\ \times \langle \lambda m_\lambda SM_S|JM_J\rangle |k_p l_p k_q l_q, \lambda m_\lambda\rangle |SM_S\rangle, \end{aligned} \tag{5.53}$$

where we have used the definition $\hat{x} = \sqrt{2x+1}$. If we now use the laboratory to RCM transformation (5.48), do the recoupling $\lambda m_\lambda SM_S \longrightarrow JM_J\lambda S$, and use the $9j$ coefficient relation (A4.27) in Ref. [228], we get

$$\begin{aligned}|(k_p l_p j_p)(k_q l_q j_q)(JM_J)\rangle = \sum_{\lambda S}\sum_{lL}\int dk \int dK \hat{j}_p\hat{j}_q\hat{\lambda}\hat{S} \begin{Bmatrix} l_p & l_q & \lambda \\ \frac{1}{2} & \frac{1}{2} & S \\ j_p & j_q & J \end{Bmatrix} \\ \times \langle klKL, \lambda|k_p l_p k_q l_q, \lambda\rangle |klKL(\lambda)SJM_J\rangle. \end{aligned} \tag{5.54}$$

To get the desired basis on the right-hand side, we must further do the recoupling of three angular momenta $lL(\lambda)SJM_J \longrightarrow lL(\mathcal{J})SJM_J$, diagrammatically sketched as [228, p. 461]

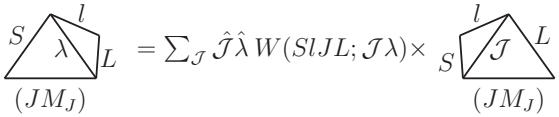

where $W(SlJL;\mathcal{J}\lambda)$ is a Racah coefficient (see Refs. [277] and [227, p. 291]). When

we apply this recoupling, we get the expression

$$
\begin{aligned}
|(k_p l_p j_p)(k_q l_q j_q)(JM_J)\rangle = \sum_{\lambda S}\sum_{lL}\sum_{\mathcal{J}}\int dk \int dK \hat{j_p}\hat{j_q}\hat{\lambda}^2\hat{S}\hat{\mathcal{J}} \\
\times \left\{ \begin{array}{ccc} l_p & l_q & \lambda \\ \frac{1}{2} & \frac{1}{2} & S \\ j_p & j_q & J \end{array} \right\} \langle klKL,\lambda|k_p l_p k_q l_q,\lambda\rangle \\
\times W(LlJS;\lambda\mathcal{J})|klKL(\mathcal{J})SJM_J\rangle. \qquad (5.55)
\end{aligned}
$$

Here we have used some symmetry relations for Racah coefficients. If we now use the relation between Racah coefficients and $6j$ symbols, and include the isospin degree of freedom, we obtain

$$
\begin{aligned}
|(k_p l_p j_p)(k_q l_q j_q)(JM_J m_{t_p} m_{t_q})\rangle = \sum_{\lambda S}\sum_{lL}\sum_{\mathcal{J}}\int dk \int dK\, \hat{j_p}\hat{j_q}\hat{\lambda}^2\hat{S}\hat{\mathcal{J}} \\
\times (-1)^{L+l+J+S} \left\{ \begin{array}{ccc} l_p & l_q & \lambda \\ \frac{1}{2} & \frac{1}{2} & S \\ j_p & j_q & J \end{array} \right\} \\
\times \langle klKL,\lambda|k_p l_p k_q l_q,\lambda\rangle \left\{ \begin{array}{ccc} L & l & \lambda \\ S & J & \mathcal{J} \end{array} \right\} \\
\times |klKL(\mathcal{J})SJM_J m_{t_p} m_{t_q}\rangle. \qquad (5.56)
\end{aligned}
$$

The corresponding antisymmetrized vector is obtained by multiplying the right-hand side of Eq. (5.56) by $\mathcal{A}^{lSM_T}$, where $M_T = m_{t_p} + m_{t_q}$ and the antisymmetrization factor is defined in Eq. (A.5). The transformation in Eq. (5.56) differs from the expressions in Refs. [274, 276] by a phase factor $(-1)^{(J-\lambda)-(\mathcal{J}-l)}$, which is one owing to triangular relations.

Using the transformation (5.56), a two-body interaction matrix element may now be written as

$$
\begin{aligned}
&\langle k_p l_p j_p k_q l_q j_q JTM_T|V|k_r l_r j_r k_s l_s j_s JTM_T\rangle \\
&= \sum_{lL\lambda S\mathcal{J}}\int_0^\infty dk \int_0^\infty dK \left\{ \begin{array}{ccc} l_p & l_q & \lambda \\ \frac{1}{2} & \frac{1}{2} & S \\ j_p & j_q & J \end{array} \right\} \\
&\times (-1)^{\lambda+\mathcal{J}-L-S}\hat{\mathcal{J}}\hat{\lambda}^2\hat{j_p}\hat{j_q}\hat{S} \left\{ \begin{array}{ccc} L & l & \lambda \\ S & J & \mathcal{J} \end{array} \right\} \\
&\times (4\pi)^2\delta\left(k^2 + \frac{1}{4}K^2 - \frac{1}{2}(k_p^2 + k_q^2)\right) \\
&\times \theta\left(1 - \frac{(k_p^2 - k^2 - \frac{1}{4}K^2)^2}{k^2K^2}\right) A\left(\frac{k_p^2 - k^2 - \frac{1}{4}K^2}{kK}\right)
\end{aligned}
$$

$$
\begin{aligned}
&\times \sum_{l'\lambda'} \int_0^\infty dk' \int_0^\infty dK' \left\{ \begin{array}{ccc} l_r & l_s & \lambda' \\ \frac{1}{2} & \frac{1}{2} & S \\ j_r & j_s & J \end{array} \right\} \\
&\times (-1)^{\lambda'+\mathcal{J}-L-S} \hat{\mathcal{J}} \hat{\lambda}' \hat{j}_r \hat{j}_s \hat{S} \left\{ \begin{array}{ccc} L & l' & \lambda' \\ S & J & \mathcal{J} \end{array} \right\} \\
&\times (4\pi)^2 \delta \left(k'^2 + \frac{1}{4} K'^2 - \frac{1}{2}(k_r^2 + k_s^2) \right) \\
&\times \theta \left(1 - \frac{(k_r^2 - k'^2 - \frac{1}{4}K'^2)^2}{k'^2 K'^2} \right) A \left(\frac{k_r^2 - k'^2 - \frac{1}{4}K'^2}{k'K'} \right) \\
&\times \langle klKL(\mathcal{J})SJTM_T|V|k'l'K'L(\mathcal{J})SJTM_T\rangle,
\end{aligned}
\tag{5.57}
$$

where the vector brackets are given explicitly using Eq. (5.49). We assume that the antisymmetrization factors are incorporated implicitly in the relative-coordinate two-body interaction. Here we have used normalizations as in Eq. (5.46) for relative and laboratory-frame momentum radial coordinates. The interaction-matrix elements should therefore be evaluated in a basis similar to Eq. (5.47).

The nuclear interaction is generally diagonal in $\mathcal{J}$, S, M_T, K, L, J, and T, and independent on the latter four. Let us separate the quantum numbers that the interaction depends on, and use the normalization

$$\langle K|K'\rangle = \delta(K - K'),$$

similarly as in Eq. (5.46). After reorganizing the different terms, the transformation becomes

$$
\begin{aligned}
&\langle k_p l_p j_p k_q l_q j_q JTM_T|V|k_r l_r j_r k_s l_s j_s JTM_T\rangle \\
&= (4\pi)^4 \sum_{lL\lambda S\mathcal{J}} \sum_{l'\lambda'} (-1)^{\lambda+\lambda'} \hat{\mathcal{J}}^2 \hat{\lambda}^2 \hat{\lambda}'^2 \hat{S}^2 \hat{j}_p \hat{j}_q \hat{j}_r \hat{j}_s \\
&\times \left\{ \begin{array}{ccc} L & l & \lambda \\ S & J & \mathcal{J} \end{array} \right\} \left\{ \begin{array}{ccc} L & l' & \lambda' \\ S & J & \mathcal{J} \end{array} \right\} \left\{ \begin{array}{ccc} l_p & l_q & \lambda \\ \frac{1}{2} & \frac{1}{2} & S \\ j_p & j_q & J \end{array} \right\} \left\{ \begin{array}{ccc} l_r & l_s & \lambda' \\ \frac{1}{2} & \frac{1}{2} & S \\ j_p & j_q & J \end{array} \right\} \\
&\times \int_0^\infty dk' \frac{1}{\tilde{k}\tilde{K}} \langle \tilde{k} l(\mathcal{J})SM_T|V|k'l'(\mathcal{J})SM_T\rangle \\
&\times \theta \left(1 - \frac{(k_p^2 - \tilde{k}^2 - \frac{1}{4}\tilde{K}^2)^2}{\tilde{k}^2 \tilde{K}^2} \right) A \left(\frac{k_p^2 - \tilde{k}^2 - \frac{1}{4}\tilde{K}^2}{\tilde{k}\tilde{K}} \right) \\
&\times \theta \left(1 - \frac{(k_r^2 - k'^2 - \frac{1}{4}\tilde{K}^2)^2}{k'^2 \tilde{K}^2} \right) A \left(\frac{k_r^2 - k'^2 - \frac{1}{4}\tilde{K}^2}{k'\tilde{K}} \right),
\end{aligned}
\tag{5.58}
$$

where we have used the definitions

$$\tilde{K} = 2 \left(\frac{1}{2} \left(k_p^2 + k_q^2 \right) - k'^2 \right)^{1/2},$$

$$\tilde{k} = \left(\frac{1}{2} \left(k_p^2 + k_q^2 - k_r^2 - k_s^2 \right) + k'^2 \right)^{1/2} . \tag{5.59}$$

To remove the Dirac delta distributions, we have defined the new integration variables

$$\begin{aligned} s &= \frac{1}{4} K^2 + k^2 - \frac{1}{2} \left(k_p^2 + k_q^2 \right) , \\ t &= k'^2 + \frac{1}{4} K^2 - \frac{1}{2} \left(k_r^2 + k_s^2 \right) , \end{aligned} \tag{5.60}$$

and simplified the integral as explained in Appendix B.1.

The reference energy is given algebraically in Eq. (5.12). Next we want to write the reference energy in the coupled partial-wave basis (5.43). A bra vector can be transformed as

$$\begin{aligned} &\sum_{m_{s_p} m_{s_q}} \sum_{m_{t_p} m_{t_q}} \langle \mathbf{k}_p \mathbf{k}_q | \langle m_{s_p} m_{s_q} | \langle m_{t_p} m_{t_q} | \\ &\quad = \frac{1}{k_p k_q} \sum_{\substack{l_p l_q \\ m_{l_p} m_{l_q}}} \sum_{\substack{m_{s_p} m_{s_q} \\ m_{t_p} m_{t_q}}} \sum_{\substack{j_p j_q \\ m_{j_p} m_{j_q}}} \sum_{JM_J} \\ &\quad \times \langle l_p s_p m_{l_p} m_{s_p} | j_p m_{j_p} \rangle \langle l_q s_q m_{l_q} m_{s_q} | j_q m_{j_q} \rangle \langle j_p j_q m_{j_p} m_{j_q} | JM_J \rangle \\ &\quad \times \langle k_p j_p l_p, k_q j_q l_q ; JM_J | \langle m_{t_p} m_{t_q} | Y_{l_p m_{l_p}} (\hat{\mathbf{k}}_p) Y_{l_q m_{l_q}} (\hat{\mathbf{k}}_q) , \end{aligned} \tag{5.61}$$

where we have used completeness relations similar to Eqs. (3.35) and (3.36), as well as coupling of angular momenta as in Eq. (3.41). If we use the angular-momentum expansion (5.61), the orthogonality of spherical harmonics, and the relation [228, p. 427]

$$\sum_{m_p m_q} (j_p j_q m_p m_q | JM_J)(j_p j_q m_p m_q | J' M'_J) = \delta_{JJ'} \delta_{M_J M'_J} \tag{5.62}$$

for Clebsch-Gordan coefficients, the reference energy per particle becomes

$$\begin{aligned} \frac{E_{REF}}{A} &= \frac{1}{5\pi^2} \frac{\hbar^2 k_F^5}{m\rho} + \frac{1}{2A} \int_0^{k_F} dk_1 \int_0^{k_F} dk_2 \\ &\quad \times \sum_{\substack{l_1 l_2 \\ j_1 j_2}} \sum_J \sum_{m_{t_1} m_{t_2}} (2J+1) \\ &\quad \times \langle k_1 j_1 l_1, k_2 j_2 l_2 ; J m_{t_1} m_{t_2} | \tilde{v} | k_1 j_1 l_1, k_2 j_2 l_2 ; J m_{t_1} m_{t_2} \rangle , \end{aligned} \tag{5.63}$$

where A is the number of nucleons and $\rho = A/\Omega$ is the nucleon density. In Eq. (5.63), we need an explicit expression for the number of particles, which in principle is an infinitely large number. When evaluating Eq. (5.63), we hope that the expansion in partial waves may be truncated after a reasonably small number of angular momenta. On the other hand, we have assumed above that the momentum points are infinitely

dense. The total number of particles, therefore, becomes infinitely large. Assuming that convergence has been obtained in the partial-wave expansion, the number of nucleons is

$$\begin{aligned} A &= \sum_{m_s} \sum_{m_t} \frac{\Omega}{(2\pi)^3} \int_{|\mathbf{k}| \leq k_F} d\mathbf{k} \\ &= \Omega \frac{2k_F^3}{3\pi^2} \end{aligned} \tag{5.64}$$

in the special case of symmetric nuclear matter. A practical problem arises here: The expression for the number of particles (5.64) depends on the volume Ω of the nuclear matter system. When deriving Eqs. (5.58) and (5.63), we have assumed that the volume is infinitely large. Unfortunately, there is no volume term in Eq. (5.58) that cancels the volume in the expression for the number of particles. Dimensional analysis of the given expressions also gives correct units for the energy per particle. The approach described above can therefore not be used to calculate the binding energy of nuclear matter.

The problem with infinite numbers can be avoided by discretizing the radial momentum explicitly [278]. This corresponds to using eigenstates of a spherical well. Following Liboff [273, p. 422], a spherical well has the single-particle wave functions

$$\psi_{nlm_l}(r, \theta_r, \phi_r) \equiv \langle \mathbf{r} | nlm_l \rangle = j_l(k_{nl} r) Y_{lm_l}(\theta_r, \phi_r) \tag{5.65}$$

and single-particle energies

$$\varepsilon_{nl} = \frac{\hbar^2 k_{nl}^2}{2m}, \tag{5.66}$$

where $j_l(x)$ is the spherical Bessel function. The discrete momenta k_{nl} are obtained from the Dirichlet boundary condition

$$\psi_{nlm_l}(R, \theta_r, \phi_r) = 0, \tag{5.67}$$

where R is the radius of the spherical box [273, pp. 422–423]. Including spin and isospin, the single-particle states may be written as

$$\psi_{njm_jlsm_t}(r, \theta_r, \phi_r) = \sum_{m_l m_s} \langle lm_l sm_s | jm_j ls \rangle j_l(k_{nl} r) Y_{lm_l}(\theta_r, \phi_r) | m_s m_t \rangle, \tag{5.68}$$

where spin and orbital angular momentum have been coupled to a total single-particle angular momentum.

Similarly as in a more general case, the Fermi vacuum state is constructed by choosing the A single-particle states $|njm_jlm_t\rangle$ with the lowest single-particle energies.

To be able to use single-reference coupled-cluster theory, the number of particles must be chosen such that all energy shells below the Fermi level are fully occupied. Similarly, one may choose the unoccupied single-particle states such that a given number of energy shells above the Fermi level are filled.

Assume we have A nucleons inside a spherical box. For simplicity, we assume that the particle density inside the box is constant. This assumption is valid in the limit of an infinite box radius, but finite systems will always have surface effects. The particle density of a sphere with radius R filled by A nucleons is then by definition

$$\rho = \frac{A}{\Omega(R)}, \tag{5.69}$$

where $\Omega(R) = 4\pi R^3/3$ is the spherical volume. Given a density ρ and a number of nucleons A, the radius can now be written as

$$R = \left(\frac{3A}{4\pi\rho}\right)^{1/3}. \tag{5.70}$$

The discrete spherical Bessel single-particle basis is useful for nuclear matter studies if the energy per particle converges fast with the number of occupied and unoccupied single-particle states. This requires that the surface effects are small in the spherical systems.

Above we concluded that the continuous radial basis $|kjm_jlm_t\rangle$ gives problems with infinite numbers, and we, therefore, want to replace this basis with the discrete equivalent $|njm_jlm_t\rangle$, which corresponds to eigenstates of a spherical well. Our task is now to rewrite the transformation given in Eq. (5.56) into a discrete form. The only part that is problematic is the vector bracket, which is defined for continuous radial states. One alternative is to derive a new discrete counterpart to the vector bracket. However, there is another well-known transformation coefficient between discrete laboratory and RCM states, which is the Moshinsky bracket [228, p. 205–206], defined for harmonic-oscillator states. If we use Moshinsky coefficients to transform the interaction matrix elements to laboratory-frame harmonic-oscillator states, matrix elements in the discrete radial basis $|njm_jlm_t\rangle$ can be obtained as

$$\langle pq|v|rs\rangle = \sum_{\substack{\alpha\leq\beta\\ \gamma\leq\delta}} \langle pq|\alpha\beta\rangle\langle\alpha\beta|v|\gamma\delta\rangle\langle\gamma\delta|rs\rangle, \tag{5.71}$$

where p, q, r, s represent radial single-particle states and $\alpha, \beta, \gamma, \delta$ harmonic-oscillator states. Hagen *et al.* [279] have used a similar transformation from the harmonic oscillator basis to a Gamow basis. As given in Ref. [279], the two-particle overlaps are

$$\langle pq|\alpha\beta\rangle = \begin{cases} \frac{\langle p|\alpha\rangle\langle q|\beta\rangle - (-1)^{J-j_\alpha-j_\beta}\langle p|\beta\rangle\langle q|\alpha\rangle}{\sqrt{(1+\delta_{pq})(1+\delta_{\alpha\beta})}}, & \text{if } m_{t_p} = m_{t_q},\\ \langle p|\alpha\rangle\langle q|\beta\rangle, & \text{if } m_{t_p} \neq m_{t_q}. \end{cases} \tag{5.72}$$

When doing the transformation from the harmonic-oscillator basis to the discrete radial single-particle basis, the single-particle overlaps are [279]

$$\langle p|\alpha\rangle = \delta_{j_p j_\alpha}\delta_{l_p l_\alpha}\delta_{m_{t_p} m_{t_\alpha}} \int_0^R dr r^2 j_{l_p}(k_{n_p l_p} r) R_{n_\alpha l_\alpha}(Cr), \tag{5.73}$$

where

$$C = \sqrt{m\omega/\hbar},$$

the variable ω is the harmonic oscillator strength, and $R_{n_\alpha l_\alpha}(Cr)$ is the radial part of the harmonic-oscillator wave function. Numerical calculations should include sufficiently many harmonic-oscillator single-particle states to get a result that is only weakly dependent on the oscillator strength. Similarly as done in Ref. [279] with the Gamow basis, the CM correction term can be calculated directly in the Bessel basis.

A proper numerical study of nuclear matter in a finite spherical box has still to be done, but is beyond the scope of this thesis. Next, we discuss how CC theory can be applied to the homogeneous electron gas.

5.3 Applications for the electron gas

Another important homogeneous system beside nuclear matter is the electron gas. In the earliest CC studies of the electron gas [50–53, 59, 60], the system was treated at the thermodynamic limit. In Paper III, infinite nuclear matter was approximated using finite boxes of nucleons. Some of the most accurate calculations of the electron gas [84, 194, 207, 208, 215] have been done using finite boxes and Monte Carlo methods. Recently, CC theory has been applied in several studies [54–58] to finite-particle approximations of the three-dimensional electron gas. Freeman has done CC studies of the two-dimensional electron gas including only ring [59] or only particle-particle ladder [60] diagrams from the CCD approximation, but to the best of our knowledge, a complete CCD calculation of the two-dimensional homogeneous electron gas is not available in the literature. As an extension of the CC calculations by Shepherd *et al.* [54–57] and Roggero *et al.* [58], we study the two-dimensional electron gas in the CCD approximation using a finite number of particles. We validate our methods by comparing results for the three-dimensional electron gas with Shepherd *et al.* [54, 210]. The single-particle basis consists of state vectors as given in Eq. (3.23), with the momentum discretized in Cartesian coordinates. Similarly as in Refs. [54–58], we neglect finite-size effects.

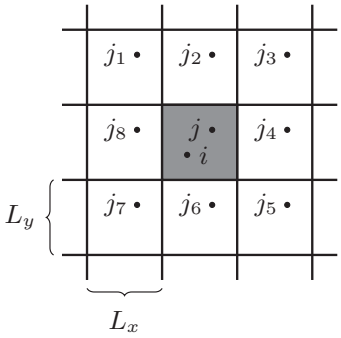

Figure 5.5: The electron gas is approximated using a finite box, or simulation cell (marked gray in the figure), with periodic boundary conditions. The Ewald interaction is an effective Coulomb interaction, which takes into account interactions between electrons in the simulation cell, as well as interactions between electrons in the simulation cell and image charges outside the finite box [77, 78]. In the figure, the charges i and j reside inside the simulation cell, whereas $j_1, \ldots, j_8$ are the nearest image charges of the charge j. The image charges of charge j are located at $\mathbf{r}_j + \mathbf{R}$, where $\mathbf{R}$ is the translational vector of the system. In two dimensions, the translational vector is $\mathbf{R} = L_x n_x \mathbf{u}_x + L_y n_y \mathbf{u}_y$, where n_x and n_y are integers.

5.3.1 Finite-box approximations of the electron gas

The homogeneous electron gas is defined as an infinite system consisting of electrons distributed with a constant density through the entire real space. The system is assumed to contain a constant positive background charge which cancels the negative charges of the electrons. The Hamiltonian operator of the homogeneous electron gas can be written as [192, p. 21]

$$\hat{H} = \hat{H}_{\text{kin}} + \hat{H}_{ee} + \hat{H}_{eb} + \hat{H}_{bb}, \tag{5.74}$$

where $\hat{H}_{\text{kin}}$ is the kinetic-energy operator, $\hat{H}_{ee}$ models the electron-electron interaction, $\hat{H}_{eb}$ represents the interaction between electrons and the positive background charge, and the operator $\hat{H}_{bb}$ gives the interaction energy of the background charge with itself.

Similarly as in Refs. [54–58], we approximate the homogeneous electron gas by a finite hypercube filled with electrons. Using periodic boundary conditions, we should also take into account interactions between electrons in the finite box and image charges in other boxes in the infinite space. We illustrate the setting in Figure 5.5. The summation over an infinite number of Coulomb-interaction terms can be efficiently calculated using, for example, Ewald's summation technique [76, 77]. Ewald's approach

is designed to give faster convergence by splitting the Coulomb interaction into a short-range part, which is calculated in real space, and a long-range part, which is summed in Fourier space [79]. The kinetic energy operator is

$$\hat{H}_{\text{kin}} = -\frac{\hbar^2}{2m}\sum_{i=1}^{N}\nabla_i^2, \tag{5.75}$$

where the sum is taken over all particles in the finite box. The Ewald electron-electron interaction operator can be written as [79]

$$\hat{H}_{ee} = \sum_{i<j}^{N} v_E\left(\mathbf{r}_i - \mathbf{r}_j\right) + \frac{1}{2}Ne^2v_0, \tag{5.76}$$

where $v_E(\mathbf{r})$ is the effective two-body interaction and v_0 is a corresponding self-interaction, defined as $v_0 = \lim_{\mathbf{r}\to 0}\left\{v_E(\mathbf{r}) - 1/r\right\}$. The Ewald interaction models the Coulomb interactions between all pairs of electrons inside the simulation cell, as well as all possible interactions between an electron in the simulation cell and an image charge (see Figure 5.5 and Refs. [77, 78]).

The negative electron charges are neutralized by a positive, homogeneous background charge [77, 78]. In Appendix A of Ref. [77], Fraser *et al.* explain how the electron-background and background-background terms, $\hat{H}_{eb}$ and $\hat{H}_{bb}$, vanish when using Ewald's interaction for the three-dimensional electron gas. Using the same arguments, these terms are also zero in the corresponding two-dimensional system.

In the three-dimensional electron gas, the Ewald interaction is [79]

$$v_E(\mathbf{r}) = \sum_{\mathbf{k}\neq\mathbf{0}}\frac{4\pi e^2}{L^3k^2}e^{i\mathbf{k}\cdot\mathbf{r}}e^{-\eta^2k^2/4} + \sum_{\mathbf{R}}\frac{e^2}{|\mathbf{r}-\mathbf{R}|}\operatorname{erfc}\left(\frac{|\mathbf{r}-\mathbf{R}|}{\eta}\right) - \frac{\pi e^2\eta^2}{L^3}, \tag{5.77}$$

where L is the box side length, $\operatorname{erfc}(x)$ is the complementary error function, and η is a free parameter that can take any value in the interval $(0,\infty)$. The translational vector

$$\mathbf{R} = L\left(n_x\mathbf{u}_x + n_y\mathbf{u}_y + n_z\mathbf{u}_z\right), \tag{5.78}$$

where $\mathbf{u}_i$ is the unit vector for dimension i, is defined for all integers n_x, n_y, and n_z. These vectors are used to obtain all image cells in the entire real space. The parameter η decides how the Coulomb interaction is divided into a short-range and long-range part and does not alter the total function. However, the number of operations needed to calculate the Ewald interaction with a desired accuracy depends on η, and η is, therefore, often chosen to optimize the convergency as a function of the simulation-cell size [79]. In our calculations, we choose η to be an infinitesimally small positive

number, similarly as done in Refs. [54–58]. This gives an interaction that is evaluated only in Fourier space.

When studying the two-dimensional electron gas, we use an Ewald interaction that is quasi two-dimensional. The interaction is derived in three dimensions, with Fourier discretization in only two dimensions [78, 280, 281]. When using the quasi two-dimensional interaction, we restrict the particles to move in only two dimensions and periodic boundary conditions are imposed in the plane in which the particles move. The Ewald effective interaction has the form [78]

$$\begin{aligned} v_E(\mathbf{r}) = &\sum_{\mathbf{k}\neq\mathbf{0}} \frac{\pi e^2}{L^2 k} \left\{ e^{-kz} \operatorname{erfc}\left(\frac{\eta k}{2} - \frac{z}{\eta}\right) + e^{kz} \operatorname{erfc}\left(\frac{\eta k}{2} + \frac{z}{\eta}\right) \right\} e^{i\mathbf{k}\cdot\mathbf{r}_{xy}} \\ &+ \sum_{\mathbf{R}} \frac{e^2}{|\mathbf{r}-\mathbf{R}|} \operatorname{erfc}\left(\frac{|\mathbf{r}-\mathbf{R}|}{\eta}\right) \\ &- \frac{2\pi e^2}{L^2} \left\{ z \operatorname{erf}\left(\frac{z}{\eta}\right) + \frac{\eta}{\sqrt{\pi}} e^{-z^2/\eta^2} \right\}, \end{aligned} \tag{5.79}$$

where the Fourier vectors $\mathbf{k}$ and the position vector $\mathbf{r}_{xy}$ are defined in the (x, y) plane. When applying the interaction $v_E(\mathbf{r})$ to two-dimensional systems, we set the z coordinate to zero. Similarly as in the three-dimensional case, and as suggested in Ref. [79] for two dimensions, also here we choose η to approach zero from above. The resulting Fourier-transformed interaction is

$$v_E^{\eta=0,z=0}(\mathbf{r}) = \sum_{\mathbf{k}\neq\mathbf{0}} \frac{2\pi e^2}{L^2 k} e^{i\mathbf{k}\cdot\mathbf{r}_{xy}}. \tag{5.80}$$

The self-interaction v_0 gives a constant in the Hamiltonian operator, as in Eq. (5.11).

In the three-dimensional electron gas, the antisymmetrized matrix elements are

$$\begin{aligned} &\langle \mathbf{k}_p m_{s_p} \mathbf{k}_q m_{s_q} | \tilde{v} | \mathbf{k}_r m_{s_r} \mathbf{k}_s m_{s_s} \rangle_{AS} \\ &= \frac{4\pi e^2}{L^3} \delta_{\mathbf{k}_p+\mathbf{k}_q,\mathbf{k}_r+\mathbf{k}_s} \left\{ \delta_{m_{s_p} m_{s_r}} \delta_{m_{s_q} m_{s_s}} \left(1 - \delta_{\mathbf{k}_p \mathbf{k}_r}\right) \frac{1}{|\mathbf{k}_r - \mathbf{k}_p|^2} \right. \\ &\left. - \delta_{m_{s_p} m_{s_s}} \delta_{m_{s_q} m_{s_r}} \left(1 - \delta_{\mathbf{k}_p \mathbf{k}_s}\right) \frac{1}{|\mathbf{k}_s - \mathbf{k}_p|^2} \right\}, \end{aligned} \tag{5.81}$$

where the Kronecker delta functions $\delta_{\mathbf{k}_p\mathbf{k}_r}$ and $\delta_{\mathbf{k}_p\mathbf{k}_s}$ ensure that the contribution with zero momentum transfer vanishes. Similarly, the matrix elements for the two-dimensional electron gas are

$$\begin{aligned} &\langle \mathbf{k}_p m_{s_p} \mathbf{k}_q m_{s_q} | v | \mathbf{k}_r m_{s_r} \mathbf{k}_s m_{s_s} \rangle_{AS} \\ &= \frac{2\pi e^2}{L^2} \delta_{\mathbf{k}_p+\mathbf{k}_q,\mathbf{k}_r+\mathbf{k}_s} \left\{ \delta_{m_{s_p} m_{s_r}} \delta_{m_{s_q} m_{s_s}} \left(1 - \delta_{\mathbf{k}_p \mathbf{k}_r}\right) \frac{1}{|\mathbf{k}_r - \mathbf{k}_p|} \right. \\ &\left. - \delta_{m_{s_p} m_{s_s}} \delta_{m_{s_q} m_{s_r}} \left(1 - \delta_{\mathbf{k}_p \mathbf{k}_s}\right) \frac{1}{|\mathbf{k}_s - \mathbf{k}_p|} \right\}, \end{aligned} \tag{5.82}$$

where the single-particle momentum vectors $\mathbf{k}_{p,q,r,s}$ are now defined in two dimensions.

In our calculations, the self-interaction constant is included in the reference energy, as in Eq. (5.12). We, therefore, get the Fock-operator matrix elements

$$\langle \mathbf{k}_p m_{s_p} | f | \mathbf{k}_q m_{s_q} \rangle = \frac{\hbar^2 k_p^2}{2m} \delta_{\mathbf{k}_p,\mathbf{k}_q} \delta_{m_{s_p} m_{s_q}} + \sum_{\mathbf{k}_i} \sum_{m_{s_i}} \langle \mathbf{k}_p m_{s_p} \mathbf{k}_i m_{s_i} | v | \mathbf{k}_q m_{s_q} \mathbf{k}_i m_{s_i} \rangle_{AS}. \tag{5.83}$$

In Ref. [56], the Hamiltonian operator was defined with the self-interaction constant included as a matrix element of the two-body interaction. This gives Fock-operator matrix elements with a gap constant. The definition used in Ref. [56] may give numerically more stable calculations, as the gap constant prevents the energy denominator from becoming too small in the vicinity of the Fermi surface. However, when using Fock matrix elements as defined in Eq. (5.83), the energy denominator in the CC equations never vanishes unless the numerator is zero. We discuss this point in Paper II.

When using periodic boundary conditions, the discrete-momentum single-particle basis functions

$$\phi_{\mathbf{k}}(\mathbf{r}) = e^{i\mathbf{k}\cdot\mathbf{r}}/L^{d/2}$$

are associated with the single-particle energy

$$\varepsilon_{n_x,n_y} = \frac{\hbar^2}{2m} \left(\frac{2\pi}{L}\right)^2 \left(n_x^2 + n_y^2\right) \tag{5.84}$$

for two-dimensional systems and

$$\varepsilon_{n_x,n_y,n_z} = \frac{\hbar^2}{2m} \left(\frac{2\pi}{L}\right)^2 \left(n_x^2 + n_y^2 + n_z^2\right) \tag{5.85}$$

for three-dimensional systems. Similarly as in, for example, Refs. [58, 84] and Paper III, we choose the single-particle basis such that both the occupied and unoccupied single-particle spaces have a closed-shell structure. This means that all single-particle states corresponding to energies below a chosen cutoff are included in the basis. We study only the unpolarized spin phase, in which all orbitals are occupied by one spin-up and one spin-down electron. Below, we explain how we utilize the symmetries of this system to write the CC equations in block-diagonal form, and thereby improving the computational scaling of the CC calculations, similarly as is usually done in studies of chemical systems [221]. Table 5.1 shows the lowest-lying spin-orbitals and the cumulative numbers of single-particle states for a two-dimensional electron box with periodic boundary conditions. The CCD energy is obtained by solving the energy equations (5.12) and (5.13) together with the $\hat{T}_2$ amplitude equation (5.16) using the discrete momentum basis.

$n_x^2 + n_y^2$	n_x	n_y	$N_{\uparrow\downarrow}$	$N_{\uparrow\uparrow}$
0	0	0	2	1
1	-1	0		
	1	0		
	0	-1		
	0	1	10	5
2	-1	-1		
	-1	1		
	1	-1		
	1	1	18	9
4	-2	0		
	2	0		
	0	-2		
	0	2	26	13
5	-2	-1		
	2	-1		
	-2	1		
	2	1		
	-1	-2		
	-1	2		
	1	-2		
	1	2	42	21

Table 5.1: Illustration of how single-particle energies fill energy shells in a two-dimensional electron box. Here n_x and n_y are the momentum quantum numbers, $n_x^2 + n_y^2$ determines the single-particle energy level, $N_{\uparrow\downarrow}$ represents the cumulative number of spin-orbitals in an unpolarized spin phase, and $N_{\uparrow\uparrow}$ stands for the cumulative number of spin-orbitals in a spin-polarized system.

Implementation

As can be seen from Eqs. (5.81) and (5.82), the Coulomb interaction is diagonal in the CM momentum $\mathbf{K}$ and total spin projection M_S. Because of these symmetries, we store the two-body interaction and $\hat{T}_2$ amplitude matrices in blocks of $(\mathbf{K}, M_S)$. In quantum chemistry, the CC equations are commonly simplified by utilizing symmetries in a similar way [221]. From a computational point of view, the storage in blocks saves a considerable amount of memory and processor time. In the CCD equations (5.13) and (5.16), the terms with summation over two particle states or two hole states can straightforwardly be written as matrix-matrix multiplications. Unfortunately, the terms in the CCD amplitude equation with summation over one particle and one hole state cannot be calculated directly using matrix-matrix multiplications. To circumvent this problem, we use a similar cross-coupling technique as introduced by Kuo *et al.* for coupling of angular momenta [282]. In the discretized Cartesian momentum basis, all diagrams of the CCD equations can therefore be implemented using matrix-matrix multiplications (see also Paper III).

Let us explain the basic principles of the cross-coupling of matrix elements in the discrete momentum basis. Consider an antisymmetrized matrix element

$$\langle pq|v|rs\rangle.$$

In a diagram with summation over the two ket states, for example, we set up the matrix elements as

$$V_{\alpha(p,q),\beta(r,s)} \equiv \langle pq|v|rs\rangle$$

and sum over the two-particle states labeled with β. In this case, the blocks are set up such that the conservation requirements

$$\mathbf{k}_p + \mathbf{k}_q = \mathbf{k}_r + \mathbf{k}_s$$

and

$$m_{s_p} + m_{s_q} = m_{s_r} + m_{s_s}$$

are fulfilled. This gives blocks in total momentum $\mathbf{K}$ and total spin projection M_S. On the other hand, if the original summation is over the states s and q, for example, the matrix elements can be set up as

$$V_{\gamma(p,r),\delta(s,q)} \equiv \langle pq|v|rs\rangle, \tag{5.86}$$

where the summation is taken over the two-particle states δ. To ensure conservation of total momentum and spin projection, the matrices must be stored in blocks such that

$$\mathbf{k}_p - \mathbf{k}_r = \mathbf{k}_s - \mathbf{k}_q$$

and

$$m_{s_p} - m_{s_r} = m_{s_s} - m_{s_q}.$$

The blocks are now in relative momentum $\tilde{\mathbf{k}}$ and relative spin projection $\tilde{m}_s$. We call matrix elements set up as in Eq. (5.86) cross-coupled matrix elements.

Let us show how the particle-hole diagrams are calculated with matrix-matrix multiplications using cross-coupled matrices. Consider the particle-hole term

$$\langle ab|I_{ph}|ij\rangle \equiv \sum_{kc}\langle ac|t|ik\rangle \left\{ \langle kb|v|cj\rangle + \frac{1}{2}\sum_{ld}\langle kl|v|cd\rangle\langle db|t|lj\rangle \right\}, \tag{5.87}$$

which is part of the CCD amplitude equation. We cross-couple the matrix I_{ph} using the matrix-element transformation

$$\langle ab|I_{ph}|ij\rangle \longrightarrow \langle bj|I^*_{ph}|ia\rangle, \tag{5.88}$$

where the star denotes that the matrix has been cross-coupled from a particle-particle-hole-hole form to a particle-hole-hole-particle form. Technically, the matrix-element transformation is a relocation of matrix elements. The cross-coupled matrix I^*_{ph} is now written as the matrix-matrix product

$$\langle bj|I^*_{ph}|ia\rangle = \sum_{kc}\langle bj|I^*_2|ck\rangle\langle ck|t^*|ia\rangle, \tag{5.89}$$

where the matrix t^* is obtained using a similar element-transformation as in Eq. (5.88) and

$$\langle bj|I^*_2|ck\rangle = \langle bj|v^{\#}|ck\rangle + \frac{1}{2}\sum_{ld}\langle bj|t^*|ld\rangle\langle ld|v^*|ck\rangle. \tag{5.90}$$

Again, the matrices v^* and $v^{\#}$ are obtained with an element-transformation of the type shown in Eq. (5.88). The matrix v^* has been obtained by cross-coupling a matrix with hole-hole-particle-particle configuration, whereas the matrix $v^{\#}$ has been obtained by cross-coupling a hole-particle-particle-hole matrix. Equations (5.89) and (5.90) are straightforwardly implemented as matrix-matrix multiplications. Finally, the matrix I^*_{ph} is transformed back to the normal coupling scheme, and blocks of I_{ph} are added to the CCD amplitude equation. The implementation of matrix-matrix multiplications

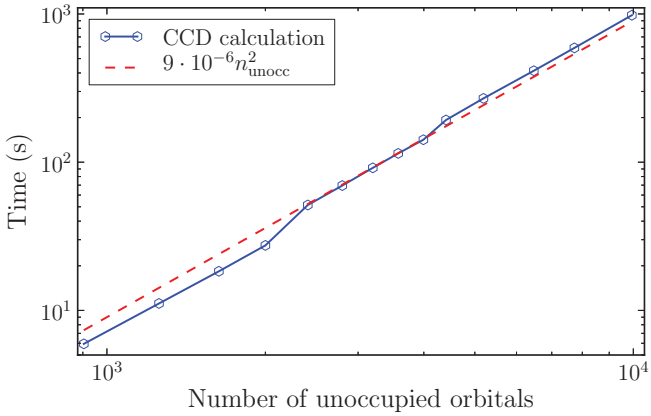

Figure 5.6: The computing time scales quadratically as a function of unoccupied single-particle orbits n_{unocc}. The CCD calculations were done for the two-dimensional electron gas with ten electrons at $r_s = 0.5$, without MPI parallelization and with a fixed number of cpus on a single computing node.

for all diagrams gives a significant speedup of the computer program. Figure 5.6 shows that the total computing time scales quadratically with the number of unoccupied orbitals, n_{unocc}, when utilizing block diagonalization and matrix-matrix multiplications as described above.

To be able to use large-scale distributed computing clusters, we have parallelized the CC program in Cartesian momentum coordinates using the Message Passing Interface (MPI) Standard [266, 267]. In our implementation, both the cross-coupled and normally coupled matrices are stored in arrays containing matrix blocks. Most of the matrix arrays are divided into subarrays that are distributed to different MPI processes (see Figure 5.7). A given subarray containing matrices is then stored only locally on the computing node where the corresponding MPI process resides. In addition to parallelizing the computing operations, this arrangement reduces the memory consumption on each node. Some of the matrices, such as the cross-coupled amplitude matrix and the normally coupled matrix of the particle-hole diagrams must be communicated to all nodes. We, therefore, chose to store complete matrix arrays of these parts on every node. For example, different parts of the normally coupled particle-hole diagrams, I_{ph}, are calculated locally on different computing nodes, and finally all parts are summed up, and the resulting matrix array is distributed to all nodes.

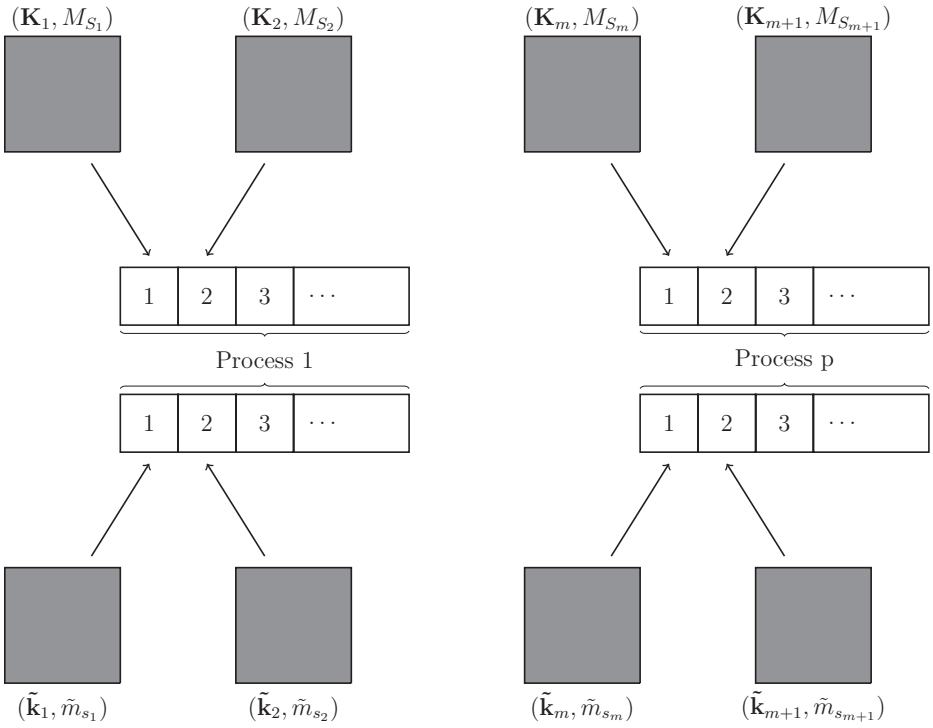

Figure 5.7: The big matrices are divided into matrix blocks, each being an element of an array. Subarrays of the different matrix lists are associated with different MPI processes. There are different matrix lists for normally coupled and cross-coupled matrices.

r_s	n_{basis}	E_{CCD}	$E_{IM-SRG(2)}$ [81]	E^L_{FCIQMC} [85]	E^S_{FCIQMC} [210]
0.5	114	−0.073145	−0.073638	−0.073842	−0.07384
	186	−0.079047	−0.079582	−0.07986	−0.07984
	358	−0.081954	−0.082504	−0.08284	−0.08281
1.0	114	−0.063987	−0.065290	−0.06583	−0.06587
	186	−0.069360	−0.070779	−0.07152	−0.07156
	358	−0.071789	−0.073235	−0.07413	−0.07412
2.0	114	−0.051114	−0.053746	−0.05487	−0.05489

Table 5.2: Correlation energies per particle for 14 electrons in a three-dimensional cubic box, as obtained with the CCD, IM-SRG [80], and FCIQMC [83] methods. The energies are given in Rydbergs, and n_{basis} denotes the size of the single-particle basis. The IM-SRG(2) results are by Reimann [81, 82], the energies marked by E^L_{FCIQMC} are results of Leikanger [85, 86], whereas the energies E^S_{FCIQMC} are FCIQMC results from Ref. [210]. The FCIQMC calculations were done using the initiator approximation [283]. Similarly as can be seen from Figure 5 of Ref. [54], we find that the CCD approximation lacks important correlations. The IM-SRG(2) method gives results much closer to the almost exact FCIQMC energy estimates. For comparison, Ceperley and Alder [53, 211] and Bishop and Lührmann [53] obtained at $r_s = 1.0$ as thermodynamic-limit estimates of the correlation energy −0.121 Ry and −0.123 Ry when using the GFMC and CC methods, respectively.

Verification and results

First, we tested our general implementation of the CCSD approximation by comparing ground-state energies of a two-dimensional parabolic quantum dot with results of Pedersen Lohne *et al.* [75]. Energies for two-particle quantum dots with different numbers of excited single-particle states were found to agree with Ref. [75] to six digits. To verify our CCD approximation for periodic systems, we compared results for the three-dimensional electron gas with similar calculations of Shepherd *et al.* [54]. As far as we understand Ref. [54], they define the Fock matrix elements with a contribution from the self-energy v_0, whereas we have defined the Fock matrices without this constant. Despite the slightly different definition of the CC algorithm, our correlation energies for 14 electrons in a cubic box agreed with the CCD results in Figure 5 (a) of Ref. [54] to the accuracy that can be read from the figure by careful inspection. The difference between our results and those of Shepherd *et al.* [54] was less than 0.001 Ha for selected points.

As is common in studies of the electron gas, we use the unitless radius r_s, which is

defined by [192, p. 25]

$$\frac{1}{(4\pi r_1^3)/3} = \frac{N}{\Omega}, \qquad r_s \equiv \frac{r_1}{r_B}, \tag{5.91}$$

where N is the number of electrons, Ω is the volume of the considered system, $r_B = \hbar^2/(m_e e^2)$ is the Bohr radius, m_e is the electron mass, and e is the electron charge. On average, every electron occupies a volume

$$\Omega^{(1)}(r_s) = \frac{4\pi r_B^3 r_s^3}{3}, \tag{5.92}$$

and r_s may, therefore, be considered as a dimensionless measure of the average distance between electrons in the system.

In Table 5.2, we compare correlation energies per particle for a three-dimensional electron-gas system consisting of 14 particles in a box, calculated at different densities. Energies obtained using the CCD approximation are benchmarked against FCIQMC results of Shepherd *et al.* [210]. In addition, we have included in-medium-SRG (IM-SRG) [80] results of Reimann [81, 82] and FCIQMC results of Leikanger [85, 86]. All FCIQMC results presented in this section have been calculated using the initiator approximation (i-FCIQMC) [283], and the IM-SRG results were obtained in the IM-SRG(2) approximation, in which the operators are truncated at the two-body level [284]. To the best of our knowledge, the electron gas has not been studied before using the IM-SRG approach, and the CCD and FCIQMC approximations have not been applied to the two-dimensional electron gas. The IM-SRG(2) results for the three-dimensional system are close to those of the virtually exact FCIQMC method, whereas the CCD energies clearly deviate from the other results. From the results of Table 5.2, we may conclude that the CCD approximation is insufficient to deal with the correlations in the three-dimensional electron gas, when approximated by a 14-electron box. It seems, therefore, necessary to include contributions from the triples amplitudes in CC calculations of this system. As expected, the CCD approach is best at high densities, and the error increases when going to lower densities. This behavior is expected, as the correlations become stronger when the density decreases [53]. A similar comparison between the CCD and FCIQMC methods for the three-dimensional electron gas is given in Figure 5 of Ref. [54], and the latter results show the same features as we see in Table 5.2.

Let us compare the finite-size calculations in Table 5.2 with previous studies of the three-dimensional electron gas at the thermodynamic limit. Ceperley and Alder [53, 211] obtained the correlation energy -0.121 Ry, when extrapolating GFMC results at $r_s = 1.0$ to the thermodynamic limit. Similarly, Bishop and Lührmann [53] obtained

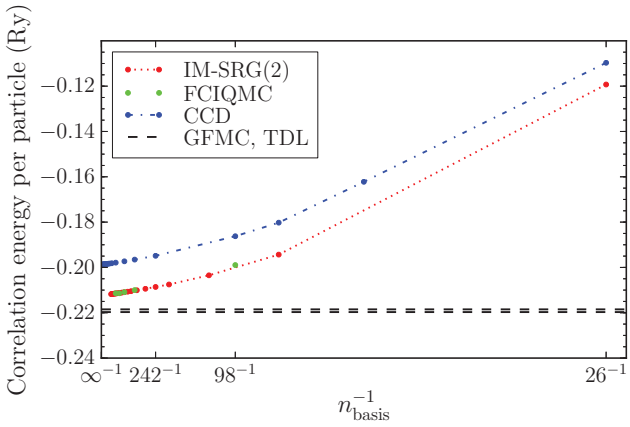

Figure 5.8: Correlation energy per particle as function of the number of single-particle orbits for a ten-particle electron gas at $r_s = 1.0$. The IM-SRG(2) correlation energies [81, 82] are in excellent agreement with the almost exact FCIQMC results [85, 86]. Similarly as was observed with the CC particle-hole ring-diagram approximation of Freeman [51, 59], the CCD truncation is less accurate for the two-dimensional electron gas than for the three-dimensional counterpart. For comparison, we have marked the correlation energy in the thermodynamic limit, as obtained by extrapolating GFMC energies [215]. The width of the horizontal line shows the statistical error of the GFMC calculations.

at the same density the correlation energy −0.123 Ry, when using a CC approximation defined in the limit of infinitely many particles. The finite-size results in Table 5.2 and Ref. [54], which were obtained using finite single-particle bases, are remarkably far from the estimates for the thermodynamic limit given in Refs. [53, 211].

Next, we consider the two-dimensional electron gas, which we have chosen to focus on. First, we compare the CCD approximation with the IM-SRG(2) and FCIQMC methods. Figure 5.8 shows results for a ten-electron system at $r_s = 1.0$. As can be seen from Figure 5.8, IM-SRG(2) gives very accurate energy estimates [81, 82], in close agreement with FCIQMC [85, 86]. For this system, the CCD approximation is clearly insufficient to describe the most important correlations. Freeman studied both the two- [59] and three-dimensional [51] electron gas in the thermodynamic limit using a particle-hole ring approximation derived from CC theory. According to these studies, the ring approximation is fairly successful in three dimensions, but fails more seriously to describe the two-dimensional system [51, 59]. Here we find that the CCD approximation is less accurate for the finite-size two-dimensional electron gas than for

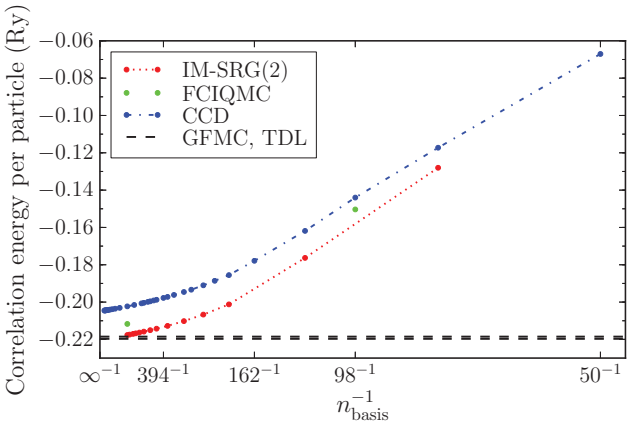

Figure 5.9: Same as Figure 5.8, but for a 26-particle two-dimensional electron gas. In contrast to the results for a ten-particle system, given in Figure 5.8, the IM-SRG(2) results for the 26-particle system [81, 82] deviate significantly from the virtually exact FCIQMC values [85, 86].

the three-dimensional system, but in both systems the CCD approximation gives results that deviate several percent from the more accurate FCIQMC values. The finite-size error can be estimated from Figure 5.8 as the difference between the FCIQMC results and the horizontal line, which shows the correlation energy at the thermodynamic limit, obtained by extrapolation of GFMC results [215].

In Figure 5.9 we show a similar plot as Figure 5.8, but here for a 26-particle electron-gas system. As for the ten-particle system, the CCD energies are far from the FCIQMC results. In addition, the IM-SRG(2) results deviate considerably more than for the ten-particle system with respect to the FCIQMC energy estimates. This suggests that the IM-SRG(2) method is less accurate than one could expect by only considering the ten-particle results. Observe that the IM-SRG method is nonvariational [284], and the approximate energies are, therefore, not upper limits of the exact value. The IM-SRG(2) approach has recently been applied to finite nuclei [284]. When compared to CC theory in the CCSD and Λ-CCSD(T) [285, 286] approximations, where the latter approximation treats the triples amplitudes only noniteratively, the IM-SRG(2) results were closer to the Λ-CCSD(T) than to the CCSD approximation [284]. Reimann *et al.* [82, 287] have recently studied two-dimensional parabolic quantum dots using IM-SRG(2), CCD, and DMC. They found better agreement between IM-SRG(2) and DMC than between CCD and DMC in systems with not too strong correlations [82, 287].

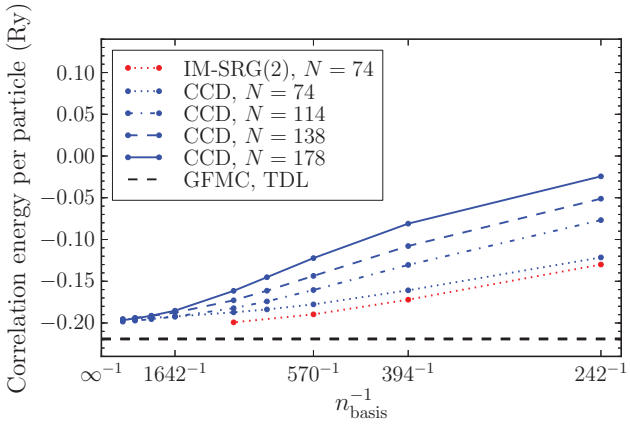

Figure 5.10: Correlation energy as a function of the number of single-particle basis functions, as calculated for the two-dimensional electron gas at $r_s = 1.0$. Finite-size approximations with different numbers of particles seem to converge to almost the same energy in the limit of a large single-particle basis. For comparison, we show IM-SRG(2) results [81, 82], which are more accurate than the CCD energies, and a GFMC estimate for the thermodynamic limit, obtained by extrapolation from finite-size calculations [215]. The error bar of the GFMC calculations is marked by the width of the horizontal line.

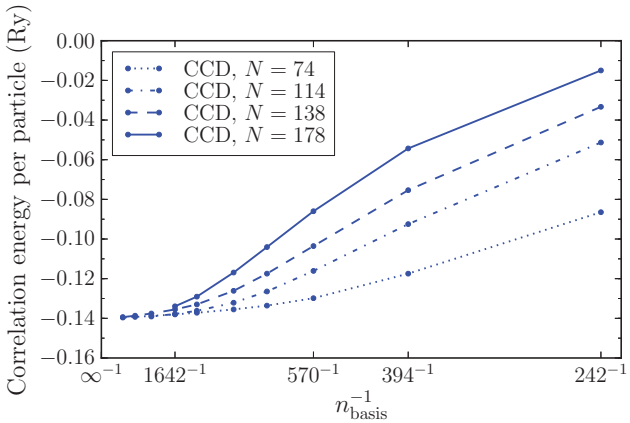

Figure 5.11: Correlation energy as a function of the number of single-particle basis functions, as calculated for the two-dimensional electron gas at $r_s = 2.0$. Similarly as at $r_s = 1.0$, the correlation energies for systems of different sizes approach the same value in the limit of a large single-particle basis.

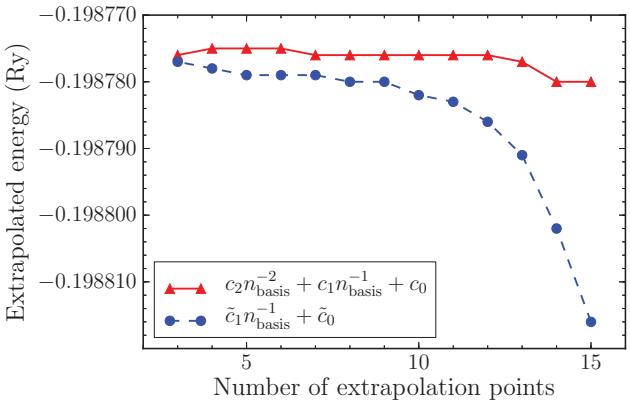

Figure 5.12: Extrapolated correlation energies for a ten-particle two-dimensional electron gas at $r_s = 1.0$. The extrapolation converges faster when fitting the results to an equation quadratic in n_{basis}^{-1} than when using an expression that is linear in the inverted number of single-particle states, n_{basis}^{-1}. The parameters c_i, where $i \in \{0, 1, 2\}$ and $\tilde{c}_j$, where $j \in \{0, 1\}$, were obtained using a least-squares fitting [255, pp. 77–84].

We have approximated the two-dimensional electron gas using different numbers of electrons. Figure 5.10 shows CCD correlation energies as function of the single-particle basis size for systems with 74, 114, 138, and 178 particles, calculated at $r_s = 1.0$. The CCD results for different finite systems seem to converge to approximately the same energy when the basis size approaches infinity. The difference between the almost converged CCD results and the thermodynamic-limit estimate of Kwon *et al.* [215] must therefore be mostly due to missing correlations in the CCD approximation. Similarly as for the ten-particle system, IM-SRG(2) gives a lower energy estimate [81, 82] than CCD for a 74-particle electron gas. As can be seen from Figure 5.11, the energy of finite systems of different sizes converge to almost the same value also when $r_s = 2.0$.

In Table 5.3 we compare different approximations of CCD, as calculated for a two-dimensional electron-gas system with ten particles at $r_s = 1.0$. The PPHHM-LAD-M approximation contains particle-particle, hole-hole and mixed ladders, as well as the so-called mosaics diagrams [56]. This approximation is obtained from the CCD equations by setting the intermediate I_2 in Eq. (5.18) to zero. The PP-LAD approximation was defined for nuclear matter above and contains only particle-particle ladder diagrams. The PP-LAD equations are obtained by neglecting all intermediates from the CCD approximation. The PP-LAD* truncation is otherwise as PP-LAD, but the single-particle

Thermodyn. limit:	ΔE_{corr}			
GFMC [215]	-0.2191 ± 0.0006			
CC-R$^{\mathrm{F}}$ [59]	-0.2308			
PP-LAD$^{\mathrm{F}}$ [60]	-0.22			
Ten-particle approximation:	$\Delta E_{\mathrm{corr}}^{\mathrm{extrap}}$ $(= c_0)$	c_1	c_2	$\Delta E_{\mathrm{corr}}^{n_{\mathrm{basis}}=9946}$
CCD	-0.1988	0.7750	7.779	-0.1987
PPHHM-LAD-M	-0.2046	0.8224	71.47	-0.2045
PP-LAD*	-0.2418	0.7660	70.57	-0.2418
PP-LAD	-0.2579	0.7537	67.34	-0.2578
PPHHM-LAD	-0.2586	0.7912	69.36	-0.2586
CC-R	-0.3627	2.554	125.2	-0.3624

Table 5.3: Correlation energies per particle in Rydbergs, as obtained with different approximations derived from CC theory. In the table, we compare the CCD method with approximations of CCD in which we have included only certain diagrammatic classes. We obtained the extrapolated correlation energy $\Delta E_{\mathrm{corr}}^{\mathrm{extrap}}$ by fitting results calculated with n_{basis} between 2010 and 9946 to the formula $c_2 n_{\mathrm{basis}}^{-2} + c_1 n_{\mathrm{basis}}^{-1} + c_0$, where c_i, $i \in \{0, 1, 2\}$, are optimization parameters. The two-dimensional electron gas was approximated by ten electrons in a box and was calculated at $r_s = 1.0$. For comparison, we have included a GFMC result of Kwon *et al.* [215], a CC ring approximation (CC-R$^{\mathrm{F}}$) result of Freeman [59], and a CC particle-particle ladder approximation (PP-LAD$^{\mathrm{F}}$) result of Freeman [60], all calculated in the thermodynamic limit. As we describe in the text, the CC-R$^{\mathrm{F}}$ and PP-LAD$^{\mathrm{F}}$ approximations of Freeman are defined differently than our CC-R, PP-LAD, and PP-LAD*.

energies are calculated using only kinetic energies. The PPHHM-LAD approximation contains particle-particle, hole-hole, and mixed ladder diagrams, which means that the intermediates I_2, I_3, and I_4 are set to zero. Finally, the CC-R, or CC ring, approximation is obtained by removing the particle-particle ladder diagrams, given by the second line on the right-hand side of Eq. (5.18), as well as all intermediates. Shepherd *et al.* [56] have applied similar approximations of CC theory to the three-dimensional electron gas. The approximations PPHHM-LAD-M, PPHHM-LAD, and CC-R correspond to the truncations called lmCCD, lCCD, and rCCD, respectively, in Ref. [56]. Observe that Shepherd *et al.* define the Fock matrices differently, with a self-energy constant in the single-particle energies [56]. When comparing with the results for the three-dimensional electron gas given in Ref. [56], we get similar energies for the CCD approximation, whereas other approximations deviate more.

The correlation energies given in the second column of Table 5.3 were obtained by extrapolating to the limit of an infinitely large single-particle basis. The extrapolation was done using the quadratic polynomial form

$$p(n_{\text{basis}}^{-1}) = c_2 n_{\text{basis}}^{-2} + c_1 n_{\text{basis}}^{-1} + c_0, \tag{5.93}$$

where n_{basis} is the size of the single-particle basis. In the cases we consider, the extrapolation curve is close to linear in n_{basis}^{-1}, and our formula can therefore be considered as a variation of the n_{basis}^{-1} extrapolation used by Shepherd *et al.* [54, 56, 210]. As illustrated in Figure 5.12, we obtained slightly faster convergence in the extrapolation when using the expression (5.93) than when assuming that the extrapolation is linear in n_{basis}^{-1}. We observed the same qualitative difference between linear and quadratic extrapolations as seen in Figure 5.12 for the PP-LAD, PP-LAD*, PPHHM-LAD, CC-R, and PPHHM-LAD-M approximations. Based on this empirical fact, we chose to use the quadratic extrapolation formula. Shepherd *et al.* [54] have shown analytically that the energy in MBPT(2) converges proportionally to the inverse of the number of single-particle basis functions. An extrapolation proportional to n_{basis}^{-1} was also used in the CC calculations of Ref. [56]. When calculating the values given in the the second column of Table 5.3, we used a least-squares fitting based on results calculated for ten different values of n_{basis}, between 2010 and 9946 single-particle states.

As can be seen from Table 5.3, the different partial summations of CCD give quite different correlation energies. According to these results, the PPHHM-LAD-M approximation, which only neglects the ring diagrams given by I_2, describes most of the correlations present in CCD. The CC-R result deviates most from both the GFMC and CCD energies. Shepherd *et al.* [56] studied the three-dimensional electron gas using

an approximation they called mCCD, or CC mosaics truncation, in which the particle-particle ladders and the intermediates I_1 and I_2 of the CCD equations are set to zero. In the three-dimensional system, the mCCD approximation gave results close to the CCD approach [56]. When applying the mCCD truncation to the two-dimensional electron gas, we had problems with convergency as a function of n_{basis}, and the results were around -0.34 Rydbergs, thus far from the CCD energy for the considered ten-electron system at $r_s = 1.0$. We conclude that the correlation energy is sensitive to the chosen many-body approximation, and it may not be justifiable to leave out classes of diagrams from the CCD approximation for the two-dimensional electron gas. Instead, higher-order contributions are needed to describe the relevant correlations in this system. Shepherd *et al.* also found large differences between different partial summations of the CCD approximation in their studies of the three-dimensional electron gas [56].

For comparison, in Table 5.3 we have included correlation energies at the thermodynamic limit, as given in Refs. [59, 60, 215]. In contrast to our CC approximations, the CC ring (CC-R$^{\text{F}}$) and CC particle-particle ladder (PP-LAD$^{\text{F}}$) approximations of Freeman are defined with not antisymmetrized interaction-matrix elements in the CC amplitude equations [59, 60]. Apart from this difference, our PP-LAD*, which has only kinetic energies in the energy denominator, is defined as the PP-LAD$^{\text{F}}$ approximation. As mentioned above, Freeman got for the two-dimensional electron gas results in closer agreement with the GFMC energies of Tanatar and Ceperley [197] when using the particle-particle ladder approximation [60] than with the ring approximation [59]. Similarly, we find that the PP-LAD approximation performs better than CC-R for a ten-particle system in two dimensions. However, the ladder- and ring-approximation correlation energies deviate much more for the finite system than what was observed at the thermodynamic limit.

In this chapter, we have discussed CC approaches for infinite-matter systems. We have given short introductions to Papers I–III, in which CC theory is applied to symmetric nuclear matter and neutron matter. The implementation and verification of our CC ladder approximation have been explained, and we have also pointed on difficulties related to an extension of the partial-wave ladder approximation to a full CCD approximation. A spherical model for nuclear matter has been mentioned, in which the single-particle basis consists of spherical Bessel functions. Finally, we have presented new results for the two-dimensional electron gas, calculated in the CCSD approximation using a finite number of electrons.

Chapter 6

Conclusions

The most important goal of this thesis has been to reintroduce CC theory as a tool to study infinite nuclear matter. As a first application, we have studied symmetric nuclear matter and neutron matter using a particle-particle and hole-hole ladder approximation derived from CC theory. In our approach, which is described in detail in Paper II, the CC ladder equations are written in a partial-wave basis using exact Pauli exclusion operators, with angular-average approximations only in the single-particle energies. As explained by, for example, Bishop and Lührmann [52], a CCD approximation contains many important classes of diagrams beyond the particle-particle and hole-hole ladder approximation. It is, therefore, interesting to study infinite nuclear matter in a full CCD approximation. Our collaborators have introduced another CC approach, in which they approximate infinite nuclear matter by a finite box containing a limited number of particles. In Paper III, they use the latter method to study infinite nuclear matter in the CCD and the CCD(T) approximations.

To verify and get insight in our CC ladder approximation, we have compared the method with other many-body approaches. In Paper II, we compare the ladder approximation with the well-known BHF method [7, 8, 65–67], as defined with continuous single-particle energies [68, 69]. The symmetric nuclear matter equations of state are similar for both methods, giving approximately 6 % less binding with the CC ladder method than with the BHF approach, when the CC ladder calculations are done using exact Pauli operators whereas angular-averaged Pauli operators are used in the BHF approach. When the Pauli exclusion operators are averaged in both methods, the differences are larger (see Paper II).

The accuracy of the CC ladder approach of Paper II is limited by a truncation in the total angular momentum, resulting in an error of less than 0.3 MeV. Another source of error is the angular-average approximation used in the energy denominator. We have not been able directly to quantify the error related to the angular-average

approximations used in the energy denominators. However, in Paper III we compare the CC ladder approximation of Paper II with a particle-particle and hole-hole ladder approximation of the CC approach formulated using a finite number of nucleons. In the latter CC method, infinite nuclear matter is approximated by averaging over different twisted boundary conditions. When comparing the two CC ladder approximations, we find that the differences in energy are always smaller than the error related to the cutoff in angular momentum (see Paper III). This good agreement between these quite different approaches, calculated in the thermodynamic limit and with finite particle numbers, respectively, indicates that the error of the angular-averaged single-particle energies is small. Simultaneously, the agreement shows that the twist-average approximation gives a good estimate of the thermodynamic limit for nuclear matter.

In Paper III, we also compare the CC ladder approach defined at the thermodynamic limit with the AFDMC method [73]. Using the Minnesota potential [74], we calculate the neutron matter equation of state. At densities below the saturation point of nuclear matter, the partial-wave-expanded CC ladder approach, the CCD approximation of Paper III, and the AFDMC method give almost the same equation of state. At least when using the Minnesota potential, correlations beyond the ladder approximation seem to be small in pure neutron matter. On the other hand, results in Paper III show that, for symmetric nuclear matter, the CCD truncation contains significant correlations compared to the CC ladder approximation. It is uncertain whether the difference between the CCD and the CC ladder approximations is due to contributions from particle-hole ring diagrams, or possibly other classes of diagrams. When Shepherd *et al.* analyzed contributions from different subapproximations of the CCD truncation in the electron gas, they found that so-called mosaics terms were particularly important [56]. It would be interesting to analyze the CCD approximation for nuclear matter further, to get a deeper understanding of where the correlation contributions come from.

Our collaborators studied infinite nuclear matter in the CCD(T) approximation, where the triples amplitudes are approximated by perturbative contributions. They also included nuclear three-body forces, as obtained from chiral perturbation theory. According to these calculations, which are presented in Paper III, the CC triples amplitudes give a significant contribution to the energy of symmetric nuclear matter. In the triples amplitudes, the full three-body force, without any normal-ordered approximations, is required. The CC studies of Paper III showed challenges related to the chiral three-body interaction, such as a strong regulator dependency and failure to simultaneously reproduce the binding energies of both the triton and symmetric nuclear

matter. It seems that further development of chiral interactions is necessary to significantly improve the CC calculations for symmetric nuclear matter (see Paper III). In conclusion, the results of Paper III illustrate how symmetric nuclear matter can be used to test nuclear interaction models.

As part of this thesis, we have also studied the electron gas using CC methods. In particular, we have concentrated on the two-dimensional electron gas, which has not been studied before in the CCD approximation. In our calculations, we have approximated the electron gas using finite boxes, as in Refs. [54–58]. First, we verified our method by studying the three-dimensional electron gas and comparing with results of Shepherd *et al.* [54, 210]. Our results for the two-dimensional electron gas were compared with IM-SRG [80] results of Reimann [81, 82] and FCIQMC [83] correlation-energy estimates of Leikanger [85, 86]. We found that the CCD approximation misses important correlations in the two-dimensional electron gas, and inclusion of triples correlations is, therefore, necessary to get accurate results. We also studied different partial summations of the CCD approximation, such as the CC particle-particle ladder and CC particle-hole ring approaches, in a similar way as was done in Ref. [56] for the three-dimensional electron gas. As in Ref. [56], we observed large differences between different approximations of CCD, which indicates that such partial summations are not sufficient to reliably model the finite-size two-dimensional electron gas.

Further studies

The CC ladder approximations of Paper II could be extended to asymmetric nuclear matter by modifying the Pauli exclusion operators to have different Fermi momenta for protons and neutrons [143, 151, 152]. This would open up for many applications in astrophysics, including the study of neutron star matter at β equilibrium [143, 151, 152]. The CC ladder calculations of Paper II could also be extended to contain three-body forces in a normal-ordered two-body approximation, similarly as in Paper III.

As mentioned above, the results of Paper III indicate that improvements in the chiral interaction are necessary to obtain realistic equations of state. It would be interesting to do CC calculations for nuclear matter with chiral two- and three-body interactions including Δ resonances. Such nuclear forces would be an extension of the models we used, in which only pions and unexcited nucleons are taken into account (see, for example, Ref. [16] for a discussion on this subject). With an improved and more realistic equation of state, one could extract a density functional or Skyrme force, as has been done using the BHF approximation [25, 26]. Coupled-cluster theory could also be used to study momentum distributions in nuclear matter, similarly as has been

done recently with the SCGF method [180]. In quantum chemistry, coupled-cluster theory has been generalized to relativistic systems [288]. As far as we know, infinite nuclear matter has not yet been studied using such approaches, and it is, therefore, of interest to investigate possible implementations.

Shepherd *et al.* [55] have studied the three-dimensional electron gas using perturbative triples correlations. According to their investigations, a CCD(T) approximation, which includes only a perturbative approximation of the triples amplitudes, causes a diverging energy in the thermodynamic limit [55]. As far as we know, a complete CCSDT calculation has not been done even for the smallest finite-size electron-gas systems in two and three dimensions. It would be interesting to do such an extension for very small systems. In our CC studies of the electron gas, we have neglected finite-size effects. Finite-size effects in the electron gas have been accounted for using different approaches [72, 77, 79, 199]. In the CC calculations, finite-size effects could be decreased by, for example, using averaging over different twisted boundary conditions [72], as was done for nuclear matter in Paper III. Momentum distributions [180] and pair-correlation functions [60] of the electron gas could also be studied using different CC approximations.

Bibliography

[1] The Committee on the Assessment of, Outlook for Nuclear Physics; Board on Physics, Astronomy; Division on Engineering, and Physical Sciences; National Research Council. *Nuclear Physics: Exploring the Heart of Matter*. The National Academies Press, 2013. Available from: `http://www.nap.edu/openbook.php?record_id=13438`.

[2] B. D. Day. *Rev. Mod. Phys.*, 39:719, 1967.

[3] H. Heiselberg and M. Hjorth-Jensen. *Phys. Rep.*, 328:237, 2000.

[4] J. M. Lattimer and M. Prakash. *Science*, 304:536, 2004.

[5] J. M. Lattimer. *Annu. Rev. Nucl. Part. Sci.*, 62:485, 2012.

[6] C. J. Horowitz, E. F. Brown, Y. Kim, W. G. Lynch, R. Michaels, et al. arxiv:1401.5839v1 [nucl-th]. 2014.

[7] K. A. Brueckner, C. A. Levinson, and H. M. Mahmoud. *Phys. Rev.*, 95:217, 1954.

[8] K. A. Brueckner and J. L. Gammel. *Phys. Rev.*, 109:1023, 1958.

[9] C. Fuchs. The relativistic dirac-brueckner approach to nuclear matter. In G. A. Lalazissis, P. Ring, and D. Vretenar, editors, *Extended Density Functionals in Nuclear Structure Physics*. Springer, Berlin, 2004.

[10] J. R. Stone and P.-G. Reinhard. *Prog. Part. Nucl. Phys.*, 58:587, 2007.

[11] J. Carlson, V. R. Pandharipande, and R. B. Wiringa. *Nucl. Phys. A*, 401:59, 1983.

[12] B. S. Pudliner, V. R. Pandharipande, J. Carlson, and R. B. Wiringa. *Phys. Rev. Lett.*, 74:4396, 1995.

[13] B. S. Pudliner, V. R. Pandharipande, J. Carlson, Steven C. Pieper, and R. B. Wiringa. *Phys. Rev. C*, 56:1720, 1997.

[14] R. Machleidt and I. Slaus. *J. Phys. G*, 27:R69, 2001.

[15] E. Epelbaum, H.-W. Hammer, and Ulf-G. Meißner. *Rev. Mod. Phys.*, 81:1773, 2009.

[16] R. Machleidt and D. R. Entem. *Phys. Rep.*, 503:1, 2011.

[17] B. D. Day and G. Zabolitzky. *Nucl. Phys. A*, 366:221, 1981.

[18] H. Q. Song, M. Baldo, G. Giansiracusa, and U. Lombardo. *Phys. Rev. Lett.*, 81:1584, 1998.

[19] J. Carlson, J. Morales, V. R. Pandharipande, and D. G. Ravenhall. *Phys. Rev. C*, 68:025802, 2003.

[20] S. Gandolfi, F. Pederiva, S. Fantoni, and K. E. Schmidt. *Phys. Rev. Lett.*, 98:102503, 2007.

[21] V. Somà and P. Bożek. *Phys. Rev. C*, 78:054003, 2008.

[22] K. Hebeler, S. K. Bogner, R. J. Furnstahl, A. Nogga, and A. Schwenk. *Phys. Rev. C*, 83:031301, 2011.

[23] A. Carbone, A. Polls, and A. Rios. *Phys. Rev. C*, 88:044302, 2013.

[24] UNEDF SciDAC Collaboration. Universal Nuclear Energy Density Functional. Accessed: 2014-04-14. Available from: `http://unedf.org`.

[25] M. Baldo, C. Maieron, P. Schuck, and X. Vias. *Nucl. Phys. A*, 736:241, 2004.

[26] L. G. Cao, U. Lombardo, C. W. Shen, and N. Van Giai. *Phys. Rev. C*, 73:014313, 2006.

[27] E. van Dalen and H. Müther. *Int. J. Mod. Phys. E*, 19:2077, 2010.

[28] J. E. Drut, R. J. Furnstahl, and L. Platter. *Prog. Part. Nucl. Phys.*, 64:120, 2010.

[29] F. Coester. *Nucl. Phys.*, 7:421, 1958.

[30] F. Coester and H. Kümmel. *Nucl. Phys.*, 17:477, 1960.

[31] J. Čížek. *J. Chem. Phys.*, 45:4256, 1966.

[32] J. Čížek and J. Paldus. *Int. J. Quantum Chem.*, 5:359, 1971.

[33] R. Bartlett and M. Musiał. *Rev. Mod. Phys.*, 79:291, 2007.

[34] J. H. Heisenberg and B. Mihaila. *Phys. Rev. C*, 59:1440, 1999.

[35] D. J. Dean and M. Hjorth-Jensen. *Phys. Rev. C*, 69:054320, 2004.

[36] K. Kowalski, D. J. Dean, M. Hjorth-Jensen, T. Papenbrock, and P. Piecuch. *Phys. Rev. Lett.*, 92:132501, 2004.

[37] G. Hagen, T. Papenbrock, D. J. Dean, A. Schwenk, A. Nogga, M. Włoch, and P. Piecuch. *Phys. Rev. C*, 76:034302, 2007.

[38] G. Hagen, T. Papenbrock, D. J. Dean, and M. Hjorth-Jensen. *Phys. Rev. Lett.*, 101:092502, 2008.

[39] R. Roth, J. R. Gour, and P. Piecuch. *Phys. Rev. C*, 79:054325, 2009.

[40] G. Hagen, T. Papenbrock, and M. Hjorth-Jensen. *Phys. Rev. Lett.*, 104:182501, 2010.

[41] G. Hagen, M. Hjorth-Jensen, G. R. Jansen, R. Machleidt, and T. Papenbrock. *Phys. Rev. Lett.*, 109:032502, 2012.

[42] S. Binder, P. Piecuch, A. Calci, J. Langhammer, P. Navrátil, and R. Roth. *Phys. Rev. C*, 88:054319, 2013.

[43] H. Kümmel, K. H. Lührmann, and J. G. Zabolitzky. *Phys. Rep.*, 36:1, 1978.

[44] G. Hagen, T. Papenbrock, M. Hjorth-Jensen, and D. J. Dean. *Rep. Prog. Phys.*, in press (2014).

[45] Z. H. Li, U. Lombardo, H.-J. Schulze, W. Zuo, L. W. Chen, and H. R. Ma. *Phys. Rev. C*, 74:047304, 2006.

[46] E. Epelbaum, H. Krebs, D. Lee, and U.-G. Meißner. *Eur. Phys. J. A*, page 199, 2009.

[47] I. Tews, T. Krüger, K. Hebeler, and A. Schwenck. *Phys. Rev. Lett.*, 110:032504, 2013.

[48] J. W. Holt, N. Kaiser, and W. Weise. *Phys. Rev. C*, 87:014338, 2013.

[49] G. Giuliani and G. Vignale. *Quantum Theory of the Electron Liquid*. Cambridge University Press, 2005.

[50] C. M. Singal and T. P. Das. *Phys. Rev. B*, 8:3675, 1973.

[51] D. L. Freeman. *Phys. Rev. B*, 15:5512, 1977.

[52] R. F. Bishop and K. H. Lührmann. *Phys. Rev. B*, 17:3757, 1978.

[53] R. F. Bishop and K. H. Lührmann. *Phys. Rev. B*, 26:5523, 1982.

[54] J. J. Shepherd, A. Grüneis, G. H. Booth, G. Kresse, and A. Alavi. *Phys. Rev. B*, 86:035111, 2012.

[55] J. J. Shepherd and A. Grüneis. *Phys. Rev. Lett.*, 110:226401, 2013.

[56] J. J. Shepherd, T. M. Henderson, and G. E. Scuseria. arxiv:1310.6806v2 [physics.chem-ph]. 2013.

[57] J. J. Shepherd, T. M. Henderson, and G. E. Scuseria. arxiv:1310.6425v3 [physics.chem-ph]. 2013.

[58] A. Roggero, A. Mukherjee, and F. Pederiva. *Phys. Rev. B*, 88:115138, 2013.

[59] D. L. Freeman. *Solid State Commun.*, 26:289, 1978.

[60] D. L. Freeman. *J. Phys. C*, 16:711, 1983.

[61] I. Shavitt and R. J. Bartlett. *Many-Body Methods in Chemistry and Physics*. Cambridge University Press, 2009.

[62] W. H. Dickhoff and C. Barbieri. *Prog. Part. Nucl. Phys.*, 52:377, 2004.

[63] W. H. Dickhoff and D. Van Neck. *Many-Body Theory Exposed! Propagator Description of Quantum Mechanics in Many-Body Systems*. World Scientific, second edition, 2008.

[64] K. Suzuki, R. Okamoto, M. Kohno, and S. Nagata. *Nucl. Phys. A*, 665:92, 2000.

[65] H. A. Bethe. *Annu. Rev. Nucl. Sci.*, 21:93, 1971.

[66] B. D. Day. *Rev. Mod. Phys.*, 50:495, 1978.

[67] M. I. Haftel and F. Tabakin. *Nucl. Phys. A*, 158:1, 1970.

[68] C. Mahaux, P. F. Bortignon, and R. A. Broglia. *Phys. Rep.*, 120:1, 1985.

[69] C. Mahaux and R. Sartor. *Phys. Rev. C*, 40:1833, 1989.

[70] D. R. Entem and R. Machleidt. *Phys. Rev. C*, 68:041001(R), 2003.

[71] S. C. Pieper. Monte carlo calculations of nuclei. In J. Navarro and A. Polls, editors, *Microscopic Quantum Many-Body Theories and Their Applications. Lecture Notes in Physics*. Springer, Berlin, 1998.

[72] C. Lin, F. H. Zong, and D. M. Ceperley. *Phys. Rev. E*, 64:016702, 2001.

[73] K. E. Schmidt and S. Fantoni. *Phys. Lett. B*, 446:99, 1999.

[74] D. R. Thompson, M. Lemere, and Y. C. Tang. *Nucl. Phys. A*, 286:53, 1977.

[75] M. Pedersen Lohne, G. Hagen, M. Hjorth-Jensen, S. Kvaal, and F. Pederiva. *Phys. Rev. B*, 84:115302, 2011.

[76] P. P. Ewald. *Ann. Phys. (Leipzig)*, 369:253, 1921.

[77] L. M. Fraser, W. M. C. Foulkes, G. Rajagopal, R. J. Needs, S. D. Kenny, and A. J. Williamson. *Phys. Rev. B*, 53:1814, 1996.

[78] B. Wood, W. M. C. Foulkes, M. D. Towler, and N. D. Drummond. *J. Phys.: Cond. Matt.*, 16:891, 2004.

[79] N. D. Drummond, R. J. Needs, A. Sorouri, and W. M. C. Foulkes. *Phys. Rev. B*, 78:125106, 2008.

[80] S. K. Bogner, R. J. Furnstahl, and A. Schwenk. *Prog. Part. Nucl. Phys.*, 65:94, 2010.

[81] S. Reimann. Private communication, 2013.

[82] S. Reimann. Master's thesis, University of Oslo, 2013.

[83] G. H. Booth, A. J. W. Thom, and A. Alavi. *J. Chem. Phys.*, 131:054106, 2009.

[84] J. J. Shepherd, G. Booth, A. Grüneis, and A. Alavi. *Phys. Rev. B*, 85:081103, 2012.

[85] K. R. Leikanger. Private communication, 2013.

[86] K. R. Leikanger. Master's thesis, University of Oslo, 2013.

[87] V. Bârsan and A. Aldea, editors. *Trends in Nanophysics. Theory, experiment and Technology*. Springer, 2010.

[88] F. Mandl and G. Shaw. *Quantum Field Theory.* John Wiley & Sons, 1984.

[89] B. R. Martin. *Nuclear and Particle Physics. An Introduction.* John Wiley & Sons Ltd, second edition, 2009.

[90] M. Riordan. *Science*, 256:1287, 1992.

[91] P. Braun-Munzinger and J. Wambach. *Rev. Mod. Phys.*, 81:1031, 2009.

[92] S. S. M. Wong. *Introductory Nuclear Physics.* Prentice-Hall, 1990.

[93] H.-T. Janka. *Annu. Rev. Nucl. Part. Sci.*, 62:407, 2012.

[94] Heavy ions and quark-gluon plasma. Accessed: 2013-11-28. Available from: `http://home.web.cern.ch/about/physics/heavy-ions-and-quark-gluon-plasma`.

[95] A New Area of Physics. Accessed: 2013-11-28. Available from: `http://www.bnl.gov/rhic/newPhysics.asp`.

[96] M. Arnould, S. Goriely, and K. Takahashi. *Phys. Rep.*, 450:97, 2007.

[97] R. N. Boyd. *An Introduction to Nuclear Astrophysics.* The University of Chicago Press, 2008.

[98] H. A. Bethe. *Rev. Mod. Phys.*, 62:801, 1990.

[99] S. Goriely, A. Bauswein, and H.-T. Janka. *J. Phys.: Conf. Ser.*, 337:012039, 2012.

[100] J. M. Lattimer and M. Prakash. *Astrophys. J.*, 550:426, 2001.

[101] A. Akmal, V. R. Pandharipande, and D. G. Ravenhall. *Phys. Rev. C*, 58:1804, 1998.

[102] T. Frick and H. Müther. *Phys. Rev. C*, 68:034310, 2003.

[103] E. N. E. van Dalen and H. Müther. *Phys. Rev. C*, 80:037303, 2009.

[104] M. Baldo, A. Polls, A. Rios, H.-J. Schulze, and I. Vidaña. *Phys. Rev. C*, 86:064001, 2012.

[105] F. Sammarruca, B. Chen, L. Coraggio, N. Itaco, and R. Machleidt. *Phys. Rev. C*, 86:054317, 2012.

[106] G. Hagen, T. Papenbrock, A. Ekström, K. A. Wendt, G. Baardsen, S. Gandolfi, M. Hjorth-Jensen, and C. J. Horowitz. *Phys. Rev. C*, 89:014319, 2014.

[107] S. R. Beane, E. Chang, S. D. Cohen, W. Detmold, H.-W. Lin, T. C. Luu, K. Orginos, A. Parreño, M. J. Savage, and A. Walker-Loud. *Phys. Rev. Lett.*, 109:172001, 2012.

[108] H. Müther, M. Prakash, and T. L. Ainsworth. *Phys. Lett. B*, 199:469, 1987.

[109] L. Engvik, M. Hjorth-Jensen, R. Machleidt, H. Müther, and A. Polls. *Nucl. Phys. A*, 627:85, 1997.

[110] C.-H. Lee, T. T. S. Kuo, G. Q. Li, and G. E. Brown. *Phys. Rev. C*, 57:3488, 1998.

[111] I. Vidaña, C. Providência, A. Polls, and A. Rios. *Phys. Rev. C*, 80:045806, 2009.

[112] A. Carbone, A. Polls, and A. Rios. *Europhys. Lett.*, 97:22001, 2012.

[113] A. S. Botvina and I. N. Mishustin. *Phys. Lett. B*, 584:233, 2004.

[114] C. J. Pethick. *Rev. Mod. Phys.*, 64:1133, 1992.

[115] J. M. Lattimer and M. Prakash. *Phys. Rep.*, 333334:121, 2000.

[116] P. Danielewicz, R. Lacey, and W. G. Lynch. *Science*, 298:1592, 2002.

[117] W. G. Lynch, M. B. Tsang, Y. Zhang, P. Danielewicz, M. Famiano, Z. Li, and A. W. Steiner. *Prog. Part. Nucl. Phys.*, 62:427, 2009.

[118] H. Müther and A. Polls. *Prog. Part. Nucl. Phys.*, 45:243, 2000.

[119] M. Bender, P.-H. Heenen, and P.-G. Reinhard. *Rev. Mod. Phys.*, 75:121, 2003.

[120] A. Lejeune, U. Lombardo, and W. Zuo. *Phys. Lett. B*, 477:45, 2000.

[121] S. Gandolfi, A. Yu. Illarionov, S. Fantoni, J. C. Miller, F. Pederiva, and K. E. Schmidt. *Mon. Not. R. Astron. Soc.: Lett.*, 404:L35, 2010.

[122] R. M. Dreizler and E. K. U. Gross. *Density Functional Theory. An Approach to the Quantum Many-Body Problem.* Springer-Verlag, 1990.

[123] M. R. Anastasio, L. S. Celenza, W. S. Pong, and C. M. Shakin. *Phys. Rep.*, 100:327, 1983.

[124] R. Brockmann and R. Machleidt. *Phys. Lett. B*, 149:283, 1984.

[125] C. J. Horowitz and B. D. Serot. *Phys. Lett. B*, 137:287, 1984.

[126] B. ter Haar and R. Malfliet. *Phys. Rep.*, 149:207, 1987.

[127] C. J. Horowitz and B. D. Serot. *Nucl. Phys. A*, 464:613, 1987.

[128] R. Brockmann and R. Machleidt. *Phys. Rev. C*, 42:1965, 1990.

[129] S. C. Pieper and R. B. Wiringa. *Annu. Rev. Nucl. Part. Sci.*, 51:53, 2001.

[130] P. Navrátil, S. Quaglioni, I. Stetcu, and B. R Barrett. *J. Phys. G*, 36:083101, 2009.

[131] R. Roth, A. Calci, J. Langhammer, and S. Binder. arxiv:1311.3563 [nucl-th]. 2013.

[132] A. Cipollone, C. Barbieri, and P. Navrátil. *Phys. Rev. Lett.*, 111:062501, 2013.

[133] H.-W. Hammer, A. Nogga, and A. Schwenk. *Rev. Mod. Phys.*, 85:197, 2013.

[134] J. D. Walecka. *Theoretical Nuclear and Subnuclear Physics.* World Scientific, 2004.

[135] E. Chabanat, P. Bonche, P. Haensel, J. Meyer, and R. Schaeffer. *Nucl. Phys. A*, 627:710, 1997.

[136] C. Mahaux and R. Sartor. Nuclear matter with nonrelativistic potentials: Present status. In M.Soyeur, H. Flocard, B. Tamain, and M. Porneuf, editors, *Nuclear Matter and Heavy Ion Collisions*, NATO ASI Series B. Physics, vol. 205. Plenum Press, New York, 1989.

[137] F. Coester, S. Cohen, B. Day, and C. M. Vincent. *Phys. Rev. C*, 1:769, 1970.

[138] K. A. Brueckner and C. A. Levinson. *Phys. Rev.*, 97:1344, 1955.

[139] K. A. Brueckner. *Phys. Rev.*, 100:36, 1955.

[140] A. D. Jackson. *Annu. Rev. Nucl. Part. Sci.*, 33:105, 1983.

[141] A. Lejeune, P. Grange, M. Martzolff, and J. Cugnon. *Nucl. Phys. A*, 453:189, 1986.

[142] M. Baldo, I. Bombaci, G. Giansiracusa, and U. Lombardo. *J. Phys. G*, 16:L263, 1990.

[143] L. Engvik, E. Osnes, M. Hjorth-Jensen, G. Bao, and E. Østgaard. *Astrophys. J.*, 469:794, 1996.

[144] E. Schiller, H. Müther, and P. C. Czerski. *Phys. Rev. C*, 60:059901(E), 1999.

[145] I. Vidaña, A. Polls, A. Ramos, M. Hjorth-Jensen, and V. G. J. Stoks. *Phys. Rev. C*, 61:025802, 2000.

[146] W. Zuo, A. Lejeune, U. Lombardo, and J. F. Mathiot. *Nucl. Phys. A*, 706:418, 2002.

[147] W. Zuo, Z. H. Li, A. Li, and G. C. Lu. *Phys. Rev. C*, 69:064001, 2003.

[148] G. F. Burgio. *J. Phys. G*, 35:014048, 2008.

[149] I. Vidaña, A. Polls, and C. Providência. *Phys. Rev. C*, 84:062801, 2011.

[150] T. Inoue, S. Aoki, T. Doi, T. Hatsuda, Y. Ikeda, N. Ishii, K. Murano, H. Nemura, and K. Sasaki. *Phys. Rev. Lett.*, 111:112503, 2013.

[151] I. Bombaci and U. Lombardo. *Phys. Rev. C*, 44:1892, 1991.

[152] W. Zuo, A. Lejeune, U. Lombardo, and J. F. Mathiot. *Eur. Phys. J. A*, 14:469, 2002.

[153] H.-J. Schulze, M. Baldo, U. Lombardo, J. Cugnon, and A. Lejeune. *Phys. Rev. C*, 57:704, 1998.

[154] B. D. Day. *Phys. Rev. C*, 24:1203, 1981.

[155] H. Q. Song, M. Baldo, G. Giansiracusa, and U. Lombardo. *Phys. Lett. B*, 411:237, 1997.

[156] R. Rajaraman and H. A. Bethe. *Rev. Mod. Phys.*, 39:745, 1967.

[157] F. E. Harris, H. J. Monkhorst, and D. L. Freeman. *Algebraic and diagrammatic methods in many-fermion theory.* Oxford University Press, 1992.

[158] S. K. Bogner, A. Schwenk, R. J. Furnstahl, and A. Nogga. *Nucl. Phys. A*, 763:59, 2005.

[159] K. Hebeler and A. Schwenk. *Phys. Rev. C*, 82:014314, 2010.

[160] R. J. Furnstahl and K. Hebeler. *Rep. Prog. Phys.*, 76:126301, 2013.

[161] W. H. Dickhoff, A. Faessler, and H. Müther. *Nucl. Phys. A*, 389:492, 1982.

[162] Z. Y. Ma and T. T. S. Kuo. *Phys. Lett. B*, 127:137, 1983.

[163] T. T. S. Kuo, Z. Y. Ma, and R. Vinh Mau. *Phys. Rev. C*, 33:717, 1986.

[164] L. Engvik, E. Osnes, M. Hjorth-Jensen, and T. T. S. Kuo. *Nucl. Phys. A*, 622:553, 1997.

[165] H. Q. Song, S. D. Yang, and T. T. S. Kuo. *Nucl. Phys. A*, 462:491, 1987.

[166] M. F. Jiang, T. T. S. Kuo, and H. Müther. *Phys. Rev. C*, 38:2408, 1988.

[167] L.-W. Siu, J. W. Holt, T. T. S. Kuo, and G. E. Brown. *Phys. Rev. C*, 79:054004, 2009.

[168] W. H. Dickhoff and H. Müther. *Rep. Prog. Phys.*, 55:1947, 1992.

[169] Y. Dewulf, W. H. Dickhoff, D. Van Neck, E. R. Stoddard, and M. Waroquier. *Phys. Rev. Lett.*, 90:152501, 2003.

[170] P. Bożek. *Phys. Lett. B*, 586:239, 2004.

[171] Kh. S. A. Hassaneen and H. Müther. *Phys. Rev. C*, 70:054308, 2004.

[172] T. Frick, H. Müther, A. Rios, A. Polls, and A. Ramos. *Phys. Rev. C*, 71:014313, 2005.

[173] P. Bożek, D. J. Dean, and H. Müther. *Phys. Rev. C*, 74:014303, 2006.

[174] V. Somà and P. Bożek. *Phys. Rev. C*, 74:045809, 2006.

[175] Kh. Gad and Kh. S. A. Hassaneen. *Nucl. Phys. A*, 793:67, 2007.

[176] V. Somà and P. Bożek. *Phys. Rev. C*, 80:025803, 2009.

[177] V. Somà and P. Bożek. *Prog. Part. Nucl. Phys.*, 62:371, 2009.

[178] A. Rios, A. Polls, and I. Vidaña. *Phys. Rev. C*, 79:025802, 2009.

[179] A. Rios and V. Somà. *Phys. Rev. Lett.*, 108:012501, 2012.

[180] A. Rios, A. Polls, and W. H. Dickhoff. *Phys. Rev. C*, 89:044303, 2014.

[181] S. Fantoni and A. Faborchini. Correlated basis function theory for fermion systems. In J. Navarro and A. Polls, editors, *Microscopic Quantum Many-Body Theories and Their Applications*, Lecture Notes in Physics. Springer, Berlin, 1998.

[182] V. R. Pandharipande and R. B. Wiringa. *Rev. Mod. Phys.*, 51:821, 1979.

[183] R. B. Wiringa, V. Fiks, and A. Fabrocini. *Phys. Rev. C*, 38:1010, 1988.

[184] A. Akmal and V. R. Pandharipande. *Phys. Rev. C*, 56:2261, 1997.

[185] S. Gandolfi, A. Yu. Illarionov, K. E. Schmidt, F. Pederiva, and S. Fantoni. *Phys. Rev. C*, 79:054005, 2009.

[186] J. M. Thijssen. *Computational Physics*. Cambridge University Press, second edition, 2007.

[187] B. L. Hammond, W. A. Lester Jr., and P. J. Reynolds. *Monte Carlo Methods in Ab Initio Quantum Chemistry*. World Scientific Publishing, 1994.

[188] A. Gezerlis and J. Carlson. *Phys. Rev. C*, 81:025803, 2010.

[189] S. Gandolfi, A. Yu. Illarionov, F. Pederiva, K. E. Schmidt, and S. Fantoni. *Phys. Rev. C*, 80:045802, 2009.

[190] B. Borasoy, E. Epelbaum, H. Krebs, D. Lee, and U.-G. Meißner. *Eur. Phys. J. A*, 35:357, 2008.

[191] J. W. Holt, N. Kaiser, and W. Weise. *Prog. Part. Nucl. Phys.*, 73:35, 2013.

[192] A. L. Fetter and J. D. Walecka. *Quantum theory of many-particle systems*. McGraw-Hill Book Company, 1971.

[193] G. E. Brown and A. D. Jackson. *The nucleon-nucleon interaction*. North-Holland Publishing Company, 1976.

[194] D. M. Ceperley and B. J. Alder. *Phys. Rev. Lett.*, 45:566, 1980.

[195] E. Wigner. *Phys. Rev.*, 46:1002, 1934.

[196] D. Ceperley. *Phys. Rev. B*, 18:3126, 1978.

[197] B. Tanatar and D. M. Ceperley. *Phys. Rev. B*, 39:5005, 1989.

[198] W. M. C. Foulkes, L. Mitas, R. J. Needs, and G. Rajagopal. *Rev. Mod. Phys.*, 73:33, 2001.

[199] S. Chiesa, D. M. Ceperley, R. M. Martin, and M. Holzmann. *Phys. Rev. Lett.*, 97:076404, 2006.

[200] H. Bruus and K. Flensberg. *Many-Body Quantum Theory in Condensed Matter Physics. An introduction*. Oxford University Press, 2004.

[201] M. Gell-Mann and K. A. Brueckner. *Phys. Rev.*, 106:364, 1957.

[202] K. S. Singwi, M. P. Tosi, R. H. Land, and A. Sjölander. *Phys. Rev.*, 176:589, 1968.

[203] D. N. Lowy and G. E. Brown. *Phys. Rev. B*, 12:2138, 1975.

[204] L. J. Lantto. *Phys. Rev. B*, 22:1380, 1980.

[205] Y. Kwon, D. M. Ceperley, and R. M. Martin. *Phys. Rev. B*, 58:6800, 1998.

[206] M. Holzmann, D. M. Ceperley, C. Pierleoni, and K. Esler. *Phys. Rev. E*, 68:046707, 2003.

[207] P. López Ríos, A. Ma, N. D. Drummond, M. D. Towler, and R. J. Needs. *Phys. Rev. E*, 74:066701, 2006.

[208] I. G. Gurtubay, R. Gaudoin, and J. M. Pitarke. *J. Phys.: Cond. Matt.*, 22:065501, 2010.

[209] G. Ortiz and P. Ballone. *Phys. Rev. B*, 50:1391, 1994.

[210] J. J. Shepherd, G. H. Booth, and A. Alavi. *J. Chem. Phys.*, 136:244101, 2012.

[211] D. M. Ceperley and B. J. Alder. Lawrence Berkley Laboratory Report No. LBL-10813 (UC-4) (unpublished). Technical report.

[212] A. K. Rajagopal and J. C. Kimball. *Phys. Rev. B*, 15:2819, 1977.

[213] M. Jonson. *J. Phys. C*, 9:3055, 1976.

[214] H.-K. Sim, R. Tao, and F. Y. Wu. *Phys. Rev. B*, 34:7123, 1986.

[215] Y. Kwon, D. M. Ceperley, and R. M. Martin. *Phys. Rev. B*, 48:12037, 1993.

[216] F. Rapisarda and G. Senatore. *Aust. J. Phys.*, 49:161, 1996.

[217] C. Attaccalite, S. Moroni, P. Gori-Giorgi, and G. B. Bachelet. *Phys. Rev. Lett.*, 88:256601, 2002.

[218] N. D. Drummond and R. J. Needs. *Phys. Rev. B*, 79:085414, 2009.

[219] N. D. Drummond and R. J. Needs. *Phys. Rev. Lett.*, 102:126402, 2009.

[220] F. Schwabl. *Advanced Quantum Mechanics*. Springer-Verlag, fourth edition, 2008.

[221] T. D. Crawford and H. F. Schaefer. *Rev. Comp. Chem.*, 14:33, 2000.

[222] T. Helgaker, P. Jørgensen, and J. Olsen. *Molecular Electronic-Structure Theory*. John Wiley & Sons, 2000.

[223] K. A. Brueckner, S. A. Coon, and J. Dabrowski. *Phys. Rev.*, 168:1184, 1968.

[224] J. J. MacKenzie. *Phys. Rev.*, 179:1002, 1969.

[225] À. Ramos Gómez. PhD thesis, University of Barcelona, 1988.

[226] K. L. G. Heyde. *The Nuclear Shell Model*. Springer-Verlag, first edition, 1990.

[227] D. A. Varshalovich, A. N. Moskalev, and V. K. Khersonskii. *Quantum Theory of Angular Momentum*. World Scientific, 1988.

[228] R. D. Lawson. *Theory of the Nuclear Shell Model*. Oxford University Press, 1980.

[229] E. Rutherford. *Philos. Mag.*, 21:669, 1911.

[230] N. Ishii, S. Aoki, and T. Hatsuda. *Phys. Rev. Lett.*, 99:022001, 2007.

[231] H. Nemura, N. Ishii, S. Aoki, and T. Hatsuda. *Phys. Lett. B*, 673:136, 2009.

[232] V. G. J. Stoks, R. A. M. Klomp, M. C. M. Rentmeester, and J. J. de Swart. *Phys. Rev. C*, 48:792, 1993.

[233] P. Ring and P. Schuck. *The Nuclear Many-Body Problem*. Springer-Verlag, first edition, 2004.

[234] R. Machleidt. *Adv. Nucl. Phys.*, 19:189, 1989.

[235] L. E. Engvik. PhD thesis, University of Oslo, 1999.

[236] H. Yukawa. *Proc. Physico-Math. Soc. Japan. 3rd Series*, 17:48, 1935.

[237] S. Abbas. *Eur. Phys. J. A*, 49:1, 2013.

[238] V. G. J. Stoks, R. A. M. Klomp, C. P. F. Terheggen, and J. J. de Swart. *Phys. Rev. C*, 49:2950, 1994.

[239] R. B. Wiringa, V. G. J. Stoks, and R. Schiavilla. *Phys. Rev. C*, 51:38, 1995.

[240] R. Machleidt. *Phys. Rev. C*, 63:024001, 2001.

[241] P. Grangé, A. Lejeune, M. Martzolff, and J.-F. Mathiot. *Phys. Rev. C*, 40:1040, 1989.

[242] M. Lacombe, B. Loiseau, J. M. Richard, R. Vinh Mau, J. Côté, P. Pirès, and R. de Tourreil. *Phys. Rev. C*, 21:861, 1980.

[243] W. N. Cottingham, M. Lacombe, B. Loiseau, J. M. Richard, and R. Vinh Mau. *Phys. Rev. D*, 8:800, 1973.

[244] E. Epelbaum. *Prog. Part. and Nucl. Phys.*, 57:654, 2006.

[245] E. Epelbaum. arxiv:1001.3229v1 [nucl-th]. 2010.

[246] D. R. Entem and R. Machleidt. *Phys. Rev. C*, 68:041001, 2003.

[247] E. Epelbaum, W. Glöckle, and U.-G. Meißner. *Nucl. Phys. A*, 747:362, 2005.

[248] M. Kortelainen, T. Lesinski, J. Moré, W. Nazarewicz, J. Sarich, N. Schunck, M. V. Stoitsov, and S. Wild. *Phys. Rev. C*, 82:024313, 2010.

[249] T. Munson, J. Sarich, S. M. Wild, S. Benson, and L. C. McInnes. Technical Memorandum ANL/MCS-TM-322, Argonne National Laboratory, Argonne, Illinois (2012). Available from: `http://www.mcs.anl.gov/tao/docs/tao_manual.pdf`.

[250] A. R. Conn, K. Scheinberg, and L. N. Vicente. *Introduction to Derivative-Free Optimization*. Society for Industrial and Applied Mathematics, 2009.

[251] M. Hjorth-Jensen, T. T. S. Kuo, and E. Osnes. *Phys. Rep.*, 261:125, 1995.

[252] A. Ramos, A. Polls, and W. H. Dickhoff. *Nucl. Phys. A*, 503:1, 1989.

[253] The NIST Reference on Constants, Units, and Uncertainty. Accessed: 2014-04-26. Available from: `http://physics.nist.gov/cuu/Constants/index.html`.

[254] W. H. Press, S. A. Teukolosky, W. T. Vetterling, and B. P. Flannery. *Numerical Recipes in Fortran. The Art of Scientific Computing*. Cambridge University Press, second edition, 1992.

[255] L. N. Trefethen and D. Bau. *Numerical Linear Algebra*. Society for Industrial and Applied Mathematics, 1997.

[256] J. Paldus. The beginnings of coupled-cluster theory: An eyewitness account. In C. E. Dykstra, G. Frenking, K. S. Kim, and G. E. Scuseria, editors, *Theory and Applications of Computational Chemistry*. Elsvier, Amsterdam, 2005.

[257] G. Hagen, D. J. Dean, M. Hjorth-Jensen, T. Papenbrock, and A. Schwenk. *Phys. Rev. C*, 76:044305, 2007.

[258] G. Hagen, P. Hagen, H.-W. Hammer, and L. Platter. *Phys. Rev. Lett.*, 111:132501, 2013.

[259] Ø. Jensen, G. Hagen, T. Papenbrock, D. J. Dean, and J. S. Vaagen. *Phys. Rev. C*, 82:014310, 2010.

[260] D. A. Pigg, G. Hagen, H. Nam, and T. Papenbrock. *Phys. Rev. C*, 86:014308, 2012.

[261] G. E. Scuseria, C. L. Janssen, and H. F. Schaefer. *J. Chem. Phys.*, 89:7382, 1988.

[262] A. Baran, A. Bulgac, M. McNeil Forbes, G. Hagen, W. Nazarewicz, N. Schunck, and M. V. Stoitsov. *Phys. Rev. C*, 78:014318, 2008.

[263] D. J. Dean, J. R. Gour, G. Hagen, M. Hjorth-Jensen, K. Kowalski, T. Papenbrock, P. Piecuch, and M. Włoch. *Nucl. Phys. A*, 752:299c, 2005.

[264] G. Allaire and S. M. Kaber. *Numerical Linear Algebra*. Springer New York, 2008.

[265] G. H. Golub and C. F. van Loan. *Matrix Computations*. The John Hopkins University Press, third edition, 1996.

[266] W. Gropp, E. Lusk, and A. Skjellum. *Using MPI: portable parallel programming with the message-passing interface*. MIT Press, second edition, 1999.

[267] J. L. Träff, S. Benkner, and J. J. Dongarra. *Recent Advances in the Messsage Passing Interface. 19th European MPI Users' Group Meeting, EuroMPI 2012, Vienna, Austria, September 23-26, 2012. Proceedings*. Springer, 2012.

[268] B. Chapman, G. Jost, and R. van der Pas. *Using OpenMP. Portable Shared Memory Parallel Programming.* The MIT Press, 2008.

[269] M. Baldo and A. Fiasconaro. *Phys. Lett. B*, 491:240, 2000.

[270] J. A. Rekkedal. Master's thesis, University of Oslo, 2009.

[271] G. Hagen, T. Papenbrock, D. J. Dean, and M. Hjorth-Jensen. *Phys. Rev. C*, 82:034330, 2010.

[272] C. W. Wong and D. M. Clement. *Nucl. Phys. A*, 183:210, 1972.

[273] R. L. Liboff. *Introductory Quantum Mechanics.* Addison Wesley, fourth edition, 2003.

[274] C. L. Kung, T. T. S. Kuo, and K. F. Ratcliff. *Phys. Rev. C*, 19:1063, 1979.

[275] R. Balian and E. Brezin. *Nuovo Cimento*, 61:403, 1969.

[276] M. Hjorth-Jensen, M. Borromeo, H. Müther, and A. Polls. *Nucl. Phys. A*, 551:580, 1993.

[277] G. Racah. *Phys. Rev.*, 62:438, 1942.

[278] T. Papenbrock. Private communication, 2010.

[279] G. Hagen, M. Hjorth-Jensen, and N. Michel. *Phys. Rev. C*, 73:064307, 2006.

[280] D. E. Parry. *Surf. Sci.*, 49:433, 1975.

[281] D. E. Parry. *Surf. Sci.*, 54:195, 1976.

[282] T. T. S. Kuo, J. Shurpin, K. C. Tam, E. Osnes, and P. J. Ellis. *Ann. Phys. (N.Y.)*, 132:237, 1981.

[283] D. Cleland, G. H. Booth, and A. Alavi. *J. Chem. Phys.*, 132:041103, 2010.

[284] H. Hergert, S. K. Bogner, S. Binder, A. Calci, J. Langhammer, R. Roth, and A. Schwenk. *Phys. Rev. C*, 87:034307, 2013.

[285] S. A. Kucharski and R. J. Bartlett. *J. Chem. Phys.*, 108:5243, 1998.

[286] A. G. Taube and R. J. Bartlett. *J. Chem. Phys.*, 128:044110, 2008.

[287] S. Reimann *et al.*, 2014. to be published.

[288] E. Ilyabaev and U. Kaldor. *Chem. Phys. Lett.*, 194:95, 1992.

[289] R. F. Bishop and W. A. Lahoz. *J. Phys. A*, 20:4203, 1987.

[290] J. J. Callahan. *Advanced Calculus. A Geometric View.* Springer, 2010.

Appendix A

Technical details

A.1 Antisymmetrization

When transforming the Brueckner-Hartree-Fock and coupled-cluster equations to a coupled angular momentum - relative momentum basis, one needs to consider anti-symmetrized interaction matrix elements

$$\begin{aligned}
&\langle \mathbf{k}_p m_{s_p} m_{t_p} \mathbf{k}_q m_{s_q} m_{t_q} | \hat{v} | \mathbf{k}_r m_{s_r} m_{t_r} \mathbf{k}_s m_{s_s} m_{t_s} \rangle_{AS} \\
=&\langle \mathbf{k}_p m_{s_p} m_{t_p} \mathbf{k}_q m_{s_q} m_{t_q} | \hat{v} | \mathbf{k}_r m_{s_r} m_{t_r} \mathbf{k}_s m_{s_s} m_{t_s} \rangle \\
-&\langle \mathbf{k}_p m_{s_p} m_{t_p} \mathbf{k}_q m_{s_q} m_{t_q} | \hat{v} | \mathbf{k}_s m_{s_s} m_{t_s} \mathbf{k}_r m_{s_r} m_{t_r} \rangle. \qquad \text{(A.1)}
\end{aligned}$$

Let us transform only the ket vector of Eq. (A.1) to the coupled angular momentum - relative momentum basis

$$|k \mathcal{J} m_{\mathcal{J}} (lS) m_{t_1} m_{t_2} \rangle.$$

Using the angular-momentum-algebra relations of Eqs. (3.35) - (3.37) and (3.39) - (3.42) and assuming that the two nucleons are both either protons or neutrons, we get

$$\begin{aligned}
&\left[|\mathbf{k}_p m_{s_p} \mathbf{k}_q m_{s_q} \rangle - |\mathbf{k}_q m_{s_q} \mathbf{k}_p m_{s_p} \rangle \right] \\
=&\left[|\mathbf{k}\mathbf{K} m_{s_p} m_{s_q} \rangle - | -\mathbf{k}\mathbf{K} m_{s_q} m_{s_p} \rangle \right] \\
=&\sum_{SM_S} \left[|\mathbf{k}\mathbf{K} \rangle - (-1)^{1-S} | -\mathbf{k}\mathbf{K} \rangle \right] \\
&\times |SM_S\rangle \langle SM_S | s m_{s_p} s m_{s_q} \rangle \\
=&\sum_{SM_S} \sum_{l m_l} \left[|\mathbf{k}\mathbf{K} \rangle - (-1)^{1-S+l} | -\mathbf{k}\mathbf{K} \rangle \right] \\
&\times \langle l m_l | \hat{\mathbf{k}} \rangle | SM_S l m_l \rangle \langle SM_S | s m_{s_p} s m_{s_q} \rangle \\
=&\sum_{SM_S} \sum_{l m_l} \sum_{\mathcal{J} m_{\mathcal{J}}} (1 - (-1)^{1-S+l}) | k \mathbf{K} \mathcal{J} m_{\mathcal{J}} l S \rangle \\
&\times \langle l m_l | \hat{\mathbf{k}} \rangle \langle SM_S | s m_{s_p} s m_{s_q} \rangle \langle \mathcal{J} m_{\mathcal{J}} l S | l m_l S M_S \rangle, \qquad \text{(A.2)}
\end{aligned}$$

where $\mathbf{k}$ and $\mathbf{K}$ are relative and CM momenta, respectively, as defined in Eq. (3.31). Whereas two creation operators related to one type of particle anticommute, creation operators of different particle species commute with each other [289]. Instead of antisymmetric matrix elements as defined in Eq. (A.1), we get matrix elements

$$2\langle \mathbf{k}_p m_{s_p} m_{t_p} \mathbf{k}_q m_{s_q} m_{t_q} | \hat{v} | \mathbf{k}_r m_{s_r} m_{t_r} \mathbf{k}_s m_{s_s} m_{t_s} \rangle \tag{A.3}$$

when the particles r and s are of different nucleon types. The ket vector then becomes

$$\begin{aligned} & 2|\mathbf{k}_p m_{s_p} \mathbf{k}_q m_{s_q}\rangle \\ =& 2 \sum_{SM_S} \sum_{lm_l} \sum_{\mathcal{J}m_\mathcal{J}} |k\mathbf{K}\mathcal{J}m_\mathcal{J} lS\rangle \\ & \times \langle lm_l|\hat{\mathbf{k}}\rangle \langle SM_S|sm_{s_p}sm_{s_q}\rangle \langle \mathcal{J}m_\mathcal{J} lS|lm_l SM_S\rangle, \end{aligned} \tag{A.4}$$

where we now have a factor 2 insted of the antisymmetrization factor $(1-(-1)^{1-S+l})$. In the proton-neutron representation, we define the antisymmetrization operator

$$\mathcal{A}^{lSM_T} = \begin{cases} \sqrt{2}, & \text{if } M_T = 0, \\ \left(1-(-1)^{l+S+1}\right)/\sqrt{2}, & \text{if } |M_T| = 1. \end{cases} \tag{A.5}$$

When written in the basis (A.2), all interaction matrix elements are assumed to be multiplied by a product $\mathcal{A}^{lSM_T}\mathcal{A}^{l'SM_T}$ to get the correct antisymmetrization. Observe that the antisymmetrization operator $\mathcal{A}$ is defined differently here than in Paper II.

The antisymmetrization operator $\mathcal{B}^{M_T,\pm}$ is defined for symmetric nuclear matter as

$$\begin{aligned} & \mathcal{B}^{M_T,\pm}\langle k\mathcal{J}(lS)|\hat{O}|k\mathcal{J}(lS)\rangle = \langle k\mathcal{J}(lS)|\hat{O}(M_{T'}=0)|k\mathcal{J}(lS)\rangle \\ & + \left(1-(-1)^{1+l+S}\right)\langle k\mathcal{J}(lS)|\hat{O}(M_{T'}=M_T\pm\delta_{M_T0})|k\mathcal{J}(lS)\rangle \end{aligned} \tag{A.6}$$

and for pure neutron matter as

$$\begin{aligned} & \mathcal{B}^{M_T,\pm}\langle k\mathcal{J}(lS)|\hat{O}|k\mathcal{J}(lS)\rangle = \left(1-(-1)^{1+l+S}\right) \\ & \times \langle k\mathcal{J}(lS)|\hat{O}(M_{T'}=1)|k\mathcal{J}(lS)\rangle, \end{aligned} \tag{A.7}$$

where $\hat{O}$ is a general two-particle operator.

Appendix B

Mathematical tools

B.1 Coupled delta distributions

Assume that $f : (x, y) \to \mathbb{R}$ and $g : (x, y) \to \mathbb{R}$ are functions with continuous derivatives on the domain $(x, y) \in \Omega(x, y) \subset \mathbb{R}^2$, and $h : (x, y) \to \mathbb{R}$ is an arbitrary function. We want to calculate an integral with two coupled delta distributions

$$\begin{aligned} &\iint_{\Omega(x,y)} \delta(f(x,y))\delta(g(x,y))h(x,y)dxdy \\ &\quad = \iint_{\Omega(x,y)} \delta^{(2)}(f(x,y), g(x,y))h(x,y)dxdy. \end{aligned} \tag{B.1}$$

On right-hand side we have defined the two-dimensional delta distribution $\delta^{(2)}(s, t)$. This integral can be evaluated by changing to the variables

$$s = f(x, y), \qquad t = g(x, y). \tag{B.2}$$

The integration measure transforms accordingly as [290, p. 339]

$$dxdy \quad \longrightarrow \quad \left| \begin{array}{cc} \frac{\partial x}{\partial s} & \frac{\partial x}{\partial t} \\ \frac{\partial y}{\partial s} & \frac{\partial y}{\partial t} \end{array} \right| dsdt, \tag{B.3}$$

where the new measure contains the absolute value of a Jacobian determinant. Let the direction of integration of the new integration domain $\tilde{\Omega}(s, t)$ be the same as in the old domain $\Omega(x, y)$. If the initial integration domain $\Omega(x, y)$ is chosen such that there exist unique inverse mappings

$$\begin{aligned} \eta &= x(s, t), \\ \xi &= y(s, t), \end{aligned} \tag{B.4}$$

we can write the integral as

$$\begin{aligned}
&\iint_{\Omega(x,y)} \delta(f(x,y))\delta(g(x,y))h(x,y)dxdy \\
&\quad = \iint_{\tilde{\Omega}(s,t)} \delta^{(2)}(s,t)\tilde{h}(s,t) \left| \begin{array}{cc} \frac{\partial x}{\partial s} & \frac{\partial x}{\partial t} \\ \frac{\partial y}{\partial s} & \frac{\partial y}{\partial t} \end{array} \right| dsdt \\
&\quad = \tilde{h}(s,t) \left| \frac{\partial x}{\partial s} \cdot \frac{\partial y}{\partial t} - \frac{\partial x}{\partial t} \cdot \frac{\partial y}{\partial s} \right| \Bigg|_{s=t=0} \\
&\quad = \frac{\tilde{h}(s,t)}{\left| \frac{\partial s}{\partial x} \cdot \frac{\partial t}{\partial y} - \frac{\partial t}{\partial x} \cdot \frac{\partial s}{\partial y} \right|} \Bigg|_{s=t=0},
\end{aligned} \tag{B.5}$$

where we have defined $\tilde{h}(s,t) \equiv h(x(s,t), y(s,t))$. In the last equality, we have applied the inverse function theorem [290, p. 169].

Appendix C

Erratum to Paper II

After the publication of Paper II, we have found that the BHF results in Figures 7 and 8 have an error. These results were obtained by summing BHF correlation contributions up to the partial wave $\mathcal{J} = 9$, and treating the remaining potential energy in the Born approximation for partial waves up to $\mathcal{J} = 24$. By accident, we summed contributions in the Born approximation in the interval $9 \leq \mathcal{J} \leq 24$ instead of $10 \leq \mathcal{J} \leq 24$, as should have been done. The BHF results in Table II, as well as other numbers given in Paper II, are not affected by this error. In Figure C.1, a nuclear matter equation of state is given, as obtained with corrected BHF results.

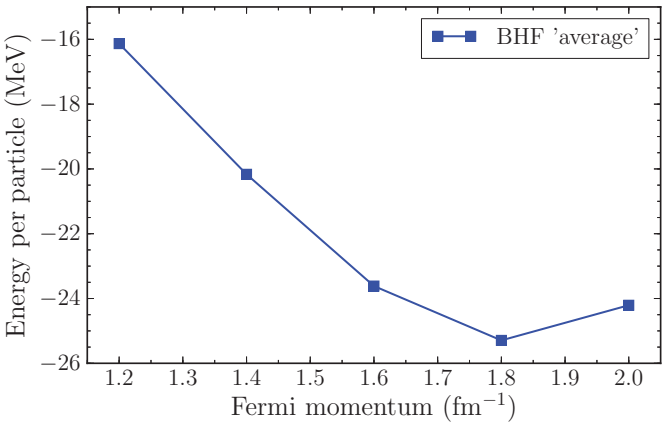

Figure C.1: The same BHF equation of state as given in Figures 7 and 8 of Paper II, but here the results have been corrected to contain partial-wave contributions in the Born approximation for $10 \leq \mathcal{J} \leq 24$, instead of $9 \leq \mathcal{J} \leq 24$, as was wrongly used in the original paper.

I

Optimized Chiral Nucleon-Nucleon Interaction at Next-to-Next-to-Leading Order

A. Ekström,[1,2] G. Baardsen,[1] C. Forssén,[3] G. Hagen,[4,5] M. Hjorth-Jensen,[1,2,6] G. R. Jansen,[4,5] R. Machleidt,[7] W. Nazarewicz,[5,4,8] T. Papenbrock,[5,4] J. Sarich,[9] and S. M. Wild[9]

[1]*Department of Physics and Center of Mathematics for Applications, University of Oslo, N-0316 Oslo, Norway*
[2]*National Superconducting Cyclotron Laboratory, Michigan State University, East Lansing, Michigan 48824, USA*
[3]*Department of Fundamental Physics, Chalmers University of Technology, SE-412 96 Göteborg, Sweden*
[4]*Physics Division, Oak Ridge National Laboratory, Oak Ridge, Tennessee 37831, USA*
[5]*Department of Physics and Astronomy, University of Tennessee, Knoxville, Tennessee 37996, USA*
[6]*Department of Physics and Astronomy, Michigan State University, East Lansing, Michigan 48824, USA*
[7]*Department of Physics, University of Idaho, Moscow, Idaho 83844, USA*
[8]*Faculty of Physics, University of Warsaw, ul. Hoża 69, 00-681 Warsaw, Poland*
[9]*Mathematics and Computer Science Division, Argonne National Laboratory, Argonne, Illinois 60439, USA*

(Received 19 March 2013; published 7 May 2013)

We optimize the nucleon-nucleon interaction from chiral effective field theory at next-to-next-to-leading order (NNLO). The resulting new chiral force $\mathrm{NNLO_{opt}}$ yields $\chi^2 \approx 1$ per degree of freedom for laboratory energies below approximately 125 MeV. In the $A = 3$, 4 nucleon systems, the contributions of three-nucleon forces are smaller than for previous parametrizations of chiral interactions. We use $\mathrm{NNLO_{opt}}$ to study properties of key nuclei and neutron matter, and we demonstrate that many aspects of nuclear structure can be understood in terms of this nucleon-nucleon interaction, without explicitly invoking three-nucleon forces.

DOI: 10.1103/PhysRevLett.110.192502 PACS numbers: 21.30.−x, 21.10.−k, 21.45.−v, 12.39.Fe

Introduction.—Interactions from chiral effective field theory (EFT) employ symmetries and the pattern of spontaneous symmetry breaking of quantum chromodynamics [1,2]. In this approach, the exchange of pions within chiral perturbation theory yields the long-ranged contributions of the nuclear interaction, while short-ranged components are included as contact terms. The interaction is parametrized in terms of low-energy constants (LECs) that are determined by their fit to experimental data. The interactions from chiral EFT exhibit a power counting in the ratio Q/Λ, with Q being the low-momentum scale being probed and Λ the cutoff, which is of the order of 1 GeV. At next-to-next-to-leading order (NNLO), three-nucleon forces (3NFs) enter, while four-nucleon forces (4NFs) enter at next-to-next-to-next-to-leading order ($\mathrm{N^3LO}$). For laboratory energies below 125 MeV, the nucleon-nucleon (NN) force exhibits a quality of fit with $\chi^2 \approx 10$/datum at NNLO [3], while a high-precision potential $\mathrm{N^3LO_{EM}}$, with a $\chi^2 \approx 1$/datum up to 290 MeV, was obtained by Entem and Machleidt [4].

The 3NFs at NNLO that accompany the current $\mathrm{N^3LO}$ NN potentials play a pivotal role in nuclear structure calculations [5]. They determine the ground-state spin of ^{10}B [6], correctly set the drip line in oxygen isotopes [7,8], and make ^{48}Ca a doubly magic nucleus [9,10]. While it might seem surprising that smaller corrections at NNLO are so decisive for basic nuclear structure properties, the 3NF contains spin-orbit and tensor contributions that clearly are important for the currently employed chiral interactions. The contributions of 3NFs at $\mathrm{N^3LO}$ have also been worked out [11,12], and there are on-going efforts to compute even higher orders [13].

While the quest for higher orders is important, this approach will result in higher accuracy only if the optimization at lower orders was carried out accurately. Thus, it is important and timely to revisit the optimization question. We note in particular that the fits of the currently employed chiral interactions [3,4,14] date back about a decade and that there has been a considerable recent progress in developing tools for the derivative-free nonlinear least-squares optimization [15]. Furthermore, the quantification of theoretical uncertainties is a long-term objective of nuclear structure theory, and this requires a covariance analysis of the interaction parameters with respect to the experimental uncertainties of the nucleon-nucleon elastic scattering observables; see, for example, Refs. [15,16]. This Letter takes the first step toward this goal. We present a state-of-the-art optimization of the NN chiral EFT interaction at NNLO. This yields a much-improved χ^2 and a high-precision NN potential $\mathrm{NNLO_{opt}}$. The 3NF at NNLO is adjusted to the binding energies in $A = 3$, 4 nuclei. We present computations of three-nucleon and four-nucleon bound states, and we employ $\mathrm{NNLO_{opt}}$ to ground states and excited states in ^{10}B, masses and excited states of oxygen and calcium isotopes, and neutron matter.

Optimizing the NN interaction at NNLO.—For the optimization of the chiral NN interaction we use the Practical Optimization Using No Derivatives (for Squares) algorithm, POUNDERS [15], as implemented in [17]. This derivative-free algorithm employs a quadratic model and

TABLE I. Parameters of $\mathrm{NNLO_{opt}}$ at $\Lambda = 500$ MeV and $\Lambda_{\mathrm{SFR}} = 700$ MeV [3,21]: c_i (in GeV^{-1}), $\tilde{C}$ (in 10^4 GeV^{-2}), and C (in 10^4 GeV^{-4}). The number of decimal digits in the parameters ensure that the phase shifts, in degrees, are computed with a four decimal digit precision.

LEC	Value	LEC	Value	LEC	Value
c_1	−0.918 639 53	c_3	−3.888 687 49	c_4	4.310 327 16
$\tilde{C}^{pp}_{^1S_0}$	−0.151 366 04	$\tilde{C}^{np}_{^1S_0}$	−0.152 141 09	$\tilde{C}^{nn}_{^1S_0}$	−0.151 764 75
$C_{^1S_0}$	2.404 021 94	$C_{^3S_1}$	0.928 384 66	$\tilde{C}_{^3S_1}$	−0.158 434 18
$C_{^1P_1}$	0.417 045 54	$C_{^3P_0}$	1.263 390 76	$C_{^3P_1}$	−0.782 658 50
$C_{^3S_1-{}^3D_1}$	0.618 141 42	$C_{^3P_2}$	−0.677 808 51		

is particularly useful for computationally expensive objective functions. We optimize the three pion-nucleon (πN) couplings (c_1, c_3, c_4), and 11 partial wave contact parameters C and $\tilde{C}$, while we keep the axial-vector coupling constant g_A, the pion-decay constant f_π, and all masses fixed. In the optimization, we minimize the objective function

$$f(\vec{x}) = \sum_{q=1}^{N_q} \left(\frac{\delta_q^{\mathrm{NNLO}}(\vec{x}) - \delta_q^{\mathrm{Nijm93}}}{w_q} \right)^2, \qquad (1)$$

where δ^{NNLO} are NNLO phase shifts, δ^{Nijm93} are experimental phase shifts from the Nijmegen multienergy partial-wave analysis [18], $\vec{x}$ denotes the parameters of the chiral interaction, and w_q are weighting factors. Note that Eq. (1) is not the χ^2 with respect to experimental data. The actual χ^2 is calculated following the POUNDERS optimization. The phase shifts δ^{NNLO} are computed from R-matrix inversion, and in the proton-proton (pp) channels we include the Coulomb interaction [19,20]. The contact terms are optimized to reproduce the Nijmegen phase shifts for each corresponding partial wave, while keeping the c_i's fixed. For the contacts, the weight w_q scales with the third power of the relative momentum q, while for the c_i's, we employ the uncertainties quoted in the Nijmegen analysis [18]. This approach can be justified by a physical argument: for the peripheral waves the higher energies still represent longer-range physics, and the need for a pedantic agreement with lower energy phase shifts can be weakened. The πN couplings c_1, c_3, and c_4 were simultaneously optimized to the peripheral partial waves $^1D_2$, $^3D_2$, $^3F_2$, E_2, $^3F_3$, $^1G_4$, and $^3F_4$. Note that the NNLO contact terms do not contribute to orbital angular momenta $L \geq 2$. We do not include other peripheral waves from the Nijmegen study since they carry extremely small uncertainties, which lead to a very noisy objective function.

Table I summarizes the optimization results. Our values should be compared with the πN couplings as determined from πN scattering data, where $c_1 = -0.81 \pm 0.15$, $c_3 = -4.69 \pm 1.34$, and $c_4 = +3.40 \pm 0.04$ have been obtained [22]. Thus, POUNDERS yields values for c_1 and c_3 that agree well with the empirical determination from πN scattering. The c_4 value, however, deviates significantly from its empirical value. The same trend was found in the construction of the N^{3}LO [4] NN interaction. A detailed statistical sensitivity analysis of the LECs with uncertainty quantification will be presented in Ref. [23].

Table II shows the χ^2/datum for $\mathrm{NNLO_{opt}}$ at various laboratory energy bins. The quality of the fit is particularly good for energies below 125 MeV. For comparison, the np NNLO interaction of Ref. [3] yields χ^2/datum of 12–27 in the range $\Lambda = 600/700 - 450/500$ MeV at energies up to 290 MeV.

Around energies of 144 MeV there exist two data sets of pp differential cross sections with a very high precision (0.5% error) [25] (47 data points). The total number of pp data in the energy interval 125–183 MeV is 343. The unusual precision of those 47 data points distorts the χ^2/datum for this interval. For this reason, Table II also shows the results without the high-precision data.

Two comments are in order. First, the χ^2 with respect to scattering observables is lower when the $^1P_1$ phase shifts are weighted with the uncertainties from the Nijmegen analysis. The P waves are accurately reproduced only when going to N^{3}LO [4]. Second, the $^3S_1 - {}^3D_1$ coupled channel is optimized with the additional constraint of reproducing the deuteron binding energy. The remaining deuteron observables, as well as the $^1S_0$ scattering observables, are predictions and reproduce the experimental values well; see Table III.

Figure 1 shows some np phase shifts of $\mathrm{NNLO_{opt}}$ and compares them with phase shifts from other potentials and partial wave analyses. Apart from the ^3P waves, the phase shifts of $\mathrm{NNLO_{opt}}$ closely agree with those obtained at N^{3}LO. Note, however, that these deviations do not spoil the good χ^2 at laboratory energies below 125 MeV.

Three-nucleon forces also appear at NNLO, and two additional LECs (c_D and c_E) enter. These are determined from calculations in the three-nucleon and four-nucleon

TABLE II. χ^2/datum for $\mathrm{NNLO_{opt}}$ at $\Lambda = 500$ MeV and $\Lambda_{\mathrm{SFR}} = 700$ MeV [3,21] with respect to the np and pp 1999 databases [24]. The values without the high-precision data sets [25] are marked by asterisks.

T_{lab} (MeV)	0–35	35–125	125–183	183–290	0–290
pp χ^2/datum	1.11	1.56	23.95 4.35*	29.26	17.10 14.03*
np χ^2/datum	0.85	1.17	1.87	6.09	2.95

TABLE III. Scattering lengths a and effective ranges r (both in fm). The superscripts N and C for the proton-proton observables refer to nuclear forces and Coulomb-plus-nuclear forces, respectively. B_D, r_D, Q_D, and P_D denote the deuteron binding energy, radius, quadrupole moment, and D-state probability, respectively. Q_D and r_D are calculated without meson-exchange currents and relativistic corrections.

	N^3LO_{EM}	$NNLO_{opt}$	Exp.	Ref.
a_{pp}^C	−7.8188	−7.8174	−7.8196(26)	[26]
			−7.8149(29)	[27]
r_{pp}^C	2.795	2.755	2.790(14)	[26]
			2.769(14)	[27]
a_{pp}^N	−17.083	−17.825		
r_{pp}^N	2.876	2.817		
a_{nn}	−18.900	−18.889	−18.95(40)	[28,29]
r_{nn}	2.838	2.797	2.75(11)	[30]
a_{np}	−23.732	−23.749	−23.740(20)	[24]
r_{np}	2.725	2.684	2.77(5)	[24]
B_D (MeV)	2.224 575	2.224 582	2.224 575(9)	[24]
r_D (fm)	1.975	1.967	1.975 35(85)	[31]
Q_D (fm^2)	0.275	0.272	0.2859(3)	[24]
P_D (%)	4.51	4.05		

systems. We find that the binding energies of ^{3}H, ^{3}He, and ^{4}He do not uniquely determine c_D and c_E, and the parametric dependence of both LECs is very similar to those found in previous studies [6,32,33]. Therefore, we choose $c_D = -0.2$ guided by the triton half life [33] and obtain $c_E = -0.36$ from optimization to the binding energies. The resulting point charge radii of ^{4}He are also in good agreement with experiment; see Table IV.

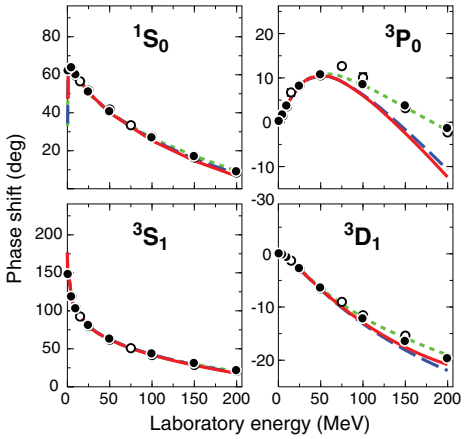

FIG. 1 (color online). Computed np phase shifts of the optimized NNLO potential of this work (solid, red line), the NNLO potential of Ref. [3] (dashed, blue line), and the N^{3}LO potential [4] (green, dotted line) compared with the Nijmegen phase shift analysis [18] (solid dots) and the VPI/GWU analysis SM99 [43] (open circles).

TABLE IV. Ground-state energies (in MeV) and point proton radii (in fm) for ^{3}H, ^{3}He, and ^{4}He using the $NNLO_{opt}$ with and without the NNLO 3NF interaction for $c_D = -0.20$ and $c_E = -0.36$.

	$E(^3H)$	$E(^3He)$	$E(^4He)$	$r_p(^4He)$
NNLO	−8.249	−7.501	−27.759	1.43(8)
NNLO+NNN	−8.469	−7.722	−28.417	1.43(8)
Experiment	−8.482	−7.717	−28.296	1.467(13)

Performance of $NNLO_{opt}$ *for light- and medium-mass nuclei and neutron matter.*—In this Letter, we apply $NNLO_{opt}$ to ^{10}B, isotopes of oxygen and calcium, and neutron matter. The considered systems are particularly interesting because the current NN chiral interactions at N^{3}LO completely fail to describe key aspects of their structure.

To study the ground state and first excited state in ^{10}B, we carry out no-core shell model (configuration interaction) calculations [34] using the bare $NNLO_{opt}$ in model spaces of up to $N_{max} = 10$ harmonic oscillator (HO) shells ($10\hbar\Omega$) above the unperturbed configuration. These model spaces are not large enough to provide fully converged results for the ground state and first excited state of ^{10}B. Still, the variational upper bounds for the energies are −54.35 MeV for the 1^+ state and −54.32 MeV for the 3^+ state. The energies are very close, in contrast to N^3LO_{EM}, which yields a level spacing of about 1.2 MeV between the $J^\pi = 1^+$ ground state and the $J^\pi = 3^+$ excited state [6].

Chiral NN interactions at N^{3}LO fail to explain the neutron drip-line in oxygen isotopes, and 3NFs have been the key element for understanding the structure of nuclei around ^{24}O [7,8]. Figure 2 shows the experimental ground-state energies of oxygen isotopes and compares the results from coupled-cluster (CC) computations in the Λ triples approximation [35–37]. Our CC calculations employ a Hartree-Fock basis built from $N_{max} = 15$ HO shells at $\hbar\Omega = 20$ MeV. Because of the "softness" of $NNLO_{opt}$, this model space is sufficiently large to converge the ground states and excited states of the nuclei

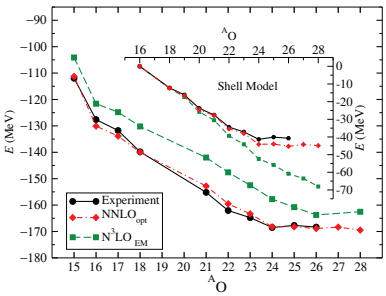

FIG. 2 (color online). The ground-state energies of oxygen isotopes obtained in CC with the $NNLO_{opt}$ and N^3LO_{EM} interactions compared with experiment. The inset shows SM results.

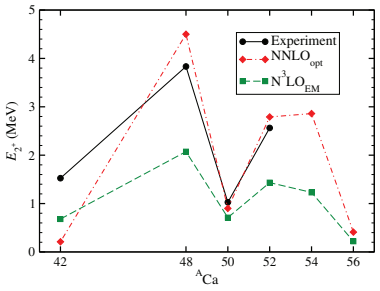

FIG. 3 (color online). The first 2^+_1 state in selected calcium isotopes obtained in CC with the NNLO$_{opt}$ and N^{3}LO$_{EM}$ interactions compared with experiment.

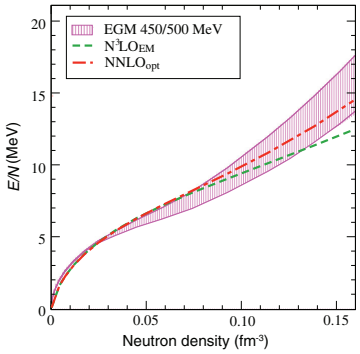

FIG. 4 (color online). Energy per nucleon for neutron matter for NNLO$_{opt}$ and N^{3}LO$_{EM}$ [4]. The calculations used the CC method with the inclusion of particle-particle ladders and a continuous single-particle spectrum. The shaded area (EGM) shows uncertainty bands for the N^{3}LO chiral effective field theory calculations of Ref. [42], including 3NFs.

considered. In addition, we performed shell-model (SM) calculations assuming the closed ^{16}O core with an effective interaction derived from many-body perturbation theory to third order in the interaction and including folded diagrams [38]. For the SM calculations, the single-particle energies were taken from the experimental ^{17}O spectrum. In both CC and SM, NNLO$_{opt}$ results are close to experiment. In contrast, the N^{3}LO$_{EM}$ case requires 3NFs to provide reasonable description of measured values.

Now we consider the heavy isotopes of calcium. Here, ^{48}Ca is doubly magic, ^{52}Ca exhibits a soft subshell closure, and ^{54}Ca is predicted to have an even softer subshell closure [10]. A signature of shell closure is the location of the first 2^+ state. We employed CC equation-of-motion methods within the singles and doubles approximation [37,39] to compute the first 2^+ state in the calcium isotopes. Figure 3 shows that N^{3}LO$_{EM}$ fails to describe the location of the first 2^+ state in ^{40,48,50,52,54,56}Ca. In contrast, NNLO$_{opt}$ yields ^{48}Ca as a doubly magic nucleus and predicts subshell closures in ^{52,54}Ca. The NNLO$_{opt}$ overbinds the calcium isotopes by about 1 MeV per nucleon. In particular, ^{40,48,52}Ca are overbound by 1.03, 1.06, and 1.04 MeV per nucleon, respectively. That is, the excess energy per nucleon is fairly constant; hence, NNLO$_{opt}$ reproduces binding energy differences, such as neutron-separation energies and low-lying excited states, rather well.

The complete description of nuclei at NNLO also requires 3NFs. We computed the first 2^+ state in ^{22,24}O and in ^{48}Ca with the 3NF compatible with the NNLO$_{opt}$ interaction. The matrix elements of the 3NF are expensive computationally, and we must at present limit their calculation to three-body energies up to $e_{3\,\max} = 2n_a + l_a + 2n_b + l_b + 2n_c + l_c = 14$. (Recall that we employ 15 major harmonic oscillator shells for the *NN* interaction.) We also used the normal ordered two-body approximation for the 3NF [40,41] with respect to a Hartree-Fock reference. With the restriction of $e_{3\,\max} = 14$, we were not able to obtain fully converged results for the binding energies of oxygen and calcium isotopes. However, excitation energies relative to the ground state converge somewhat better. Our results for the first 2^+ state in ^{22,24}O and in ^{48}Ca are 2.3(3), 3.5(5), and 4.8(7) MeV, respectively. We estimate the uncertainty by varying $\hbar\Omega$ in the interval 16–22 MeV. The results obtained by using NNLO$_{opt}$ *NN* interaction alone yields 2.5, 5.0, and 4.5 MeV in ^{22,24}O and ^{48}Ca, respectively. These preliminary results suggest that the 3NFs may not dramatically change the results that were obtained with the NNLO$_{opt}$ *NN* interaction alone.

It is instructive to compare the predictions of NNLO$_{opt}$ and N^{3}LO$_{EM}$ for the neutron matter equation of state at subsaturation densities with the results of *ab initio* calculations of Refs. [42]. Figure 4 shows that the performance of NNLO$_{opt}$ is on par with the EGM results of Ref. [42], which take into account the effects of 3NFs and 4NFs. The predictions of N^{3}LO$_{EM}$ deviate from other results at higher densities.

Conclusions.—We constructed the new *NN* chiral EFT interaction NNLO$_{opt}$ at next-to-next-to-leading order using the optimization tool POUNDERS in the phase-shift analysis. The optimization of the low-energy constants in the *NN* sector at NNLO yields a χ^2/datum of about one for laboratory scattering energies below 125 MeV. The NNLO$_{opt}$ *NN* interaction yields very good agreement with binding energies and radii for $A = 3$, 4 nuclei. Key aspects of nuclear structure, such as excitation spectra, the position of the neutron drip line in oxygen, shell-closures in calcium, and the neutron matter equation of state at subsaturation densities, are reproduced by NNLO$_{opt}$ interaction alone, without resorting to 3NFs. We performed the initial calculation of the first 2^+ states in ^{22,24}O and ^{48}Ca with NNLO$_{opt}$ supplemented by a 3NF and found the effects of 3NFs to be small and in good agreement with experimental excitation energies. The precise role of 3NFs in medium-mass nuclei, the quantification of theoretical uncertainties, and optimizations at higher-order chiral interactions will be addressed in forthcoming investigations.

We thank M. P. Kartamyshev, B. D. Carlsson, and H. T. Johansson for discussions and related code development. This work was supported by the Research Council of Norway under contract ISP-Fysikk/216699; by the Office of Nuclear Physics, U.S. Department of Energy (Oak Ridge National Laboratory), under Grants No. DE-FG02-03ER41270 (University of Idaho), No. DE-FG02-96ER40963 (University of Tennessee), No. DE-AC02-06CH11357 (Argonne), and No. DE-SC0008499 (NUCLEI SciDAC collaboration); by the Swedish Research Council (dnr 2007-4078), and by the European Research Council (ERC-StG-240603). Computer time was provided by the Innovative and Novel Computational Impact on Theory and Experiment (INCITE) program. This research used resources of the Oak Ridge Leadership Computing Facility located in the Oak Ridge National Laboratory, which is supported by the Office of Science of the Department of Energy under Contract No. DE-AC05-00OR22725, and used computational resources of the National Center for Computational Sciences, the National Institute for Computational Sciences, and the Notur project in Norway.

[1] U. van Kolck, Phys. Rev. C **49**, 2932 (1994).
[2] E. Epelbaum, H.-W. Hammer, and U.-G. Meißner, Rev. Mod. Phys. **81**, 1773 (2009); R. Machleidt and D. Entem, Phys. Rep. **503**, 1 (2011).
[3] E. Epelbaum, W. Glöckle, and U.-G. Meißner, Eur. Phys. J. A **19**, 401 (2004); E. Epelbaum, A. Nogga, W. Glöckle, H. Kamada, U.-G. Meißner, and H. Witała, Eur. Phys. J. A **15**, 543 (2002).
[4] D. R. Entem and R. Machleidt, Phys. Rev. C **68**, 041001(R) (2003).
[5] H.-W. Hammer, A. Nogga, and A. Schwenk, Rev. Mod. Phys. **85**, 197 (2013).
[6] P. Navrátil, V. G. Gueorguiev, J. P. Vary, W. E. Ormand, and A. Nogga, Phys. Rev. Lett. **99**, 042501 (2007).
[7] T. Otsuka, T. Suzuki, J. D. Holt, A. Schwenk, and Y. Akaishi, Phys. Rev. Lett. **105**, 032501 (2010).
[8] G. Hagen, M. Hjorth-Jensen, G. R. Jansen, R. Machleidt, and T. Papenbrock, Phys. Rev. Lett. **108**, 242501 (2012).
[9] J. D. Holt, T. Otsuka, A. Schwenk, and T. Suzuki, J. Phys. G **39**, 085111 (2012).
[10] G. Hagen, M. Hjorth-Jensen, G. R. Jansen, R. Machleidt, and T. Papenbrock, Phys. Rev. Lett. **109**, 032502 (2012).
[11] S. Ishikawa and M. R. Robilotta, Phys. Rev. C **76**, 014006 (2007).
[12] V. Bernard, E. Epelbaum, H. Krebs, and U.-G. Meißner, Phys. Rev. C **77**, 064004 (2008); V. Bernard, E. Epelbaum, H. Krebs, and U.-G. Meißner, Phys. Rev. C **84**, 054001 (2011).
[13] H. Krebs, A. Gasparyan, and E. Epelbaum, Phys. Rev. C **85**, 054006 (2012).
[14] E. Epelbaum, A. Nogga, W. Glöckle, H. Kamada, U.-G. Meißner, and H. Witała, Phys. Rev. C **66**, 064001 (2002).
[15] M. Kortelainen, T. Lesinski, J. Moré, W. Nazarewicz, J. Sarich, N. Schunck, M. V. Stoitsov, and S. Wild, Phys. Rev. C **82**, 024313 (2010).
[16] P.-G. Reinhard and W. Nazarewicz, Phys. Rev. C **81**, 051303 (2010).
[17] T. Munson, J. Sarich, S. M. Wild, S. Benson, and L. C. McInnes, Technical Memorandum ANL/MCS-TM-322, Argonne National Laboratory, Argonne, Illinois (2012), see http://www.mcs.anl.gov/tao.
[18] V. G. J. Stoks, R. A. M. Klomp, M. C. M. Rentmeester, and J. J. de Swart, Phys. Rev. C **48**, 792 (1993).
[19] C. M. Vincent and S. C. Phatak, Phys. Rev. C **10**, 391 (1974).
[20] D. H. Lu, T. Mefford, R. H. Landau, and G. Song, Phys. Rev. C **50**, 3037 (1994).
[21] E. Epelbaum, Prog. Part. Nucl. Phys. **57**, 654 (2006).
[22] P. Büttiker and U.-G. Meißner, Nucl. Phys. **A668**, 97 (2000).
[23] A. Ekström *et al.* (to be published).
[24] R. Machleidt, Phys. Rev. C **63**, 024001 (2001).
[25] G. Cox, G. Eaton, C. V. Zyl, O. Jarvis, and B. Rose, Nucl. Phys. **B4**, 353 (1968), 21 pp diff. cross section data at 144.1 MeV.O. Jarvis, C. Whitehead, and M. Shah, Phys. Lett. **36B**, 409 (1971), 26 pp diff. cross section data at 144.0 MeV.
[26] J. R. Bergervoet, P. C. van Campen, W. A. van der Sanden, and J. J. de Swart, Phys. Rev. C **38**, 15 (1988).
[27] W. A. van der Sanden, A. H. Emmen, and J. J. de Swart, Tech. Rep., Nijmegen (1983), unpublished.
[28] D. E. Gonzalez Trotter *et al.*, Phys. Rev. C **73**, 034001 (2006).
[29] Q. Chen *et al.*, Phys. Rev. C **77**, 054002 (2008).
[30] G. Miller, B. Nefkens, and I. Šlaus, Phys. Rep. **194**, 1 (1990).
[31] A. Huber, T. Udem, B. Gross, J. Reichert, M. Kourogi, K. Pachucki, M. Weitz, and T. W. Hänsch, Phys. Rev. Lett. **80**, 468 (1998).
[32] A. Nogga, P. Navrátil, B. R. Barrett, and J. P. Vary, Phys. Rev. C **73**, 064002 (2006).
[33] D. Gazit, S. Quaglioni, and P. Navrátil, Phys. Rev. Lett. **103**, 102502 (2009).
[34] B. Barrett, P. Navrátil, and J. P. Vary, Prog. Part. Nucl. Phys. **69**, 131 (2013).
[35] S. A. Kucharski and R. J. Bartlett, J. Chem. Phys. **108**, 5243 (1998).
[36] A. G. Taube and R. J. Bartlett, J. Chem. Phys. **128**, 044110 (2008).
[37] G. Hagen, T. Papenbrock, D. J. Dean, and M. Hjorth-Jensen, Phys. Rev. C **82**, 034330 (2010).
[38] M. Hjorth-Jensen, T. T. S. Kuo, and E. Osnes, Phys. Rep. **261**, 125 (1995).
[39] G. R. Jansen, M. Hjorth-Jensen, G. Hagen, and T. Papenbrock, Phys. Rev. C **83**, 054306 (2011).
[40] G. Hagen, T. Papenbrock, D. J. Dean, A. Schwenk, A. Nogga, M. Włoch, and P. Piecuch, Phys. Rev. C **76**, 034302 (2007).
[41] S. Binder, J. Langhammer, A. Calci, P. Navrátil, and R. Roth, Phys. Rev. C **87**, 021303 (2013).
[42] I. Tews, T. Krüger, K. Hebeler, and A. Schwenk, Phys. Rev. Lett. **110**, 032504 (2013).
[43] R. A. Arndt, I. I. Strakovsky, and R. L. Workman (1999), SAID, Scattering Analysis Interactive Dial-in computer facility, George Washington University (formerly Virginia Polytechnic Institute), solution SM99 (Summer 1999); for more information see, e.g., R. A. Arndt, I. I. Strakovsky, and R. L. Workman, Phys. Rev. C **50**, 2731 (1994).

II

Coupled-cluster studies of infinite nuclear matter

G. Baardsen,[1] A. Ekström,[1,2] G. Hagen,[3,4] and M. Hjorth-Jensen[1,2,5]
[1]*Department of Physics and Center of Mathematics for Applications, University of Oslo, N-0316 Oslo, Norway*
[2]*National Superconducting Cyclotron Laboratory, Michigan State University, East Lansing, Michigan 48824, USA*
[3]*Physics Division, Oak Ridge National Laboratory, Oak Ridge, Tennessee 37831, USA*
[4]*Department of Physics and Astronomy, University of Tennessee, Knoxville, Tennessee 37996, USA*
[5]*Department of Physics and Astronomy, Michigan State University, East Lansing, Michigan 48824, USA*
(Received 24 June 2013; revised manuscript received 8 October 2013; published 14 November 2013)

Background: Coupled-cluster (CC) theory is a widely used many-body method for studying strongly correlated many-fermion systems. It allows for systematic inclusions of complicated many-body correlations beyond a mean field. Recent applications to finite nuclei have shown that first-principles approaches like CC theory can be extended to studies of medium-heavy nuclei, with excellent agreement with experiment. However, CC calculations of properties of infinite nuclear matter are rather few and date back more than 30 yr.
Purpose: The aim of this work is thus to develop the relevant formalism for performing CC calculations in nuclear matter and neutron-star matter, including thereby important correlations to infinite order in the interaction and testing modern nuclear forces based on chiral effective field theory. Our formalism includes also the exact treatment of the so-called Pauli operator in a partial-wave expansion of the equation of state.
Methods: Nuclear- and neutron-matter calculations are done using a coupled particle-particle and hole-hole ladder approximation. The coupled ladder equations are derived as an approximation of CC theory, leaving out particle-hole and nonlinear diagrams from the CC doubles amplitude equation. This study is a first step toward CC calculations for nuclear and neutron matter.
Results: We present results for both symmetric nuclear matter and pure neutron matter employing state-of-the-art nucleon-nucleon interactions based on chiral effective field theory. We employ also the newly optimized chiral interaction [Ekström *et al*., Phys. Rev. Lett. **110**, 192502 (2013)] to study infinite nuclear matter. The ladder approximation method and corresponding results are compared with conventional Brueckner-Hartree-Fock theory. The ladder approximation is derived and studied using both exact and angular-averaged Pauli exclusion operators, with angular-averaged input momenta for the single-particle potentials in all calculations. The inclusion of an exact treatment of the Pauli operators in a partial-wave expansion yields corrections of the order of 1.7%–2% of the total energy in symmetric nuclear matter. Similarly, the inclusion of both hole-hole and particle-particle ladders result in corrections of the order 0.7%–2% compared to the approximation with only particle-particle ladders. Including these effects, we get at most almost a 6% difference between our CC calculation and the standard Brueckner-Hartree-Fock approach.
Conclusions: We have performed CC calculations of symmetric nuclear matter and pure neutron matter including particle-particle and hole-hole diagrams to infinite order using an exact Pauli operator and angular-averaged single-particle energies. The contributions from hole-hole diagrams and exact Pauli operators add important changes to the final energies per particle.

DOI: 10.1103/PhysRevC.88.054312 PACS number(s): 21.65.Cd, 21.65.Mn, 21.30.−x, 26.60.Kp

I. INTRODUCTION

Nuclear matter is defined as an isotropic system consisting of infinitely many nucleons which interact only by nuclear forces. The Schrödinger equation of this system has been solved approximately using many different *ab initio* many-body methods [1–8]. As an example, diagrammatic partial summations have been derived from many-body perturbation theory to calculate the binding energy. One approach belonging to this family of methods is the Brueckner-Goldstone (BG) expansion [9], which is a Goldstone expansion where the interaction has been replaced by a well-behaved reaction matrix [10]. The Brueckner-Hartree-Fock (BHF) scheme [9,11], which is one of the standard methods of nuclear-matter theory [6,12–16], is a first-order approximation in BG theory.

Unfortunately, the BG expansion does not converge very well when using the number of reaction matrices as the order parameter [17]. A more appropriate way to include higher-order correlations is the hole-line expansion [1], where the perturbation truncation is determined by the number of independent hole lines in the the BG diagrams. The two-hole-line approximation is then equivalent to the BHF method. Calculations including up to three-hole-line diagrams indicate that the hole-line expansion converges [13,18]. Despite encouraging results for the hole-line expansion, it would still be desirable to get a deeper understanding of the accuracy of the many-body methods applied to nuclear matter. Better knowledge about the convergence of the many-body methods in nuclear matter is also necessary to validate the quality of calculations including three- and many-body interactions [19–25].

An approach that is related to the above-mentioned perturbative techniques is the coupled-cluster (CC) method [26–31]. As perturbation theory, CC theory gives a nonvariational and size-extensive method. However, in contrast to many-body perturbation theory, CC theory sums to infinite order, depending

on the level of truncation, selected many-body contributions. It is thus a nonperturbative method. The CC truncation is physical in the sense that a so-called T_n truncation includes all possible correlations arising from sets of n-particle-n-hole clusters [32–34]. During the last one and a half decades, CC theory has been successfully applied to structure calculations of finite nuclei [35–43]. Inspired by the success of the CC approach in finite nuclei, we hope that CC theory could also provide accurate results for infinite nuclear matter.

Already in the early 1980s, Day and Zabolitzky performed CC calculations for nuclear matter [2] using the Bochum truncation [44,45]. The theory of nuclear interactions has evolved a lot since that time (see for example Ref. [46]), with the construction of high-precision potentials exhibiting a χ^2 per datum close to one with respect to nucleon-nucleon scattering data [46]. Later, two- and three-body interactions have been developed based on effective field theory (EFT), which is derived using symmetries arising from quantum chromodynamics (QCD) [47]. In addition, soft low-momentum interactions based on renormalization group theory have been introduced [48]. It seems therefore necessary to perform new CC calculations for nuclear matter with modern two- and three-body interactions.

In the Bochum truncation scheme [44], the exact CC amplitude equations are approximated by setting all so-called reduced n-particle subsystem amplitudes χ_n, with n larger than a chosen truncation level, to zero. The justification for using this truncation is that all subsystem amplitudes χ_n become small inside a radius where the interaction may be very strong [44]. This truncation scheme therefore ensures that the contribution from particles interacting strongly at short distances becomes small. In their CC calculations for nuclear matter, Day and Zabolitzky included the two- and three-body subsystem amplitudes χ_2 and χ_3, and incorporated also parts of the four-body amplitude χ_4 [2,18]. Given the computing capacity in the early 1980s, it was necessary to do further approximations in the CC equations. As is explained in Refs. [2,18], the authors used angular-averaged Pauli exclusion operators, other averages over angles, and first-order Taylor expansions to approximate the dependence of the single-particle potential on the G matrix. In addition, they replaced some diagrams with estimates, which were simpler to calculate than the original diagrams [2]. Before this study, Manzke [49] did CC calculations for nuclear matter in the two-body subsystem approximation.

Coupled-cluster theory is widely used within the quantum chemistry community [31]. A commonly used CC truncation scheme in quantum chemistry is to set all cluster amplitudes in the exponential CC wave function ansatz beyond a given excitation level to zero (see Sec. II A and Refs. [32,33]). These approximations are called, for example, CC doubles (CCD), CC singles-doubles (CCSD), etc. [31], or, alternatively, SUBn approximations [50]. This truncation scheme has been applied in studies of finite nuclei [37,38,40–43], mainly using soft interactions. Our aim is to apply the same CC method to studies of the equation of state of symmetric nuclear matter and neutron matter.

The SUBn approximation includes long-range contributions, such as the forward and other ring diagrams, already at the CCD or SUB2 level [50,51]. In contrast, these correlations are included in the Bochum scheme in the subsystem amplitudes χ_3 and χ_4 [44]. Another difference between the two CC truncation schemes is the treatment of the single-particle state potentials in the energy denominator. In the Bochum CC method, the energy denominator contains single-hole state potentials with summations of particle-particle ladder diagrams to infinite order, whereas the single-particle state potentials are zero in the energy denominator. Instead, the single-particle state potential terms are part of the χ_3 and χ_4 subsystem amplitudes [44]. In contrast, in the SUBn approximation, which we employ in this work, the energy denominator contains single-particle potentials at the Hartree-Fock level for both particles and holes.

Previously, Freeman [52] has studied the two-dimensional electron gas including particle-particle ladder diagrams from the CCD approximation. In a similar way, as a first step toward CC calculations for nuclear matter, we here include particle-particle and hole-hole correlations at the two-particle-two-hole, or T_2, level. In this scheme, only the linear ladder diagrams have been included in the CC T_2 amplitude equation, whereas the linear particle-hole diagrams and all nonlinear diagrams have been neglected. When leaving out certain diagrams of the T_2 amplitude equation, our scheme may be considered as strictly not a CC approximation. However, the method shows a proof of principle of an iterative CC numerical scheme, where particle-particle and hole-hole ladder diagrams are coupled and summed to infinite order. The coupled ladder approximation is similar to the Bochum CC method including only the two-body subsystem amplitude χ_2, but the single-particle potentials are different. It ought also to be emphasized that the calculations of Day and Zabolitzky [2] included a larger set of diagrams, and thereby correlations, than the approximation used in this work.

According to the hole-line expansion calculations by Song *et al.*, the contribution of particle-particle diagrams is considerably larger than that of particle-hole diagrams [13]. Still, the contribution of particle-hole diagrams is clearly non-negligible in the hole-line expansion [13]. The results of Ref. [53] show that ring (particle-hole) diagrams are significant for the binding energy of nuclear matter. The aim is therefore to include all T_2 diagrams in a future CC calculation to get a proper CC approximation at the T_2 level.

Summation of particle-particle and hole-hole ladder diagrams is also a common approximation in self-consistent Green's function (SCGF) theory [4]. The SCGF ladder approximation has been extensively applied to studies of nuclear and neutron matter [54–58], lately including either three-body interactions or density-dependent two-body operators arising from three-body interactions [8,19]. In the SCGF ladder approximation, the energy denominator contains self-consistently solved complete off-shell self-energies including both particle-particle and hole-hole ladder diagrams. As the SCGF method, the CC ladder approximation also treats particle and hole interactions symmetrically, but from the definition of the CC equations it follows that the single-particle potentials occur in the energy denominator only up to the Hartree-Fock level.

Another similar method is the particle-particle and hole-hole ring diagram approximation [59–62], where the particle-particle and hole-hole diagrams are derived from Green's function theory, and a momentum model space is used to avoid poles in the energy denominator. The binding energy obtained in this approximation depends, however, on the model space momentum cutoff [61]. In the particle-particle and hole-hole ring diagram method the authors employed the standard angular-average approximations to decrease the computational complexity of the calculations [59].

In the present work, we analyze the partial-wave expansion of the equation of state using an exact treatment of the intermediate states, avoiding thereby the standard angle-average approximation of Pauli exclusion operators [12]. Finally, we perform calculations of the above systems using modern nucleon-nucleon interactions based on chiral perturbation theory to next-to-next-to-leading order (NNLO) [63] and next-to-next-to-next-to-leading order (N^3LO) [64].

After these introductory remarks, we present our formalism in the next three sections, followed subsequently by our results and discussion thereof in Sec. IV. Concluding remarks and perspectives are presented in Sec. V.

II. FORMALISM: MANY-BODY METHODS

The general form of the Hamiltonian operator of infinite nuclear matter is

$$\begin{aligned}\hat{H} &= \hat{K} + \hat{V}_{NN} + \hat{V}_{NNN} + \cdots \\ &= -\frac{\hbar^2}{2M}\sum_{i=1}^{A}\nabla_i^2 + \sum_{i<j}^{A}\hat{v}_{NN}(\mathbf{r}_i,\mathbf{r}_j) \\ &\quad + \sum_{i<j<k}^{A}\hat{v}_{NNN}(\mathbf{r}_i,\mathbf{r}_j,\mathbf{r}_k) + \cdots, \end{aligned} \tag{1}$$

where A is the number of nucleons, $\hat{K}$ is the kinetic energy operator, $\hat{V}_{NN}$ is a two-particle interaction operator, $\hat{V}_{NNN}$ is a three-particle interaction operator, M is the nucleon mass, and $\mathbf{r}_l$ is the position vector of particle l. In this paper, we neglect n-body interactions for n larger than two and define the Hamiltonian operator as

$$\hat{H} = \hat{K} + \hat{V} = -\frac{\hbar^2}{2M}\sum_{i=1}^{A}\nabla_i^2 + \sum_{i<j}^{A}\hat{v}(r_{ij}),$$

where $\hat{v}$ is a two-body interaction and $r_{ij} = |\mathbf{r}_i - \mathbf{r}_j|$.

In our calculations, we use the nucleon-nucleon interaction of Ref. [64]. This interaction model is given by an N^3LO approximation of chiral perturbation theory. Nuclear interactions based on EFT have the advantage that two- and many-body interactions can be derived in a mutually consistent way [47]. Furthermore, we present also results obtained with a recent nucleon-nucleon interaction at order NNLO in chiral perturbation theory. This interaction results from an optimization-based reparametrization to the available body of experimental data using the model-based, derivative-free optimization algorithm POUNDERS developed at Argonne National Laboratory [65]. The resulting new chiral interaction, labeled $NNLO_{opt}$ hereafter, exhibits a χ^2 per datum close to one for laboratory scattering energies below approximately 125 MeV in the two-body proton-proton and neutron-proton channels; see Ref. [63] for further details. In the $A = 3$ and $A = 4$ nucleon systems, this interaction gives binding energies that differ by 20 and 45 keV from the experimental values, respectively. Thus, the contributions of three-nucleon forces appear smaller than for previous parametrizations of chiral interactions.

We model infinite nuclear matter as a system of A interacting nucleons confined by a cubic box potential. The cubic box boundary condition together with the free nucleon Hamiltonian equation

$$-\frac{\hbar^2}{2M}\nabla^2\varphi(\mathbf{r}) = \varepsilon\varphi(\mathbf{r}),$$

gives the plane-wave eigenfunctions $\varphi_{\mathbf{k}}(\mathbf{r}) = e^{i\mathbf{k}\cdot\mathbf{r}}/\sqrt{\Omega}$ and eigenenergies $\varepsilon_{\mathbf{k}} = \hbar^2k^2/(2M)$. Here $\hbar\mathbf{k}$ is the momentum, $\mathbf{r}$ is the position coordinate, and Ω is the volume of the box. We therefore use plane waves as our single-particle basis, from which the Slater determinants are constructed.

A. Coupled ladder approximation

In this section, the coupled ladder equations are derived as an approximation of the CC method. The CC formalism is presented in a momentum basis. In the general expressions, we omit spin and isospin degrees of freedom.

In CC theory, the A-fermion state vector is expressed using the exponential ansatz

$$|\Psi\rangle \equiv e^{\hat{T}}\,|\Phi_0\rangle\,,$$

where $|\Phi_0\rangle$ is the uncorrelated free Fermi vacuum, and the cluster operator $\hat{T}$ is defined as the sum

$$\hat{T} = \sum_{m=1}^{A}\hat{T}_m,$$

of m-particle m-hole excitation operators

$$\hat{T}_m = \left(\frac{1}{m!}\right)^2 \sum_{\substack{\mathbf{k}_{i_1},\ldots,\mathbf{k}_{i_m}\\ \mathbf{k}_{a_1},\ldots,\mathbf{k}_{a_m}}} t^{\mathbf{k}_{a_1},\ldots,\mathbf{k}_{a_m}}_{\mathbf{k}_{i_1},\ldots,\mathbf{k}_{i_m}} c^{\dagger}_{\mathbf{k}_{a_1}}\cdots c^{\dagger}_{\mathbf{k}_{a_m}} c_{\mathbf{k}_{i_m}}\cdots c_{\mathbf{k}_{i_1}}. \tag{2}$$

We label single-particle states occupied in the Fermi vacuum determinant Φ_0 (holes) by $i, j, k, \ldots$ and excited states of the same single-particle basis (particles) by a, b, c, and so on. Indices $p, q, r, \ldots$ are used to label single-particle states that may be either holes or particles. The operators $c^{\dagger}$ and c are fermion creation and annihilation operators, respectively.

Given that the single-particle basis is complete, the A-particle Schrödinger equation can be written equivalently as the CC energy equation

$$\langle\Phi_0|e^{-\hat{T}}\hat{H}e^{\hat{T}}|\Phi_0\rangle = E, \tag{3}$$

where the cluster operator $\hat{T}$ is obtained from the corresponding set of CC amplitude equations

$$\left\langle\Phi^{\mathbf{k}_{a_1}\mathbf{k}_{a_2}\ldots\mathbf{k}_{a_k}}_{\mathbf{k}_{i_1}\mathbf{k}_{i_2}\ldots\mathbf{k}_{i_k}}\right|e^{-\hat{T}}\hat{H}e^{\hat{T}}|\Phi_0\rangle = 0 \tag{4}$$

for $k = 1, 2, 3, \ldots, A$. Here we have used the notation

$$\left|\Phi^{\mathbf{k}_{a_1}\mathbf{k}_{a_2}\ldots\mathbf{k}_{a_k}}_{\mathbf{k}_{i_1}\mathbf{k}_{i_2}\ldots\mathbf{k}_{i_k}}\right\rangle \equiv c^\dagger_{\mathbf{k}_{a_1}} c^\dagger_{\mathbf{k}_{a_2}} \cdots c^\dagger_{\mathbf{k}_{a_k}} c_{\mathbf{k}_{i_k}} \cdots c_{\mathbf{k}_{i_2}} c_{\mathbf{k}_{i_1}} |\Phi_0\rangle, \quad (5)$$

which means that the bra vector in Eq. (4) is a k-particle k-hole excitation of the Fermi vacuum state.

In almost all practical calculations, except for some very simple model systems, it is necessary to do a truncation both in the cluster operator $\hat{T}$ and in the single-particle basis. To derive the ladder expansion, we need only the approximation $\hat{T} \approx \hat{T}_2$, which is commonly called the CCD approximation. In fact, the $\hat{T}_1$ operator is found to vanish for infinite nuclear and neutron matter [44]. By symmetry considerations, the total momentum of the system of nucleons is zero. Both the kinetic energy operator $\hat{K}$ and the total Hamiltonian $\hat{H}$ are assumed to be diagonal in total momentum $\mathbf{K}$. Hence, both the reference state Φ_0 and the correlated ground state Ψ must be eigenfunctions of the operator $\hat{\mathbf{K}}$ with the corresponding eigenvalue $\mathbf{K} = \mathbf{0}$ [10].

Using abstract vectors and a momentum single-particle basis, the CC ansatz can be written as

$$|\Psi_{\mathrm{CC}}\rangle = |\Phi_0\rangle + \sum_{\mathbf{k}_i\mathbf{k}_a} t^{\mathbf{k}_a}_{\mathbf{k}_i} |\Phi^{\mathbf{k}_a}_{\mathbf{k}_i}\rangle + \frac{1}{4} \sum_{\mathbf{k}_i\mathbf{k}_j\mathbf{k}_a\mathbf{k}_b} t^{\mathbf{k}_a\mathbf{k}_b}_{\mathbf{k}_i\mathbf{k}_j} |\Phi^{\mathbf{k}_a\mathbf{k}_b}_{\mathbf{k}_i\mathbf{k}_j}\rangle + \frac{1}{2} \sum_{\mathbf{k}_i\mathbf{k}_a} \sum_{\mathbf{k}_j\mathbf{k}_b} t^{\mathbf{k}_a}_{\mathbf{k}_i} t^{\mathbf{k}_b}_{\mathbf{k}_j} |\Phi^{\mathbf{k}_a\mathbf{k}_b}_{\mathbf{k}_i\mathbf{k}_j}\rangle + \cdots, \quad (6)$$

where $\mathbf{k}_m$ is the momentum of the single-particle state m. From Eq. (6) and the conditions

$$\hat{\mathbf{K}}|\Phi_0\rangle = \mathbf{0}|\Phi_0\rangle,$$

and

$$\hat{\mathbf{K}}|\Psi_{\mathrm{CC}}\rangle = \mathbf{0}|\Psi_{\mathrm{CC}}\rangle,$$

it follows that

$$\hat{\mathbf{K}} t^{\mathbf{k}_a}_{\mathbf{k}_i} |\Phi^{\mathbf{k}_a}_{\mathbf{k}_i}\rangle = (\mathbf{k}_a - \mathbf{k}_i) t^{\mathbf{k}_a}_{\mathbf{k}_i} |\Phi^{\mathbf{k}_a}_{\mathbf{k}_i}\rangle,$$

and

$$\hat{\mathbf{K}} t^{\mathbf{k}_a\mathbf{k}_b}_{\mathbf{k}_i\mathbf{k}_j} |\Phi^{\mathbf{k}_a\mathbf{k}_b}_{\mathbf{k}_i\mathbf{k}_j}\rangle = (\mathbf{k}_a + \mathbf{k}_b - \mathbf{k}_i - \mathbf{k}_j) t^{\mathbf{k}_a\mathbf{k}_b}_{\mathbf{k}_i\mathbf{k}_j} |\Phi^{\mathbf{k}_a\mathbf{k}_b}_{\mathbf{k}_i\mathbf{k}_j}\rangle.$$

Because by definition $|\mathbf{k}_a| > |\mathbf{k}_i|$, the CC exponential ansatz becomes an eigenfunction of the operator $\hat{\mathbf{K}}$ with the eigenvalue $\mathbf{0}$ only if all coefficients $t^{\mathbf{k}_a}_{\mathbf{k}_i}$ are zero and the restriction

$$\mathbf{k}_a + \mathbf{k}_b = \mathbf{k}_i + \mathbf{k}_j,$$

is fulfilled. This implies that the operator $\hat{T}_1$ is zero. In the same way, the contribution of $\hat{T}_1$ vanishes in CC calculations for the three-dimensional electron gas [50].

The CCD $\hat{T}_2$ amplitude equation can be written in laboratory momentum coordinates as (see, for example, Ref. [33])

$$\begin{aligned}
0 = {} & \langle \mathbf{k}_a\mathbf{k}_b|v|\mathbf{k}_i\mathbf{k}_j\rangle + P(\mathbf{k}_a\mathbf{k}_b) \sum_{\mathbf{k}_c} \langle \mathbf{k}_b|f|\mathbf{k}_c\rangle \langle \mathbf{k}_a\mathbf{k}_c|t|\mathbf{k}_i\mathbf{k}_j\rangle \\
& - P(\mathbf{k}_i\mathbf{k}_j) \sum_{\mathbf{k}_k} \langle \mathbf{k}_a\mathbf{k}_b|t|\mathbf{k}_i\mathbf{k}_k\rangle \langle \mathbf{k}_k|f|\mathbf{k}_j\rangle \\
& + \frac{1}{2} \sum_{\mathbf{k}_c\mathbf{k}_d} \langle \mathbf{k}_a\mathbf{k}_b|v|\mathbf{k}_c\mathbf{k}_d\rangle \langle \mathbf{k}_c\mathbf{k}_d|t|\mathbf{k}_i\mathbf{k}_j\rangle \\
& + \frac{1}{2} \sum_{\mathbf{k}_k\mathbf{k}_l} \langle \mathbf{k}_a\mathbf{k}_b|t|\mathbf{k}_k\mathbf{k}_l\rangle \langle \mathbf{k}_k\mathbf{k}_l|v|\mathbf{k}_i\mathbf{k}_j\rangle \\
& + P(\mathbf{k}_i\mathbf{k}_j) P(\mathbf{k}_a\mathbf{k}_b) \sum_{\mathbf{k}_k\mathbf{k}_c} \langle \mathbf{k}_a\mathbf{k}_c|t|\mathbf{k}_i\mathbf{k}_k\rangle \langle \mathbf{k}_k\mathbf{k}_b|v|\mathbf{k}_c\mathbf{k}_j\rangle \\
& + \frac{1}{2} P(\mathbf{k}_i\mathbf{k}_j) P(\mathbf{k}_a\mathbf{k}_b) \sum_{\mathbf{k}_k\mathbf{k}_l\mathbf{k}_c\mathbf{k}_d} \langle \mathbf{k}_k\mathbf{k}_l|v|\mathbf{k}_c\mathbf{k}_d\rangle \\
& \times \langle \mathbf{k}_a\mathbf{k}_c|t|\mathbf{k}_i\mathbf{k}_k\rangle \langle \mathbf{k}_d\mathbf{k}_b|t|\mathbf{k}_l\mathbf{k}_j\rangle \\
& - P(\mathbf{k}_i\mathbf{k}_j) \frac{1}{2} \sum_{\mathbf{k}_k\mathbf{k}_l\mathbf{k}_c\mathbf{k}_d} \langle \mathbf{k}_k\mathbf{k}_l|v|\mathbf{k}_c\mathbf{k}_d\rangle \\
& \times \langle \mathbf{k}_a\mathbf{k}_b|t|\mathbf{k}_i\mathbf{k}_k\rangle \langle \mathbf{k}_c\mathbf{k}_d|t|\mathbf{k}_j\mathbf{k}_l\rangle \\
& - P(\mathbf{k}_a\mathbf{k}_b) \frac{1}{2} \sum_{\mathbf{k}_k\mathbf{k}_l\mathbf{k}_c\mathbf{k}_d} \langle \mathbf{k}_k\mathbf{k}_l|v|\mathbf{k}_c\mathbf{k}_d\rangle \\
& \times \langle \mathbf{k}_a\mathbf{k}_c|t|\mathbf{k}_i\mathbf{k}_j\rangle \langle \mathbf{k}_b\mathbf{d}|t|\mathbf{k}_k\mathbf{k}_l\rangle \\
& + \frac{1}{4} \sum_{\mathbf{k}_k\mathbf{k}_l\mathbf{k}_c\mathbf{k}_d} \langle \mathbf{k}_k\mathbf{k}_l|v|\mathbf{k}_c\mathbf{k}_d\rangle \\
& \times \langle \mathbf{k}_c\mathbf{k}_d|t|\mathbf{k}_i\mathbf{k}_j\rangle \langle \mathbf{k}_a\mathbf{k}_b|t|\mathbf{k}_k\mathbf{k}_l\rangle, \quad (7)
\end{aligned}$$

where all two-body matrix elements are antisymmetrized and $P(pq)$ is a permutation operator that operates on a general function $y(p, q)$ according to

$$P(pq)y(p, q) = y(p, q) - y(q, p).$$

The Fock operator is defined by

$$\langle \mathbf{k}_p|f|\mathbf{k}_q\rangle = \langle \mathbf{k}_p|h_0|\mathbf{k}_q\rangle + \sum_i \langle \mathbf{k}_p\mathbf{k}_i|v|\mathbf{k}_q\mathbf{k}_i\rangle,$$

where the single-particle kinetic energy operator h_0 is $k^2/(2M)$ in momentum space. From the fact that the two-particle interaction conserves the total momentum, it follows that the Fock operator is diagonal in momentum basis. This also means that the plane-wave basis is a Hartree-Fock basis for infinite nuclear matter and, as is well known, the Hartree-Fock energy for nuclear matter is simply the same as the ground-state energy in first-order many-body perturbation theory [MBPT(1)] [66]. The CC $\hat{T}_2$ amplitude equation from Eq. (7) is given in diagrammatic representation in Fig. 1. We use diagrammatic rules as defined in Ref. [33].

The particle-particle and hole-hole ladder (PPHH-LAD) approximation is obtained by leaving out from the CCD amplitude equation all nonlinear terms, as well as the linear term with summation over one particle and one hole index. The coupled ladder equations are

$$\begin{aligned}
0 = {} & \langle \mathbf{k}_a\mathbf{k}_b|v|\mathbf{k}_i\mathbf{k}_j\rangle + P(\mathbf{k}_a\mathbf{k}_b) \sum_{\mathbf{k}_c} \langle \mathbf{k}_b|f|\mathbf{k}_c\rangle \langle \mathbf{k}_a\mathbf{k}_c|t|\mathbf{k}_i\mathbf{k}_j\rangle \\
& - P(\mathbf{k}_i\mathbf{k}_j) \sum_{\mathbf{k}_k} \langle \mathbf{k}_a\mathbf{k}_b|t|\mathbf{k}_i\mathbf{k}_k\rangle \langle \mathbf{k}_k|f|\mathbf{k}_j\rangle \\
& + \frac{1}{2} \sum_{\mathbf{k}_c\mathbf{k}_d} \langle \mathbf{k}_a\mathbf{k}_b|v|\mathbf{k}_c\mathbf{k}_d\rangle \langle \mathbf{k}_c\mathbf{k}_d|t|\mathbf{k}_i\mathbf{k}_j\rangle \\
& + \frac{1}{2} \sum_{\mathbf{k}_k\mathbf{k}_l} \langle \mathbf{k}_a\mathbf{k}_b|t|\mathbf{k}_k\mathbf{k}_l\rangle \langle \mathbf{k}_k\mathbf{k}_l|v|\mathbf{k}_i\mathbf{k}_j\rangle. \quad (8)
\end{aligned}$$

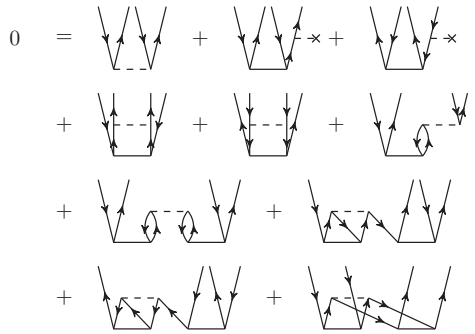

FIG. 1. Diagrammatic representation of the $\hat{T}_2$ amplitude equation in the CCD approximation. The coupled particle-particle and hole-hole ladder (PPHH-LAD) equations are obtained by leaving out the sixth diagram, which has summation over one particle and one hole state, and all the nonlinear diagrams, that is, the four last diagrams. The particle-particle ladder (PP-LAD) equations are otherwise equal to the PPHH-LAD equations; apart from that in the former case also the fifth diagram is neglected. The two-particle interaction is illustrated by a dashed line and the t amplitude by a solid line. The dashed line with a cross at one vertex represents the Fock operator. Lines with arrows pointing upwards represent particles, whereas lines with arrows pointing downwards represent holes. The interaction and t amplitude are assumed to be antisymmetric.

We define the particle-particle ladder (PP-LAD) equations as Eq. (8), where the last line, the hole-hole ladder diagram, is removed. In the PPHH-LAD approximation, the five first diagrams of Fig. 1 are retained. The PP-LAD approximation uses only the four first diagrams in the same figure.

The CC energy equation (3) becomes in the CCD approximation

$$E_{\mathrm{CCD}} = E_{\mathrm{REF}} + \Delta E_{\mathrm{CCD}},$$

where the reference energy is written as

$$E_{\mathrm{REF}} = \sum_{\mathbf{k}_i} \langle \mathbf{k}_i | h_0 | \mathbf{k}_i \rangle + \frac{1}{2} \sum_{\mathbf{k}_i \mathbf{k}_j} \langle \mathbf{k}_i \mathbf{k}_j | v | \mathbf{k}_i \mathbf{k}_j \rangle, \tag{9}$$

and the correlation correction term is simply

$$\Delta E_{\mathrm{CCD}} = \frac{1}{4} \sum_{\mathbf{k}_a \mathbf{k}_b \mathbf{k}_i \mathbf{k}_j} \langle \mathbf{k}_i \mathbf{k}_j | v | \mathbf{k}_a \mathbf{k}_b \rangle \langle \mathbf{k}_a \mathbf{k}_b | t | \mathbf{k}_i \mathbf{k}_j \rangle. \tag{10}$$

The general expressions for the CC energy are derived in, for example, Ref. [33]. A diagrammatic representation of the energy equation is given in Fig. 2. The correlation energy has more terms in a general case when the $\hat{T}_1$ amplitude does not vanish.

Let us define T as the amplitude matrix, with the matrix elements

$$[T]_{\alpha,\beta} = \langle \mathbf{k}_{p(\alpha)} \mathbf{k}_{q(\alpha)} | t | \mathbf{k}_{r(\beta)} \mathbf{k}_{s(\beta)} \rangle,$$

where p, q, r, and s are functions of the two-body configurations α and β. As explained in Ref. [33], the ladder equations

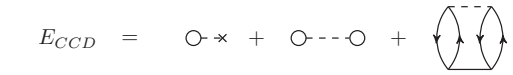

FIG. 2. The CCD energy equation, given in terms of diagrams. The two-particle interaction is given by a dashed line and the t amplitude by a solid line. The dashed line with a cross at one vertex represents the kinetic energy operator. Lines with arrows pointing upwards represent particles, lines with arrows pointing downwards represent holes, and circles are always hole lines.

can be written as the more convenient matrix equation

$$T = z(T), \tag{11}$$

where the left-hand side consists of only an amplitude matrix and the rest of the ladder equation, here written as the function z of the amplitude matrix T, is on the right-hand side. Utilizing the representation of Eq. (11), the amplitude equation can be solved by a fixed-point iteration scheme. Algorithm I (see Table I) is commonly used in CC calculations [33], and this is the procedure we have employed.

B. Brueckner-Hartree-Fock approximation

In BHF theory [12,67], the total energy is approximated by

$$E_{\mathrm{BHF}} = \sum_{\mathbf{k}_i} \langle \mathbf{k}_i | h_0 | \mathbf{k}_i \rangle + \frac{1}{2} \sum_{\mathbf{k}_i \mathbf{k}_j} \langle \mathbf{k}_i \mathbf{k}_j | g | \mathbf{k}_i \mathbf{k}_j \rangle,$$

where the G matrix is defined as

$$\langle \mathbf{k}_p \mathbf{k}_q | g | \mathbf{k}_r \mathbf{k}_s \rangle = \langle \mathbf{k}_p \mathbf{k}_q | v | \mathbf{k}_r \mathbf{k}_s \rangle + \frac{1}{2} \sum_{\mathbf{k}_c \mathbf{k}_d} \frac{\langle \mathbf{k}_p \mathbf{k}_q | v | \mathbf{k}_c \mathbf{k}_d \rangle \langle \mathbf{k}_c \mathbf{k}_d | g | \mathbf{k}_r \mathbf{k}_s \rangle}{\varepsilon_{\mathbf{k}_p} + \varepsilon_{\mathbf{k}_q} - \varepsilon_{\mathbf{k}_c} - \varepsilon_{\mathbf{k}_d}} \tag{12}$$

and the single-particle energy is

$$\varepsilon_{\mathbf{k}_p} = \langle \mathbf{k}_p | h_0 | \mathbf{k}_p \rangle + \sum_{\mathbf{k}_i} \langle \mathbf{k}_p \mathbf{k}_i | g | \mathbf{k}_p \mathbf{k}_i \rangle. \tag{13}$$

In the so-called continuous option [68,69], which we use, the single-particle energy has the form given in Eq. (13) for both particle and hole states.

Diagrams of the BHF equations are given in Figs. 3 and 4. From the diagrammatic expressions one can see that the

TABLE I. Algorithm I: Fixed-point iteration scheme for solving the ladder equations, as explained in Ref. [33]. The amplitude matrix T and the function z are defined in the text.

1. Initialize E_{old} to a large number.
2. Initialize the amplitude matrix T_{old} to zero.
3. Loop until convergence.
   (a) Calculate $T_{\mathrm{new}} = z(T_{\mathrm{old}})$.
   (b) Calculate a new binding energy
   $E_{\mathrm{new}} = \Delta E_{\mathrm{CCD}}\,(T_{\mathrm{new}})$.
   If $|E_{\mathrm{new}} - E_{\mathrm{old}}|$ is smaller than a given tolerance, stop.
   Else, set $E_{\mathrm{old}} = E_{\mathrm{new}}$ and $T_{\mathrm{old}} = T_{\mathrm{new}}$
   and return to 3(a).

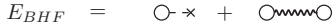

FIG. 3. The BHF energy equation in terms of diagrams. The waved line represents the G matrix, and a circle means summation over hole states.

PP-LAD and BHF equations are similar. In fact, one can show that the BHF equations become equal to the PP-LAD equations, provided that the G matrix in the single-particle energy expression (13) is replaced by the interaction matrix. We used this similarity to verify our implementation of the PP-LAD equations as well. In the PPHH-LAD approximation we have, in addition to particle-particle ladders, hole-hole ladder contributions, and the two types of ladder diagrams couple to each other.

III. FURTHER APPROXIMATIONS

Explicit expressions of the nuclear interaction are commonly given in relative momentum coordinates, whereas the CC equations are defined in laboratory coordinates. Either the interaction may be transformed to laboratory coordinates, or the many-body equations must be rewritten to relative coordinates. We chose to transform the ladder equations from laboratory to relative and center-of-mass (RCM) coordinates. Details of the transformation are shown in Appendix A 1.

In addition to transforming the equations from laboratory to RCM coordinates, we write the equations in a basis of coupled angular momenta. The basis we use is $|k(lS)\mathcal{J}m_{\mathcal{J}}M_T\rangle$, where k is the radial component of the relative momentum, l is the relative orbital angular momentum, S is the total two-particle spin, $\mathcal{J}$ is the angular momentum sum $l+S$, $m_{\mathcal{J}}$ is the z projection of $\mathcal{J}$, and M_T is the projection of the two-particle isospin. The same representation is commonly used in nuclear structure calculations, such as the BHF method [12], but owing to angular-average approximations the matrix elements are normally diagonal in $\mathcal{J}$ and $m_{\mathcal{J}}$.

As can be seen from Eq. (A4), the ladder equations in RCM coordinates depend on the particle-particle Pauli exclusion operator

$$Q^{(e)}_{pp}(\mathbf{k},\mathbf{K},k_F)=\theta(|\mathbf{k}+\mathbf{K}/2|-k_F)\theta(|-\mathbf{k}+\mathbf{K}/2|-k_F)$$

FIG. 4. Definition of the G matrix, expressed using diagrams. The wavy line represents the G-matrix interaction. All other parts are defined as in Fig. 1.

and the hole-hole Pauli exclusion operator

$$Q^{(e)}_{hh}(\mathbf{k},\mathbf{K},k_F)=\theta(k_F-|\mathbf{k}+\mathbf{K}/2|)\theta(k_F-|-\mathbf{k}+\mathbf{K}/2|),$$

where k_F is the Fermi momentum, $\mathbf{k}$ and $\mathbf{K}$ are relative and CM momenta, respectively, defined in Eq. (A3), and the superscript (e) emphasizes that these are the exact Pauli operators. A common approximation for nuclear-matter calculations is to replace the exact Pauli operators with an operator averaged over the angle between the relative and CM momentum vectors [12,54,67].

In this paper, we use a technique introduced by Suzuki *et al.* [15] to expand the exact Pauli operator in partial waves. Using the exact Pauli operator in a partial-wave expansion, we derive the CC ladder equations. We also derive the ladder equations using angular-average approximations of the Pauli operator. In both cases we use an angular-average approximation of the single-particle energies.

A. Exact Pauli operator

Expressed in the coupled partial-wave basis, the reference energy per particle is

$$E_{\mathrm{REF}}/A=\frac{3\hbar^2k_F^2}{10m}+\frac{3C}{4k_F^3}\sum_{\mathcal{J}Sl}\sum_{M_T}(2\mathcal{J}+1)\times\int_0^{2k_F}dK\,K^2\int_0^{\sqrt{k_F^2-K^2/4}}dk\,k^2\times\langle k(lS)\mathcal{J}M_T|v|k(lS)\mathcal{J}M_T\rangle x_{hh}(k,K,k_F),\quad(14)$$

where A is the number of particles, k_F is the Fermi momentum, k and K are the radial coordinates of the relative and CM momentum, respectively, and C is 1 for symmetric nuclear matter and 2 for pure neutron matter. The function x_{hh} is defined as

$$x_{hh}=\begin{cases}0, & \text{if } k>\sqrt{k_F^2-K^2/4},\\ -\frac{k^2-k_F^2+K^2/4}{kK}, & \text{if } k_F-K/2<k<\sqrt{k_F^2-K^2/4},\\ 1, & \text{otherwise,}\end{cases}\quad(15)$$

and similarly we define a function

$$x_{pp}=\begin{cases}0, & \text{if } k<\sqrt{k_F^2-K^2/4},\\ \frac{k^2-k_F^2+K^2/4}{kK}, & \text{if } \sqrt{k_F^2-K^2/4}<k<k_F+K/2,\\ 1, & \text{otherwise.}\end{cases}\quad(16)$$

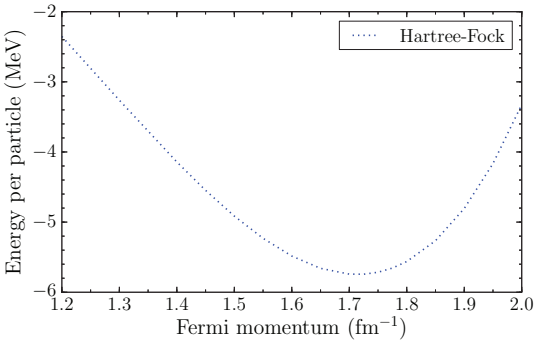

FIG. 5. (Color online) Total energy per nucleon of symmetric nuclear matter in the Hartree-Fock approximation, given as a function of Fermi momentum k_F. The calculation was done with a bare N^{3}LO two-body interaction, and the total angular momentum truncation was set to $\mathcal{J} \leqslant 24$.

In Sec. III, all interaction and t-amplitude matrix elements are assumed to be multiplied by the antisymmetrization factor $\mathcal{A}^{l'lSM_T}$ given in Eq. (A9). Because the Pauli exclusion operator is the only factor in the potential energy part of the reference energy that depends on the angle between $\mathbf{k}$ and $\mathbf{K}$, the expression for the reference energy is the same when using exact and angular-averaged Pauli operators. As mentioned above, the reference energy is also the Hartree-Fock energy when using the plane-wave basis for this particular system. In the limit of an untruncated basis, the reference energy expressed in a partial-wave basis, given in Eq. (14), equals the Hartree-Fock energy. Because we calculate the reference energy with a high cutoff in angular momentum, we refer to the reference energy (14) as the Hartree-Fock energy. However, one should notice that the partial-wave basis is not a Hartree-Fock basis for infinite nuclear matter. The reference energy is plotted in Fig. 5.

In the algorithm used to solve the PP-LAD and PPHH-LAD equations, it is necessary to store all t-amplitude matrix elements to be able to calculate the binding energy at each iteration step. When using a sufficient number of integration grid points and angular momentum partial waves to reach necessary accuracy, the size of the CC amplitude matrix would typically exceed standard memory capacities at most high-performance computing facilities. When the ladder equations are written in the coupled partial-wave basis we used, it is possible to calculate the t-amplitude matrix for only one angular direction of the CM momentum $\mathbf{K}$ and then obtain the other matrix elements by performing a rotation [15]. This is a major advantage, because the memory requirements for storing the t amplitude decreases significantly.

The size of the t-amplitude matrix can be further decreased by removing the dependency on the angular parts of the relative momenta, that is, $\hat{\mathbf{k}}$ and $\hat{\mathbf{k}}'$. As can be seen from Eq. (A4), the only dependency on these vectors in the ladder amplitude equations that cannot be separated out occurs in the single-particle energies. In RCM coordinates, the single-particle energies are functions of $|\pm\mathbf{k} + \mathbf{K}/2|$ or $|\pm\mathbf{k}' + \mathbf{K}/2|$, as shown in Eq. (A11). To remove the dependency of the t-amplitude matrix on $\hat{\mathbf{k}}$ and $\hat{\mathbf{k}}'$, we use an angular-average approximation of the arguments $|\pm\mathbf{k} + \mathbf{K}/2|$ in the single-particle energy [54,67,70]. Because nuclear matter is an isotropic medium, the single-particle energy must be a symmetric function, and the single-particle energy can be approximated as a finite polynomial with only even powers. Following Ramos [54,70], we replace the input momentum

$$k_p = |\pm\mathbf{k} + \mathbf{K}/2|,$$

with the angular-average approximation

$$\overline{k_p} = \sqrt{k^2 + K^2/4 \pm kK\sqrt{\langle\cos^2\theta_{\mathbf{kK}}\rangle}}, \tag{17}$$

where

$$\langle\cos^2\theta_{\mathbf{kK}}\rangle = \begin{cases} x^3_{hh}(k, K)/3, & \text{if } k_p \leqslant k_F, \\ x^3_{pp}(k, K)/3, & \text{if } k_p > k_F, \end{cases}$$

and $\theta_{\mathbf{kK}}$ is the angle between the relative and CM momentum vectors.

If we use the above-mentioned rotation of the t-amplitude matrix, given explicitly in Eq. (A18), and apply the angular-average approximation in Eq. (17), we can write the correlation energy per particle as

$$\begin{aligned}\Delta E_{\mathrm{CCD}}/A = \frac{3C}{32k_F^3} \sum_{\mathcal{J}m_{\mathcal{J}}} \sum_{\mathcal{J}''m_{\mathcal{J}''}} \sum_{\mathcal{J}'''m_{\mathcal{J}'''}} \sum_{m_{\mathcal{J}'}} \sum_{SM_T} \sum_{ll'l''l'''} \int_0^{2k_F} K^2 dK \int_{-1}^{1} d\cos\theta_K \int_0^{\sqrt{k_F^2 - K^2/4}} k^2 dk \int_{\sqrt{k_F^2 - K^2/4}}^{\infty} k'^2 dk' \\ \times d^{\mathcal{J}''}_{m_{\mathcal{J}''}m_{\mathcal{J}'}}(\theta_K) d^{\mathcal{J}'''}_{m_{\mathcal{J}'''}m_{\mathcal{J}'}}(\theta_K) \langle k(lS)\mathcal{J}M_T|v|k'(l'S)\mathcal{J}M_T\rangle \langle k'(l''S)\mathcal{J}''m_{\mathcal{J}'}M_T|t(K)|k(l'''S)\mathcal{J}'''m_{\mathcal{J}'}M_T\rangle \\ \times Q_{hh}(l'''\mathcal{J}'''m_{\mathcal{J}'''}, l\mathcal{J}m_{\mathcal{J}}; SM_T kK\theta_K) Q_{pp}(l'\mathcal{J}m_{\mathcal{J}}, l''\mathcal{J}''m_{\mathcal{J}''}; SM_T k'K\theta_K),\end{aligned} \tag{18}$$

where the Wigner D function has been defined through

$$D^J_{MM'}(\alpha, \beta, \gamma) = e^{-iM\alpha} d^J_{MM'}(\beta) e^{-iM'\gamma}, \tag{19}$$

and the function $d^J_{MM'}(\beta)$ is given in Ref. [71]. In Eq. (18), the t-amplitude is independent on the angles $\hat{\mathbf{k}}$ and $\hat{\mathbf{k}}'$, and we have used the definitions

$$Q_{hh}(l''\mathcal{J}''m_{\mathcal{J}''}, l'''\mathcal{J}m_{\mathcal{J}}; SM_TkK\theta_K\phi_K) = \mathcal{A}^{l''l'''SM_T}\frac{1}{2}\sum_{m_{l''}m_{l'''}}\sum_{M_S}\int d\hat{\mathbf{k}}Y^*_{l''m_{l''}}(\hat{\mathbf{k}})Y_{l'''m_{l'''}}(\hat{\mathbf{k}})\langle l'''m_{l'''}SM_S|\mathcal{J}m_{\mathcal{J}}\rangle\langle l''m_{l''}SM_S|\mathcal{J}''m_{\mathcal{J}''}\rangle \times\theta(k_F-|\mathbf{k}+\mathbf{K}/2|)\theta(k_F-|-\mathbf{k}+\mathbf{K}/2|) \tag{20}$$

and

$$\begin{aligned}Q_{pp}&(l''\mathcal{J}'m_{\mathcal{J}'}, l'''\mathcal{J}''m_{\mathcal{J}''}; SM_Tk'K\theta_K\phi_K)\\ &= \mathcal{A}^{l''l'''SM_T}\frac{1}{2}\sum_{m_{l''}m_{l'''}}\sum_{M'_S}\int d\hat{\mathbf{k}}'Y^*_{l''m_{l''}}(\hat{\mathbf{k}}')Y_{l'''m_{l'''}}(\hat{\mathbf{k}}')\\ &\quad\times\langle l''m_{l''}SM'_S|\mathcal{J}'m_{\mathcal{J}'}\rangle\langle l'''m_{l'''}SM'_S|\mathcal{J}''m_{\mathcal{J}''}\rangle\theta(|\mathbf{k}'+\mathbf{K}/2|-k_F)\theta(|-\mathbf{k}'+\mathbf{K}/2|-k_F)\end{aligned} \tag{21}$$

in a similar way as Suzuki *et al*. did in their BHF study [15]. In Eqs. (20) and (21), the brackets denote Clebsch-Gordan coefficients and the functions $Y_{lm_l}(\hat{\mathbf{k}})$ are spherical harmonics [71].

In Ref. [15], the authors have derived an expression for Q_{pp} which avoids the complicated integration limits over the space angle of $\mathbf{k}$ [15], namely,

$$\begin{aligned}Q_{pp}&(l,\mathcal{J},m_{\mathcal{J}},l'\mathcal{J}'m_{\mathcal{J}'};SM_TkK\theta_K\phi_K)\\ &= \mathcal{A}^{ll'SM_T}\frac{1}{2}\left\{x_{pp}\delta_{ll'}\delta_{\mathcal{J}\mathcal{J}'}\delta_{m_{\mathcal{J}}m_{\mathcal{J}'}} + \sum_{L>0;L=\text{even}}(-1)^{S+m_{\mathcal{J}}}\frac{(4\pi)^{1/2}\hat{l}\hat{l}'\hat{\mathcal{J}}\hat{\mathcal{J}}'}{\hat{L}}\langle l0l'0|L0\rangle\langle\mathcal{J}-m_{\mathcal{J}}\mathcal{J}'m_{\mathcal{J}'}|LM_L\rangle\right.\\ &\quad\left.\times Y_{LM_L}(\theta_K,\phi_K)W(l\mathcal{J}l'\mathcal{J}';SL)[P_{L+1}(x_{pp})-P_{L-1}(x_{pp})]\right\},\end{aligned} \tag{22}$$

where $\hat{x}\equiv\sqrt{2x+1}$, $P_L(x)$ is the Legendre polynomial, $W(l\mathcal{J}l'\mathcal{J}';SL)$ denotes the Racah coefficient [71], and x_{pp} is as defined in Eq. (16). We have used Eq. (22) to evaluate Q_{pp} and a similar expression for evaluating Q_{hh}. The expression for Q_{hh} was obtained by replacing x_{pp} with the equivalent for hole-hole states, i.e., x_{hh} given in Eq. (15). Observe that the simplified but exact Pauli operator expression (22) and the corresponding expression for the hole-hole Pauli operator could not have been used if the t amplitude was not independent on the angular vectors $\hat{\mathbf{k}}$ and $\hat{\mathbf{k}}'$. The reason for this restriction is that the Pauli operator expressions, when expanded in partial waves, as defined in Eqs. (20) and (21), are integral operators and not just real functions. The effect of the integral operators Q_{hh} and Q_{pp} can be seen clearly from the correlation energy expression in Eq. (A17). The angular-average approximation of the single-particle energies therefore simplifies the correlation energy expression significantly.

Because the exact Pauli operator is not diagonal in $\mathcal{J}$ and $m_{\mathcal{J}}$, both the G matrix [15] and the t-amplitude matrix are not diagonal in the total angular momentum $\mathcal{J}$ and its projection $m_{\mathcal{J}}$. The fact that the amplitude matrix is not diagonal in total angular momentum makes the ladder equations more complicated. Writing the PPHH-LAD equations in the basis $|k(lS)\mathcal{J}m_{\mathcal{J}}M_T\rangle$, we get

$$\begin{aligned}\Delta\tilde{\varepsilon}&(k,k',K)\langle k'(l'S)\mathcal{J}'m_{\mathcal{J}'}M_T|t(K)|k(lS)\mathcal{J}m_{\mathcal{J}}M_T\rangle\\ &= \langle k'(l'S)\mathcal{J}'m_{\mathcal{J}'}M_T|v|k(lS)\mathcal{J}m_{\mathcal{J}}M_T\rangle\delta_{\mathcal{J}\mathcal{J}'}\delta_{m_{\mathcal{J}}m_{\mathcal{J}'}} + \frac{1}{2}\sum_{\mathcal{J}''m_{\mathcal{J}''}}\sum_{l''l'''}\int_0^{k_F}h^2dh\langle k'(l'S)\mathcal{J}'m_{\mathcal{J}'}M_T|t(K)|h(l''S)\mathcal{J}''m_{\mathcal{J}''}M_T\rangle\\ &\quad\times\langle h(l'''S)\mathcal{J}m_{\mathcal{J}}M_T|v|k(lS)\mathcal{J}m_{\mathcal{J}}M_T\rangle Q_{hh}(l''\mathcal{J}''m_{\mathcal{J}''}, l'''\mathcal{J}m_{\mathcal{J}};SM_ThK\theta_K\phi_K)\\ &\quad+\frac{1}{2}\sum_{\mathcal{J}''m_{\mathcal{J}''}}\sum_{l'l'''}\int_0^{\infty}p^2dp\langle k'(l'S)\mathcal{J}'m_{\mathcal{J}'}M_T|v|p(l''S)\mathcal{J}'m_{\mathcal{J}'}M_T\rangle\langle p(l'''S)\mathcal{J}''m_{\mathcal{J}''}M_T|t(K)|k(lS)\mathcal{J}m_{\mathcal{J}}M_T\rangle\\ &\quad\times Q_{pp}(l''\mathcal{J}'m_{\mathcal{J}'}, l'''\mathcal{J}''m_{\mathcal{J}''};SM_TpK\theta_K\phi_K),\end{aligned} \tag{23}$$

where $|(lS)\mathcal{J}m_{\mathcal{J}}\rangle$ denotes a vector where l and S are coupled to $\mathcal{J}$. In Eq. (23) we have used the angular-averaged energy denominator $\Delta\tilde{\varepsilon}(k,k',K)$, which is defined in Eq. (A16). When using the rotation of the ladder amplitude matrix, given in Eq. (A18), the amplitude matrix needs to be evaluated only at a single angular coordinate of the CM momentum. The amplitude equation (23) is therefore given as a function of only the radial part of the CM momentum.

In Eq. (22), the restriction that L must be even ensures that parity is conserved [15]. This follows from the properties of the first Clebsch-Gordan coefficient in Eq. (22), which vanishes when $(-1)^l\neq(-1)^{l'}$, provided that L is even. Because the

operators Q_{hh} and Q_{pp} conserve parity, one can see from Eq. (23) that the t-amplitude of the ladder equation also conserves parity. On the contrary, the exact Pauli operators (both particle-particle and hole-hole ones) do not conserve the total angular momentum $\mathcal{J}$. Consequently, the t amplitude also becomes nondiagonal in the total angular momentum. The exact Pauli operators become diagonal in the projection $m_{\mathcal{J}}$ in the special case when the angular part of the CM momentum is zero. The t-amplitude matrix elements are therefore also diagonal in $m_{\mathcal{J}}$ when $\mathbf{K}$ is parallel with the z axis.

We later refer to the approximation with exact Pauli operators (both particle-particle and hole-hole ones) and angular-averaged single-particle energies as "exact." The angular-average approximation of the single-particle energies, given in Eq. (17), is used in all calculations presented in this work, including both the coupled ladder approximations and the BHF method.

B. Angular-averaged Pauli operators

The ladder equations can be simplified substantially by doing an angular-average approximation of the Pauli exclusion operators. The hole-hole and particle-particle exclusion operators become [15], respectively,

$$\begin{aligned} &Q_{hh}(l\mathcal{J}m_{\mathcal{J}}, l'\mathcal{J}'m_{\mathcal{J}'}; SM_T hK\theta_K\phi_K) \\ &\quad\rightarrow \overline{Q}_{hh} \\ &\quad\equiv \frac{1}{4\pi}\int d\hat{\mathbf{K}} Q_{hh}(l\mathcal{J}m_{\mathcal{J}}, l'\mathcal{J}'m_{\mathcal{J}'}; SM_T hK\theta_K\phi_K) \\ &\quad= \mathcal{A}^{llSM_T}\frac{1}{2}x_{hh}\delta_{ll'}\delta_{\mathcal{J}\mathcal{J}'}\delta_{m_{\mathcal{J}}m_{\mathcal{J}'}}, \end{aligned} \tag{24}$$

and

$$\begin{aligned} &Q_{pp}(l\mathcal{J}m_{\mathcal{J}}, l'\mathcal{J}'m_{\mathcal{J}'}; SM_T pK\theta_K\phi_K) \\ &\quad\rightarrow \overline{Q}_{pp} \\ &\quad\equiv \frac{1}{4\pi}\int d\hat{\mathbf{K}} Q_{pp}(l\mathcal{J}m_{\mathcal{J}}, l'\mathcal{J}'m_{\mathcal{J}'}; SM_T pK\theta_K\phi_K) \\ &\quad= \mathcal{A}^{llSM_T}\frac{1}{2}x_{pp}\delta_{ll'}\delta_{\mathcal{J}\mathcal{J}'}\delta_{m_{\mathcal{J}}m_{\mathcal{J}'}}, \end{aligned} \tag{25}$$

where x_{hh} and x_{pp} are as defined in Eqs. (15) and (16). We note that the angular-averaged Pauli exclusion operators are diagonal in the total angular momentum $\mathcal{J}$, in contrast to the exact operators.

When using the angular-average approximation, the PPHH-LAD equations simplify to

$$\begin{aligned} &\Delta\tilde{\varepsilon}(k,k',K)\langle k'(l'S)\mathcal{J}M_T|t(K)|k(lS)\mathcal{J}M_T\rangle \\ &\quad= \langle k'(l'S)\mathcal{J}M_T|v|k(lS)\mathcal{J}M_T\rangle \\ &\qquad+\frac{1}{2}\sum_{l''}\int_0^{k_F} h^2dh\langle k'(l'S)\mathcal{J}M_T|t(K)|h(l''S)\mathcal{J}M_T\rangle \\ &\qquad\times\langle h(l''S)\mathcal{J}M_T|v|k(lS)\mathcal{J}M_T\rangle\overline{Q}_{hh}(h,K) \\ &\qquad+\frac{1}{2}\sum_{l''}\int_0^{\infty} p^2dp\langle k'(l'S)\mathcal{J}M_T|v|p(l''S)\mathcal{J}M_T\rangle \\ &\qquad\times\langle p(l''S)\mathcal{J}M_T|t(K)|k(lS)\mathcal{J}M_T\rangle\overline{Q}_{pp}(p,K), \end{aligned} \tag{26}$$

where $\Delta\tilde{\varepsilon}(k,k',K)$ is the energy denominator with angular-averaged arguments. From the properties of the angular-averaged Pauli operators, it follows that the t amplitude is diagonal in $\mathcal{J}$, and independent on $m_{\mathcal{J}}$ and the CM momentum angles θ_K and ϕ_K. Because of these symmetries, the CC amplitude matrix is orders of magnitude smaller in the angular-averaged approximation than when using exact Pauli exclusion operators.

The CCD correlation energy per particle becomes in the angular-averaged approximation

$$\begin{aligned} \Delta E^{\text{ave}}_{\text{CCD}}/A = &\frac{3C}{16k_F^3}\sum_{\mathcal{J}}\sum_{SM_T}\sum_{ll'}(2\mathcal{J}+1) \\ &\times\int_0^{\sqrt{k_F^2-K^2/4}} k^2dk\int_{\sqrt{k_F^2-K^2/4}}^{\infty} k'^2dk' \\ &\times\int_0^{2k_F} K^2dK\langle k(lS)\mathcal{J}M_T|v|k'(l'S)\mathcal{J}M_T\rangle \\ &\times\langle k'(l'S)\mathcal{J}M_T|t(K)|k(lS)\mathcal{J}M_T\rangle \\ &\times\overline{Q}_{hh}(k,K)\overline{Q}_{pp}(k',K). \end{aligned} \tag{27}$$

The approximation using both angular-averaged Pauli operators and angular-averaged arguments in the single-particle energies are in the following referred to as "average."

IV. RESULTS AND DISCUSSION

In the following we present results of numerical calculations using the above-mentioned ladder approximations. These approximations are compared with conventional BHF theory. We investigate also the role of angular-averaged Pauli exclusion operators and compare this with the exact treatment discussed above. In addition, we compare results obtained using the optimized NNLO_{opt} two-body interaction [63] with calculations done with the N^3LO interaction [64]. The different interaction models and many-body methods are applied to both symmetric nuclear-matter and neutron-matter systems.

In all our calculations, we have taken into account charge symmetry breaking and charge independence breaking of the chiral interactions. The BHF calculations were done using continuous single-particle energies [72], which here means that single-particle energies for both particles and holes were calculated using Eq. (13). The singularities in the G-matrix equation owing to the continuous single-particle energies were avoided by calculating the principal value of the integral in the G-matrix equation. The G-matrix equation (12) was solved in a coupled angular momentum basis $|k(lS)\mathcal{J}m_{\mathcal{J}}M_T\rangle$ using the matrix inversion method of Haftel and Tabakin [12]. Unless stated explicitly otherwise, the BHF calculations have been calculated with a truncation of the total angular momentum at $\mathcal{J}\leqslant 24$ in the Born approximation and $\mathcal{J}\leqslant 9$ for the full G matrix. The BHF calculations were done with angular-averaged Pauli operators, as described in Ref. [12].

The coupled ladder equations were solved with both exact and angular-averaged Pauli exclusion operators. We refer to these two approximations as "exact" and "average," respectively. All calculations were done with an angular-average

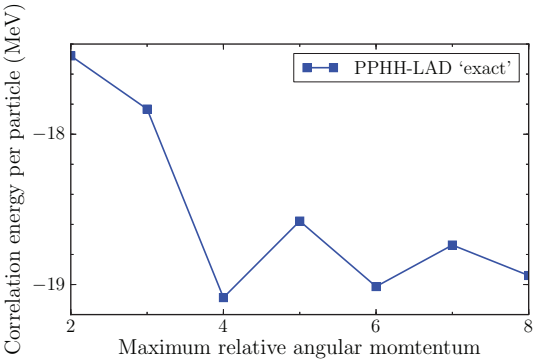

FIG. 6. (Color online) Convergence of the correlation energy of symmetric nuclear matter, given as a function of maximum total angular momentum $\mathcal{J}_{\max}$. The correlation energy was calculated for the Fermi momentum $k_F = 1.8$ fm^{-1}, using the PPHH-LAD approximation and exact Pauli exclusion operators.

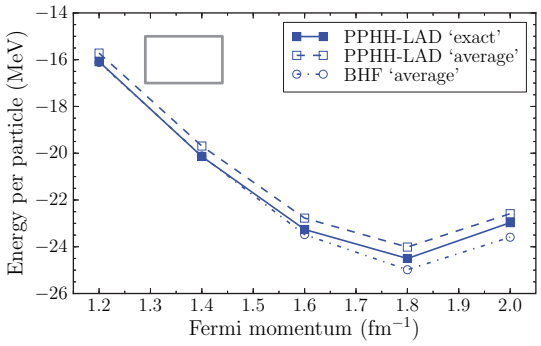

FIG. 7. (Color online) Total energy per particle as a function of the Fermi momentum, calculated for symmetric nuclear matter. The two approximations of the PPHH-LAD equations, average and exact, are compared with a BHF calculation with angular-averaged Pauli exclusion operator. These calculations were done with the N^{3}LO [64] two-body interaction. The box denotes the uncertainty region for the experimental saturation point of symmetric nuclear matter, as obtained by extrapolating from observables of finite nuclei.

approximation of the single-particle energies, as was explained in Sec. III A. The Hartree-Fock energy was calculated with a cutoff in total angular momentum at $\mathcal{J} \leqslant 24$. The correlation energy was calculated with a truncation at $\mathcal{J} \leqslant 16$ in the average approximation and $\mathcal{J} \leqslant 8$ in the exact approximation. Figure 6 shows the convergence of the correlation energy as a function of the total angular momentum cutoff $\mathcal{J}_{\max}$. Because of the high density, the angular momentum barrier cannot keep particles far apart from each other, and therefore the convergence as a function of total angular momentum is slow in infinite nuclear matter. At high angular momenta, the interaction is dominated by the one-pion exchange part, and the convergence behavior as a function of total angular momentum is therefore similar for different interaction models. Owing to restrictions in computer memory, we were not able to calculate with $\mathcal{J}_{\max}$ higher than 8 in the exact approximation.

Let us first consider symmetric nuclear matter using the N^{3}LO interaction. In Fig. 7, we compare the energy per nucleon as a function of the Fermi momentum for different approximations. The Fermi momentum at saturation is equal for all the three methods, whereas there are differences in the binding energies. The general form of the equation of state is very similar for the coupled ladder and BHF methods. As can be seen from the figure, the PPHH-LAD approximation gives less binding than the BHF approximation when the PPHH-LAD calculation is done with both angular-averaged and exact Pauli operators. The binding energy at saturation obtained with the BHF method is approximately 0.5 MeV lower than the corresponding result of Li *et al.* [6]. There are several factors that may have contributed to the difference between our BHF results and those of Li *et al.* [6]. For example, in Ref. [6] they used a complex G matrix, whereas we have used a real G matrix and treated the singularities by using a principal value integral [12]. It is also possible that we have used different angular-average approximations in the single-particle energies. As seen from Fig. 7, an exact treatment of the Pauli operators gives more binding than when using an angular-average approximation. This is in agreement with the results of Suzuki *et al.* [15] and Schiller *et al.* [14], where an exact treatment of the Pauli operator gave approximately 0.2–0.5 MeV more binding energy in the BHF approximation.

Carbone *et al.* [8] have compared correlation energies obtained with the the SCGF method at finite temperature with BHF calculations, using the same N^{3}LO two-body interaction as we have used. Similarly as in Fig. 7, they got slightly higher energies with the SCGF method, which contains both particle-particle and hole-hole ladders, compared to the BHF results. In previous studies where the SCGF method has been compared with the BHF approximation [16,55,56] using other two-body interactions, the saturation energies obtained using the SCGF method have been located several MeVs higher than the corresponding BHF result, and the saturation densities have been shifted towards lower values. As will be shown systematically in a future publication [73], we find a similar difference between the PPHH-LAD and BHF methods when using the hard-core Argonne v_{18} interaction [74]. In fact, when using the Argonne v_{18} potential, the saturation energy of the PPHH-LAD approximation is found to be only about 1 MeV below the SCGF saturation energy shown in Fig. 3 of Ref. [16], and the saturation density is almost the same for both ladder approximations. It is interesting to note that we observed a larger difference between our CC and BHF results in systems with a hard interaction compared to systems with a soft interaction. If we relate these findings with a hard-core interaction to those obtained with, for example, the Bochum CC truncation scheme [44] mentioned in the Introduction, it may be possible that the Bochum scheme will give a faster convergence than the SUBn truncation scheme when using hard-core interaction models.

Finally, we ought to mention that the way the CC equations are solved here, and in most other CC applications as well, no self-consistent solution of the pairing gap equations is

TABLE II. Total energy per nucleon at selected Fermi momenta k_F, as obtained with different approximations. For easier comparison, all these energies were calculated with the same cutoff in total angular momentum, i.e., $\mathcal{J}_{\max} = 24$ for the Hartree-Fock/Born approximation and $\mathcal{J}_{\max} = 8$ for the correlation contribution. All results were obtained with the N^{3}LO interaction [64]. Energies in units of MeV.

k_F (fm^{-1})	1.2	1.4	1.6	1.8	2.0
PPHH exact	−16.08	−20.14	−23.26	−24.50	−22.97
PPHH average	−15.74	−19.74	−22.84	−24.09	−22.56
PP exact	−15.76	−19.83	−22.98	−24.27	−22.82
PP average	−15.45	−19.45	−22.57	−23.86	−22.40
PT2 average	−15.11	−19.81	−23.35	−24.80	−23.25
BHF average	−16.18	−20.25	−23.74	−25.47	−24.42

performed. In practical terms this means that we never face instabilities in the denominators of the CC expansions owing to poles arising in the two-hole sector. In CC theory, in contrast to various SCGF approaches, there is never an explicit energy dependence in the denominators of the different amplitudes. The energy differences in the two-particle-two-hole energies that enter the computation of various denominators are never zero, by construction. There are no terms in our present formalism which thus could account for pairing instabilities in the denominators, as discussed in, for example, Refs. [75,76]. The effects of pairing instabilities and the self-consistent solution of the gap equation together with the full CCD equations (including the particle-hole terms as well), await therefore further investigations.

In Table II, we list the total energies for symmetric nuclear matter calculated with the N^{3}LO two-body interaction. For easier comparison, all results are computed with the same cutoffs in total angular momentum. We find that the difference between the PPHH-LAD energies with angular-averaged and exact Pauli operators is approximately 0.4 MeV at the saturation Fermi momentum. This makes a difference of roughly 1.7%. At the same Fermi momentum, the PPHH-LAD method with exact Pauli operators gives approximately 1 MeV more binding than the BHF method with angular-averaged Pauli operators. The 1-MeV difference corresponds to 3.8% of the total energy.

In Fig. 8 we compare the coupled PPHH-LAD with the particle-particle ladder approximation, PP-LAD. From Fig. 8 one can see that the inclusion of hole-hole ladders gives slightly more binding compared to the pure particle-particle ladder approximation. From Table II we find that the difference is approximately 0.2 MeV at saturation Fermi momentum or about 1% of the binding energy. At the saturation density, the contribution coming from including the hole-hole ladders is smaller than the error of an angular-average approximation of the Pauli exclusion operators.

As mentioned earlier, the only difference between the BHF and the PP-LAD approximations is the single-particle energy, which in the BHF method is calculated with a G matrix and in the ladder approximation with a bare interaction. Single-particle potentials with a G matrix and with a bare interaction are plotted in Fig. 9, as obtained using the N^{3}LO interaction.

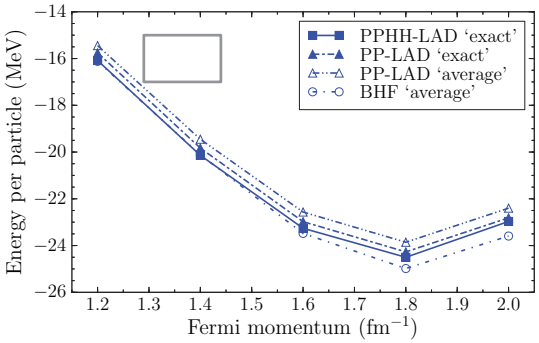

FIG. 8. (Color online) The exact PPHH-LAD and PP-LAD calculations of energy per nucleon as a function of Fermi momentum. The equation of state of a BHF calculation is also given. The box denotes the uncertainty region for the experimental saturation point of symmetric nuclear matter. All results were obtained with the N^{3}LO interaction [64].

Next we compare the two different chiral interactions N^{3}LO and NNLO$_{\rm opt}$ when applied to infinite-matter systems. In Fig. 10 we have plotted the equations of state for symmetric nuclear matter and in Fig. 11 for pure neutron matter, respectively, as obtained with the two different nuclear interaction models. When using the NNLO$_{\rm opt}$ interaction for symmetric nuclear matter, we find that the HF energy is much closer to the PPHH-LAD approximation than is the case with the N^{3}LO interaction. Thus, the optimized next-to-next-to-lowest-order interaction provides a better starting point for the perturbation series than the N^{3}LO interaction. As can be seen from Fig. 10, in the PPHH-LAD approximation the two different interactions give almost the same equation of state for Fermi

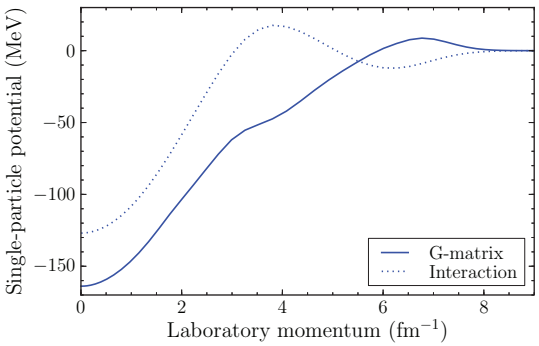

FIG. 9. (Color online) Single-particle potential as a function of laboratory frame momentum, calculated at Fermi momentum 1.8 fm^{-1} with a G matrix and with a bare interaction. In both cases, we used the N^{3}LO two-body interaction and the total angular momentum cutoff $\mathcal{J}_{\max} = 9$. The only difference between the BHF and PP-LAD equations is the single-particle energy: In BHF theory the single-particle potential is calculated using a self-consistent G matrix, whereas in the PP-LAD approximation the single-particle energy is obtained by replacing the G matrix with a bare interaction.

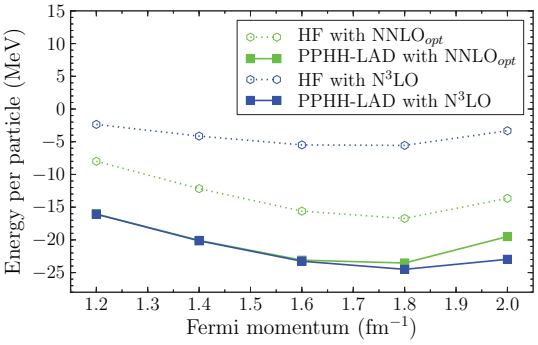

FIG. 10. (Color online) Energy per particle for symmetric nuclear matter, as calculated in the HF and PPHH-LAD approximations using the N^{3}LO and NNLO$_{opt}$ two-body interactions. In the PPHH-LAD approximation, the angular momentum cutoff was set to $\mathcal{J} \leqslant 8$ and the calculations were done with exact Pauli exclusion operators.

momenta less than 1.6 fm^{-1}. At higher Fermi momenta, the NNLO$_{opt}$ interaction gives less binding. Both the N^{3}LO and the NNLO$_{opt}$ interactions overbind considerably and saturate at too high density in symmetric nuclear matter. The similarity between the binding energies obtained with the two different two-body interactions is in contrast to the results in finite nuclei [63], where the NNLO$_{opt}$ interaction gave significantly better agreement with experiments than the N^{3}LO interaction. However, even if this may indicate that three-body forces could play a smaller role with the optimized interaction, there is no clear indication that such correlations are negligible. The N^{3}LO and NNLO$_{opt}$ interactions have also been compared in nuclear-matter calculations using the SCGF method at finite temperature [8]. The SCGF method was found to give slightly more binding when using the NNLO$_{opt}$ interaction compared to calculations with the N^{3}LO two-body interaction. The results obtained by Carbone *et al.* [8], using the SCGF

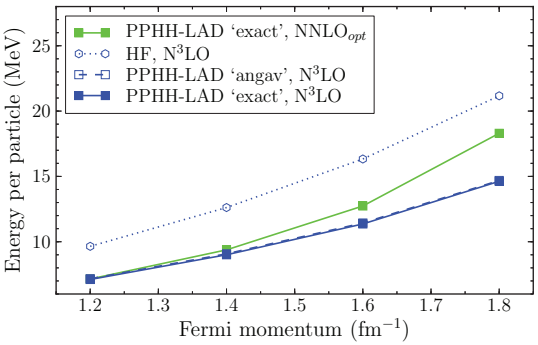

FIG. 11. (Color online) Energy per particle for pure neutron matter given as a function of Fermi momentum k_F. The figure shows results of calculations in Hartree-Fock (HF) and coupled PPHH-LAD, using the N^{3}LO and NNLO$_{opt}$ two-body interactions. The neutron-matter results obtained with exact Pauli operators have been published in Ref. [63].

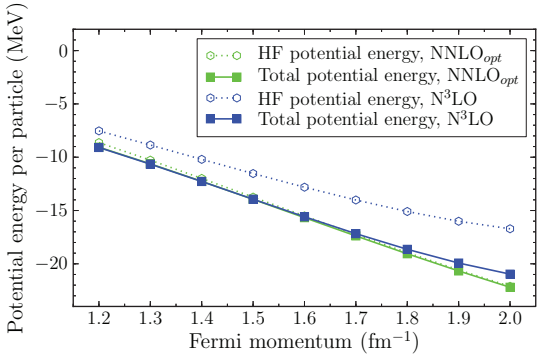

FIG. 12. (Color online) Potential energy per particle for the $^1S_0$ partial wave as function of the Fermi momentum k_F for pure neutron matter. We plot the Hartree-Fock potential energy and the total potential energy obtained by adding the correlation energies obtained from PPHH-LAD approximation with angular-averaged Pauli exclusion operators. Both potential models have been employed.

method, are rather close to those obtained with our present CCD calculations.

Equations of state for neutron matter are given in Fig. 11. As can be seen from the figure, the differences between the calculations with exact and angular-averaged Pauli operators are much smaller for neutron matter than for symmetric nuclear matter. According to these results, the angular-average approximation of the Pauli operators is a fairly good approximation in neutron-matter systems. In Ref. [63] we found that the equation of state for neutron matter with the optimized NNLO interaction was within the error estimates obtained with an N^{3}LO interaction with three-body forces [24], whereas a calculation with a two-body N^{3}LO interaction gave an equation of state that was more attractive around the empirical saturation density. Below we show that the stronger repulsion seen when using the optimized NNLO$_{opt}$ interaction stems from a poorer reproduction of the $^3P_0$ and $^3P_1$ partial-wave phase shifts of the Nijmegen analysis.

The results for symmetric nuclear matter with the two potential models result in energies that are very similar. This effect is largely attributable to the excellent reproduction of various partial waves for the proton-neutron channel, in particular the $^3S_1$ partial wave [77]. However, for pure neutron matter we see a clear deviation starting at Fermi momenta $k_F = 1.4$ fm^{-1}. To better understand this behavior, we have singled out two partial waves, namely the $^1S_0$ and the $^3P_0$ partial waves. The results for the potential energies per particle are shown in Figs. 12 and 13 for the $^1S_0$ and the $^3P_0$ partial waves, respectively. We show both the Hartree-Fock potential energy and the total potential energy by adding the results from the PPHH-LAD correlations. At the NNLO level of optimization, the P waves show larger deviations from the phase shifts deduced from the experimental cross sections [77], yielding a poorer agreement compared with the N^{3}LO interaction at laboratory energies beyond 100 MeV in energy. This applies, in particular, to the $^3P_0$ and the $^3P_1$ partial waves, resulting in a $^3P_0$ wave which is less attractive for the NNLO optimized

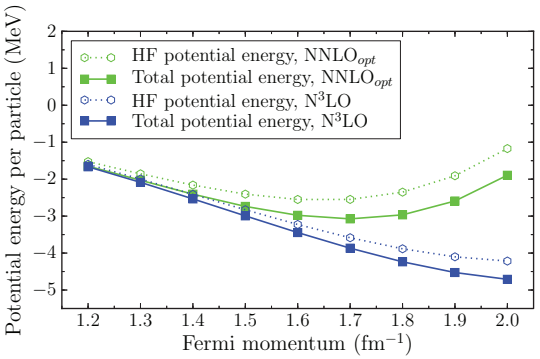

FIG. 13. (Color online) Potential energy per particle for the $^3P_0$ partial wave as function of the Fermi momentum k_F for pure neutron matter. We plot the Hartree-Fock potential energy and the total potential energy obtained by adding the correlation energies obtained from PPHH-LAD approximation with angular-averaged Pauli exclusion operators. Both potential models have been employed.

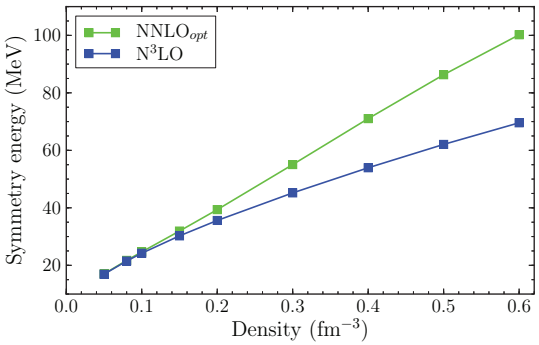

FIG. 14. (Color online) Symmetry energy as function of density, calculated in the PPHH-LAD approximation with exact Pauli exclusion operators. The empirical saturation density of symmetric nuclear matter is approximately 0.17 fm^{-3} [78].

interaction model. The contributions from the $^3P_1$ partial wave to the equation of state plays a smaller role compared with the $^3P_0$ partial wave. The differences for the $^3P_0$ partial wave is seen rather clearly in Fig. 13. The N^{3}LO interaction results in more binding than the NNLO$_{\rm opt}$ interaction model for this particular partial wave. This applies both to the Hartree-Fock potential energy and to the final potential energy that includes correlations. The discrepancy that arises from this partial wave is the main reason behind the more repulsive equation of state obtained with the NNLO$_{\rm opt}$ interaction. It will thus be interesting to see whether an optimization with respect to the experimental cross section at both the NNLO and the N^{3}LO levels will bring the results for pure neutron matter closer to the results obtained with the N^{3}LO interaction of Ref. [64]. These results will be presented in Ref. [77]. It is interesting to note also that the Hartree-Fock potential energies for the $^1S_0$ channel are rather similar to the fully correlated potential energy with the NNLO$_{\rm opt}$ interaction. This is also in line with our analysis from nuclear structure of Ref. [63], indicating that this interaction is rather soft at the two-body level. Both interaction models yield negligible differences for the full potential energy for the $^1S_0$ partial wave. In summary, the poorer reproduction of the phase shifts for two selected P waves leads to a more repulsive equation of state for pure neutron matter with the newly optimized NNLO$_{\rm opt}$ interaction. Whether three-body forces or more complicated correlations beyond the CCD approximation employed here will improve the situation remains, however, to be explored.

Finally, we present our results for the symmetry energy in Fig. 14. The symmetry energy S is defined as the difference between the binding energies of pure neutron matter and symmetric nuclear matter, that is

$$S = (E_{\rm pnm} - E_{\rm snm})/A, \tag{28}$$

where $E_{\rm pnm}/A$ and $E_{\rm snm}/A$ are the binding energies per particle for pure neutron matter and symmetric nuclear matter, respectively. The behavior of the symmetry energy at high densities is important for the understanding of several physical properties and processes of neutron stars (see Refs. [79–81] and references therein). In Fig. 14, the symmetry energy is plotted as a function of nucleon density, as obtained from a PPHH-LAD calculation with exact Pauli exclusion operators. The symmetry energies are calculated with both the N^{3}LO and the NNLO$_{\rm opt}$ two-body interactions. The symmetry energy obtained with the N^{3}LO interaction is slightly larger than what was reported in Refs. [82,83], where the calculations were done with BHF theory using the CD-Bonn interaction. At densities lower than 0.1 fm^{-1}, the two interaction models give almost the same symmetry energy. However, above the saturation density, the difference between the two models increases as a function of density. As seen from Fig. 14, the NNLO$_{\rm opt}$ interaction gives significantly larger symmetry energies than the N^{3}LO interaction at high densities. Such a large deviation between the two different two-body interactions is possible because the nuclear interactions are fitted to phase shifts for laboratory energies only up to 290 MeV [63,64].

V. CONCLUSIONS

We have studied infinite nuclear and neutron matter using a CC ladder approximation, where the equations were derived from the CCD approximation. In the coupled ladder approximation, particle-hole and nonlinear diagrams were neglected from the CCD amplitude equations. Our approach can be seen as a first step in implementing CC theory for infinite nuclear matter. The coupled ladder equations consist of particle-particle and hole-hole ladder diagrams which are coupled together. As we have shown, this method is closely related to the commonly used BHF approximation.

We have derived coupled ladder equations both with exact and angular-averaged Pauli exclusion operators, following the approach introduced by Suzuki *et al.* for the BHF approximation [15]. In all calculations we have used angular-averaged input momenta for the single-particle energies. Our method was applied numerically to both symmetric nuclear-matter and pure neutron-matter systems. The ladder approximations for symmetric nuclear matter were found to

give less binding than the BHF approximation. In symmetric nuclear matter, the contribution from the hole-hole ladder diagrams was found to be smaller than the error owing to angular-average approximations for the Pauli exclusion operators. Generally, symmetric nuclear-matter calculations with exact Pauli exclusion operators gave more binding than calculations with angular-averaged Pauli operators. This behavior is in agreement with observations made with the BHF method [14,15]. The binding energy per particle of pure neutron matter was found to be less sensitive to the Pauli exclusion operator approximation than what was the case for symmetric nuclear matter.

The ladder approximations were applied to infinite neutron and nuclear matter using two different chiral two-body interactions. An optimized NNLO interaction [63] was compared with the N^{3}LO interaction of Entem and Machleidt [64]. In symmetric nuclear matter, we found that the two interaction models gave similar binding energies. As was shown in Ref. [63], the optimized NNLO interaction gives more repulsion in neutron matter compared to the N^{3}LO two-body interaction. In the present work, we showed that the increased repulsion obtained with the NNLO interaction is attributable to differences in the $^3P_0$ and $^3P_1$ partial waves. We also calculated symmetry energies with the N^{3}LO and optimized NNLO two-body interactions.

ACKNOWLEDGMENTS

We thank Scott Bogner, Boris Carlsson, Gustav Jansen, Øyvind Jensen, Simen Kvaal, and Thomas Papenbrock for several discussions. This work was supported by the Research Council of Norway under Contract No. ISP-Fysikk/216699; by the Office of Nuclear Physics, US Department of Energy (Oak Ridge National Laboratory), under Grants No. DE-FG02-96ER40963 (University of Tennessee) and No. DE-SC0008499 (NUCLEI SciDAC collaboration). This research used computational resources of the Notur project in Norway.

APPENDIX: TECHNICAL DETAILS

1. Relative momentum basis

Infinite nuclear matter is defined in the thermodynamic limit, that is, the limit where the volume Ω and the number of particles A approach infinity, while the density of particles $\rho \equiv A/\Omega$ is kept constant. At the limit when Ω approaches infinity, the sums over momenta can be replaced by integrals:

$$\sum_{\mathbf{k}} \to \frac{\Omega}{(2\pi)^3}\int d\mathbf{k}. \tag{A1}$$

In the following we replace all sums over momenta with integrals according to Eq. (A1).

Taking the limit $\Omega \to \infty$, the ladder amplitude equations (8) may be written in laboratory momentum coordinates as

$$\begin{aligned}0 &= \langle \mathbf{k}_a\mathbf{k}_b|v|\mathbf{k}_i\mathbf{k}_j\rangle + (\varepsilon(\mathbf{k}_a)+\varepsilon(\mathbf{k}_b)\\ &\quad -\varepsilon(\mathbf{k}_i)-\varepsilon(\mathbf{k}_j))\langle \mathbf{k}_a\mathbf{k}_b|t|\mathbf{k}_i\mathbf{k}_j\rangle\\ &\quad +\frac{1}{2}\left(\frac{\Omega}{(2\pi)^3}\right)^2\int d\mathbf{k}_k\int d\mathbf{k}_l\,\langle \mathbf{k}_a\mathbf{k}_b|t|\mathbf{k}_k\mathbf{k}_l\rangle\,\langle \mathbf{k}_k\mathbf{k}_l|v|\mathbf{k}_i\mathbf{k}_j\rangle\\ &\quad \times\theta(k_F-|\mathbf{k}_k|)\theta(k_F-|\mathbf{k}_l|)\\ &\quad +\frac{1}{2}\left(\frac{\Omega}{(2\pi)^3}\right)^2\int d\mathbf{k}_c\int \mathbf{k}_d\,\langle \mathbf{k}_a\mathbf{k}_b|v|\mathbf{k}_c\mathbf{k}_d\rangle\,\langle \mathbf{k}_c\mathbf{k}_d|t|\mathbf{k}_i\mathbf{k}_j\rangle\\ &\quad \times\theta(|\mathbf{k}_c|-k_F)\theta(|\mathbf{k}_d|-k_F),\end{aligned} \tag{A2}$$

where $\theta(x)$ is the Heaviside step function and we have used the definition $\varepsilon(\mathbf{k}) \equiv \langle \mathbf{k}|f|\mathbf{k}\rangle$. Later we refer to $\varepsilon(\mathbf{k})$ as the single-particle energy.

We define the RCM momentum coordinates as

$$\begin{aligned}\mathbf{k} &= (\mathbf{k}_i-\mathbf{k}_j)/2, \quad & \mathbf{K} &= \mathbf{k}_i+\mathbf{k}_j,\\ \mathbf{k}' &= (\mathbf{k}_a-\mathbf{k}_b)/2, \quad & \mathbf{K}' &= \mathbf{k}_a+\mathbf{k}_b,\\ \mathbf{h} &= (\mathbf{k}_k-\mathbf{k}_l)/2, \quad & \mathbf{H} &= \mathbf{k}_k+\mathbf{k}_l,\\ \mathbf{p} &= (\mathbf{k}_c-\mathbf{k}_d)/2, \quad & \mathbf{P} &= \mathbf{k}_c+\mathbf{k}_d,\end{aligned} \tag{A3}$$

where i, j, k, l denote single-particle states occupied and a, b, c, d states unoccupied in the uncorrelated Fermi vacuum state. Transforming to RCM coordinates, the PPHH-LAD equations become

$$\begin{aligned}0 &= \langle \mathbf{k}'|v|\mathbf{k}\rangle + (\varepsilon(|\mathbf{k}'+\mathbf{K}/2|)+\varepsilon(|-\mathbf{k}'+\mathbf{K}/2|)\\ &\quad -\varepsilon(|\mathbf{k}-\mathbf{K}/2|)-\varepsilon(|-\mathbf{k}+\mathbf{K}/2|))\langle \mathbf{k}'|t|\mathbf{k}\rangle\\ &\quad +\frac{1}{2}\int d\mathbf{h}\langle \mathbf{k}'|t(\mathbf{K})|\mathbf{h}\rangle\langle \mathbf{h}|v|\mathbf{k}\rangle\\ &\quad \times\theta(k_F-|\mathbf{h}+\mathbf{K}/2|)\theta(k_F-|-\mathbf{h}+\mathbf{K}/2|)\\ &\quad +\frac{1}{2}\int d\mathbf{p}\langle \mathbf{k}'|v|\mathbf{p}\rangle\langle \mathbf{p}|t(\mathbf{K})|\mathbf{k}\rangle\\ &\quad \times\theta(|\mathbf{p}+\mathbf{K}/2|-k_F)\theta(|-\mathbf{p}+\mathbf{K}/2|-k_F),\end{aligned} \tag{A4}$$

where the relation

$$\langle \mathbf{k}_p\mathbf{k}_q|v|\mathbf{k}_r\mathbf{k}_s\rangle = \frac{(2\pi)^3}{\Omega}\langle \mathbf{k}|v|\mathbf{k}'\rangle\delta_{\mathbf{K}\mathbf{K}'} \tag{A5}$$

has been used. The expressions (9) and (10) for the reference and correlation energies, respectively, can be transformed to RCM coordinates in a similar way as is shown here for the ladder amplitude equations.

Owing to the isotropy of nuclear matter, we assume that the single-particle energy $\varepsilon(\mathbf{k}_p)$ depends only on the absolute value of the argument $\mathbf{k}_p$ [54,70]. In laboratory frame momentum coordinates, the single-particle energy is then

$$\varepsilon(|\mathbf{k}_p|) = \frac{\hbar^2k_p^2}{2m} + U(|\mathbf{k}_p|), \tag{A6}$$

where

$$U(|\mathbf{k}_p|) = \frac{\Omega}{(2\pi)^3}\sum_{m_sm_t}\int d\mathbf{k}_q\langle \mathbf{k}_p\mathbf{k}_q|v|\mathbf{k}_p\mathbf{k}_q\rangle\theta(k_F-|\mathbf{k}_q|). \tag{A7}$$

Because of the isotropy, we choose the direction such that $\mathbf{k}_p = (0, 0, k_p)$. The single-particle potential energy can also be written as

$$\begin{aligned}U(|\mathbf{k}_p|) &= \sum_{m_sm_t}\int d\mathbf{k}_q\,[\langle \mathbf{p}|v|\mathbf{p}\rangle - \langle \mathbf{p}|v|-\mathbf{p}\rangle]\\ &\quad \times\theta(k_F-|-\mathbf{p}+\mathbf{P}/2|),\end{aligned} \tag{A8}$$

where **p** and **P** are RCM momentum coordinates defined by $\mathbf{k}_p$ and $\mathbf{k}_q$, as in Eq. (A3).

2. Momentum and angular momentum basis

In this work, we assume that every interaction matrix element,

$$\langle k'(l'S)\mathcal{J}m_{\mathcal{J}}M_T|v|k(lS)\mathcal{J}m_{\mathcal{J}}M_T\rangle,$$

and every t-amplitude matrix element is multiplied by a factor

$$\mathcal{A}^{l'lSM_T} = \begin{cases} 1+(-1)^{l+l'}, & \text{if } M_T = 0, \\ \frac{1}{2}[1-(-1)^{l+S+1}], & \\ \times[1-(-1)^{l'+S+1}], & \text{if } |M_T| = 1, \end{cases} \tag{A9}$$

which ensures antisymmetry and conservation of parity.

Using exact Pauli exclusion operators, the ladder t-amplitude equations (A4) can be rewritten in the coupled angular momentum basis as

$$\begin{aligned}
&\Delta\varepsilon(\mathbf{k},\mathbf{k}',\mathbf{K})\langle k'(l'S)\mathcal{J}'m_{\mathcal{J}'}M_T|t(\mathbf{K},\hat{\mathbf{k}},\hat{\mathbf{k}}')|k(lS)\mathcal{J}m_{\mathcal{J}}M_T\rangle \\
&\quad = \langle k'(l'S)\mathcal{J}'m_{\mathcal{J}'}M_T|v|k(lS)\mathcal{J}m_{\mathcal{J}}M_T\rangle\delta_{\mathcal{J}\mathcal{J}'}\delta_{m_{\mathcal{J}}m_{\mathcal{J}'}} \\
&\qquad + \frac{1}{2}\sum_{\mathcal{J}''m_{\mathcal{J}''}}\sum_{l'l'''}\int_0^{k_F} h^2dh\langle k'(l'S)\mathcal{J}'m_{\mathcal{J}'}M_T|t(\mathbf{K},\hat{\mathbf{k}},\hat{\mathbf{k}}')|h(l''S)\mathcal{J}''m_{\mathcal{J}''}M_T\rangle\langle h(l'''S)\mathcal{J}m_{\mathcal{J}}M_T|v|k(lS)\mathcal{J}m_{\mathcal{J}}M_T\rangle \\
&\qquad \times Q_{hh}(l''\mathcal{J}''m_{\mathcal{J}''}, l'''\mathcal{J}m_{\mathcal{J}}; SM_T hK\theta_K\phi_K) \\
&\qquad + \frac{1}{2}\sum_{\mathcal{J}''m_{\mathcal{J}''}}\sum_{l'l'''}\int_0^{\infty} p^2dp\langle k'(l'S)\mathcal{J}'m_{\mathcal{J}'}M_T|v|p(l''S)\mathcal{J}'m_{\mathcal{J}'}M_T\rangle\langle p(l'''S)\mathcal{J}''m_{\mathcal{J}''}M_T|t(\mathbf{K},\hat{\mathbf{k}},\hat{\mathbf{k}}')|k(lS)\mathcal{J}m_{\mathcal{J}}M_T\rangle \\
&\qquad \times Q_{pp}(l''\mathcal{J}'m_{\mathcal{J}'}, l'''\mathcal{J}''m_{\mathcal{J}''}; SM_T pK\theta_K\phi_K),
\end{aligned} \tag{A10}$$

where $|(lS)\mathcal{J}m_{\mathcal{J}}\rangle$ denotes a vector where l and S are coupled to $\mathcal{J}$. In Eq. (A10) we have introduced the shorthand notation

$$\Delta\varepsilon(\mathbf{k},\mathbf{k}',\mathbf{K}) \equiv \varepsilon(|\mathbf{k}+\mathbf{K}/2|) + \varepsilon(|-\mathbf{k}+\mathbf{K}/2|) - \varepsilon(|\mathbf{k}'+\mathbf{K}/2|) - \varepsilon(|-\mathbf{k}'+\mathbf{K}/2|) \tag{A11}$$

for the energy denominator.

The sum of the single-particle energies corresponding to two-hole states can be expressed in terms of RCM coordinates as

$$\begin{aligned}
\varepsilon(|\mathbf{k}_i|) + \varepsilon(|\mathbf{k}_j|) = \varepsilon(|\mathbf{k}+\mathbf{K}/2|) + \varepsilon(|-\mathbf{k}+\mathbf{K}/2|) &= \frac{\hbar^2k^2}{m} + \frac{\hbar^2K^2}{4m} \\
&+ U^{M_T,+}(|\mathbf{k}+\mathbf{K}/2|) + U^{M_T,-}(|-\mathbf{k}+\mathbf{K}/2|),
\end{aligned} \tag{A12}$$

where

$$U^{M_T,\pm}(|\mathbf{k}_p|) = \frac{1}{4}\sum_{\mathcal{J}Sl}(2\mathcal{J}+1)\int_0^{k_F} dk_q k_q^2\int_{-1}^{1} d\cos\theta_{\mathbf{k}_q}\mathcal{B}^{M_T,\pm}\langle p\mathcal{J}lS|v|p\mathcal{J}lS\rangle\,, \tag{A13}$$

and the variable $p = |\mathbf{k}_p - \mathbf{k}_q|/2$. The antisymmetrization operator $\mathcal{B}^{M_T,\pm}$ is defined through the relation

$$\mathcal{B}^{M_T,\pm}\langle p\mathcal{J}lS|v|p\mathcal{J}l'S\rangle = \langle p\mathcal{J}lS|v(M_T'=0)|p\mathcal{J}l'S\rangle + [1-(-1)^{l'+S'+1}]\langle p\mathcal{J}lS|v(M_T'=M_T\pm\delta_{M_T,0})|p\mathcal{J}l'S\rangle \tag{A14}$$

for symmetric nuclear matter and the relation

$$\mathcal{B}^{M_T,\pm}\langle p\mathcal{J}lS|v|p\mathcal{J}l'S\rangle = [1-(-1)^{l'+S'+1}]\langle p\mathcal{J}lS|v(M_T'=1)|p\mathcal{J}l'S\rangle \tag{A15}$$

for pure neutron matter. The expressions of **k** and **K** are given in Eq. (A3). The sum of single-particle energies corresponding to two-particle states, $\varepsilon(\mathbf{k}_a) + \varepsilon(\mathbf{k}_b)$, is calculated in the same way. We define the angular-averaged energy denominator as

$$\Delta\bar{\varepsilon}(k,k',K) \equiv \varepsilon(\overline{k_i}) + \varepsilon(\overline{k_j}) - \varepsilon(\overline{k_a}) - \varepsilon(\overline{k_b}), \tag{A16}$$

where $\overline{k_p}$ for $p = i, j, a, b$ are angular-averaged input momenta defined in Eq. (17). Observe that the energy denominator is assumed to be a function of the two-particle isospin projection M_T.

The correlation energy can be written in the partial-wave expansion as

$$\begin{aligned}
\Delta E_{\mathrm{CCD}}/A = \frac{3C}{64\pi k_F^3}&\sum_{\mathcal{J}m_{\mathcal{J}}}\sum_{\mathcal{J}''m_{\mathcal{J}''}}\sum_{\mathcal{J}'''m_{\mathcal{J}'''}}\sum_{SM_T}\sum_{ll'l'''}\int_0^{\sqrt{k_F^2-K^2/4}} k^2dk\int_{\sqrt{k_F^2-K^2/4}}^{\infty} k'^2dk'\int_0^{2k_F} K^2dK \\
&\times\int_{-1}^{1} d\cos\theta_K\int_0^{2\pi} d\phi_K\langle k(lS)\mathcal{J}M_T|v|k'(l'S)\mathcal{J}M_T\rangle\hat{Q}_{hh}(l'''\mathcal{J}'''m_{\mathcal{J}'''}, l\mathcal{J}m_{\mathcal{J}}; SM_T kK\theta_K\phi_K) \\
&\times\hat{Q}_{pp}(l'\mathcal{J}m_{\mathcal{J}}, l''\mathcal{J}''m_{\mathcal{J}''}; SM_T k'K\theta_K\phi_K)\langle k'(l''S)\mathcal{J}''m_{\mathcal{J}''}M_T|t(\mathbf{K},\hat{\mathbf{k}},\hat{\mathbf{k}}')|k(l'''S)\mathcal{J}'''m_{\mathcal{J}'''}M_T\rangle,
\end{aligned} \tag{A17}$$

where the Pauli operators $\hat{Q}_{hh}$ and $\hat{Q}_{pp}$ are defined in Eqs. (20) and (21). Here we use the notations $\hat{Q}_{hh}$ and $\hat{Q}_{pp}$ instead of Q_{hh} and Q_{pp} to emphasize that these are integral operators that operate on the t-amplitude matrix. The t amplitude depends on $\hat{\mathbf{k}} \equiv (\theta_{\mathbf{k}}, \phi_{\mathbf{k}})$ and $\hat{\mathbf{k}}' \equiv (\theta_{\mathbf{k}'}, \phi_{\mathbf{k}'})$ through the energy denominator $\Delta\varepsilon(\mathbf{k}, \mathbf{k}', \mathbf{K})$, and the closed-form expression (22) can therefore generally not be used in the energy equation (A17).

When the ladder equations are written in the coupled partial-wave basis, it is possible to calculate the t-amplitude matrix for only one angular direction of the CM momentum $\mathbf{K}$, and then obtain the other matrix elements by performing a rotation [15]. Using the same technique as Suzuki *et al*., an amplitude matrix with a general CM momentum vector can be written

$$\langle k'(l''S)\mathcal{J}''m_{\mathcal{J}''}|t(\mathbf{K})|k(l'''S)\mathcal{J}'''m_{\mathcal{J}'''}\rangle = \sum_{m_{\mathcal{J}}m_{\mathcal{J}'}} D^{\mathcal{J}''}_{m_{\mathcal{J}''}m_{\mathcal{J}}}(\phi_K, \theta_K, 0) D^{\mathcal{J}'''*}_{m_{\mathcal{J}'''}m_{\mathcal{J}'}}(\phi_K, \theta_K, 0) \langle k'(l''S)\mathcal{J}''m_{\mathcal{J}}|t(K)|k(l'''S)\mathcal{J}'''m_{\mathcal{J}'}\rangle, \tag{A18}$$

where $D^{\mathcal{J}}_{m_{\mathcal{J}}m_{\mathcal{J}'}}(\alpha, \beta, \gamma)$ is the Wigner D function and α, β, and γ are Euler angles, defined in, for example, Ref. [71]. Equation (A18) can be used to obtain the correlation energy expression (18) from Eq. (A17).

[1] B. D. Day, Rev. Mod. Phys. **50**, 495 (1978).
[2] B. D. Day and G. Zabolitzky, Nucl. Phys. A **366**, 221 (1981).
[3] A. Akmal and V. R. Pandharipande, Phys. Rev. C **56**, 2261 (1997).
[4] W. Dickhoff and C. Barbieri, Prog. Part. Nucl. Phys. **52**, 377 (2004).
[5] S. Gandolfi, F. Pederiva, S. Fantoni, and K. E. Schmidt, Phys. Rev. Lett. **98**, 102503 (2007).
[6] Z. H. Li, U. Lombardo, H.-J. Schulze, W. Zuo, L. W. Chen, and H. R. Ma, Phys. Rev. C **74**, 047304 (2006).
[7] A. Lovato, O. Benhar, S. Fantoni, A. Y. Illarionov, and K. E. Schmidt, Phys. Rev. C **83**, 054003 (2011).
[8] A. Carbone, A. Polls, and A. Rios, Phys. Rev. C **88**, 044302 (2013).
[9] K. A. Brueckner, Phys. Rev. **100**, 36 (1955).
[10] B. D. Day, Rev. Mod. Phys. **39**, 719 (1967).
[11] K. A. Brueckner and C. A. Levinson, Phys. Rev. **97**, 1344 (1955).
[12] M. I. Haftel and F. Tabakin, Nucl. Phys. A **158**, 1 (1970).
[13] H. Q. Song, M. Baldo, G. Giansiracusa, and U. Lombardo, Phys. Rev. Lett. **81**, 1584 (1998).
[14] E. Schiller, H. Müther, and P. Czerski, Phys. Rev. C **60**, 059901(E) (1999).
[15] K. Suzuki, R. Okamoto, M. Kohno, and S. Nagata, Nucl. Phys. A **665**, 92 (2000).
[16] M. Baldo, A. Polls, A. Rios, H.-J. Schulze, and I. Vidaña, Phys. Rev. C **86**, 064001 (2012).
[17] R. Rajaraman and H. A. Bethe, Rev. Mod. Phys. **39**, 745 (1967).
[18] B. D. Day, Phys. Rev. C **24**, 1203 (1981).
[19] V. Somà and P. Bozek, Phys. Rev. C **78**, 054003 (2008).
[20] I. Vidaña, C. Providência, A. Polls, and A. Rios, Phys. Rev. C **80**, 045806 (2009).
[21] K. Hebeler, S. K. Bogner, R. J. Furnstahl, A. Nogga, and A. Schwenk, Phys. Rev. C **83**, 031301 (2011).
[22] A. W. Steiner and S. Gandolfi, Phys. Rev. Lett. **108**, 081102 (2012).
[23] K. Hebeler and R. J. Furnstahl, Phys. Rev. C **87**, 031302 (2013).
[24] I. Tews, T. Krüger, K. Hebeler, and A. Schwenk, Phys. Rev. Lett. **110**, 032504 (2013).
[25] T. Krüger, I. Tews, K. Hebeler, and A. Schwenk, Phys. Rev. C **88**, 025802 (2013).
[26] F. Coester, Nucl. Phys. **7**, 421 (1958).
[27] F. Coester and H. Kümmel, Nucl. Phys. **17**, 477 (1960).
[28] J. Čížek, J. Chem. Phys. **45**, 4256 (1966).
[29] J. Čížek, in *Advances in Chemical Physics* (Wiley & Sons, New York, 2007), p. 35.
[30] J. Čížek and J. Paldus, Int. J. Quant. Chem. **5**, 359 (1971).
[31] R. Bartlett and M. Musiał, Rev. Mod. Phys. **79**, 291 (2007).
[32] I. Shavitt and R. J. Bartlett, *Many-Body Methods in Chemistry and Physics* (Cambridge University Press, Cambridge, U.K., 2009).
[33] T. D. Crawford and H. F. Schaefer, Rev. Comp. Chem. **14**, 33 (2000).
[34] F. E. Harris, H. J. Monkhorst, and D. L. Freeman, *Algebraic and Diagrammatic Methods in Many-Fermion Theory* (Oxford University Press, Oxford, U.K., 1992).
[35] J. H. Heisenberg and B. Mihaila, Phys. Rev. C **59**, 1440 (1999).
[36] B. Mihaila and J. H. Heisenberg, Phys. Rev. C **61**, 054309 (2000).
[37] D. J. Dean and M. Hjorth-Jensen, Phys. Rev. C **69**, 054320 (2004).
[38] J. R. Gour, P. Piecuch, M. Hjorth-Jensen, M. Włoch, and D. J. Dean, Phys. Rev. C **74**, 024310 (2006).
[39] J. R. Gour, M. Horoi, P. Piecuch, and B. A. Brown, Phys. Rev. Lett. **101**, 052501 (2008).
[40] G. Hagen, T. Papenbrock, D. J. Dean, and M. Hjorth-Jensen, Phys. Rev. C **82**, 034330 (2010).
[41] G. R. Jansen, M. Hjorth-Jensen, G. Hagen, and T. Papenbrock, Phys. Rev. C **83**, 054306 (2011).
[42] O. Jensen, G. Hagen, T. Papenbrock, D. J. Dean, and J. S. Vaagen, Phys. Rev. C **82**, 014310 (2010).
[43] R. Roth, S. Binder, K. Vobig, A. Calci, J. Langhammer, and P. Navrátil, Phys. Rev. Lett. **109**, 052501 (2012).
[44] H. Kümmel, K. H. Lührmann, and J. G. Zabolitzky, Phys. Rep. **36**, 1 (1978).
[45] R. F. Bishop, Theor. Chim. Acta **80**, 95 (1991).
[46] R. Machleidt and I. Slaus, J. Phys. G: Nucl. Part. Phys. **27**, R69 (2001).
[47] R. Machleidt and D. R. Entem, Phys. Rep. **503**, 1 (2011).
[48] S. K. Bogner, A. Schwenk, R. J. Furnstahl, and A. Nogga, Nucl. Phys. A **763**, 59 (2005).
[49] W. Manzke, Diplomarbeit, Bochum University, 1974.
[50] R. F. Bishop and K. H. Lührmann, Phys. Rev. **17**, 3757 (1978).
[51] D. L. Freeman, Phys. Rev. B **15**, 5512 (1977).
[52] D. L. Freeman, J. Phys. C: Solid State Phys. **16**, 711 (1983).
[53] W. Dickhoff, A. Faessler, and H. Müther, Nucl. Phys. A **389**, 492 (1982).

[54] A. Ramos, A. Polls, and W. H. Dickhoff, Nucl. Phys. A **503**, 1 (1989).
[55] P. Bozek, Eur. Phys. J. A **15**, 325 (2002).
[56] Y. Dewulf, W. H. Dickhoff, D. Van Neck, E. R. Stoddard, and M. Waroquier, Phys. Rev. Lett. **90**, 152501 (2003).
[57] T. Frick and H. Müther, Phys. Rev. C **68**, 034310 (2003).
[58] A. Rios, A. Polls, and I. Vidaña, Phys. Rev. C **79**, 025802 (2009).
[59] H. Song, S. Yang, and T. Kuo, Nucl. Phys. A **462**, 491 (1987).
[60] M. F. Jiang, T. T. S. Kuo, and H. Müther, Phys. Rev. C **38**, 2408 (1988).
[61] L. Engvik, E. Osnes, M. Hjorth-Jensen, and T. Kuo, Nucl. Phys. A **622**, 553 (1997).
[62] L.-W. Siu, J. W. Holt, T. T. S. Kuo, and G. E. Brown, Phys. Rev. C **79**, 054004 (2009).
[63] A. Ekström, G. Baardsen, C. Forssén, G. Hagen, M. Hjorth-Jensen, G. R. Jansen, R. Machleidt, W. Nazarewicz, T. Papenbrock, J. Sarich, and S. M. Wild, Phys. Rev. Lett. **110**, 192502 (2013).
[64] D. R. Entem and R. Machleidt, Phys. Rev. C **68**, 041001(R) (2003).
[65] T. Munson, J. Sarich, S. M. Wild, S. Benson, and L. Curfman McInnes, *TAO 2.0 Users Manual*, Technical Memorandum ANL/MCS-TM-322 (Argonne National Laboratory, Argonne, Illinois, 2012), http://www.mcs.anl.gov/uploads/cels/papers/TM-322.pdf.
[66] J. J. MacKenzie, Phys. Rev. **179**, 1002 (1969).
[67] K. A. Brueckner and J. L. Gammel, Phys. Rev. **109**, 1023 (1958).
[68] C. Mahaux, P. F. Bortignon, and R. A. Broglia, Phys. Rep. **120**, 1 (1985).
[69] C. Mahaux and R. Sartor, Phys. Rev. C **40**, 1833 (1989).
[70] À. G. Ramos, Ph.D. thesis, University of Barcelona, 1988.
[71] D. A. Varshalovich, A. N. Moskalev, and V. K. Khersonskii, *Quantum Theory of Angular Momentum* (World Scientific, Singapore, 1988).
[72] M. Baldo, I. Bombaci, L. S. Ferreira, G. Giansiracusa, and U. Lombardo, Phys. Rev. C **43**, 2605 (1991).
[73] A. Polls *et al*. (unpublished).
[74] R. B. Wiringa, V. G. J. Stoks, and R. Schiavilla, Phys. Rev. C **51**, 38 (1995).
[75] B. Vonderfecht, W. Dickhoff, A. Polls, and A. Ramos, Nucl. Phys. A **555**, 1 (1993).
[76] D. J. Dean and M. Hjorth-Jensen, Rev. Mod. Phys. **75**, 607 (2003).
[77] A. Ekström (unpublished).
[78] W. D. Myers and W. J. Swiatecki, Ann. Phys. **204**, 401 (1990).
[79] J. M. Lattimer, Annu. Rev. Nucl. Part. Science **62**, 485 (2012).
[80] B.-A. Li, Phys. Rev. Lett. **88**, 192701 (2002).
[81] J. Erler, C. J. Horowitz, W. Nazarewicz, M. Rafalski, and P.-G. Reinhard, Phys. Rev. C **87**, 044320 (2013).
[82] L. Engvik, M. Hjorth-Jensen, R. Machleidt, H. Müther, and A. Polls, Nucl. Phys. A **627**, 85 (1997).
[83] H. Heiselberg and M. Hjorth-Jensen, Phys. Rep. **328**, 237 (2000).

III

Coupled-cluster calculations of nucleonic matter

G. Hagen,[1,2] T. Papenbrock,[1,2] A. Ekström,[3,4] K. A. Wendt,[1,2] G. Baardsen,[3] S. Gandolfi,[5] M. Hjorth-Jensen,[3,4,6] and C. J. Horowitz[7]

[1]*Physics Division, Oak Ridge National Laboratory, Oak Ridge, Tennessee 37831, USA*
[2]*Department of Physics and Astronomy, University of Tennessee, Knoxville, Tennessee 37996, USA*
[3]*Department of Physics and Center of Mathematics for Applications, University of Oslo, N-0316 Oslo, Norway*
[4]*National Superconducting Cyclotron Laboratory, Michigan State University, East Lansing, Michigan 48824, USA*
[5]*Theoretical Division, Los Alamos National Laboratory Los Alamos, New Mexico 87545, USA*
[6]*Department of Physics and Astronomy, Michigan State University, East Lansing, Michigan 48824, USA*
[7]*Indiana University, Bloomington, Indiana 47405, USA*

(Received 13 November 2013; published 27 January 2014)

Background: The equation of state (EoS) of nucleonic matter is central for the understanding of bulk nuclear properties, the physics of neutron star crusts, and the energy release in supernova explosions. Because nuclear matter exhibits a finely tuned saturation point, its EoS also constrains nuclear interactions.
Purpose: This work presents coupled-cluster calculations of infinite nucleonic matter using modern interactions from chiral effective field theory (EFT). It assesses the role of correlations beyond particle-particle and hole-hole ladders, and the role of three-nucleon forces (3NFs) in nuclear matter calculations with chiral interactions.
Methods: This work employs the optimized nucleon-nucleon (NN) potential $\mathrm{NNLO_{opt}}$ at next-to-next-to leading order, and presents coupled-cluster computations of the EoS for symmetric nuclear matter and neutron matter. The coupled-cluster method employs up to selected triples clusters and the single-particle space consists of a momentum-space lattice. We compare our results with benchmark calculations and control finite-size effects and shell oscillations via twist-averaged boundary conditions.
Results: We provide several benchmarks to validate the formalism and show that our results exhibit a good convergence toward the thermodynamic limit. Our calculations agree well with recent coupled-cluster results based on a partial wave expansion and particle-particle and hole-hole ladders. For neutron matter at low densities, and for simple potential models, our calculations agree with results from quantum Monte Carlo computations. While neutron matter with interactions from chiral EFT is perturbative, symmetric nuclear matter requires nonperturbative approaches. Correlations beyond the standard particle-particle ladder approximation yield non-negligible contributions. The saturation point of symmetric nuclear matter is sensitive to the employed 3NFs and the employed regularization scheme. 3NFs with nonlocal cutoffs exhibit a considerably improved convergence than their local cousins. We are unable to find values for the parameters of the short-range part of the local 3NF that simultaneously yield acceptable values for the saturation point in symmetric nuclear matter and the binding energies of light nuclei.
Conclusions: Coupled-cluster calculations with nuclear interactions from chiral EFT yield nonperturbative results for the EoS of nucleonic matter. Finite-size effects and effects of truncations can be controlled. For the optimization of chiral forces, it might be useful to include the saturation point of symmetric nuclear matter.

DOI: 10.1103/PhysRevC.89.014319 PACS number(s): 21.65.Mn, 21.30.−x, 21.60.De

I. INTRODUCTION

Bulk nucleonic matter is interesting for several reasons. The equation of state (EoS) of neutron matter, for instance, determines properties of supernova explosions [1], and of neutron stars [2–7], and it links the latter to neutron radii in atomic nuclei [8–10] and symmetry energy [11,12]. Likewise, the compressibility of nuclear matter is probed in giant dipole excitations [13], and the symmetry energy of nuclear matter is related to the difference between proton and neutron radii in atomic nuclei [14–16]. The saturation point of nuclear matter determines bulk properties of atomic nuclei, and is therefore an important constraint for nuclear energy-density functionals and mass models (see, e.g., Refs. [17,18]).

The determination and our understanding of the EoS for nuclear matter is intimately linked with our capability to solve the nuclear many-body problem. Here, correlations beyond the mean field play an important role. Theoretical studies of nuclear matter and the pertinent EoS span back to the very early days of nuclear many-body physics. Early computations are nicely described in the 1967 review by Day [19]. These early calculations were performed using Brueckner-Bethe-Goldstone theory [20,21]; see Refs. [3,22,23] for recent reviews and developments. In these calculations, mainly particle-particle correlations were summed to infinite order. Other correlations were often included in a perturbative way. Coupled-cluster calculations of nuclear matter were performed already during the late 1970s and early 1980s [24,25]. In recent years, there has been a considerable algorithmic development of first-principle methods for solving the nuclear many-body problem. A systematic inclusion of other correlations in a nonperturbative way are nowadays accounted for in Monte Carlo methods [26–30], self-consistent Green's function approaches [23,31–34],

nuclear density functional theory [16,18], and coupled-cluster theory [35,36].

Similar progress has been made in the derivation of nuclear forces based on chiral effective field theory (EFT) [37,38]. Nuclear Hamiltonians from chiral EFT are now used routinely in nucleonic matter calculations, with the three-nucleon forces (3NFs) [39,40] being front and center of many studies [34,41–48]. We note finally that there are also approaches to nucleonic matter based on lattice quantum chromodynamics [49].

In this work we study the EoS of nucleonic matter, using modern NN interactions and 3NFs from chiral EFT, and an implementation of the coupled-cluster method [50,51] that has become a standard in quantum chemistry [52,53]. We employ a Cartesian momentum space basis with periodic boundary conditions, similar to the recent coupled-cluster based calculations of the electron gas [54,55]. Our calculations are based on coupled cluster with doubles (CCD) approximation [56–58]. This is the lowest-order truncation for closed-shell systems in a momentum-space basis, and we will also explore the role of selected triples clusters. We employ a recent parametrization [36] of the NN force from chiral EFT at next-to-next-to-leading order, with inclusion of the 3NF that enters at the same chiral order.

The recent work by Baardsen *et al.* [35] used coupled-cluster theory in the thermodynamic limit, formulated in the relative center-of-mass frame using a partial-wave expansion, to compute the EoS of nuclear matter using modern NN chiral interactions. Baardsen *et al.* [35] summed particle-particle and hole-hole ladders to infinite order ($\mathrm{CCD_{ladd}}$), while neglecting particle-hole and other nonlinear terms that enter in the CCD approximation. In this work we include all terms that enter at the CCD cluster truncation level, and we can therefore assess the role of these correlations by comparing to the method developed in [35]. Further, the current implementation of CCD in the laboratory frame using PBC facilitates the inclusion of 3NFs considerably, and we also study effects of selected triples excitations to the EoS.

This paper is organized as follows. In the next section we present the coupled-cluster formalism for infinite matter that includes 3NFs and perturbative triples corrections. The calculations are performed in Cartesian coordinates with a discrete momentum basis and twisted periodic boundary conditions [59–61]. This avoids the tedious partial-wave expansion of the nuclear forces, and it eases considerably the numerical evaluation of 3NFs. Averaging over twisted periodic boundary conditions minimizes finite-size effects and provides us with a good convergence towards the thermodynamic limit. Section II also presents computational results for finite-size effects and a few benchmark calculations. Our results for symmetric nuclear matter and pure neutron matter are presented in Sec. III. Concluding remarks are given in Sec. IV.

II. METHOD

In this section we present the coupled-cluster formalism for infinite matter. We discuss the inclusion and treatment of NN forces and 3NFs from chiral effective field theory (EFT), correlations up to three-particle–three-hole excitations and finite-size effects. Several benchmark calculations give us confidence in the validity of our approach.

A. Interaction and model space

Our Hamiltonian is

$$H = T_{\mathrm{kin}} + V_{NN} + V_{\mathrm{3NF}}.$$

Here, T_{kin} denotes the kinetic energy, and V_{NN} and V_{3NF} denote the translationally invariant NN interaction and 3NF. The NN interaction and 3NF are from chiral effective field theory [37,38] at next-to-next-to-leading order (NNLO). We employ the parametrization $\mathrm{NNLO_{opt}}$ for the NN interaction [36], and the local 3NF [62]. This 3NF has a local regulator, i.e., the cutoff is in the momentum transfer, and thereby differs from implementations of the 3NF [40] that employ the cutoff in the relative Jacobi momenta. We note that the numerical implementation of the 3NF in the discrete momentum basis is much simpler than in the harmonic oscillator basis commonly used for finite nuclei, because essentially no transformation of matrix elements is necessary. Nevertheless, the sheer number of matrix elements (and associated function calls) of the 3NF is huge, and this is computationally still a limiting factor.

For the model space, we choose a cubic lattice in momentum space with $(2n_{\mathrm{max}}+1)^3$ momentum points. The spin (spin-isospin) degeneracy of each momentum point is $g_s = 2$ ($g_s = 4$) for pure neutron matter (nuclear matter). Thus, filling of the lattice yields shell closures for "Fermi spheres" with $g_s n$ fermions, and $n = 1,7,19,27,33,57,\ldots$. We note that one could also use noncubic lattices. Any periodic lattice permits one to implement momentum conservation exactly. For fixed particle number $A = g_s n$ and density $\rho = g_s k_F^3/(6\pi^2)$ (or Fermi momentum k_F), one computes the volume of the cubic box $V = L^3 = A/\rho$, and the box length L that determines the lattice spacing $\Delta k = 2\pi/L$. We note that the computed results exhibit a dependence on the shell closure n. However, Sec. II D shows that shell effects and finite-size effects can be mitigated and controlled, and that the dependence on the parameter n becomes very small.

The second parameter of our lattice is n_{max}. We note that $n_{\mathrm{max}}\Delta k$ is the momentum cutoff of our single-particle basis. One has to increase n_{max} until the computed results (e.g., the energy per nucleon) is practically independent of this parameter. For the results reported below we find that $n_{\mathrm{max}} = 4$ is sufficient.

B. Coupled-cluster theory for infinite systems

In this section we present the coupled-cluster equations for nucleonic matter. Our calculations of nucleonic matter are based on the recently optimized chiral nucleon-nucleon interaction at $\mathrm{NNLO_{opt}}$ [36] with the 3NF at the same chiral order. The low-energy constants (LECs) of the 3NF were determined by fitting the constants c_E and c_D to reproduce the experimental half-life and binding energy of the triton. The optimized 3NF LECs are $c_E = -0.389$ and $c_D = -0.39$. With these values the ^{4}He binding energy is -28.47 MeV [63]. We employ single-particle states

$$|\vec{p},s_z,t_z\rangle \equiv |\mathbf{k}\rangle,$$

with momentum $\vec{p}$, spin projection s_z and isospin projection t_z. Discrete values of the momentum variable $\vec{p} = \hbar\vec{k}$ result from periodic boundary conditions in a cubic box with length L, that is

$$k_{n_i} = \frac{2\pi n_i}{L}, \quad n_i = 0, \pm 1, \ldots \pm n_{\max}, \quad i = x, y, z.$$

In this basis, the nuclear Hamiltonian with nucleon-nucleon and three-nucleon interactions is

$$\begin{aligned} H = & \sum_{pq} \langle \mathbf{k}_p | T_{\rm kin} | \mathbf{k}_q \rangle a_p^\dagger a_q \\ & + \frac{1}{4} \sum_{pqrs} \langle \mathbf{k}_p \mathbf{k}_q | V_{\rm NN} | \mathbf{k}_r \mathbf{k}_s \rangle a_p^\dagger a_q^\dagger a_s a_r \\ & + \frac{1}{36} \sum_{pqrstu} \langle \mathbf{k}_p \mathbf{k}_q \mathbf{k}_r | V_{\rm 3NF} | \mathbf{k}_s \mathbf{k}_t \mathbf{k}_u \rangle a_p^\dagger a_q^\dagger a_r^\dagger a_u a_t a_s . \end{aligned} \quad (1)$$

The kinetic energy is diagonal in the discrete momentum basis $\langle \mathbf{k}_p | T_{\rm kin} | \mathbf{k}_q \rangle = \frac{\hbar^2}{2m} \vec{k}_p^2 \delta_{pq}$. The operators $a_p^\dagger$ and a_p create and annihilate a nucleon in state $|\mathbf{k}_p\rangle$, respectively.

The discrete momentum basis allows us to respect translational invariance of the NN potential and the 3NFs. Momentum is conserved, meaning that the two- and three-body matrix elements of the Hamiltonian (1) vanish unless

$$\vec{k}_p + \vec{k}_q = \vec{k}_r + \vec{k}_s,$$

and

$$\vec{k}_p + \vec{k}_q + \vec{k}_r = \vec{k}_s + \vec{k}_t + \vec{k}_u.$$

Note also that the chiral nucleon-nucleon and three-nucleon interactions conserve the total isospin projection, but not the total spin projection.

In single-reference coupled-cluster theory the correlated wave-function is written in the form

$$|\Psi\rangle = e^T |\Phi_0\rangle.$$

Here $|\Phi_0\rangle = \prod_{i=1}^A a_i^\dagger |0\rangle$ is a product state and serves as the reference. The cluster operator T is a linear combination of n-particle–n-hole (np-nh) excitation operators, i.e., $T = T_1 + T_2 + \cdots + T_n$. In the discretized momentum basis the reference state is the closed shell Fermi vacuum, and is obtained by filling the A states with the lowest kinetic energy. We limit ourselves to spin saturated reference state, meaning that each momentum orbital of the reference state is doubly occupied. In this case the nuclear interaction does not induce 1p-1h excitations of the reference state, and we have $T_1 = 0$. Thus, the cluster operator becomes

$$T = \frac{1}{4} \sum_{ijab} \langle \mathbf{k}_a \mathbf{k}_b | t | \mathbf{k}_i \mathbf{k}_j \rangle a_a^\dagger a_b^\dagger a_j a_i + \cdots .$$

Here and in what follows, indices i,j,k,l (a,b,c,d) label occupied (unoccupied) states. Truncating T at the 2p-2h excitation level ($T \approx T_2$) gives the coupled-cluster doubles (CCD) approximation. The CCD energy and amplitude equations can be written in compact form

$$E_{\rm CCD} = E_0 + \langle \Phi_0 | \overline{H}_N | \Phi_0 \rangle, \quad (2)$$

$$0 = \langle \Phi_{ij}^{ab} | \overline{H}_N | \Phi_0 \rangle. \quad (3)$$

Here

$$\begin{aligned} E_0 = & \langle \Phi_0 | H | \Phi_0 \rangle \\ = & \sum_i \langle \mathbf{k}_i | f | \mathbf{k}_i \rangle + \frac{1}{2} \sum_{i,j} \langle \mathbf{k}_i \mathbf{k}_j | v | \mathbf{k}_i \mathbf{k}_j \rangle \\ & + \frac{1}{6} \sum_{ijk} \langle \mathbf{k}_i \mathbf{k}_j \mathbf{k}_k | w | \mathbf{k}_i \mathbf{k}_j \mathbf{k}_k \rangle \end{aligned} \quad (4)$$

is the vacuum expectation value (which in the case of no 1p-1h corresponds to the Hartree-Fock energy), $|\Phi_{ij}^{ab}\rangle$ is a 2p-2h excitation of the reference state, and $\overline{H}_N \equiv e^{-T} H_N e^T$ is the similarity transformation of the normal-ordered Hamiltonian:

$$\begin{aligned} H_N = & \sum_{pq} \langle \mathbf{k}_p | f | \mathbf{k}_q \rangle : a_p^\dagger a_q : \\ & + \frac{1}{4} \sum_{pqrs} \langle \mathbf{k}_p \mathbf{k}_q | v | \mathbf{k}_r \mathbf{k}_s \rangle : a_p^\dagger a_q^\dagger a_s a_r : \\ & + \frac{1}{36} \sum_{pqrstu} \langle \mathbf{k}_p \mathbf{k}_q \mathbf{k}_r | w | \mathbf{k}_s \mathbf{k}_t \mathbf{k}_u \rangle : a_p^\dagger a_q^\dagger a_r^\dagger a_u a_t a_s : . \end{aligned} \quad (5)$$

Here $: a_p^\dagger \cdots a_{p'} \cdots :$ is the normal ordered string of operators with respect to the reference state. The normal-ordered one-body operator is given in terms of the Fock matrix elements

$$\begin{aligned} \langle \mathbf{k}_p | f | \mathbf{k}_q \rangle = & \langle \mathbf{k}_p | t | \mathbf{k}_q \rangle + \sum_i \langle \mathbf{k}_p \mathbf{k}_i | V_{\rm NN} | \mathbf{k}_q \mathbf{k}_i \rangle \\ & + \frac{1}{2} \sum_{ij} \langle \mathbf{k}_p \mathbf{k}_i \mathbf{k}_j | V_{\rm 3NF} | \mathbf{k}_q \mathbf{k}_i \mathbf{k}_j \rangle . \end{aligned} \quad (6)$$

The normal-ordered two-body operator has matrix elements

$$\begin{aligned} \langle \mathbf{k}_p \mathbf{k}_q | v | \mathbf{k}_r \mathbf{k}_s \rangle = & \langle \mathbf{k}_p \mathbf{k}_q | V_{\rm NN} | \mathbf{k}_r \mathbf{k}_s \rangle \\ & + \sum_i \langle \mathbf{k}_p \mathbf{k}_q \mathbf{k}_i | V_{\rm 3NF} | \mathbf{k}_i \mathbf{k}_r \mathbf{k}_s \rangle . \end{aligned} \quad (7)$$

Finally, the normal-ordered three-body operator w has matrix elements

$$\langle \mathbf{k}_p \mathbf{k}_q \mathbf{k}_r | w | \mathbf{k}_s \mathbf{k}_t \mathbf{k}_u \rangle = \langle \mathbf{k}_p \mathbf{k}_q \mathbf{k}_r | V_{\rm 3NF} | \mathbf{k}_s \mathbf{k}_t \mathbf{k}_u \rangle . \quad (8)$$

In most of this work, we will neglect all elements of w when solving the CCD equations. In this normal-ordered two-body approximation, the 3NF enters in the vacuum expectation value (4), the Fock matrix (6), and the normal-ordered two-body operator (7), but the three-body operator w that changes the orbitals of all three nucleons is neglected.

We note that coupled-cluster theory with full inclusion of 3NFs was worked out in the singles and doubles approximation (CCSD) [64], and very recently with triples corrections included [65].

For an efficient numerical implementation one writes the CCD equations (3) in a factorized (quasilinear) form,

$$0 = \langle \mathbf{k}_a\mathbf{k}_b|v|\mathbf{k}_i\mathbf{k}_j\rangle + P(ab)\sum_c \langle \mathbf{k}_b|\chi|\mathbf{k}_c\rangle\langle \mathbf{k}_a\mathbf{k}_c|t|\mathbf{k}_i\mathbf{k}_j\rangle - P(ij)\sum_k \langle \mathbf{k}_k|\chi|\mathbf{k}_j\rangle\langle \mathbf{k}_a\mathbf{k}_b|t|\mathbf{k}_i\mathbf{k}_k\rangle + \frac{1}{2}\sum_{cd}\langle \mathbf{k}_a\mathbf{k}_b|\chi|\mathbf{k}_c\mathbf{k}_d\rangle\langle \mathbf{k}_c\mathbf{k}_d|t|\mathbf{k}_i\mathbf{k}_j\rangle$$
$$+\frac{1}{2}\sum_{kl}\langle \mathbf{k}_a\mathbf{k}_b|t|\mathbf{k}_k\mathbf{k}_l\rangle\langle \mathbf{k}_k\mathbf{k}_l|\chi|\mathbf{k}_i\mathbf{k}_j\rangle + P(ij)P(ab)\sum_{kc}\langle \mathbf{k}_a\mathbf{k}_c|t|\mathbf{k}_i\mathbf{k}_k\rangle\langle \mathbf{k}_k\mathbf{k}_b|\chi|\mathbf{k}_c\mathbf{k}_j\rangle$$
$$+\frac{1}{2}P(ij)\sum_{cdk}\langle \mathbf{k}_a\mathbf{k}_k\mathbf{k}_b|w|\mathbf{k}_i\mathbf{k}_c\mathbf{k}_d\rangle\langle \mathbf{k}_c\mathbf{k}_d|t|\mathbf{k}_k\mathbf{k}_j\rangle - \frac{1}{2}P(ab)\sum_{ckl}\langle \mathbf{k}_a\mathbf{k}_k\mathbf{k}_l|w|\mathbf{k}_i\mathbf{k}_c\mathbf{k}_j\rangle\langle \mathbf{k}_c\mathbf{k}_b|t|\mathbf{k}_k\mathbf{k}_l\rangle. \quad (9)$$

Here, $P(pq) \equiv 1 - P_{pq}$ is an antisymmetrization operator, and we employed the intermediates

$$\langle \mathbf{k}_b|\chi|\mathbf{k}_c\rangle = \langle \mathbf{k}_b|f|\mathbf{k}_c\rangle - \frac{1}{2}\sum_{kld}\langle \mathbf{k}_b\mathbf{k}_d|t|\mathbf{k}_k\mathbf{k}_l\rangle\langle \mathbf{k}_k\mathbf{k}_l|v|\mathbf{k}_c\mathbf{k}_d\rangle + \frac{1}{4}\sum_{edkl}\langle \mathbf{k}_k\mathbf{k}_l\mathbf{k}_b|w|\mathbf{k}_e\mathbf{k}_d\mathbf{k}_c\rangle\langle \mathbf{k}_e\mathbf{k}_d|t|\mathbf{k}_k\mathbf{k}_l\rangle, \quad (10)$$

$$\langle \mathbf{k}_k|\chi|\mathbf{k}_j\rangle = \langle \mathbf{k}_k|f|\mathbf{k}_j\rangle + \frac{1}{2}\sum_{kcd}\langle \mathbf{k}_k\mathbf{k}_l|v|\mathbf{k}_c\mathbf{k}_d\rangle\langle \mathbf{k}_c\mathbf{k}_d|t|\mathbf{k}_j\mathbf{k}_l\rangle + \frac{1}{4}\sum_{cdln}\langle \mathbf{k}_l\mathbf{k}_n\mathbf{k}_k|w|\mathbf{k}_c\mathbf{k}_d\mathbf{k}_j\rangle\langle \mathbf{k}_c\mathbf{k}_d|t|\mathbf{k}_l\mathbf{k}_n\rangle, \quad (11)$$

$$\langle \mathbf{k}_k\mathbf{k}_l|\chi|\mathbf{k}_i\mathbf{k}_j\rangle = \langle \mathbf{k}_k\mathbf{k}_l|v|\mathbf{k}_i\mathbf{k}_j\rangle + \frac{1}{2}\sum_{cd}\langle \mathbf{k}_k\mathbf{k}_l|v|\mathbf{k}_c\mathbf{k}_d\rangle\langle \mathbf{k}_c\mathbf{k}_d|t|\mathbf{k}_i\mathbf{k}_j\rangle + \frac{1}{2}P(ij)\sum_{cdn}\langle \mathbf{k}_n\mathbf{k}_k\mathbf{k}_l|w|\mathbf{k}_c\mathbf{k}_d\mathbf{k}_j\rangle\langle \mathbf{k}_c\mathbf{k}_d|t|\mathbf{k}_n\mathbf{k}_i\rangle, \quad (12)$$

$$\langle \mathbf{k}_k\mathbf{k}_b|\chi|\mathbf{k}_c\mathbf{k}_j\rangle = \langle \mathbf{k}_k\mathbf{k}_b|v|\mathbf{k}_c\mathbf{k}_j\rangle + \sum_{ld}\langle \mathbf{k}_k\mathbf{k}_l|v|\mathbf{k}_c\mathbf{k}_d\rangle\langle \mathbf{k}_c\mathbf{k}_d|t|\mathbf{k}_l\mathbf{k}_j\rangle - \frac{1}{2}\sum_{dln}\langle \mathbf{k}_l\mathbf{k}_k\mathbf{k}_n|w|\mathbf{k}_d\mathbf{k}_j\mathbf{k}_c\rangle\langle \mathbf{k}_d\mathbf{k}_b|t|\mathbf{k}_l\mathbf{k}_n\rangle$$
$$+\frac{1}{2}\sum_{del}\langle \mathbf{k}_l\mathbf{k}_k\mathbf{k}_b|w|\mathbf{k}_d\mathbf{k}_e\mathbf{k}_c\rangle\langle \mathbf{k}_d\mathbf{k}_e|t|\mathbf{k}_l\mathbf{k}_j\rangle, \quad (13)$$

$$\langle \mathbf{k}_a\mathbf{k}_b|\chi|\mathbf{k}_c\mathbf{k}_d\rangle = \langle \mathbf{k}_a\mathbf{k}_b|v|\mathbf{k}_c\mathbf{k}_d\rangle - \frac{1}{2}P(ab)\sum_{ekl}\langle \mathbf{k}_k\mathbf{k}_l\mathbf{k}_b|w|\mathbf{k}_e\mathbf{k}_c\mathbf{k}_d\rangle\langle \mathbf{k}_e\mathbf{k}_a|t|\mathbf{k}_k\mathbf{k}_l\rangle. \quad (14)$$

In Eqs. (9)–(14) the numerically expensive sums that involve products of two-body operators can all be implemented efficiently as matrix-matrix multiplications. The momentum conservation reduces the computational cost of the CCD equations to $n_o n_u^3$, where n_o (n_u) is the number of occupied (unoccupied) momentum states. This is a considerable reduction in computational cycles as compared to the normal cost of the CCD equations which is $n_o^2 n_u^4$ [52], and similar to the reduction of computational cost achieved in the angular momentum coupled scheme [66,67].

The coupled-cluster equations (9) are solved numerically by iteration and yield the matrix elements of T_2. The CCD energy (2) is given in algebraic form by

$$E_{\mathrm{CCD}} = E_0 + \frac{1}{4}\sum_{ijab}\langle \mathbf{k}_i\mathbf{k}_j|v|\mathbf{k}_a\mathbf{k}_b\rangle\langle \mathbf{k}_a\mathbf{k}_b|t|\mathbf{k}_i\mathbf{k}_j\rangle.$$

Below, we will also employ an approximation (denoted as $\mathrm{CCD_{ladd}}$) that only uses the particle-particle and hole-hole ladders in the CCD equations, i.e.,

$$0 = \langle \mathbf{k}_a\mathbf{k}_b|v|\mathbf{k}_i\mathbf{k}_j\rangle + P(ab)\sum_c \langle \mathbf{k}_b|f|\mathbf{k}_c\rangle\langle \mathbf{k}_a\mathbf{k}_c|t|\mathbf{k}_i\mathbf{k}_j\rangle - P(ij)\sum_k \langle \mathbf{k}_k|f|\mathbf{k}_j\rangle\langle \mathbf{k}_a\mathbf{k}_b|t|\mathbf{k}_i\mathbf{k}_k\rangle$$
$$+\frac{1}{2}\sum_{cd}\langle \mathbf{k}_a\mathbf{k}_b|v|\mathbf{k}_c\mathbf{k}_d\rangle\langle \mathbf{k}_c\mathbf{k}_d|t|\mathbf{k}_i\mathbf{k}_j\rangle + \frac{1}{2}\sum_{kl}\langle \mathbf{k}_a\mathbf{k}_b|t|\mathbf{k}_k\mathbf{k}_l\rangle\langle \mathbf{k}_k\mathbf{k}_l|v|\mathbf{k}_i\mathbf{k}_j\rangle\,. \quad (15)$$

The $\mathrm{CCD_{ladd}}$ approximation was used in Ref. [35] within coupled-cluster theory, and a similar approximation was also employed in other computations of nucleonic matter, see, e.g., Refs. [42,43].

Let us also discuss the inclusion of three-body clusters. When going beyond the CCD approximation and considering triples excitations, one might question whether the residual three-body part w can safely be neglected. After all, three-body forces directly induce excitations of three-body clusters. Below we will include the residual part w when considering contributions from triples excitations to the correlation energy, and study the accuracy of the normal-ordered two-body approximation in the presence of triples excitations in neutron and symmetric nuclear matter. Very recently, Binder *et al.* employed chiral interactions softened via the similarity renormalization group transformation [68,69], studied the effect of triples corrections in the presence of 3NFs in nuclei such as ^{16}O and ^{40}Ca, and found it to be small [65].

The full inclusion of triples in the presence of three-body forces is demanding and computationally expensive. Some effects of triples can be included in the CCD(T) approximation [70] that we extend to 3NFs. In CCD(T) the

triples excitation amplitude is approximated as

$$t_{ijk}^{abc} \equiv \langle \mathbf{k}_a \mathbf{k}_b \mathbf{k}_c | t | \mathbf{k}_i \mathbf{k}_j \mathbf{k}_k \rangle \approx \left\langle \Phi_{ijk}^{abb} \right| (v+w)(1+\hat{T}_2) |\Phi_0\rangle / \epsilon_{abc}^{ijk}. \quad (16)$$

Here

$$\epsilon_{abc}^{ijk} \equiv f_i^i + f_j^j + f_k^k - f_a^a - f_b^b - f_c^c \,. \quad (17)$$

The CCD(T) correction to the energy is

$$\Delta E_{\mathrm{CCD(T)}} = \frac{1}{36} \sum_{ijkabc} \left| t_{ijk}^{abc} \right|^2 / \epsilon_{abc}^{ijk}. \quad (18)$$

Employing the triples amplitude (16) with the inclusion of w yields the energy correction $\Delta E_{\mathrm{CCD(T)}}$. We also consider the following approximations. Neglecting the residual three-body part w yields the normal-ordered two-body approximation to the CCD(T) energy correction, denoted as $\Delta E_{\mathrm{CCD(T:w=0)}}$. Omitting the term wT_2 in Eq. (16) gives the energy correction $\Delta E_{\mathrm{CCD(T:}wT_2=0)}$. Note that the numerically expensive term wT_2 in Eq. (16) consist of three distinct diagrams in which one sums over pp, hh, and ph intermediate states, respectively. Below we will investigate the contributions of these three diagrams to the CCD(T) energy correction in neutron and symmetric nuclear matter.

C. Ladder approximation in a partial-wave basis

In Ref. [35], the ladder approximation of the coupled-cluster equations for nuclear matter is presented in an alternative formulation. Historically, the equations for nuclear matter, for example in the hole-line approximation [71], have often been expressed explicitly in a partial-wave basis [72–74]. Similarly, in the method presented in Ref. [35], the ladder approximation is formulated in a partial-wave basis, assuming that the thermodynamic limit is reached and therefore using integrals over relative and center-of-mass momenta. In the partial-wave expanded equations, the Pauli exclusion operators are treated exactly, using a technique introduced for the Brueckner-Hartree-Fock approximation by Suzuki *et al.* [74]. Apart from the truncation in partial waves, the only approximation in this method is in the single-particle potentials, where an angular-average approximation was used for the laboratory momentum argument [35,75].

D. Finite-size effects

We would like to quantify the error due to finite-size effects and the accuracy of our coupled-cluster calculations of neutron and nuclear matter. Using periodic boundary conditions (PBC) one could increase the number of particles in the box until convergence to the thermodynamic limit is reached. However, due to variations of the shell effects at different closed shell configurations, there is no guarantee that increasing the number of particles will lead to a systematic and smooth convergence to the thermodynamic limit. Furthermore, the computational cost of many-body methods such as the AFDMC and coupled-cluster methods increases rapidly with increasing particle number, and one would therefore like to employ a method that controls finite-size effects already for modest particle numbers. This can be achieved with averaging over phases of Bloch waves that correspond to different boundary conditions [59–61].

Consider a free particle in a box of size L subject to twisted boundary condition, that is, the wave function with momentum k fulfills the condition for so-called Bloch waves, namely, $\psi_k(x+L) = e^{i\theta}\psi_k(x)$. By averaging over the twist angle θ, shell effects can be eliminated for free Fermi systems [59], and they are much suppressed for interacting systems [60,61]. In this way, one obtains a much more systematic and smooth convergence towards the thermodynamic limit. The twisted boundary conditions are defined by

$$k_{n_i} = \frac{(2\pi n_i + \theta_i)}{L}, \quad n_i = 0, \pm 1, \ldots \pm n_{\max}, \; i = x, y, z,$$

with the twist angle $\theta \in [0, \pi]$ for systems with time-reversal invariance [61]. This amounts to letting the particles pick up a complex phase when they wrap around the boundary of the cubic box. By integrating or averaging over a finite number of twists in each x, y, z direction we obtain the twist-averaged boundary conditions (TABC). In our implementation of TABC we integrate over the twist angles θ using a finite number of Gauss-Legendre quadrature points in $[0, \pi]$. Note that $\theta = 0$ ($\theta = \pi$) corresponds to (anti)periodic boundary conditions.

In order to quantify the finite-size effects using PBC and TABC we compute the kinetic and potential energy contribution to the Hartree-Fock energy for several closed shell configurations ranging from tens to several hundreds of nucleons, and compare with the thermodynamic limit for these quantities. In Fig. 1 we show the relative error of the kinetic energy in pure neutron matter for the Fermi momentum $k_F = 1.6795$ fm^{-1} computed using standard PBC and TABC. We used 10 Gauss-Legendre points for the twist angle θ_i of the $i = x, y, z$ direction in the integration interval $[0, \pi]$. Clearly, we obtain a much faster and smoother convergence to the thermodynamic limit using TABC. Generally we get about an order of magnitude reduction in the relative error when using

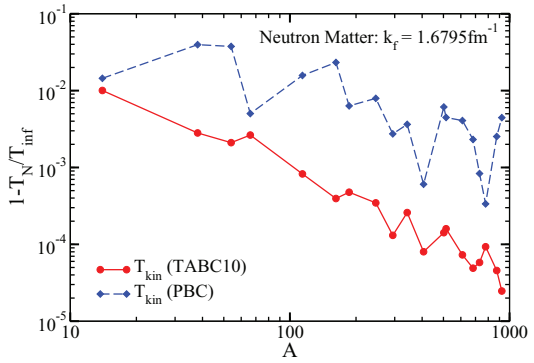

FIG. 1. (Color online) Relative finite-size corrections for the kinetic energy in pure neutron matter at the Fermi momentum $k_F = 1.6795$ fm^{-1} vs the neutron number A. TABC10 are twist-averaged boundary conditions with 10 Gauss-Legendre points in each spatial direction.

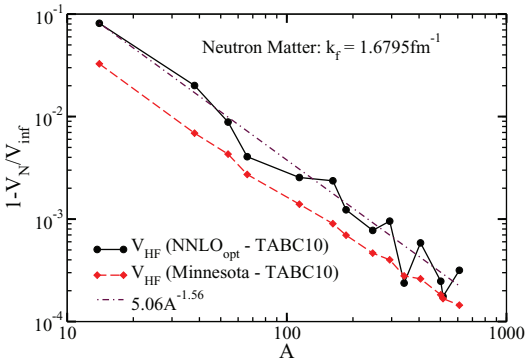

FIG. 2. (Color online) Relative finite-size corrections for the Hartree-Fock energy of the NNLO$_{opt}$ (full line) and Minnesota (dashed line) potentials in pure neutron matter at the Fermi momentum $k_F = 1.6795$ fm^{-1} vs the neutron number A. TABC10 are twist-averaged boundary conditions with 10 Gauss-Legendre points in each spatial direction. The dashed-dotter line shows a power law fit to the NNLO$_{opt}$ results.

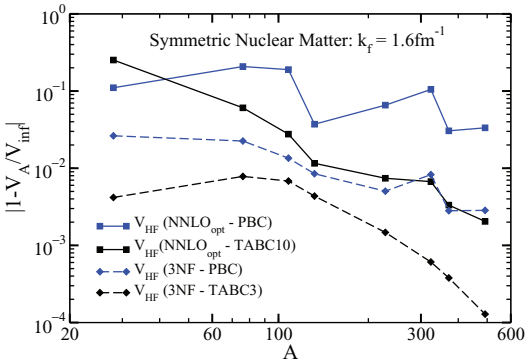

FIG. 3. (Color online) Relative finite-size corrections for the Hartree-Fock energy of the NN potential NNLO$_{opt}$ and the 3NF potential in symmetric nuclear matter at the Fermi momentum $k_F = 1.6$ fm^{-1} vs the nucleon number A. PBC: periodic boundary conditions. TABC10 and TABC3 are twist-averaged boundary conditions with 10 and 3 Gauss-Legendre points in each spatial direction, respectively.

TABC as compared to PBC. Finite size effects are particularly small for PBC and $N = 66$ neutrons. This was also seen in AFDMC calculations [27].

Figure 2 shows the relative error of the potential energy to the Hartree-Fock energy in pure neutron matter for the Fermi momentum $k_F = 1.6795$ fm^{-1} computed with TABC. We compute the potential energy from NNLO$_{opt}$ and from the Minnesota potential. We see that the finite-size effects in the potential energy are comparable to the finite-size effects in the kinetic energy shown in Fig. 1. We note that finite-size effects vanish as the power law $A^{-1.56}$ in the neutron number A.

Finally, we would also like to assess the finite-size effects in symmetric nuclear matter. In Fig. 3 we show the relative error of the potential energy to the Hartree-Fock energy in symmetric nuclear matter for the Fermi momentum $k_F = 1.6$ fm^{-1} computed using PBC and TABC. We consider the Hartree-Fock potential energy contribution from the nucleon-nucleon interaction NNLO$_{opt}$ and the 3NF at order NNLO separately. In particular it is seen that the relative error in the potential energy contribution from the 3NF is about an order of magnitude smaller than the relative error coming from the nucleon-nucleon interaction alone using both PBC and TABC. In the case of symmetric nuclear matter there is no systematic convergence trend using PBC, and for 132 nucleons the relative error for PBC is around $\sim$4%, while using TABC the error is reduced to $\sim$1%. It is interesting to note that finite size effects for NNLO$_{opt}$ with TABC decrease as $A^{-1.59}$ with increasing nucleon number A. This exponent is similar to the exponent found in neutron matter (see Fig. 2).

Coupled-cluster calculations of nucleonic matter using TABC are very expensive. Using 10 twist angles in each direction requires 10^3 coupled-cluster calculations, although symmetry considerations can reduce this number considerably. In Ref. [61] it was shown that one can find a specific choice of twist angles (known as special points), in which the Hartree-Fock energy exactly corresponds to the Hartree-Fock energy in the thermodynamic limit. In the following we compute these special points for neutron and nuclear matter using both NN interactions and 3NFs, and compare with calculations using PBC and TABC.

E. Benchmarks

It is interesting to compare the results for various boundary conditions with the infinite matter results by Baardsen *et al.* [35]. Figure 4 shows the CCD$_{ladd}$ results for neutron matter computed with the nucleon-nucleon potential NNLO$_{opt}$. In a finite system, the neutron number $N = 66$ is very close to

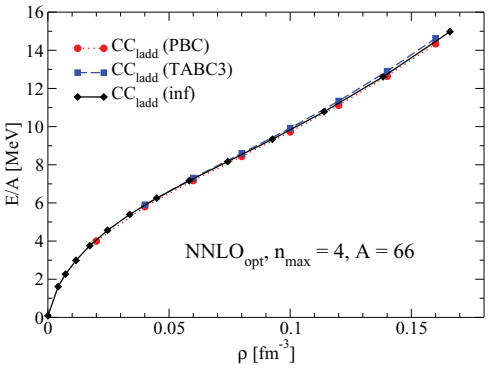

FIG. 4. (Color online) Energy per particle of neutron matter for NNLO$_{opt}$ computed in the CCD$_{lad}$ approximation with periodic boundary conditions (circles), twist-averaged boundary conditions (squares), and for infinite matter (diamonds). The latter results are from Ref. [36]. The calculations used $A = 66$ neutrons and $n_{max} = 4$.

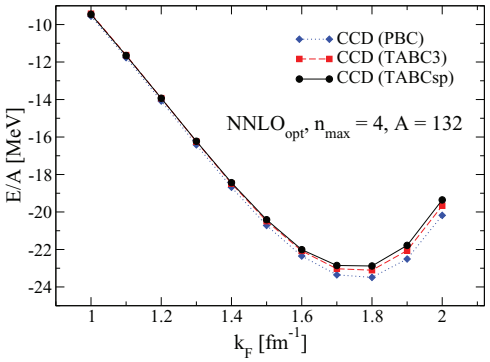

FIG. 5. (Color online) Energy per particle of symmetric nuclear matter for NNLO$_{opt}$ computed in the CCD approximation with periodic boundary conditions (diamonds), twist-averaged boundary conditions (squares), and with a special point and twisted boundary conditions (circles). The calculations used $A = 132$ nucleons and $n_{max} = 4$.

the infinite matter results for both periodic and twist-averaged boundary conditions.

For symmetric nuclear matter, the CCD results are more sensitive to the choice of the boundary conditions, with results shown in Fig. 5. At higher Fermi momenta ($k_F > 1.6$ fm^{-1}), the energy per nucleon for periodic boundary conditions differs by ∼0.5 MeV from the result obtained with twist-averaged boundary conditions. A calculation with a special point in the twist is very close to the twist-averaged results. However, for Fermi momenta $k_F < 1.6$ fm^{-1}, the difference between the PBC and TABC is less than 200 keV per nucleon.

Figure 6 compares nuclear matter results calculated in the ladder approximation with the CC$_{ladd}$ of Ref. [35]. The latter were obtained by taking the thermodynamic limit in the relative and center-of mass frame and by summing over partial

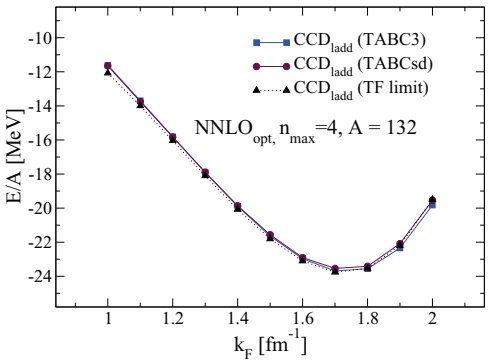

FIG. 6. (Color online) Energy per particle of symmetric nuclear matter for NNLO$_{opt}$ computed in the CCD$_{ladd}$ approximation in the thermodynamic limit using partial-wave expansion (triangles) (partly adapted from Ref. [35]), with twist averaged boundary conditions (squares), and with a special point and twisted boundary conditions (circles). The calculations used $A = 132$ nucleons and $n_{max} = 4$.

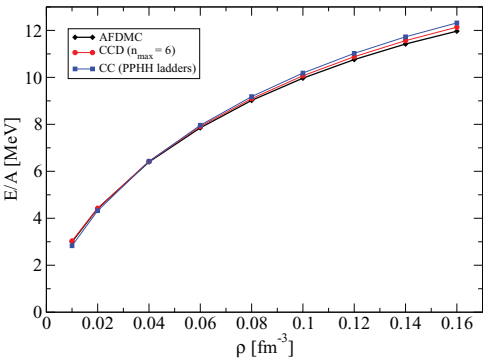

FIG. 7. (Color online) Energy per particle of neutron matter, computed with the Minnesota potential. Diamonds: AFDMC, circles: CCD, squares: CCD limited to pp and hh ladders.

waves. The summation over intermediate particle-particle and hole-hole configurations is performed with an exact Pauli operator, while the single-particle energies are computed using an angle-averaging procedure, see Ref. [35] for further details. For these results, the angle-average approximation, together with a truncation in the number of partial waves included, represent the sources of possible errors in the thermodynamic limit. It is therefore very satisfactory that the results from different methods are close to each other.

Let us also consider a simple potential model and benchmark the results of our coupled-cluster calculations against virtually exact results from the auxiliary field diffusion Monte Carlo (AFDMC) method [76]. The Minnesota potential [77] is a semirealistic nucleon-nucleon interaction that can be solved accurately with AFDMC. It depends only on the relative momenta and spin, but lacks spin-orbit or tensor contributions. The matrix elements of this potential are real numbers. For the benchmark we employ periodic boundary conditions, $A = 66$ neutrons, and $n_{max} = 6$.

Figure 7 compares the energy per neutron of our lattice CCD results (circles), and our CCD$_{ladd}$ in the thermodynamic limit, see Ref. [35], to the AFDMC benchmark. Overall, the agreement is good between all methods. As expected, the CCD results are more accurate than the CCD$_{ladd}$ approximation.

Finally, we turn to 3NFs. The inclusion of 3NFs—even in the normal-ordered approximation—is still numerically expensive due to the large number of required matrix elements. We also study different approximations for 3NFs, and compare the results for symmetric nuclear matter when 3NFs only enter in the normal-ordered approximation as zero-body, one-body, or up to two-body forces. Figure 8 clearly shows that normal-ordered two-body forces are relevant.

III. RESULTS FOR CHIRAL INTERACTIONS

In this section, we present our results for coupled-cluster computations of neutron matter and symmetric nuclear matter. As shown in the previous section, the finite size effects (and the differences between PBC and TABC) are small for

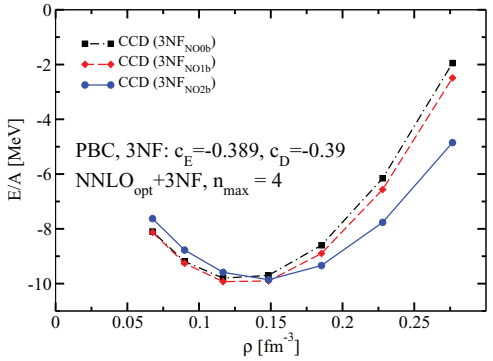

FIG. 8. (Color online) Energy per particle of symmetric nuclear matter computed in the CCD approximation with $\mathrm{NNLO_{opt}} + 3\mathrm{NF}$ ($c_E = -0.389$, $c_D = -0.39$). The 3NF is included in the zero-body (black dashed-dotted line), one-body (red dashed line), and in the two-body (blue solid line) normal-ordered approximations. The calculations used $A = 132$ nucleons and $n_{\max} = 4$.

$A = 66$ neutrons and $A = 132$ nucleons when calculating neutron matter and symmetric nuclear matter, respectively. For this reason, many of the expensive calculations involving 3NFs are only performed with PBC at these specific particle numbers.

A. Neutron matter

Figure 9 shows the energy per neutron as a function of density based on NN interactions alone and compares various many-body methods. The employed NN interaction $\mathrm{NNLO_{opt}}$ is perturbative in neutron matter, with second-order many-body perturbation theory (MBPT2), CCD and $\mathrm{CCD_{ladd}}$ giving

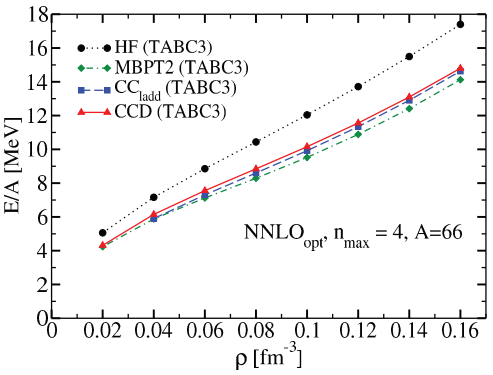

FIG. 9. (Color online) Energy per particle in neutron matter with $\mathrm{NNLO_{opt}}$ (NN only). The black dashed line is Hartree-Fock (HF), the green dashed-dotted line is second-order many-body perturbation theory (MBPT2), the blue dashed line is coupled-cluster doubles ladder approximation ($\mathrm{CCD_{ladd}}$), and the red solid line is coupled-cluster doubles (CCD). The calculations used $A = 66$ neutrons, $n_{\max} = 4$, and TABC3.

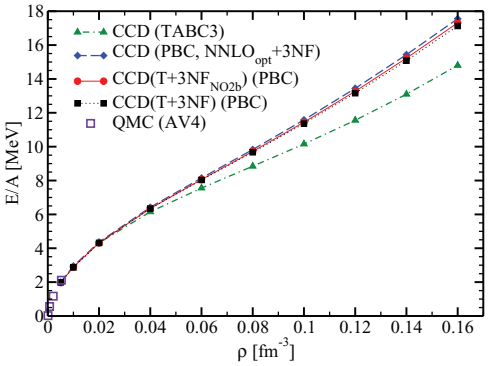

FIG. 10. (Color online) Energy per particle in neutron matter with $\mathrm{NNLO_{opt}}$ (NN only) and with inclusion of 3NF computed in the CCD and CCD(T) approximations. The 3NF LECs are given by $c_E = -0.389$ and $c_D = -0.39$. The calculations used $A = 66$ neutrons, $n_{\max} = 4$, and PBC and TABC. The QMC results are from Refs. [28,30].

similar results that differ by less than 1 MeV per neutron at nuclear saturation density.

Figure 10 shows the effect of 3NFs in CCD calculations of the EoS for neutron matter. We consider several approximations involving 3NFs, and it is seen that they yield very similar results. We note that three-nucleon forces act repulsively. The results for neutron matter reported here are consistent with the recent calculations of Krueger *et al.* [46], and our results for the EoS fall within their NNLO uncertainty band. The CCD calculation that includes the normal-ordered 3NFs is shown as diamonds. Triples corrections that are limited to the inclusion of up to two-body terms from the normal-ordered 3NF are shown as circles, while triples corrections that include also the residual 3NF are shown as squares. For neutron matter, the effects of triples are small and account for about 0.3 MeV per neutron at high densities, and the residual 3NFs contribute little to the triples corrections. At very low densities, the coupled-cluster results are in agreement with results from quantum Monte Carlo (QMC) calculations [27,28,30,78]. In this low-density regime the physics is dominated by the large scattering length, and the EoS becomes independent of the short-ranged parts of the nuclear interaction.

B. Nuclear matter

In this subsection we perform coupled-cluster calculations of symmetric nuclear matter using chiral NN and 3NF interactions at NNLO. Figure 11 shows the energy per nucleon in symmetric nuclear matter for a wide range of densities computed in MBPT2, the $\mathrm{CCD_{ladd}}$, and in the CCD approximation with the NN potential $\mathrm{NNLO_{opt}}$. In these calculations we used $A = 132$ nucleons, $n_{\max} = 4$, and TABC based on 3^3 angles. We observe that the saturation point is at a too-large density, and we get a considerable overbinding. These results for $\mathrm{NNLO_{opt}}$ are in good agreement with the recent self-consistent Green's function (SCGF) calculations

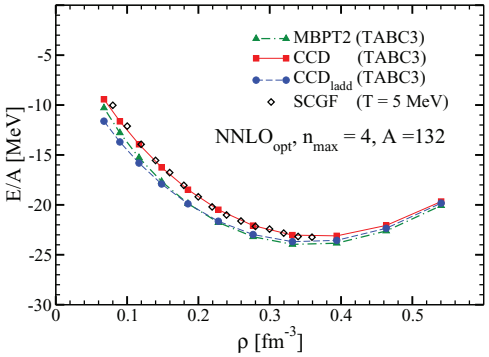

FIG. 11. (Color online) Energy per particle in symmetric nuclear matter with NNLO$_{opt}$ (NN only) computed in the MBPT2 (triangles with green dashed-dotted line), CCD$_{ladd}$ (circles with blue dashed line), and CCD (squares with solid red line) approximations. The calculations used 132 nucleons, $n_{max} = 4$, and TABC3. Diamonds are results from self-consistent Green's function (SCGF) at the finite temperature $T = 5$ MeV, taken from Ref. [34].

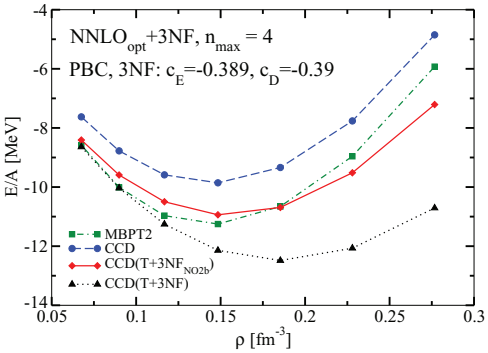

FIG. 12. (Color online) Energy per particle in symmetric nuclear matter with NNLO$_{opt}$ and 3NF computed in the MBPT2 (squares with green dashed-dotted line), CCD (circles with blue dashed line), and CCD(T) with 3NF in the normal-ordered two-body approximation (diamonds with solid red line), and including the residual 3NF in leading order (triangles with dotted black line). The 3NF LECs are given by $c_E = -0.389$ and $c_D = -0.39$. The calculations used 132 nucleons, $n_{max} = 4$, and PBC.

of nuclear matter [34], and the CCD$_{ladd}$ calculations of Ref. [35]. The difference between MBPT2 and CCD is about 2 MeV below saturation energy and about three times as large as for neutron matter. The difference between the CCD$_{ladd}$ approximation and the full CCD calculations is around 1 MeV per nucleon around saturation density. We can conclude that—in contrast to neutron matter—for nuclear matter and the NNLO$_{opt}$ interaction (which is rather soft), nonlinear terms in the T_2 amplitude and particle-hole excitations yield non-negligible contributions. These results indicate that nuclear matter for the NNLO$_{opt}$ chiral interaction is not perturbative. We note also that the coupled-cluster calculations are difficult to converge for Fermi momenta smaller than about 0.8 fm^{-1}. This is presumably due to the clustering of nuclear matter at low densities [79]. We also note that the results shown Fig. 11 at high densities are beyond the presumed valididy of the underlying EFT.

Let us turn to 3NFs. Figure 12 shows the energy per nucleon in symmetric nuclear matter for a wide range of densities computed with MBPT2, CCD, and the CCD(T) approximation. The CCD calculations included the 3NF in the normal-ordered two-body approximation. The CCD(T) calculations were performed with 3NFs in the normal-ordered two-body approximation [CCD(T+3NF$_{NO2b}$)], and going beyond the normal-ordered two-body approximation by including the leading-order residual 3NF contribution to the perturbative estimate for the T_3 amplitude [CCD(T+3NF$_{NO3b}$)]. In these calculations we used $A = 132$ nucleons with PBC and $n_{max} = 4$. For the densities we consider here, the difference between PBC and TABC is small.

In contrast to calculations of neutron matter, the contribution from the perturbative triples corrections is sizable in nuclear matter, and about 1 MeV per nucleon in the range of densities shown when including the 3NF in the normal-ordered two-body approximation. Furthermore, we find that the contribution of the residual 3NF to the CCD(T) energy is significant around saturation density, indicating that the normal-ordered two-body approximation for the 3NF might not be sufficient in symmetric nuclear matter. We checked that the contribution of the residual 3NF to the CCD amplitude equations is negligible, and therefore it might be sufficient to include the full 3NF in the perturbative triples amplitude. In order to check the accuracy of the perturbative triples approximation [CCD(T)] in nuclear matter we also performed non-perturbative, iterative CCDT-1 (see Refs. [80,81]) calculations for $A = 28$ and $n_{max} = 3$ at two different densities $k_F = 1.3$ fm^{-1} and $k_F = 1.6$ fm^{-1}. We found that the difference between CCD(T) and CCDT-1 in this range of densities is at most 0.1 MeV per nucleon. Therefore, we conclude that the CCD(T) approximation is accurate for the NN potential NNLO$_{opt}$ and chiral 3NFs in symmetric nuclear matter.

C. Scheme dependence of three-nucleon forces

In this subsection, we try to further illuminate the role of 3NFs in nucleonic matter. We study different regularization schemes, and compute the energy per particle in pure neutron matter and symmetric nuclear matter. The 3NF employed in the previous subsections exhibits a cutoff of $\Lambda = 500$ MeV. This cutoff is in the momentum transfer, and therefore local in position space [62]. This choice of regulator for the 3NF is different from the regularization scheme that is used in the nucleon-nucleon sector, and from other regularizations of the 3NF that exhibit cutoffs on Jacobi momenta [40]. We note that regulators that cut off initial and final Jacobi momenta lead to nonlocal interactions. Here, the cutoff function is

$$f_R(\vec{p},\vec{q}) = \exp\left[-\left(\frac{4p^2+3q^2}{4\Lambda^2}\right)^n\right],$$

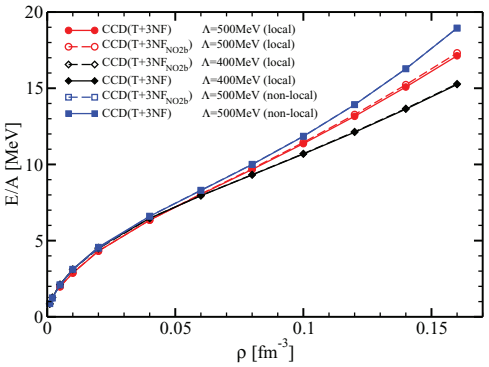

FIG. 13. (Color online) Energy per particle in pure neutron matter with NNLO$_{\rm opt}$ and 3NF computed in the CCD(T) approximation including 3NFs in the normal ordered two-body approximation and including the residual 3NF in the CCD(T: $wT_2 = 0$) approximation. For the 3NF we used a local regulator with cutoffs $\Lambda = 400$ and $\Lambda = 500$ MeV. The 3NF LECs are given by $c_E = -0.389$ and $c_D = -0.39$ for the $\Lambda = 500$ MeV local regulator, while for the $\Lambda = 400$ MeV local regulator we used $c_E = -0.27$ and $c_D = -0.39$ with c_E adjusted to the ^{4}He binding energy. For the nonlocal regulator with $\Lambda = 500$ MeV cutoff we used $c_E = -0.791$ and $c_D = -2$ adjusted to the triton and ^{3}He binding energies. The calculations used 66 neutrons, $n_{\rm max} = 4$, and PBC.

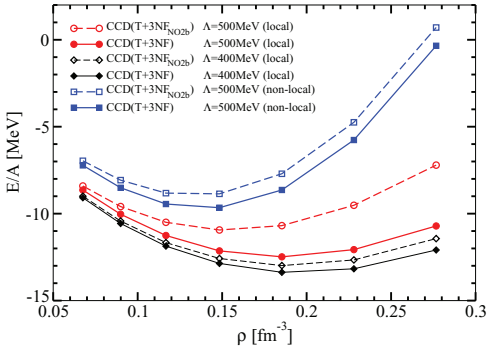

FIG. 14. (Color online) Same caption as in Fig. 13, except that the energy per particle is for symmetric nuclear matter. The calculations used 132 nucleons, $n_{\rm max} = 4$, and PBC.

with $\vec{p} = (\vec{k}_1 - \vec{k}_2)/2$ and $q = [\vec{k}_3 - (\vec{k}_1 - \vec{k}_2)/2](2/3)$. This regulator reduces to the regulator used in the NN sector for $\vec{q} = 0$. In the NN potential NNLO$_{\rm opt}$ we use $n = 3$, while for the local regulator of the 3NF defined in Ref. [62] we use $n = 2$ in the exponential. In what follows, we compare the NNLO$_{\rm opt}$ interaction with a 3NF that also uses a local regulator but a lower cutoff of $\Lambda = 400$ MeV, and with a 3NF that employs a nonlocal regulator and a cutoff $\Lambda = 500$ MeV in relative Jacobi momenta.

Figure 13 shows the energy per particle in pure neutron matter computed in the CCD(T) approximation. Here we included 3NFs in the normal ordered two-body approximation, and in the CCD(T: $wT_2 = 0$) approximation. For the latter, we went beyond the normal ordered two-body approximation and included the residual three-body term w that enters at first order in the triples equation for T_3. In neutron matter the contribution from the residual 3NF w to the energy per particle is small. This indicates that the normal-ordered two-body approximation works very well. In the EoS calculation with the local regulator and the lower cutoff $\Lambda = 400$ MeV we adjusted the LECs of the three-body contact term to $c_E = -0.27$ and kept c_D unchanged. Then, the binding energies of the triton and the nuclei ^{3,4}He are close to the experimental values. For the nonlocal regulator with cutoff $\Lambda = 500$ and power $n = 2$ in the exponential, the LECs $c_E = -0.791$ and $c_D = -2$ reproduce the triton and ^{3}He binding energies. In pure neutron matter the contributions from the 3NF contact terms with the LECs c_E and c_D vanish for a nonlocal regulator, and the contribution to the EoS depends only on the pion-nucleon couplings c_1 and c_3 of the long-range two-pion exchange term of the 3NF [42]. However, for a local regulator the 3NF contact terms do not vanish in neutron matter [29]. The results for the EoS for pure neutron matter show a regulator dependence at densities beyond $\rho = 0.08$ fm^{-3}. The band obtained from the different 3NF regulators are within the corresponding band for neutron matter obtained in Ref. [46].

Figure 14 shows the corresponding plot for the energy per particle in symmetric nuclear matter. Here the results for the local regulator with a cutoff $\Lambda = 500$ MeV exhibit a considerable enhancement of the contribution from the residual 3NF w to the energy per particle at densities above the saturation densities. The sizeable triples contribution of the residual 3NF w questions the usually observed hierarchy of the coupled-cluster approximation. The results from the lower cutoff $\Lambda = 400$ MeV are much more satisfactory in the sense that the contribution from the residual three-body part w to the binding energy per particle is considerably smaller, and at the order of 0.5 MeV or less for the densities considered. Likewise, the results obtained with the non-local regulator at the cutoff 500 MeV are also satisfactory in the sense that the contribution from the residual 3NF w is at most 1 MeV to the energy per particle at densities beyond the saturation point. One might speculate whether this problematic feature of the local regulator with a cutoff 500 MeV is related to the large cutoff dependence found in finite nuclei using this regulator [69]. Naively one would expect that regulator dependencies are higher-order corrections in an EFT. The large scheme dependencies observed in Fig. 14 might therefore suggest that the cutoff $\Lambda = 500$ MeV is too close to the EFT breakdown scale.

For local and nonlocal regulators we considerably underbind nuclear matter. The saturation density for the local regulators is too high, while for the nonlocal regulator the saturation density is closer to the empirical value. We tried to adjust the LECs c_E and c_D such that an acceptable result could be obtained simultaneously for the saturation point in symmetric nuclear matter and the triton binding energy. For the nonlocal regulator the result is shown in Fig. 15. The blue band shows the region where the triton binding energy is reproduced within 5%. The red band shows the region where the saturation

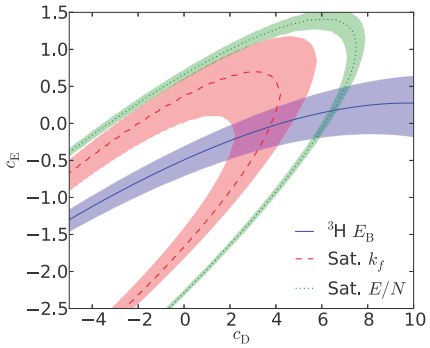

FIG. 15. (Color online) The blue band shows the region where the triton binding energy is reproduced within 5% of the experimental value. The red band shows the region where the saturation fermi momentum in symmetric nuclear matter is reproduced within 5% of its empirical value, and the green band shows the region where the energy per nucleon is within 5% of the empirical value.

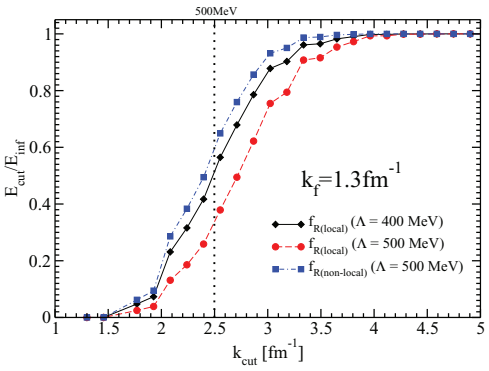

FIG. 16. (Color online) Cutoff dependent fraction of the residual 3NF contribution to the MBPT2 energy per particle in symmetric nuclear matter for different regulators. Results are shown for the local regulator with $\Lambda = 500$ MeV (diamonds), the local regulator with $\Lambda = 400$ MeV (squares), and for the non-local regulator with $\Lambda = 500$ MeV (circles). Calculations used 132 nucleons, $n_{max} = 4$, and PBC.

Fermi momentum is within 5% of its empirical value, and the green band shows the region where the energy per nucleon is within 5% of the empirical value. The nuclear matter calculations were obtained from MBPT2 calculations using 28 nucleons, and we accounted for about 1 MeV per nucleon in missing correlations energy, and about 0.5 MeV per nucleon due to finite size effects. It thus seems that a simultaneous reproduction of saturation in light nuclei and infinite matter is not possible without adjusting other LECs. As an example we considered the point $c_E = 0.3$ and $c_D = -2.0$. This yields the saturation point $k_F \approx 1.4$ fm^{-1} and $E/A \approx 15.5$ MeV, while the triton binding energy is -13.53 MeV.

We would like to understand better the role that different regulators and cutoffs play for the chiral 3NF. Unfortunately, it is difficult to visualize 3NFs in momentum space [82,83]. We therefore compute the MBPT2 contribution of the residual 3NF w and cut off the involved momentum integrations at a single-particle momentum k_{cut}. Figure 16 shows the fractional contribution of the MBPT2 energy correction of the residual 3NF as a function of k_{cut} at the Fermi momentum $k_F = 1.3$ fm^{-1}. The chiral cutoff of $\Lambda = 500$ MeV is also shown as a dashed line for comparison. We see that for the local cutoff $\Lambda = 500$ MeV most contributions to the MBPT2 result are from high single-particle momenta that are well above the nominal chiral cutoff. The situation is improved for the local regulator with lower cutoff $\Lambda = 400$ MeV and even more so for the nonlocal regulator with cutoff $\Lambda = 500$ MeV. For a discussion of different cutoff schemes and convergence issues in calculations of the homogeneous electron gas see Ref. [54].

Let us finally note that issues with 3NFs also arose in other calculations. Lovato *et al.* [29] pointed out that the equivalence of different chiral 3NF contact terms [40] is spoiled by local regulators. Roth *et al.* [84] used SRG evolution to soften the chiral NN interaction of Ref. [85] combined with the local 3NF of Ref. [62], and found that the results in medium-mass nuclei depend considerably on the SRG evolution scale. This dependence is reduced for a cutoff $\Lambda = 400$ MeV in the local 3NF [69]. Clearly, more studies of chiral 3NFs are necessary to fully understand regularization scheme dependences.

IV. SUMMARY

We have performed coupled-cluster calculations of nucleonic matter with interactions from chiral EFT at NNLO. The single-particle states consist of a discrete lattice in momentum space, and the implementation of twist-averaged boundary conditions mitigates shell oscillations and finite-size effects. Our benchmark calculations agree well with other well established methods. We find that neutron matter is perturbative, while symmetric nuclear matter is not perturbative, with significant contributions beyond perturbation theory and particle ladders.

For the employed NN potential NNLO$_{opt}$ and 3NFs, the neutron matter results fall within the error estimates of previous calculations for chiral interactions, with 3NFs acting repulsively. For nuclear matter, the empirical saturation could not be reproduced, and the results are very sensitive to the employed regulator (local vs nonlocal) and cutoff. At larger chiral cutoffs, the nonlocal regulator is preferred over the local one because it corresponds closer to the cutoff generated by the finite single-particle basis. It seems that the variation of the 3NF contact terms alone is insufficient to achieve both an acceptable saturation point of nuclear matter and an acceptable binding of light nuclei.

ACKNOWLEDGMENTS

We thank S. K. Bogner, E. Epelbaum, R. J. Furnstahl, A. Mukherjee, and F. Pederiva for discussions. This work was supported by the Office of Nuclear Physics, U.S. Department of Energy (Oak Ridge National Laboratory), under DE-FG02-96ER40963 (University of Tennessee), DE-FG02-87ER40365

(Indiana University), DE-SC0008499 and DE-SC0008808 (NUCLEI SciDAC collaboration), the Field Work Proposal ERKBP57 at Oak Ridge National Laboratory, the LDRD program at Los Alamos National Laboratory, and the Research Council of Norway under Contract No. ISP-Fysikk/216699. Computer time was provided by the Innovative and Novel Computational Impact on Theory and Experiment (INCITE) program. This research used resources of the Oak Ridge Leadership Computing Facility located in the Oak Ridge National Laboratory, which is supported by the Office of Science of the Department of Energy under Contract No. DE-AC05-00OR22725, and used computational resources of the National Center for Computational Sciences, the National Institute for Computational Sciences, and the Notur project in Norway. Computing time has also been provided by Los Alamos Open Supercomputing. This research also used resources of the National Energy Research Scientific Computing Center, which is supported by the Office of Science of the U.S. Department of Energy under Contract No. DE-AC02-05CH11231.

[1] A. Burrows, Rev. Mod. Phys. **85**, 245 (2013).
[2] F. Weber, *Pulsars as Astrophysical Laboratories for Nuclear and Particle Physics* (IOP, London, 1999).
[3] H. Heiselberg and M. Hjorth-Jensen, Phys. Rep. **328**, 237 (2000).
[4] J. M. Lattimer and M. Prakash, Phys. Rep. **442**, 109 (2007).
[5] F. Sammarruca, Int. J. Mod. Phys. E **19**, 1259 (2010).
[6] J. M. Lattimer, Annu. Rev. Nucl. Part. Sci. **62**, 485 (2012).
[7] K. Hebeler, J. M. Lattimer, C. J. Pethick, and A. Schwenk, Astrophys. J. **773**, 11 (2013).
[8] B. A. Brown, Phys. Rev. Lett. **85**, 5296 (2000).
[9] C. J. Horowitz and J. Piekarewicz, Phys. Rev. Lett. **86**, 5647 (2001).
[10] S. Gandolfi, J. Carlson, and S. Reddy, Phys. Rev. C **85**, 032801 (2012).
[11] M. B. Tsang, J. R. Stone, F. Camera, P. Danielewicz, S. Gandolfi, K. Hebeler, C. J. Horowitz, J. Lee, W. G. Lynch, Z. Kohley *et al.*, Phys. Rev. C **86**, 015803 (2012).
[12] A. W. Steiner and S. Gandolfi, Phys. Rev. Lett. **108**, 081102 (2012).
[13] S. Shlomo and D. H. Youngblood, Phys. Rev. C **47**, 529 (1993).
[14] S. Abrahamyan, Z. Ahmed, H. Albataineh, K. Aniol, D. S. Armstrong, W. Armstrong, T. Averett, B. Babineau, A. Barbieri, V. Bellini *et al.* (PREX Collaboration), Phys. Rev. Lett. **108**, 112502 (2012).
[15] P.-G. Reinhard, J. Piekarewicz, W. Nazarewicz, B. K. Agrawal, N. Paar, and X. Roca-Maza, Phys. Rev. C **88**, 034325 (2013).
[16] J. Erler, C. J. Horowitz, W. Nazarewicz, M. Rafalski, and P.-G. Reinhard, Phys. Rev. C **87**, 044320 (2013).
[17] M. Kortelainen, T. Lesinski, J. Moré, W. Nazarewicz, J. Sarich, N. Schunck, M. V. Stoitsov, and S. Wild, Phys. Rev. C **82**, 024313 (2010).
[18] D. Lunney, J. M. Pearson, and C. Thibault, Rev. Mod. Phys. **75**, 1021 (2003).
[19] B. D. Day, Rev. Mod. Phys. **39**, 719 (1967).
[20] K. A. Brueckner, C. A. Levinson, and H. M. Mahmoud, Phys. Rev. **95**, 217 (1954).
[21] K. A. Brueckner, Phys. Rev. **100**, 36 (1955).
[22] M. Baldo and G. F. Burgio, Rep. Prog. Phys. **75**, 026301 (2012).
[23] M. Baldo, A. Polls, A. Rios, H.-J. Schulze, and I. Vidaña, Phys. Rev. C **86**, 064001 (2012).
[24] H. Kümmel, K. H. Lührmann, and J. G. Zabolitzky, Phys. Rep. **36**, 1 (1978).
[25] B. D. Day and G. Zabolitzky, Nucl. Phys. A **366**, 221 (1981).
[26] J. Carlson, J. Morales, V. R. Pandharipande, and D. G. Ravenhall, Phys. Rev. C **68**, 025802 (2003).
[27] S. Gandolfi, A. Y. Illarionov, K. E. Schmidt, F. Pederiva, and S. Fantoni, Phys. Rev. C **79**, 054005 (2009).
[28] A. Gezerlis and J. Carlson, Phys. Rev. C **81**, 025803 (2010).
[29] A. Lovato, O. Benhar, S. Fantoni, and K. E. Schmidt, Phys. Rev. C **85**, 024003 (2012).
[30] A. Gezerlis, I. Tews, E. Epelbaum, S. Gandolfi, K. Hebeler, A. Nogga, and A. Schwenk, Phys. Rev. Lett. **111**, 032501 (2013).
[31] W. Dickhoff and C. Barbieri, Prog. Part. Nucl. Phys. **52**, 377 (2004).
[32] V. Somà and P. Bożek, Phys. Rev. C **78**, 054003 (2008).
[33] A. Rios and V. Somà, Phys. Rev. Lett. **108**, 012501 (2012).
[34] A. Carbone, A. Polls, and A. Rios, Phys. Rev. C **88**, 044302 (2013).
[35] G. Baardsen, A. Ekström, G. Hagen, and M. Hjorth-Jensen, Phys. Rev. C **88**, 054312 (2013).
[36] A. Ekström, G. Baardsen, C. Forssén, G. Hagen, M. Hjorth-Jensen, G. R. Jansen, R. Machleidt, W. Nazarewicz, T. Papenbrock, J. Sarich *et al.*, Phys. Rev. Lett. **110**, 192502 (2013).
[37] R. Machleidt and D. Entem, Phys. Rep. **503**, 1 (2011).
[38] E. Epelbaum, H.-W. Hammer, and U.-G. Meißner, Rev. Mod. Phys. **81**, 1773 (2009).
[39] U. van Kolck, Phys. Rev. C **49**, 2932 (1994).
[40] E. Epelbaum, A. Nogga, W. Glöckle, H. Kamada, U.-G. Meißner, and H. Witała, Phys. Rev. C **66**, 064001 (2002).
[41] E. Epelbaum, H. Krebs, D. Lee, and U.-G. Meißner, Euro. Phys. J. A **40**, 199 (2009).
[42] K. Hebeler and A. Schwenk, Phys. Rev. C **82**, 014314 (2010).
[43] K. Hebeler, S. K. Bogner, R. J. Furnstahl, A. Nogga, and A. Schwenk, Phys. Rev. C **83**, 031301 (2011).
[44] J. Holt, N. Kaiser, and W. Weise, Nucl. Phys. A **876**, 61 (2012).
[45] H.-W. Hammer, A. Nogga, and A. Schwenk, Rev. Mod. Phys. **85**, 197 (2013).
[46] T. Krüger, I. Tews, K. Hebeler, and A. Schwenk, Phys. Rev. C **88**, 025802 (2013).
[47] L. Coraggio, J. W. Holt, N. Itaco, R. Machleidt, and F. Sammarruca, Phys. Rev. C **87**, 014322 (2013).
[48] C. Drischler, V. Somá, and A. Schwenk, arXiv:1310.5627.
[49] T. Inoue, S. Aoki, T. Doi, T. Hatsuda, Y. Ikeda, N. Ishii, K. Murano, H. Nemura, and K. Sasaki (HAL QCD Collaboration), Phys. Rev. Lett. **111**, 112503 (2013).
[50] D. J. Dean and M. Hjorth-Jensen, Phys. Rev. C **69**, 054320 (2004).
[51] K. Kowalski, D. J. Dean, M. Hjorth-Jensen, T. Papenbrock, and P. Piecuch, Phys. Rev. Lett. **92**, 132501 (2004).
[52] R. J. Bartlett and M. Musiał, Rev. Mod. Phys. **79**, 291 (2007).

[53] I. Shavitt and R. J. Bartlett, *Many-body Methods in Chemistry and Physics* (Cambridge University Press, Cambridge, 2009).
[54] J. J. Shepherd, A. Grüneis, G. H. Booth, G. Kresse, and A. Alavi, Phys. Rev. B **86**, 035111 (2012).
[55] A. Roggero, A. Mukherjee, and F. Pederiva, Phys. Rev. B **88**, 115138 (2013).
[56] F. E. Harris, H. J. Monkhorst, and D. L. Freeman, *Algebraic and Diagrammatic Methods in Many-Fermion Theory* (Oxford University Press, Oxford, 1992).
[57] D. L. Freeman, Phys. Rev. B **15**, 5512 (1977).
[58] R. F. Bishop and K. H. Lührmann, Phys. Rev. B **17**, 3757 (1978).
[59] C. Gros, Zeitschrift für Physik B Condensed Matter **86**, 359 (1992).
[60] C. Gros, Phys. Rev. B **53**, 6865 (1996).
[61] C. Lin, F. H. Zong, and D. M. Ceperley, Phys. Rev. E **64**, 016702 (2001).
[62] P. Navrátil, Few-Body Syst. **41**, 117 (2007).
[63] P. Navrátil, S. Quaglioni, and D. Gazit (private communication).
[64] G. Hagen, T. Papenbrock, D. J. Dean, A. Schwenk, A. Nogga, M. Włoch, and P. Piecuch, Phys. Rev. C **76**, 034302 (2007).
[65] S. Binder, P. Piecuch, A. Calci, J. Langhammer, P. Navrátil, and R. Roth, Phys. Rev. C **88**, 054319 (2013).
[66] G. Hagen, T. Papenbrock, D. J. Dean, and M. Hjorth-Jensen, Phys. Rev. Lett. **101**, 092502 (2008).
[67] G. Hagen, T. Papenbrock, D. J. Dean, and M. Hjorth-Jensen, Phys. Rev. C **82**, 034330 (2010).
[68] S. K. Bogner, R. J. Furnstahl, and R. J. Perry, Phys. Rev. C **75**, 061001 (2007).
[69] R. Roth, S. Binder, K. Vobig, A. Calci, J. Langhammer, and P. Navrátil, Phys. Rev. Lett. **109**, 052501 (2012).
[70] K. Raghavachari, J. Chem. Phys. **82**, 4607 (1985).
[71] B. D. Day, Rev. Mod. Phys. **50**, 495 (1978).
[72] B. D. Day, Phys. Rev. C **24**, 1203 (1981).
[73] M. I. Haftel and F. Tabakin, Nucl. Phys. A **158**, 1 (1970).
[74] K. Suzuki, R. Okamoto, M. Kohno, and S. Nagata, Nucl. Phys. A **665**, 92 (2000).
[75] K. A. Brueckner and J. L. Gammel, Phys. Rev. **109**, 1023 (1958).
[76] K. Schmidt and S. Fantoni, Phys. Lett. B **446**, 99 (1999).
[77] D. Thompson, M. Lemere, and Y. Tang, Nucl. Phys. A **286**, 53 (1977).
[78] S. Gandolfi, A. Y. Illarionov, F. Pederiva, K. E. Schmidt, and S. Fantoni, Phys. Rev. C **80**, 045802 (2009).
[79] C. Horowitz and A. Schwenk, Nucl. Phys. A **776**, 55 (2006).
[80] Y. S. Lee and R. J. Bartlett, J. Chem. Phys. **80**, 4371 (1984).
[81] Y. S. Lee, S. A. Kucharski, and R. J. Bartlett, J. Chem. Phys. **81**, 5906 (1984).
[82] K. Hebeler, Phys. Rev. C **85**, 021002 (2012).
[83] K. A. Wendt, Phys. Rev. C **87**, 061001 (2013).
[84] R. Roth, J. Langhammer, A. Calci, S. Binder, and P. Navrátil, Phys. Rev. Lett. **107**, 072501 (2011).
[85] D. R. Entem and R. Machleidt, Phys. Rev. C **68**, 041001 (2003).